

Assessment of the Risk of Internal Erosion of Water Retaining Structures: Dams, Dykes and Levees

Intermediate Report of the European Working Group of ICOLD

Contributions to the Symposium on 17–19 September 2007 in Freising, Germany



DEUTSCHES **T**ALSPERREN**K**OMITEE e.V.

Postfach 10 09 31
45009 Essen
Germany

Geschäftsstelle:
Kronprinzenstraße 37
45128 Essen
Germany

Tel.: +49 (0)201 178-2630
Fax.: +49 (0)201 178-2605
info@talsperrenkomitee.de



Technische Universität München

Lehrstuhl für Wasserbau und Wasserwirtschaft

80290 München, Arcisstraße 21 Tel.: 089 / 289 23161
Germany Fax: 089 / 289 23172
 E-Mail: wabau @ bv.tum.de

Versuchsanstalt für Wasserbau und Wasserwirtschaft (Oskar von Miller - Institut)

82432 Obernach, Walchensee Tel.: 08858 / 9203 0
Germany Fax: 08858 / 9203 33
 E-Mail: obernach @ bv.tum.de

ISSN 1437-3513

ISBN 978-3-940476-04-3

Berichte des Lehrstuhls und der Versuchsanstalt für
Wasserbau und Wasserwirtschaft

Herausgegeben von Prof. Peter Rutschmann
Ordinarius für Wasserbau und Wasserwirtschaft, TU München

Druck und Einband: Meissner Druck GmbH, Oberaudorf

Preface 1

Since there are embankment dams, there are problems with internal erosion. Phenomena related with these mechanisms are often difficult to identify and to estimate. In a certain way the early detection of internal erosion and the reliable assessment of the resulting risk for the dam stability have to be considered as supreme discipline in embankment dam engineering. Despite the enormous quantity and the outstanding quality of many research activities in this field there is still a lot of research work to do.

The German National Committee on Large Dams (Deutsches TalsperrenKomitee e.V.) as national organisation of ICOLD (International Committee on Large Dams) is organising the 14th German Dam Symposium and 7th European Club Dam Symposium in Freising. Within the scope of this international conference we will deal with the *Public Awareness of Dams*, with *Benefits and Risks of Hydraulic Structures* and of course with the discussion of *Ongoing Projects in Germany and Abroad*.

Considering their important relevance in embankment dam engineering the German National Committee places special emphasis on *Leakage Detection* and *Internal Erosion*. We appreciate so much the activities of the European Working Groups established by the ICOLD European Club. One of these groups, the *European Working Group on Internal Erosion in Embankment Dams*, was working intensively on a summarizing report during the last years. You have this report now in your hands. We all know that again this report will not be the last one in this difficult field of research. Anyway, the German National Committee is convinced that this publication is a significant step ahead.

The production of the report is jointly financed by the German National Committee and the Institute of Hydraulic and Water Resources Engineering of the Technische Universität München. We have to thank the former head of this institute, Prof. Theodor Strobl, who was responsible for this agreement, and his successor Prof. Peter Rutschmann, who overtook this commitment and who is acting now as publisher of the report. The editorial work was done in close cooperation between Electricité de France (EDF), Tiroler Wasserkraft (TIWAG) and Innsbruck University.

The essential work of the report was done by the very active members of the working group. There were many meetings and there was a lot of coordination work to do. The key role in this procedure played Monsieur Jean-Jacques Fry (EDF), the chairman of the working group. Merci beaucoup, Jean Jacques!

Beuerberg, 29th July 2007

Markus Aufleger

Vice-President

German National Committee on Large Dams

Preface 2

Internal erosion and piping in embankments and theirs foundations is the main cause of failures and accidents to embankment dams. In Europe, many existing dams, dykes and levees were not provided with filters and are susceptible to internal erosion failure. This has been recognized by the European Club of ICOLD and a Working Group was devoted to that problem. The members of the European Working Groups are young researchers and experts. Every year, in a symposium, the researchers present their latest research results and compare them to practice and experience from experts. The objective of the task is to give guidance for practitioners in charge to assessing the safety of water retaining structures. The method is being developed in three deliverables:

The first step is a companion book delivering the main definitions of physical processes, describing the framework upon which the safety assessment of all the internal erosion incidents can be based and assessing the current research needs. The title is "Internal erosion of Dams and theirs Foundations" published by Taylor & Francis, London, ISBN 978-0-415-43724-0. This book records the proceedings of a symposium organised by EDF AND IREX and chaired by Robin FELL.

The second step is a research report, developing research and compiling first results in the framework of the assessment of the internal erosion process through a water retaining structure conducted in a systematic way, so that all internal erosion phases are considered for each failure mode and loading condition. Height steps are detailed by different papers written by researchers or engineers. These papers are submitted to discussion. The reader is invited to exchange his remarks, his approval or his contradictory experience with the authors. Email addresses are at the end of every paper. It is clear that some important research results or validation of practice are missing. For instance, framework of probabilistic modelling exists and awaits application, piping modelling is not achieved, comparison between methods of leakage detection has not been completed and foundation problems were not paid sufficient attention. For all this reasons, that report is an intermediate report.

The third step shall bring up to date experience and research on internal erosion and shall propose the guidelines for engineers. Based on the research under development and on discussion with international experts, the intermediate report will be modified and completed in order to give a strong support to practitioners.

Le Bourget, July 2007

Jean-Jacques Fry

Chairman

European Working Group on Internal Erosion in Embankment Dams

Authors of the report

ALEM A.	GOLTZ Matthias
ARTIÈRES Olivier	GRAVELAT Serge
AUFLEGER Markus	GUIDOUX Cyril
BARTSCH Maria	HUBER Nils P.
BENAHMED Nadia	JOHANSSON Sam
BENAMAR Ahmed	KOELEWIJN André R.
BLAIS Jean-Paul	KONRAD Jean-Marie
BOLEVÉ Alexandre	MAROT Didier
BONELLI Stéphane	MUCKENTHALER Peter
BRIDLE Rodney	NILSSON Åke
BROWN Alan J.	PERZLMAIER Sebastian
CALLE E.O.F.	RADZICKI Krzysztof
CHOPIN Michel	REVIL André
COURIVAUD Jean-Robert	ROYET Paul
DAHLIN Torleif	SAUCKE Ulrich
DELGADO Fernando	SELLMEIJER Hans J.B.
DORNSTÄDTER Jürgen	SJÖDAHL Pontus
ELKAWAFI A.	TERNAT Fabien
FABRE Jean-Paul	VAZINKHOO S.
FOILLARD René	VUOLA Pekka
FRY Jean-Jacques	VEDRENNE Christophe
GARNER Steve J.	WÖRMAN Anders

Editorial Board of the report

AUFLEGER Markus, Professor at University of Innsbruck

FRY Jean-Jacques, expert at EDF and Professor at Ecole Centrale de Lyon

GOLTZ Matthias, Scientific Staff at University of Innsbruck

PERZLMAIER Sebastian, Dam Engineer at TIWAG

Acknowledgement

Thanks to EDF, IREX, Technische Universität München and Vattenfall for hosting the annual meetings of the European Working Group on Internal Erosion in the years 2003 to 2007.

Thanks to Prof. Robin FELL, IREX, GTC and Hydroresearch for their long term support of the working group.

Thanks to the University of Innsbruck and TIWAG for the editorial work.

Thanks to the Technische Universität München for publishing this report.

Thanks to the DTK for sponsoring it.

Inhaltsverzeichnis / Table of Contents

01	1
Jean Jacques Fry	
Context and Framework of the Report of the European Working Group on Internal Erosion	
02	13
Pekka Vuola, Jean-Marie Konrad, Maria Bartsch	
Effects of Frost and Thaw on Dams	
03	21
J.-M. Konrad	
Evaluating the Changes in Hydraulic Conductivity of Compacted Soils Subjected to Freeze-Thaw Cycles	
04	30
S. Perzlmaier, P. Muckenthaler, A.R. Koelewijn	
Hydraulic Criteria for Internal Erosion in Cohesionless Soil	
05	45
S. Bonelli, D. Marot, F. Ternat, N. Benahmed	
Criteria of Erosion for Cohesive Soils	
06	60
Jean-Jacques Fry	
Current Practice and new View on Granular Filters	
07	70
Rodney Bridle, Fernando Delgado and Nils P Huber	
Internal Erosion: Continuation and Filtration: Current Approaches Illustrated by a Case History	
08	86
A. Benamar, A. Elkawafi, A. Alem, H. Wang	
Clogging Evaluation Opermeable Soil Filters	
09	96
A. Wörman, U. Saucke, E.O.F. Calle, J.B. Sellmeijer and A.R. Koelewijn	
Probabilistic Aspects of Geomechanical Filter Design	

10		110
J.B. Sellmeijer & A.R. Koelewijn		
Engineering Tools for Piping – Neural Networks Created using FEM		
11		132
Jean-Jacques Fry, Jean-Paul Blais, Sebastian Perzlmaier, Markus Aufleger and Matthias Goltz		
Introduction to the Detection of Internal Erosion		
12		144
Jean-Paul Blais, Serge Gravelat, René Foillard		
Detection of Leakage by non Destructive Methods : EDF Experience		
13		154
S.J. Garner, S. Vazinkhoo		
Analysis of Conventional Monitoring and Cross-Hole Seismic Data for Detection of Internal Erosion in an Earthfill Dam		
14		167
A. Revil, A. Bolève		
Self-Potential as a Detection Method to Evaluate Fluid Flow		
15		180
Pontus Sjödahl, Torleif Dahlin and Sam Johansson		
Detection of Internal Erosion and Seepage Evaluation using Resistivity Monitoring		
16		186
Sam Johansson and Pontus Sjödahl		
Seepage Measurements and Internal Erosion Detection using the Passive Temperature Method		
17		193
S. Perzlmaier, M. Aufleger, J. Dornstädter		
Detection of Internal Erosion by Means of the Active Temperature Method		
18		208
Jean-Jacques Fry and Michel Chopin		
Dam Strengthening by Diaphragm Walls		

19	222
Maria Bartsch and Åke Nilsson	
Function Analysis and Strengthening by Adding a d/s Berm	
20	235
Olivier Artières, Stéphane Bonelli, Jean-Paul Fabre, Cyril Guidoux, Krzysztof Radzicki, Paul Royet, Christophe Vedrenne	
Active and Passive Defences against Internal Erosion	
21	245
Jean-Robert Courivaud and Jean-Jacques Fry	
Dam Breaching – Case Studies	
22	255
A.J Brown	
A Framework for the Management of Risk from Internal Erosion	

Context and Framework of the Report of the European Working Group on Internal Erosion

By Jean Jacques Fry

Abstract

The European Working Group on Internal Erosion of Embankment Dams delivers its final report in Freising at the ICOLD European Club Dam Symposium. Previously five meetings were held in Paris (2004), Aussois (2005), Obernach (2005), Stockholm (2006) and Aix-les-bains (2007). This paper presents the context, the background, the definitions and the framework of the task. The internal erosion assessment is an 8 step process : location, situation, initiation of erosion, filtration, progression, detection, intervention, and prevention.

According to the statistics collected by ICOLD (1995), embankment dams are more vulnerable than concrete or masonry dams (table 1) :

Table 1: Failure/year/dam in the world (without China) from 1970 to 1990

Type	Number of dams	Number of failures	N° of Dam Failures 100 000_year*dam
Concrete or masonry	5500	2	2/100 000
Embankment	16 500	26	9/100 000

Three modes of failure threaten embankment dams and dykes : external erosion (mostly during flooding due to overtopping and sometimes by toe scour), internal erosion and sliding. From ICOLD statistics (ICOLD 1995), the most frequent hazard is the flood (table 2), however, in the years to come due to the progress of hydrological studies (PMF, Safety flood, etc.) and weather forecasting the most likely hazard should be internal erosion.

Table 2: Failure rate in the world (without China form 1970 to 1989 - ICOLD 1995)

Modes of failure	Number of Failures 1970-1979 N° of dams	Number of Failures 1980-1989 Number of dams
Internal erosion	0,0020	0,0016
External erosion	0,0026	0,0019
sliding	0,0004	0,0001

The current annual probability of failure depends of the type of construction and the age of the structure. It can be estimated from statistics collected by Fell (Table 3- Forster and Fell 2000).

Table 3: Estimated annual probabilities of failure depending on type of design

Type of embankment built before 2000	estimated annual probability
Homogeneous earthfill	$2,1 \times 10^{-4}$
homogeneous with rock toe	$1,8 \times 10^{-4}$
Concrete face earthfill	1×10^{-4}
Puddle core earthfill	6×10^{-5}
earthfill with filter	6×10^{-5}
Central core earth and rockfill	$< 6 \times 10^{-5}$
Zoned earthfill or earth and rockfill	5×10^{-5}
Concrete face earthfill	$< 4 \times 10^{-5}$
Earthfill with core wall	$< 3 \times 10^{-5}$

A large number of old embankments and dykes are in operation in Europe. Internal erosion is the major potential mode of failure of these structures. In view of this, the European club wishes to improve its methods for assessing the likelihood of internal erosion of its dams and dykes.

1 Background: Five Annual Meetings

The European Club of ICOLD has nominated a European Working Group (EWG), with the objective to gather together researchers and experts and to update ideas on internal erosion. The task was piloted by Dr. Andrew Charles, from the Building Research Establishment, from 1994 to 2001 and by Dr Jean-Jacques Fry, from Electricité de France (EDF) from 2003 to 2007. EDF was, and still is, very keen to increase the safety of its structures. Currently EDF owns 400 dams (including 150 large embankment dams) and 584 km of dykes the majority of which are very old. In France, the task has been supported by the Institut pour la Recherche Appliquée et l'Expérimentation (IREX). In France IREX has launched a research program on internal erosion of dams and dykes, named ERINOH (2006-2009). Since 2004, the method has been developed during a series of 5 meetings attended by 40 to 60 specialists. IREX and EDF sponsored the three meetings held in France.

The first meeting was held in Paris, France, on 26th and 27th April 2004 with two objectives : Firstly to present the European research programmes and incident data base and secondly to present information on early detection with optical fibres.

The second was organized with Prof. Robin Fell, Australia, from 25th to 27th April 2005 in Aussois, France, with two objectives : Firstly the definition of the framework upon which the safety assessment of any internal erosion incident of a dam can be based and secondly an assessment of current research needs.

The third was held on 13th and 14th June 2005 in Obernach, Germany, sponsored by Technische Universitat of Munchen (TUM) and GTC Kappelmeyer, devoted to recent Research results and detection of leakages by fibre optic sensors.

The fourth was held in Stockholm, Sweden, on 11th and 12th September 2006, sponsored by VATTENFAL and ELFORSK, with 3 topics : analysis of mechanisms, experimentation and modelling and methods of detection.

The last meeting, in Aix-les Bains, France, on 16th and 17th April 2007 was designed to focus technical papers and discussions on the final report. The objective was the presentation of the final report to the European Symposium of ICOLD in Freising, Germany, from on 17th to 19th September 2007 .

2 Definitions

Given the sometimes contradictory meaning of certain words, for the purposes of the EWG, the following definitions were agreed by the attendees in the Aussois meeting (Fell and Fry, 2007).

Heave (or ‘blow out’ or ‘liquefaction’). Heave occurs in cohesionless soils when seepage pore pressures are such that the effective stress becomes zero (pore pressure equals total stress). ‘Heave’ may often be followed by backward erosion if the seepage gradient remains high at the surface.

Hydraulic fracture. Hydraulic fracture occurs in the core of embankment dams when the minor principal stress becomes zero and the pressure of the water seeping through the core exceeds the remaining compressive stress and forms a crack or further opens an existing crack in which internal erosion may start.

Internal erosion. Occurs when soil particles within an embankment dam or its foundation, are carried downstream by seepage flow. Internal erosion can be initiated by concentrated leakage, backward erosion, suffusion or soil contact erosion.

Concentrated leakage erosion. Erosion by a concentrated leakage may occur through a crack in an embankment or its foundation, caused by differential settlement, desiccation, freezing and thawing, hydraulic fracture; voids adjacent to a concrete wall, or it may occur in a poorly compacted material which forms a system of large interconnecting voids.

Backward erosion. Backward erosion involves the detachment of soils particles when the seepage exits to a free unfiltered surface.

Piping. Piping is the mode of failure of internal erosion which forms due to backward erosion or concentrated leakage erosion in a highly permeable zone and results in the formation of a continuous tunnel called a ‘pipe’ between the upstream and the downstream side of the embankment or its foundation.

Soil contact erosion (or ‘external suffusion’ or ‘surface suffusion’). Soil contact erosion is a form of internal erosion which involves selective erosion of fine particles from the contact with a coarser layer, for instance along the contact between silt and gravel sized particles.

Suffusion (or ‘suffosion’). Suffusion is a form of internal erosion, which involves selective erosion of fine particles from the matrix of coarser particles (coarse particles are not floating in

the fine particles). The fine particles are removed through the voids between the larger particles by seepage flow, leaving behind an intact soil skeleton formed by the coarser particles.

Internal instability. Soils, which are susceptible to suffusion, are internally unstable. Coarse graded and gap graded soils where the volume of fines is less than the volume of voids between the coarse particles, are susceptible to suffusion.

3 Framework for Risk Assessment

The process of internal erosion of a water retaining structure is best considered in a systematic way, so that all internal erosion phases are considered for each failure mode and loading condition. 8 steps have to be detailed (Table 4 - Fell and Fry, 2007).

Step 1 Loading Condition. A loading condition is a theoretical combination of different loads exerted on a dam at a given time for analysis purposes. The loading condition is the start point for the internal erosion assessment.

Step 2 Location where erosion starts. This is the physical point where internal erosion starts in the structure such as in the embankment, foundation, along a conduit or along a spillway interface.

Step 3 Initiation. Initiation is the first phase of internal erosion, when particles become detached. The four ways this can occur, concentrated leak, backward erosion, suffusion and soil contact erosion were defined at the meeting in Aussois.

Step 4 Filtration. Filtration (also described as Continuation) is the phase where the relationship between the particle size distribution of the base (core) material and the filter controls whether or not erosion will continue. Foster and Fell (1999b, 2001) define four levels of severity of continuation from 'no erosion' to 'continuing erosion'.

Step 5 Progression. Progression is the phase of internal erosion where the enlargement of the pipe and the increase in pore pressure and seepage occur. The main issues are the mechanical condition whether the pipe will collapse, and the hydraulic condition whether upstream zones may control the erosion process by flow limitation and whether hydraulic shear stresses within the eroding soil may or may not lead to the enlargement of the pipe.

Step 6 Detection. Detection is the ability to detect the internal erosion process during one of the erosion phases.

Step 7 Intervention. Intervention is the ability to stop the internal erosion process during one of the first three phases and prior to the formation of a breach.

Step 8 Breach Prediction. Breach is the final phase of internal erosion. It may occur by one of four phenomena:

- Gross enlargement of the pipe (or piping).
- Slope instability of the downstream slope (general instability).
- Unravelling of the downstream face (local instability, or skin sliding).
- Overtopping (e.g. due to settlement of the crest).

Table 4: the 8 steps to assess the risks of internal erosion

Phases	Content
1 Load condition	1 HYDROSTATIC : Frequent water level, Rare flood, Safety flood 2 SEISMIC : OBE and MDE 3 ENVIRONMENTAL : animals, sun shrinkage, frost and thawing
2 Location	1 EMBANKMENT : Upper, Lower, Conduit, Wall, 2 FOUNDATION : Valley, Abutment, 3 EMBANKMENT TO FOUNDATION
3 Initiation	1 BACKWARD EROSION, 2 CONCENTRATED LEAK, 3 CONTACT EROSION, 4 SUFFUSION
4 Filtration	1 NO EROSION VAUGHAN, 2 NO EROSION SHERARD, 3 SOME EROSION, 4 EXCESSIVE EROSION, 5 CONTINUING EROSION
5 Progression	1 MECHANICAL CONDITION. Will pipe stay open? 2 HYDRAULICAL CONDITION. Rate of erosion? Upstream and downstream flow limitation? Critical gradient or velocity reaches?
6 Detection	Piping mode monitoring? Type of effective Surveillance? Continuous temperature measurement?
7 Intervention	Structural measures for repair? Diaphragm wall? Filter and Rock toe?
8 Breach Prediction and population protection	1 st mode of failure : GROSS ENLARGEMENT, 2 nd mode of failure : LOSS OF FREEBOARD - CREST SETTLEMENT, 3 rd mode of failure : SLOPE INSTABILITY, 4 th mode of failure : UNRAVELLING

This final step gives potential breach characteristics that enable emergency plans to be prepared, both in terms of the available time and maximum peak discharge for the emergency and in terms of actions to prevent failure in the event of a serious incident.

4 Loading Conditions

A loading condition is a theoretical combination of different loads exerted on a dam at a given time for analysis purposes. The main loads exerted on a dam are :

- Hydrostatic load which is related to the reservoir level (**Figure 1**)
- Seismic loads which were designed in terms of Operating Base Earthquake and Maximum Design Earthquake by ICOLD and which may be expressed in terms of earthquake magnitude, Peak Ground Acceleration (PGA), spectra and return period.

Other potential loads include :

- Environmental loads : rat holes, desiccation crack, tree roots.
- Human loads : explosion, acts of terrorism, vandalism or accidents.

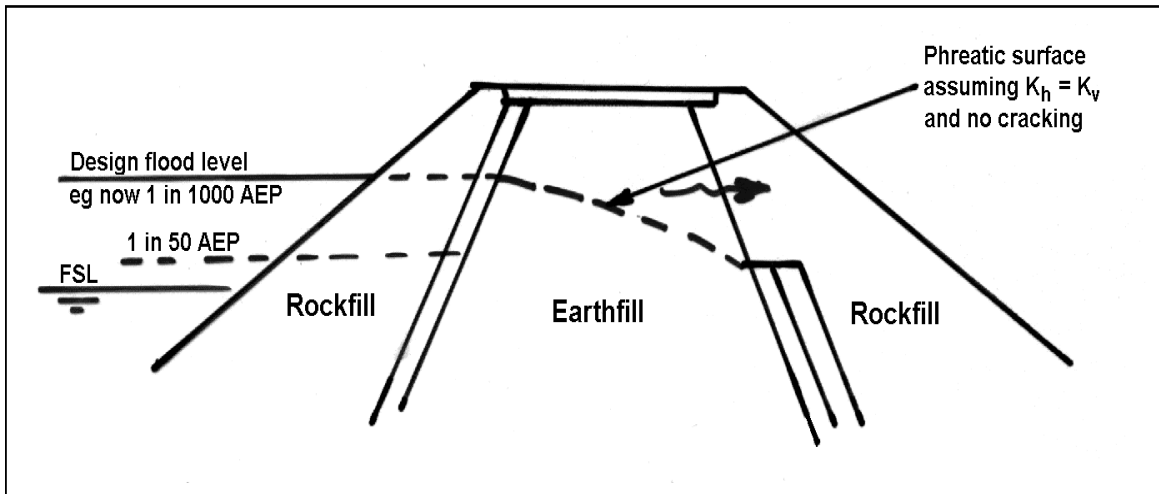


Figure 1: Example of possible situation triggering internal erosion

The scenario of loading conditions is the sum of all the loading conditions. An example of the loading conditions that should be considered is shown in table 1.

The likelihood of a given load may be expressed as the annual probability or frequency that the load is within a certain range. The selection of frequency F , or return period $T = 1/F$, make quantitative assessment easy. The successive internal erosion phases can be presented using flowcharts. The flowcharts enable multiple failure modes to be shown graphically and set up event trees to quantify the likelihood of the failure modes presented.

Foster and Fell (2000) proposed such quantitative assessment. In that report, the emphasis is not put on quantitative assessment, but on physical processes. The basic idea is to give additional guidance by modelling the progression phase or by comparing some key factors (hydraulic gradient, Darcy velocity) to a threshold determined from new laboratory tests.

Table 1: Example of loading conditions for assessing the likelihood of internal erosion

Loading number	Reservoir Loading conditions	Return period-(years)	Earthquake & return period	Return period-(years)
1	Frequent Water Level	1	No	
2	Maximum Water Level	100	No	
3	Maximum flood level reached cracks in the core or overtopping of the core	> 1000	No	
4	Probable Maximum Flood	> 10 000	No	
5	Full Supply Level	1	OBE	150 to 500
6	Full Supply Level	1	sufficient to cause cracking to below Full Supply Level	1 000
7	Full Supply Level	1	MDE	10 000

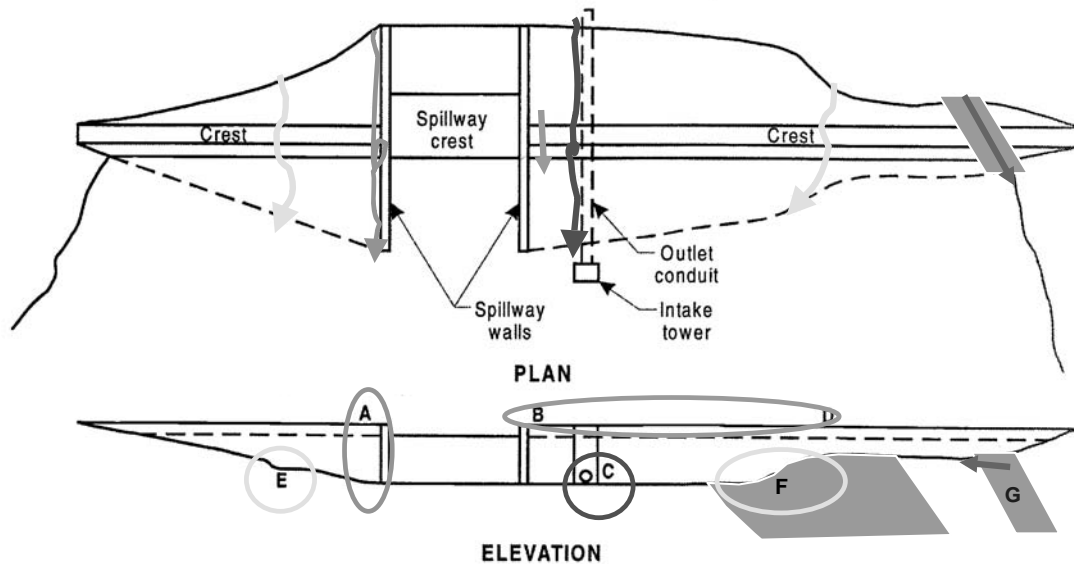
5 Locations where Internal Erosion Starts

5.1 Internal Erosion Path

In theory, the previous process of internal assessment is considered for all internal erosion paths. The internal erosion path is the potential path along which eroded particles are moved from the location where internal erosion starts in the dam and its foundation (**Figure 2**).

There are three categories of internal erosion paths in a typical analysis. These were developed by Foster and Fell (1999) from work by Von Thun (1996) and are as follows.

- Internal erosion in the dam embankment. This is the most frequent path, it is the cause of 39 dam failures out of 136 reported in the world (1/3 of the failed dams whose cause has been determined) by Foster and Fell (2000). They are mainly related to erosion starting adjacent to conduits, along the interface of the core with the spillway, through cracks caused by differential settlement, through construction joints created due to winter or wet season shut downs and river diversion closures and at the contact between foundation and core.
- Internal erosion in the foundation. This path is responsible for 19 dam failures out of 136. The total figure includes 60 piping failures reported in the world by Foster and Fell (2000). Internal erosion in the foundation is only a problem for soil and erodible rock foundations. Internal erosion from the embankment into the foundation may occur where the foundation is composed of coarse soils such as gravels or open jointed rock.
- Internal erosion from the dam embankment into the foundation. Two failures are reported by Foster and Fell (2000) out of 136 failures and 60 piping failures.



LEGEND

A - Adjacent spillway walls.	D - Related to irregularities in the foundation profile.
B – Crest : poor design and dessication cracks	F - In the foundation
C - Adjacent outlet conduit.	G - From embankment to foundation

Figure 2: Main locations where internal erosion could possibly be initiated

5.2 Data Collection and Models Identification

A lot of data is required for the safety assessment. Data collection is very important. It may be checked by creating 4 models of the dam and its foundation :

Geometrical model: the geometrical model gathers all the information describing the shape and the dimensions of the dam and its foundation layers. "As built drawings" are required, however experience shows that many "as built drawings" are incorrect. Levelling of the crest and bore holes are required to reinterpret the drawings. Shear wave investigations are used to draw the contour of the bedrock and weathered rock.

Geological model: Geological model considers lithology (positions and nature of soft soils, weathered rock and bedrock), structural analysis (tectonic, position of discontinuities : joints, faults, etc...) and geological background (earthquake, geomorphology). The susceptibility to erosion of weathered or soft rock and quality of joints (opening and content) are the key factors.

Geotechnical model: Geotechnical model is the compilation of the mechanical properties required for internal erosion assessment and stability analysis, including laboratory properties like bulk density, cohesion, friction angle, modulus and in situ properties like cone strength value, friction ratio. In situ tests are useful to get the variability of properties (mean, standard deviation, and autocorrelation parameters). A new CPT test named Permeafor enables continuous profiles of cone resistance and permeability to be plotted and is well suited to define the extent of contact erosion.

Hydraulic model : Hydraulic model quantifies the flow parameters through the dam body and its foundation. Two kinds of input data are required : soil characteristics and border limits

(piezometric heads and discharge). Soil characteristics include porosity, vertical and horizontal permeability and erosion parameters like critical shear stress and erosion coefficient k_d investigated with the Hole Erosion Test (see chapter on initiation). In practice leaking areas are investigated by Geophysical investigations (temperature, resistivity, streaming potential and radar, ...).

These 4 models are the basis for both stability and internal erosion analysis.

5.3 Location of Internal Erosion Depending on Dam Zoning

By comparing the zoning of the dams that have experienced failures, the location and how the erosion started, Foster and Fell (2000) assessed the relative influence of dam zoning on the likelihood of internal erosion.

Homogeneous dams: dams which have no zoning of materials have the highest frequency of failure, nearly five times higher than the average of all the other types of dam combined. Failures have generally been associated with concentrated leakage around conduits passing through the dam (9 cases), and backward erosion and/or concentrated leakage by piping (16 cases) through poorly compacted fill materials (12 cases) and piping through dispersive soils (4 cases). For Europe, it is noteworthy to remember that the average frequency of failure of homogeneous earthfill dams constructed prior to 1900 is about 10 times higher than that for dams constructed after 1950.

Earthfill dams with rock toe: they have one of the highest frequencies of failure by internal erosion. 9 Failures have occurred, associated with a path through embankment (5 cases), or with a path through foundation (3 cases) and from embankment into foundation (1 case). Their failure have generally been the result of concentrated leakage around an outlet conduit, backward erosion of the fill into coarse rockfill materials and sometimes concentrated leakage through cracks created through the dam due to irregularities in the foundation or steep abutments.

Zoned earthfill dams: these dams have a relatively low probability of failure. This is due to the fact that they were constructed after the Second World War using better construction procedures. It is worth noting that 3 of the 4 dams failed just after the first filling.

Puddle clay core dams: these dams have a relatively high average failure frequency through the embankment. Of the 4 failures of large dams, 3 were constructed before 1865 and in each case concentrated leakage occurred following hydraulic fracturing of the thin core which is not protected by zoned material. More than half of the piping accidents occurred after 50 years of operation. The failure of the 5 m high Clandeboye Dam occurred after 80 years of operation and was attributed to the collapse of a wooden conduit that passed through the embankment.

Embankment dams with upstream earth core and downstream rockfill zone: they have a low incidence of failure due to piping. There is only one dam failure, Avalon dam in 1904. This dam failed from backward erosion at the core rockfill contact that was not protected by a filter.

Earthfill dams with filter drains: these types of dam have a relatively low probability of failure. Failures have been associated with concentrated leakage and/or backward erosion through dispersive fill materials around outlet conduits passing through the dam (3 cases) or at the contact with concrete spillway structure (1 case). Failures occurred in zones where filters were

not provided : the 2 failures of embankments with a vertical filter were caused by backward erosion where no filter was provided around the conduit. In the 2 other cases, only a horizontal filter was provided.

Upstream faced rockfill dams: 5 Failures occurred, associated with a path through the embankment (2 cases), or with a path through the foundation (3 cases). The cause of failure was attributed to problems associated with the connection of the conduit to the upstream face in two cases and in the third case as a result of settlement and rupture of the conduit within the embankment.

Concrete faced rockfill dams: they have a very low incidence of internal erosion through the embankment, probably due to the good quality of the foundation, the drainage capacity and the stability of the rock body. Only one failure is reported by Zhang and Qu Chen (2007) : that is the Gouhou dam where piping is suspected in the stratified rockfill.

Central core earthfill and rockfill shoulders dams: no failure was reported for this type of dam. However 21 accidents were reported. 15 of these involved suffusion of broadly graded core materials of glacial origin into coarse or segregated filters. That a relatively large number of accidents have occurred but no failures have taken place indicates that these dams have a low frequency of failure because they are slow to progress to breaching. Review of these accidents suggests that breaching is slow to progress due to the slowness of suffusion process, effect of filters and stability and drainage capacity of the downstream rockfill shoulder.

6 Content of the Report

The content of the final report illustrates the framework upon which the safety assessment of any internal erosion incident can be based. The different steps of the risk assessment are successively presented. However, case studies are described in Fell and Fry (2007) and new complements are given in that report.

Step 1 and 2: Loading Condition and location

The general principles of loading conditions and locations are briefly presented in this paper. In the following two papers emphasis is given to the Nordic weather conditions and to the frost and thaw damaging effects on dams by Konrad J-M, Vuola P and Bartsch M.

Step 3 Initiation. The key point of this step is the detachment criteria. It is noteworthy for engineers that global relationships can be proposed. Hydraulic criteria in cohesionless soils are compiled from literature by Sebastian Perzlmaier, Peter Muckenthaler, Meindert Van, Matthias Goltz, and in cohesive soils by Stéphane Bonelli, Didier Marot and Fabien Ternat.

Step 4 Filtration. Rodney Briddle, Fernando Delgado and Nils P. Huber sum up the key factors required by engineers for assessing the filtering capability of a dam. The probabilistic approach is a potential tool developed by Anders Wörman Ulrich Saulke, Hans Sellmeijer, André Koelewijn. Ahmed Benamar gives informations on internal clogging of filter.

Step 5 Progression. Progression is the phase of internal erosion where the enlargement of the pipe and the increase in pore pressure and seepage occurs. The main issues are the mechanical condition whether the pipe will collapse, and the hydraulic condition whether upstream zones may control the erosion process by flow limitation and whether hydraulic shear stresses within the eroding soil may or may not lead to the enlargement of the pipe. New

engineering tools based on stochastic modelling developed mainly by Geodelft are available for engineers.

Meindert Van and André Koelewijn present one of these most promising ways to quantify the likelihood of internal erosion progression.

Step 6 Detection. Detection is the ability to detect the internal erosion process during one of the erosion phases. Currently, this is the step where the major progresses were noticed in the task group and where the risk is mainly controlled. Three methods of leakage determination have been developed, based on resistivity, streaming potential and the most effective on temperature measurements. Current strategies of seepage investigations and detection are introduced by Jean-Jacques Fry, Sebastian Perzlmaier, Markus Aufleger, Mattias Goltz and Jean-Paul Blais. Investigations for remedial maintenance are the scope of Jean-Paul Blais, Serge Gravelat and René Foillard. S.J. Garner and S. Vazinkhoo illustrate the analysis of conventional monitoring and cross-hole seismic data for detection of internal erosion. Preventive maintenance based on detection of internal erosion and seepage evaluation using resistivity monitoring are developed by Pontus Sjödahl and Sam Johansson, using streaming potential method by André Revil and Alexandre Bolève, using passive temperature method by Sam Johansson, Pontus Sjödahl, Christophe Vedrenne, Jean-Paul Fabre, Krysztof Radzicki, Stéphane Bonelli, and Jean-Marie Konrad and using active temperature method by Sebastian Perzlmaier, Markus Aufleger, Jürgen Dornstädter and Mattias Goltz.

Step 7 Intervention. Intervention is the ability to stop the internal erosion process during one of the first three phases and prior to the formation of a breach. Repairs based on diaphragm walls are introduced by Jean-Jacques Fry and Michel Chopin, construction of rock toe-berms for dams is presented by A. Nilsson, Maria Bartsch, and for dykes by Olivier Artières, Cyril Guidoux and Paul Royet.

Step 8 Breach Prediction. Breach is the final phase of internal erosion. It may occur in one of the four following ways:

- Gross enlargement of the pipe.
- Slope instability of the downstream slope.
- Unravelling of the downstream face.
- Overtopping (e.g. due to settlement of the crest).

This final step gives potential breach characteristics when preparing emergency plans, both in terms of the available time and maximum peak discharge for the emergency and in terms of actions to prevent failure. Breaching modelling is presented by Stéphane Bonelli, with some information from case studies given by J-R Courivaud. Finally, risk management is presented by Alan Brown.

7 Conclusions

This intermediate report summarises the main points for dam engineers who are charged with assessing the safety of embankment dams. The report is focused on the risk of internal erosion. The methodology is described from the international experts point of view. Significant emphasis is put describing new methods of detection.

A couple of years or more shall be required to investigate interpretation of new laboratory tests and application of new promising modelling and deliver the real final report of the task.

Literature

- [1] ICOLD (1995) Ruptures de barrages. Analyse statistique. Bulletin 99
- [2] FELL R., (1995) Application of risk assesment techniques to the zoning of embankment dams. Malaysian water association international conference on dam engineering. 1-2 August 1995. Kuala Lumpur
- [3] FELL R. and FRY J-J (2007) Internal erosion of dams and theirs foundations. Taylor and Francis 2007
- [4] FOSTER M., FELL R. and SPANNAGLE M. (2000) The statistics of embankment dam failures and accidents. Canadian Geotechnic J.37 pages 1000-1024
- [5] FOSTER M., FELL R. (2000) Use of event trees to estimate the probability of failure of embankment dams by internal erosion and piping ICOLD Beijing Congress Q76 R16
- [6] ZHANG, QU CHEN (2007) Seepage failure mechanism Soil and Foundations pages 557-567

Authors Name and Affiliation

Dr. Jean-Jacques Fry
EDF CIH Centre d'Ingénierie Hydraulique
73 373 Le Bourget du Lac Cédex
.jean-jacques.fry@edf.fr

Effects of Frost and Thaw on Dams

Pekka Vuola, Jean-Marie Konrad, Maria Bartsch

Abstract

Frost and thaw damage dams in a way that can be compared to how they damage e.g. roads and buildings: cracking, loosening, slope sliding and reduced bearing capacity. Climate change may be a new threat to dams. The threat to dams in the form of potential damage and some recorded incidents are presented in this paper, as well as means to reduce the effects of frost and thaw.

1 Favourable Conditions for Frost and Thaw

1.1 General

Frost can be divided into two basic categories: annual frost and permanent frost or permafrost. Frost action in dams includes both freezing and thawing effects. It is essentially controlled on the one hand by climate and on the other hand by construction techniques and sequence as well as soil type used in the different zones of the dam. One type of damage induced by frost is presented in figure 1.



Figure 1: Longitudinal frost crack in a) a minor earth dam in Yläiesjoki in Finland, photo by A. Leskelä and b) the zoned Grytfors rock fill dam in Sweden, photo by I. Ekström.

1.2 Climate

The world climate is usually classified by using the Köppen climate classification system. The system consists of classes A...E, where D and E are cold areas. Class H meaning highlands was not included in the original system.

Class D is a continental, severe i.e. micro-thermal, moist climate, with cold winters, and including a summer season. The average temperature of the coldest month is below -3 °C. Most

parts of Northern and Eastern Europe, Siberia and Canada are situated in the class D area. Class E is the polar climate area. In class H, or highland areas, the climate varies from cool to cold. The European climate is presented in figure 2, which is based on calculations by Dr. Kirsti Jylhä from the Finnish Meteorological Institute. Analysis period is 1961...1990.

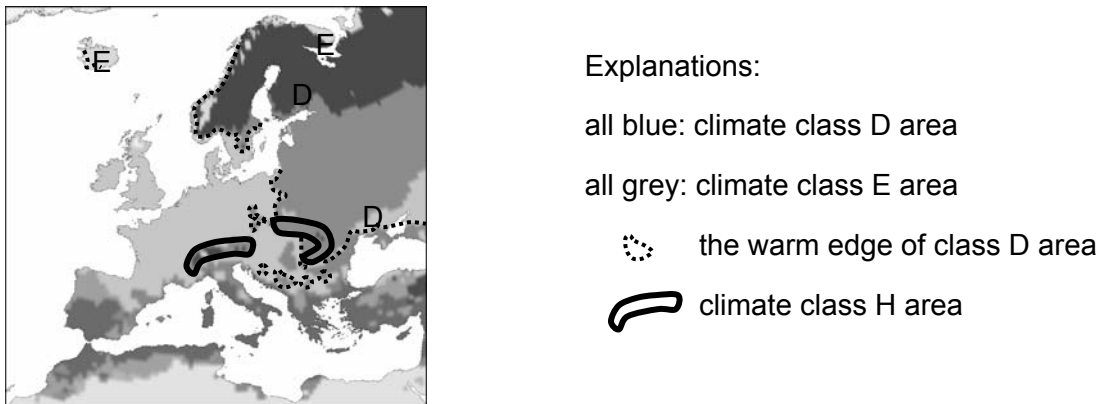


Figure 2: Climate in Europe according to the Köppen climate classification system.

Due to the climate definition, frost depth is at least 0,5 metres in the class D area, if the ground surface is free of snow. There seems to be an argument for concluding that frost action susceptibility is one of the dimensioning aspects for dams that are situated in the areas belonging to the climate classes D, E and H.

1.3 Soils

Soils are classified susceptible to frost action, if their height of capillary water rise is high enough. Silts as well as silt and sand moraines are usually susceptible to extreme frost action, because ice lens formation is noticeable in these soils. Clays are usually less susceptible. Coarse grained soils may be susceptible to frost action, if they contain a sufficient proportion of fine-grained soil fractions.

1.4 Frost and Thaw as Phenomena

Frost In frost susceptible soils, extra water rises into the frozen soil due to capillarity and forms ice lenses. The soil then tends to expand and to induce either frost heave or frost pressure and possibly cracking in the ground.

Freezing water releases freezing i.e. latent heat energy, which is conducted to the ground surface. Apart from conduction, there may be convection, if the material is coarse enough, especially rock fill.

Frost depth for a homogeneous ground can be calculated by using equation 1, where the ground surface is assumed free of snow. The value of coefficient κ is on the order of magnitude 0,01 for all soils. Based on research (Kuusiniemi 1995), the value is 0,012 in case of wide moraine dams.

$$Z = \kappa \cdot \sqrt{F} \quad (1)$$

Z = frost depth in the case of a one layer system [m], κ = coefficient for the units m, h and $^{\circ}\text{C}$, $F = \Sigma(t^*T^-)$ freezing index [$\text{h}^*^{\circ}\text{C}$], where T^- is the temperature below zero.

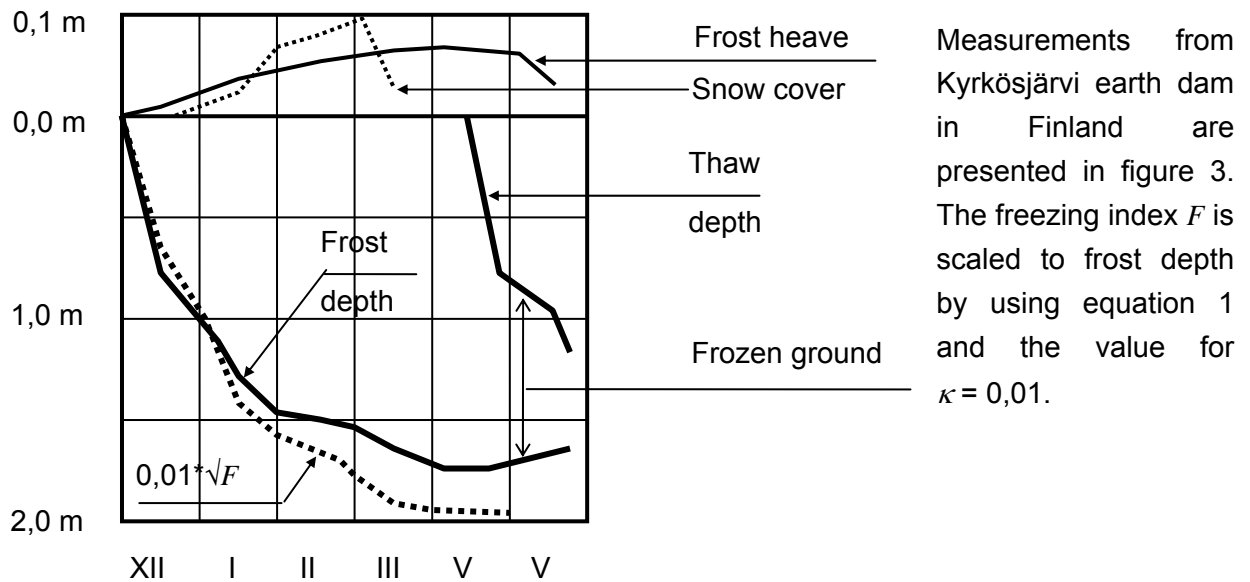


Figure 3: Measured values from Kyrkösärvi earth dam in western Finland in winter 1986...1987. Original values presented in (Kuusiniemi 1995) are redrawn.

Thaw There are potential problems, especially while the thaw is proceeding. Thawing ice lenses and possibly rain or melting snow may saturate the thawed zone. Saturation, linked with seepage parallel to the slope or shear deformations, may lead to slope sliding or loss of bearing capacity. Vertical and horizontal cracks and deformations in the dam induce soil loosening. In addition, these cracks are thorough or localized concentrated leaks through the dam.

2 Threat to Dams: Theory and some recorded Incidents

2.1 Period of Construction

Frozen soil cannot be compacted properly, if the aim is to obtain a high relative density. Dam slope slides and loss of bearing capacity of roads may occur during the thaw. If the dam construction can't be completed in one warm season, the frozen soil may loosen when thawing, or the thaw may set in during the first filling of the reservoir.

2.2 Period of Operation

2.2.1 Stationary Climate

The appearance of frost in dams is presented in figure 4. The vertical crack is usually longitudinal, but vertical cross cracks through the core or the whole dam are also possible. Causes include at least non-uniform formation of ice lenses and thermal contraction.

A photo from Grytfors dam in Skellefte River in northern Sweden is presented in figure 1b. Notably, the dams have developed large longitudinal cracks reaching down several metres. The large frost depth in excess of 3 metres is apparently due to convection in the rock fill on the crest.

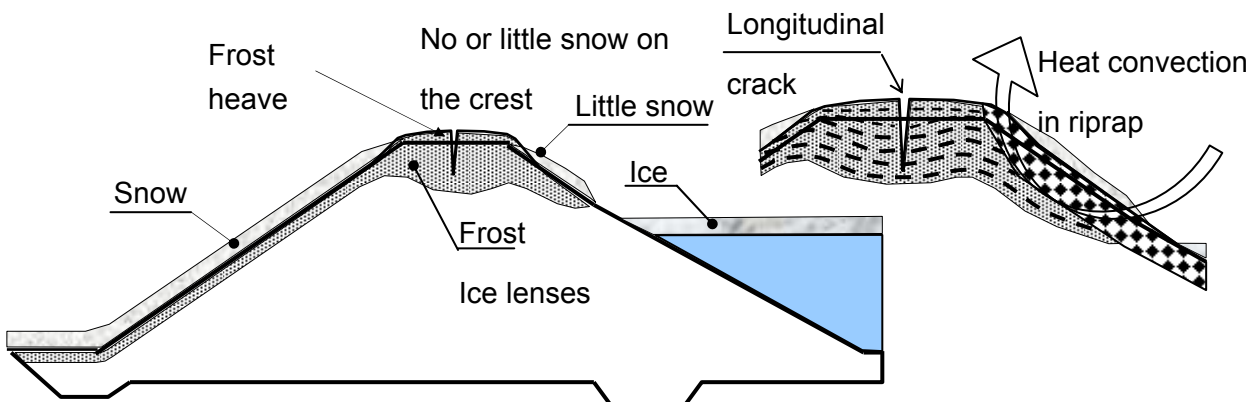


Figure 4: Frost in a wide-core i.e. 'homogeneous' earth dam.

The drainage system may be obstructed by frost, if the drainage level is above the frost depth. Ventilation in the pipes cools them possibly in a detrimental way. The ditches and outlets may be filled with ice.

Major destructive thaw phenomena are presented in figure 5. A series of events like this occurred in Hautaperä wide-core earth dam in Finland in 1976 during the first filling, but slope sliding was only local (Körkkö et.al. 1983). Another case occurred in Finland in Uljua zoned rock fill dam in 1970 soon after the first filling; internal erosion resulted in piping through the core and filters.

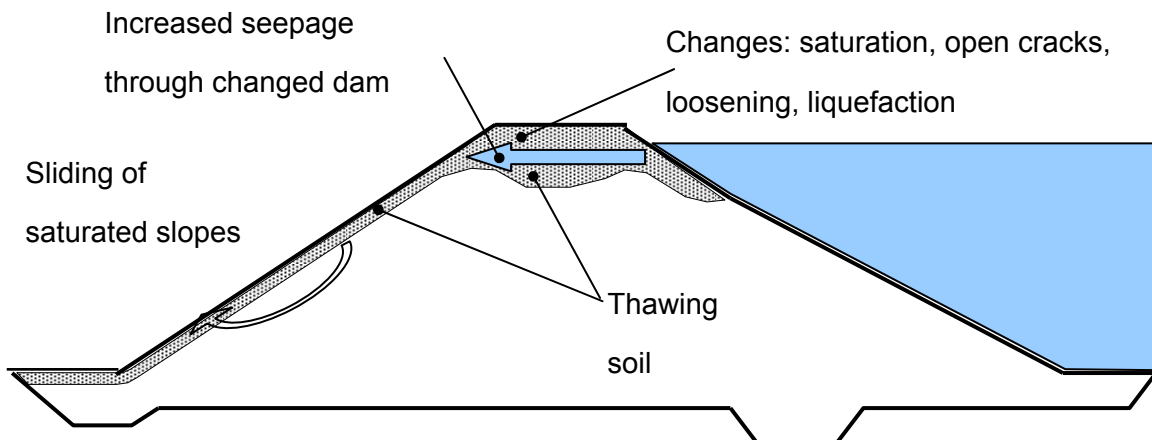


Figure 5: Damaging phenomena possibly occurring in earth dams during the thaw.

A typical spillway construction is presented in figure 6. The ice lenses are vertical in the deeper part of the core of the earth dam, resulting into horizontal frost pressure against the construction and the earth dam. This pressure induces deformation in the unfrozen core. The potholes on the dam crest alongside the construction may indicate such phenomena.

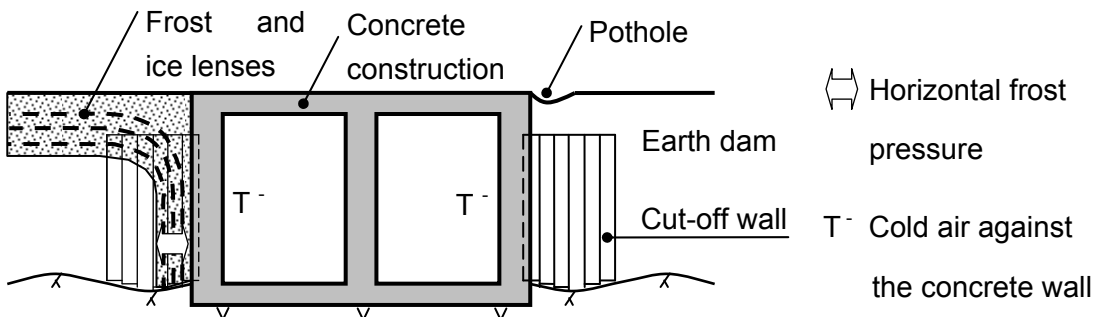


Figure 6: Effect of frost against a spillway construction.

In northern Québec, where the average freezing index is 84 000 h°C or 3 500 d°C, permafrost conditions within a homogeneous earth-structure were noticed after twelve years of operation, although the dam site was not in a permafrost area (Konrad and Ladet 1996). In the downstream toe area, only a thin permafrost layer was detected (**figure 7**), owing to snow conditions and possibly to advective heat flow from seepage through the drain. Downstream slope movement is induced by in-situ pore expansion as the active layer freezes, resulting in a solifluction deformation process. Finally, it appears that the horizontal drain remains operative despite the presence of permafrost. Thermal simulations have shown that permafrost conditions could develop as observed in the field. It is therefore important to apply this type of thermal analysis for any new structure built in the north where freezing indices exceed 72 000 h°C or 3 000 d°C.

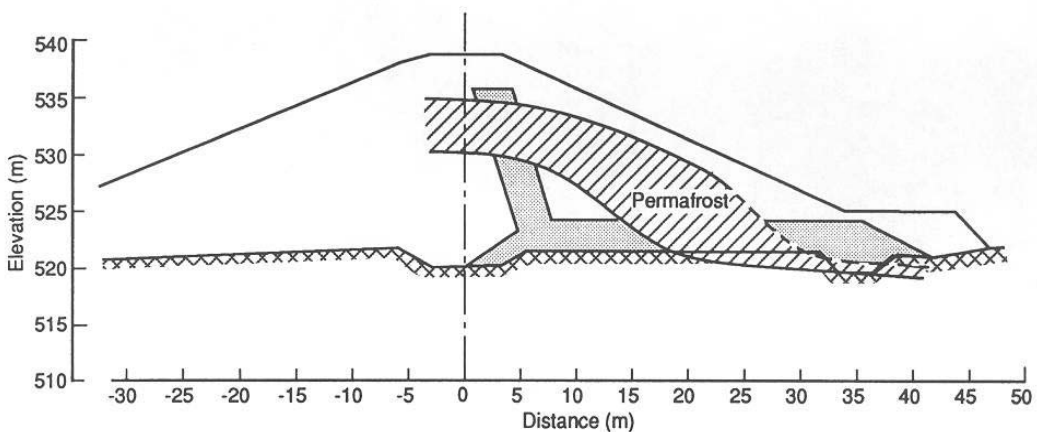


Figure 7: Observed permafrost in KA-07 /Konrad and Ladet/.

2.2.2 Climate change

Several hypotheses have been published to the effect that our climate is currently undergoing a change. Forecasts suggest that the climate is getting warmer in general. The following consequences may result from climate change:

- the freezing index may decrease, which decreases annual frost depth,
- the snow cover may decrease, which may increase real annual frost depth,
- in permafrost areas, the annual thaw depth may increase; in areas with fairly shallow permafrost or major climate change, the permafrost may thaw out.

3 Means to reduce the Effect of Frost and Thaw

3.1 Some usual structural Means

A sufficiently high freeboard is the most common solution to avoid frost problems. The Finnish practice is to dimension the freeboard for freezing index F_{10} indicating a return period of 10 years. Though frost may penetrate deeper occasionally, the hydraulic gradient through the thawing soil is usually minor; nonetheless filters on both sides of the core are desirable even in wide-core i.e. 'homogeneous' earth dams. At least the Finnish practice is to exclude the insulating effect of snow especially on the dam crest, because moderately insulating new snow remains there to a lesser degree. And on many dam crests there is a road, where snow is removed.

In wide-core earth dams in Finland, a gravel filter with a peat and grass overlay on the downstream slope has proved sufficient to prevent external erosion.

The sub-surface drains are usually placed below frost depth. The possibility of a ditch and outlet freeze-up should be taken into consideration. One solution is to guarantee water exit out of the dam through the coarse zones.

Cut-off walls have been used in the interface between an earth dam and the spillway or any cold structure, in order to increase seepage length and to reduce the effects of frost and thaw. The walls are reinforced concrete or sheet pile walls.

3.2 Industrial Insulations

Industrial insulation products can be used on the dam crest. Though insulation is not used very often, Finnish and Swedish applications have included: mainly extruded polystyrene boards in both countries, blast furnace sand in Finland and light weight foam glass aggregate in Sweden.

In the Grytfors rock fill dam mentioned in chapter 2.2.1, the moraine cores were raised inside the original crest profile, and the freeboard was reduced to 1 metre. The problem was solved by placing several layers of insulation boards on the new core, as presented in figure 8a. In the Suorva Västra dam in Sweden, part of the insulation has been sloped using light weight foam glass aggregate, surrounded by a geotextile. The working phase is presented in figure 8b. The horizontal polystyrene boards were installed later on.



Figure 8: a) Frost protection in Grytfors dam in northern Sweden: insulation of raised moraine core, photo by I. Ekström. b) Use of light weight foam glass aggregate as the sloping insulation in the Suorva Västra dam, photo by Å. Nilsson.

3.3 Dams in Permafrost Areas

Most permafrost is located in the E or polar areas and in sub-arctic D or continental high-latitude areas; alpine permafrost exists in cold H or highland areas. Permafrost is subdivided into continuous, discontinuous and sporadic frozen ground. Permafrost is always associated with a surficial unfrozen layer in the summer months, referred to as the active layer. Taliks, a Russian term for unfrozen bodies within permafrost, develop mostly in flood plains as a result of heat transfer from large rivers and lakes.

Basically, two approaches are preferred for construction and operation of dams on permafrost: the unfrozen and frozen approach. The unfrozen approach is recommended for rocky subsurfaces or in ice-poor permafrost where thaw settlement is minor. It is also important to have sufficient fine-grained soils to build an impervious core and cut-off. The frozen approach relies on an impervious barrier composed of saturated frozen material in the subsoil and in the entire body of the dam. This construction technique is favoured if thaw settlement of the subsoil would be significant, i.e. in ice-rich permafrost. Obviously, frozen impervious earth cores need to remain frozen over the life span of the dam. Global warming must now be systematically considered in the north. For instance, at higher latitudes, a more pronounced impact of climate change will occur in the winter.

Dams may thus be constructed using frozen earth cores but thawing will be permitted during operation. The effect of differential deformations of the dam must be offset by the use of adequate filters to prevent continuation of backward erosion, if the core material becomes unstable upon thawing. Another alternative is to keep the dam frozen at all times by using artificial means such as thermosyphons that operate when the air temperature is below freezing.

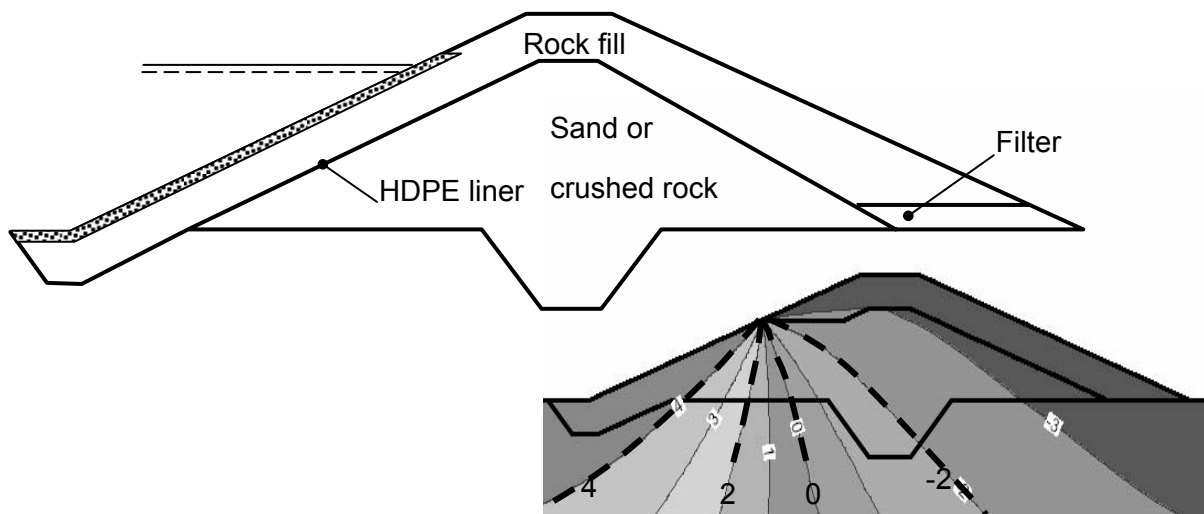


Figure 9: a) Typical dam on permafrost with frozen core and HDPE liner, b) thermal simulation of reservoir-induced melting of a dam on permafrost.

The construction sequence is also important in order to allow the collection and storage of the required quantity of sand in the summer, when the active layer is thawed, and completion of the excavations and dam construction in the winter, when the ground is frozen and conditions are well suited to the construction of a frozen core. The granular material can be mixed with water to achieve a degree of saturation of at least 85%. The following lift can only be placed once the in-

place material is frozen. To ensure an efficient cut-off, the frozen dam core would also have a HDPE liner placed on the upstream face of the core as shown in figure 9a.

Typical problems with dams on permafrost are generally associated with:

- Excessive settlement in the upstream shell and subsoil due to reservoir induced thaw (fig. 9b). Action: use relatively flat slopes 1V:3H or 1V:4H
- Core material too dry during placement which leads to high permeability and excessive seepage in the spring. Action: create some water retention structure around each lift.
- Incomplete cut-off in the ground beneath the dam
- Incomplete sub-surface investigation, e.g. undetected talik bodies
- Lack of adequate seal at each abutment, considering active layer and fissured rock.

Literature

- [1] KONRAD, J.-M. & LADET, R: Permafrost Formation and Aggradation in a 23 m High Homogeneous Dyke: A Case-Study. 1996. The Cold Regions Infrastructure, Eighth International Specialty Conference on Cold Regions Engineering, Fairbanks, Alaska, USA. pp. 700-710
- [2] KUUSINIEMI, Risto: Maapadon harjan routiminen ja routasuojaus mitoitus, 28.11.1995, Teknillinen korkeakoulu, Helsinki. (Frost action in the dam crest and frost protection dimensioning, Licentiate Thesis i.e. PhD Thesis, Helsinki University of Technology; written in Finnish)
- [3] KÖRKKÖ, Raimo, LOUKOLA, Erkki and MAIJALA, Timo: Hautaperän maapadon varmuuden tarkistus, 1983, National Board of Waters, Helsinki, Finland. Report 228. (Checking of stability of Hautaperä earth dam; written in Finnish)

Authors Name and Affiliation

Pekka Vuola, Lic.Tech. i.e. Dr.Eng.
Finnish Environment Institute (SYKE)
pekka.vuola@ymparisto.fi

Jean-Marie Konrad, ing, PhD.
Professor of civil engineering
Université Laval, Canada
jmkonrad@gci.ulaval.ca

Maria Bartsch, Lic.Eng. i.e. Dr.Eng.
Vattenfall Power Consultant AB
maria.bartsch@vattenfall.com

Evaluating the Changes in Hydraulic Conductivity of Compacted Soils subjected to Freeze-Thaw Cycles

J.-M. Konrad

Abstract

Freeze-thaw events in compacted soils produce both a change in soil fabric and in void ratio. This may, in turn, lead to a change in hydraulic conductivity. The magnitude of the change in k values depends on the type of soil, its fabric (homogeneous i.e. wet of optimum or aggregated with macropores, i.e. dry of optimum) and number of freeze-thaw cycles. For nonclay soils, horizontal ice lensing does not appear to create preferential seepage planes if arching is not present. Index properties such as the average size of the fines ($<80\mu\text{m}$) and specific surface area are useful to determine the nature of the fines.

1 Freezing Conditions in Damcrests

As outlined by Vuola et al. (2007), problems associated with dam construction and operation in cold areas (such as Northern Quebec and even southern Quebec where freezing indices range from 800 to 3500 °C.days) must be considered by the design engineer and the dam safety management team. Essentially, two situations require special attention. First, if the construction season spans over more than one year, winter construction is not allowed and it is general practice to protect the compacted till core with a 2m-thick sand layer in order to prevent undue frost penetration into the compacted till core. The following spring, the protective sand layer is removed, the till core scarified and recompacted before construction resumes. Recently, dam owners consider the possibility of avoiding using a protective sand layer allowing thus the frost to penetrate into the till core. After thaw, scarification of the upper 30 cm and recompaction will be done before resuming till placement activities. This approach is definitively more economical but it requires evaluating the hydraulic conductivity changes induced by one freeze-thaw event.

Another issue is related to the annual freeze-thaw events in the dam crest once construction is completed. When frost penetrates into the till core, ice lensing may occur if the till is frost susceptible and if there is availability of water. The thawing of the ice lenses may cause preferential seepage paths parallel to the flow lines. This, in turn, may lead to potential internal erosion if the seepage velocities are larger than a limit value. Again, it is essential for the design engineer to evaluate the change in hydraulic conductivity of the till core following several freeze-thaw cycles. This problem is further aggravated by the fact that reservoir levels may fluctuate over a relatively large range of elevations, up to several meters depending on the actual climatic conditions. This may, in turn, lead to deeper frost penetrations, and when reservoir levels are close to their highest levels of operation, seepage will occur through relatively large portions of thawed tills.

It is thus important to evaluate both the frost susceptibility of the impervious core of an embankment dam as well as the freeze-thaw induced hydraulic conductivity changes as a function of number of freeze-thaw events.

2 Frost Susceptibility from Soil Index Properties

Konrad (2005) demonstrated that a successful approach for assessing the frost susceptibility from soil index properties must consider at least the following key factors:

- grain size distribution and fines content;
- clay mineralogy;
- soil fabric;
- overburden pressure

Unfrozen water in a frozen soil can be partitioned into capillary water in the pores far from the soil particle surface and adsorbed water that can be considered as strongly influenced by the mineral surfaces. Water mobility in capillary channels is greater than that in the adsorbed water films, as the water molecules are strongly oriented and structured. Frost heave is essentially related to water flow through the network of capillary water channels in a tiny frozen zone adjacent to the frost front. As different clay minerals have different values of specific surface, the specific surface area of the fines fraction can be related to the amount of adsorbed water present in the frozen soil. Increasing adsorbed water content will be associated with increasing values of specific surface. The specific surface may also indicate, at least in a qualitative manner, the relative importance of clay minerals in the fines fraction.

Figure 1 shows the relationship between specific surface area and average particle size of the fines fraction for various soils. Soils represented by full symbols on Figure 1 have significant amounts of clay minerals while soils represented by open symbols are non plastic with nonclay fines. The reference line in Figure 1 can be used to differentiate soils with fines made of clay minerals from soils with nonclay fines, hence non plastic soils.

Frost-susceptibility can be quantified by the segregation potential SP. The use of the segregation potential parameter in geotechnical problems involving freezing is advantageous for at least two reasons. The first one is that it normalizes the response of the soil with respect to the thermal solicitation or intensity of freezing. This, in turn, makes SP an excellent parameter to assess the relative frost-susceptibility of soil and may even allow for some differences in test standards. The second advantage resides in the fact that SP permits the prediction of frost heaving for given specific geological and climatic conditions with the possibility of comparing the anticipated frost heave to an acceptable value depending on the project requirements and the risk tolerated by the designer or owner. Segregational frost heave in the field is calculated as:

$$h = 1.09 \int_0^t (SP_o e^{-ap_e} gradT_f) dt \quad (1)$$

where t represents time.

The frost heave response of the reference soils is presented in Figure 2 by the solid line which gives the values of SP_o as a function of average particles size of the fines fraction. Figure 2 also gives the value of SP_o for the other soils studied. Figure 3b presents the frost heave response of these soils in terms of normalized segregation potential and normalized specific surface for a given normalized water content w/w_L , where w_L is the liquid limit.

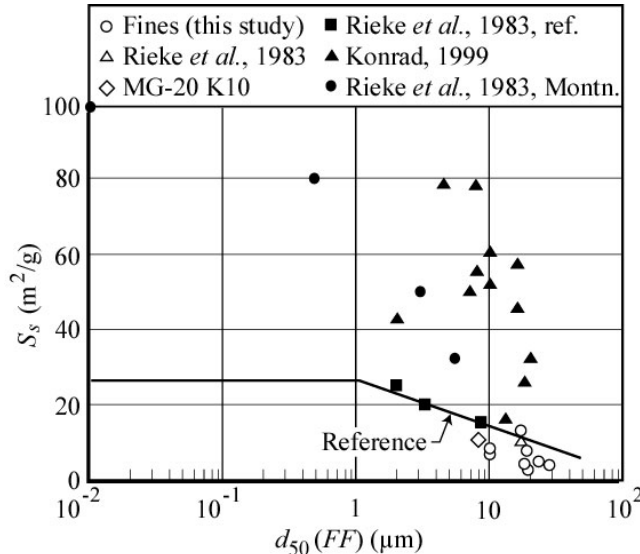


Figure 1: Specific surface area for different fines. Full symbols: clays Open symbols: nonclay fines

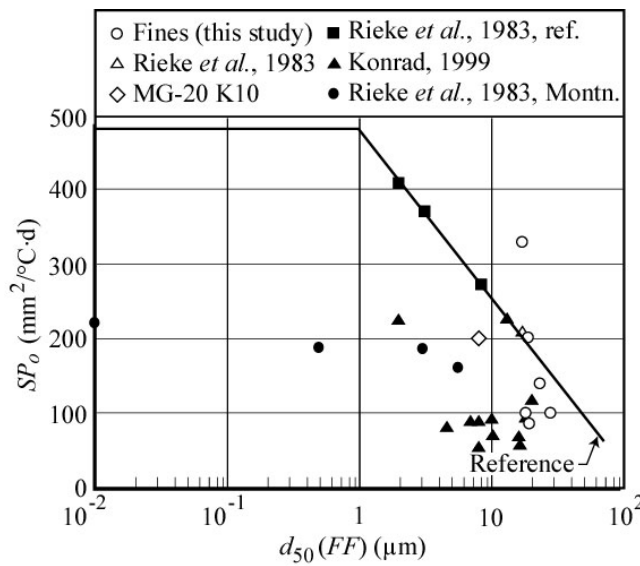


Figure 2: Segregation potential of various soils (adapted from Konrad 2005)

As anticipated, the relationships between normalized SP_o and normalized S_s depend on the type of minerals present in the fines; for soils in which the fines are essentially nonclay minerals, there is a linear relationship between normalized SP_o and normalized S_s up to the reference value of S_s , which depends essentially on average particle size of the fines fraction. For normalized values of specific surface area larger than 1, the clay minerals in the fines become

predominant and influence strongly the partition of unfrozen water content. Increasing values of S_s are associated with more adsorbed water around the clay plates and decreasing amounts of unfrozen capillary channels, thus reducing freezing-induced water migration and segregation potential. In general, the segregation-freezing temperatures in fine-grained soils such silts and clays with normalized specific surface areas of the fines fraction larger than 1 ranges between -0.1 and -0.5 °C. In soils with nonclay fines, the temperature of ice lens formation is greater than -0.1 °C, say a few hundreds of degree Celsius below 0°C. This may explain why the influence of overburden pressure is of paramount importance in these soils and that SP is extremely sensitive to small overburden pressure changes.

The frost-susceptibility of two tills from Quebec, one from the Caniapiscau dam in northern Quebec about 1000 km north of Montréal and a till from Péribonka dam, from the Lac-St-Jean region, about 400 km north of Montréal was determined from a freeze test in the laboratory. The segregation potential for consolidated slurries was 60 and 94 mm²/°C.day for Caniapiscau and Péribonka, respectively. Figure 3a shows the characteristics of these tills in terms of their index properties. The till from Caniapiscau is less frost-susceptible than the till from Péribonka because its normalized specific surface area is less than that of Péribonka till. It is stress worthy to point out that when compacted near optimum Proctor, both tills show less frost-susceptibility in terms of frost heaving owing to lower hydraulic conductivities of the unsaturated unfrozen soil.

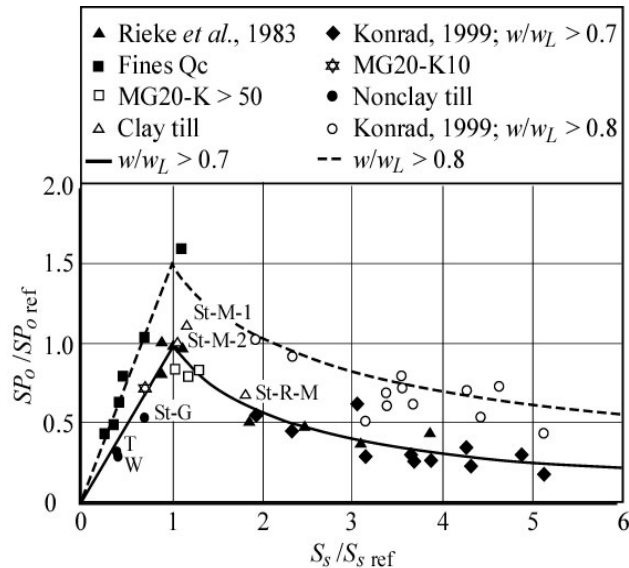


Figure 3: Characterization of two tills from Quebec

3 Factors Influencing the Change in Hydraulic Conductivity during freeze Thaw Cycles

3.1 Compacted Clays

To study the influence of freeze-thaw cycles on the hydraulic conductivity of compacted soils, an experimental setup shown in Fig. 4 was used. The relatively small height of the soil sample permits to create relatively uniform changes in the soil fabric since freezing is done under isothermal conditions by applying the same temperature at both end plates. This setup allows applying several freeze-thaw cycles and conducting constant head permeability tests at any desired step.

Tests conducted on consolidated slurries of natural silty clay and various kaolinite-silt mixtures (Konrad and Samson, 2000a,b) subjected to one freeze-thaw cycle showed that the change in hydraulic conductivity was related to the change in void ratio and to the change in soil fabric. For these frost-susceptible soils, it was also clearly established that the hydraulic conductivity of the thawed soils follows a linear relationship in a void ratio – log k space. The slope of this relationship, referred to as the permeability index S_k , depends upon the soil's clay content. The permeability index increases with decreasing freezing temperature as illustrated by Fig. 5 for the LaChute silty clay. The ultimate permeability index is related to the temperature at which no further change in unfrozen water content occurs in the soil. For the Lachute silty clay, this occurs at about -10°C to -12°C but in less clayey soils, it can occur at much higher temperatures. For instance for a 65% silt and 35% kaolinite mixture, no further change in hydraulic conductivity will occur for temperatures less than -2°C.

In very plastic clays, shrinkage cracks may lead to significant hydraulic conductivity increases. However, as water percolation continues, swelling of the clay walls closes the crack openings and ultimately leads to a decrease in hydraulic conductivity with time.

3.2 Compacted Tills

Tests conducted on compacted tills used in impervious cores of large earth dams in northern Quebec have shown that the change of hydraulic conductivity was also related to the number of freeze-thaw cycles as well as on the applied overburden pressure. For these soils, the fines are generally nonclay fines and their frost susceptibility varies with the specific surface area of the fines as discussed above.

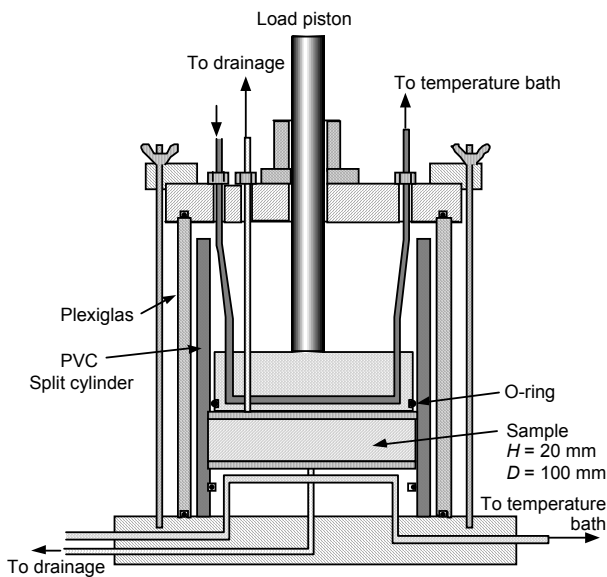


Figure 4: Experimental set-up for freeze-thaw-hydraulic conductivity tests

It is noted that the study of compacted soils is associated with additional difficulties such as assessing the actual degree of saturation after each freeze-thaw cycles and subsequent percolation or with repeatability issues as fabric is strongly influenced by initial water content. Nonetheless, when compacted close to the Proctor optimum conditions, the samples are generally close to saturation after several freeze-thaw-percolation cycles.

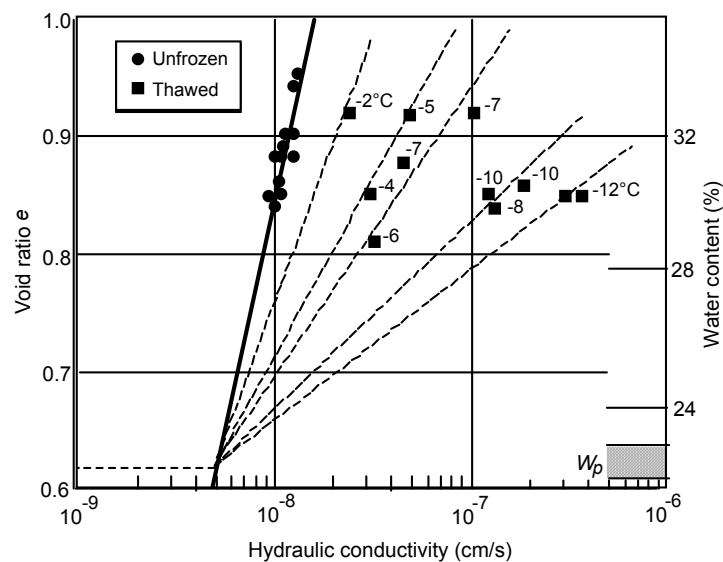


Figure 5: Influence of temperature for LaChute clay (after Konrad, 2000b)

Figure 6 shows the hydraulic conductivity changes obtained after several freeze-thaw cycles on compacted tills from Périonka and Caniapiscau. These data are also compared with data reported by Leroueil et al. (2002) on similar tills. Full lines correspond to soils with a homogeneous fabric, never frozen, dashed lines to the same soil with an aggregates and macropores, and hatched lines correspond to thawed soils after several freeze-thaw cycles.

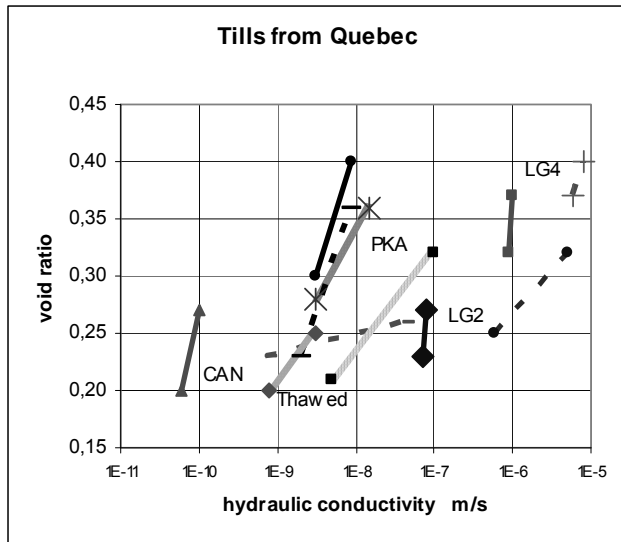


Figure 6: Hydraulic conductivity for tills from Quebec

Several observations can be drawn:

Hydraulic conductivity for compacted soils is very sensitive to compaction conditions. Wet of optimum conditions lead to a relatively homogeneous fabric while compaction dry of optimum produces an aggregated fabric with macropores as established by several authors (Daniel and Benson, 1990, Leroueil et al. 2002).

For non plastic tills, freeze-thaw cycles induce a change in fabric, which results in an increase in hydraulic conductivity for a given void ratio. However, freeze-thaw cycles also induce a reduction in void ratio. The combined effect may thus result generally in a slight decrease in hydraulic conductivity or a slight increase in k , depending on the initial void ratio.

Figure 7 shows that the average size of the fines ($<80\mu\text{m}$) can be used to estimate the hydraulic conductivity of tills compacted wet of optimum, i.e. tills with a homogeneous fabric. Clearly, when compacted dry of optimum, more variability may lead to more scatter in empirical relationships.

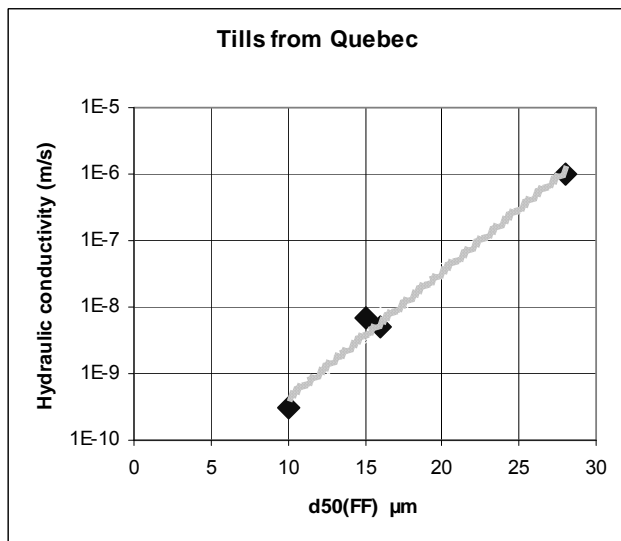


Figure 7: Relationship for tills from Quebec

4 Significance for the Potential of Internal Erosion

In these non plastic tills, ice lensing does not produce preferential seepage paths after thaw has occurred since thaw-settlements close the ice filled openings as ice melts. Special freeze-thaw cells with horizontal seepage (Konrad et al. 2000) showed identical changes in hydraulic conductivities for Caniapiscau tills subjected to vertical and horizontal seepage. The effect of freeze-thaw cycles is to create progressively a fabric with some macro pores and aggregates in which the finer particles are more densely compacted owing to the large suctions developed during freezing. Arching, however, must be minimized in the upper parts of zoned earth dams. It is also worth stressing that an increase of one order of magnitude in hydraulic conductivity in till cores that generally display a hydraulic conductivity of 10^{-7} m/s leads to a seepage velocity of about 0.5×10^{-6} m/s, which is still fairly low. Finally, all constant head permeability tests were conducted with hydraulic gradients of about 50, i.e. 100 times larger than those expected in the field. In all cases, thawed till samples were stable with respect to internal erosion.

5 Conclusions

Repeated freeze-thaw events result in hydraulic conductivity changes in compacted soils. The magnitude of these changes depends essentially upon the initial fabric created by the compaction conditions, the number of freeze-thaw cycles and the soil type. Larger changes may be expected in plastic clay soils as shrinkage cracks may induce large macrostructures. In non-plastic soils, however, hydraulic conductivity changes are generally offset by thaw-induced settlements which lead to a decrease in void ratio, hence of hydraulic conductivity.

Index properties such as the specific surface area of the fines and the average size of the fines are useful to determine whether the fines are predominantly controlled by clay minerals or if they are nonclay particles.

Finally, for dam crests, caution must be given to minimizing the potential arching effects in the core.

Literature

- [1] DANIEL, D.E. and BENSON, C.H. 1990. Water content-density criteria for compacted soil liners. *J. of Geot. Engng, ASCE*, 116(12):1811-1830.
- [2] KONRAD, J.-M., 2005. Estimation of the segregation potential of fine-grained soils using the frost heave response of two reference soils. *Can. Geotech. J.* 42, (1), 38-50.
- [3] KONRAD, J.-M. and SAMSON, M. 2000a. Hydraulic conductivity of kaolinite-silt mixtures subjected to closed-system freezing and thaw consolidation. *Canadian Geotechnical Journal* 37, No 4, 857-869.
- [4] KONRAD, J.-M. and SAMSON, M, 2000b. Influence of freezing temperature on the hydraulic conductivity of a silty clay. *Journal of Geotechnical and geoenvironmental engineering, ASCE*, Vol 126. No 2, 180-187.

- [5] KONRAD, J-M., LADET, R. LANGLOIS, P. 2000. Influence of reservoir level increase on thermal and hydraulic behaviour of frozen till cores. Can. Dam Assoc. conference, Victoria, B.C. Canada.
- [6] LEROUEIL, S., LE BIHAN, J-P, SEBAIHI, S. and ALICESCU, V. 2002. Hydraulic conductivity of compacted tills from northern Quebec. Can. Geot. J., 39: 10039-1049.
- [7] VUOLA, P., KONRAD, J-M., BARTSCH, M. 2007 Effects of frost and thaw on dams. This issue.

Authors Name and Affiliation

Jean-Marie Konrad, ing., PhD.
Professor of Civil Engineering
Université Laval, Canada
Jean-Marie.Konrad@gci.ulaval.ca

Hydraulic Criteria for Internal Erosion in Cohesionless Soil

S. Perzlmaier, P. Muckenthaler, A.R. Koelewijn

Abstract

This contribution gives an overview of hydraulic criteria for backward erosion, contact erosion and suffusion based on critical hydraulic gradients and critical flow velocities, discussing the interaction of hydraulic and geometric criteria. Since the hydraulic gradient can not sufficiently describe the transport of particles in cross flow on a micro scale, the focus is on critical pore velocities. A summary of the nonlinearity of flow through porous media leads to the derivation of critical flow velocities for internal erosion focusing on particle sink velocities, friction forces of resting particles and sediment transport criteria, which are compared to each other, to hydraulic criteria known from literature and to critical gradients observed in lab tests. The derivation of critical flow velocities forms the theoretical background to assess the likelihood of internal erosion to initiate by distributed flow velocity measurements referred to in paper 15 'Detection of internal erosion by means of the active temperature measurement'.

1 Introduction

To evaluate the likelihood of internal erosion to initiate, geometric and hydraulic criteria are known. Empirically generated geometric criteria, like filter rules for contact erosion, are often based on particle size distribution. Analytical approaches to internal erosion or suffusion compare the grain size of the particles subject to be displaced with the width of the pores to be passed. Even though movement of particles into a coarse filter, from an unfiltered exit or within the soil matrix is geometrically feasible, the hydraulic load on the particles has to exceed their drag force to initiate erosion or suffusion. This is the basis of hydraulic criteria. The hydraulic load on the particles is often described by the hydraulic gradient, averaging the force acting on the soil matrix along the flow path. Some empirical criteria use the mean gradient over the water retaining structure, while criteria focusing on point gradients (local gradient at the point where erosion might initiate) seem to be more precise. An even better description of the forces acting on single particles on a macro scale and taking the diversity of permeability into account can be obtained by the Darcian flow velocity as a volumetric current per unit of area. In fact, the pore velocity is the most descriptive parameter, characterizing the hydraulic load on a micro scale. The drag forces of the particles mainly result from their self weight and their interaction with other particles. This can be friction for coarse particles, adhesion for particles smaller than 0.2 mm and cohesion for soils with a fraction of fines ($d < 0.075$ mm) lets say larger than 15 %.

The fact that the critical ratio of filter and base particle size, e.g. defined by D_{15}/d_{85} (D_{15} : filter, d_{85} : base) in modern filter design criteria (Sherard & Dunnigan 1989) as well as in the no erosion boundary of Foster & Fell (2001), becomes larger with increasing percentage of fines shows that even geometric criteria take the growth of the drag forces into account to some extent, as cohesion increases the inter particle forces (**Figure 1**). After the ratio of filter and base particle size exceeds the critical geometric limit, the hydraulic load on the particles has to be taken into account. Nevertheless, geometric stability can be regained after some or even

excessive erosion has taken place and the interface between base and filter is clogged again as described by the empirical ‘some erosion’ and ‘excessive erosion’ boundaries given by Foster & Fell (2001). The fact that the excessive erosion boundary does not differ a lot from the no erosion boundary for soil with a very high percentage of fines (group 1) but allows for a difference in particle size between base and filter about two to three times larger for cohesionless base material (group 3) once more shows some relation to other than purely geometric influence. However, beyond the excessive erosion boundary the filter has to be classified as too coarse and erosion may initiate, if a critical hydraulic load on the particles is exceeded. As shown, there are three configurations that can be distinguished where either geometric, hydraulic or both influences dominate the process (**Figure 2**).

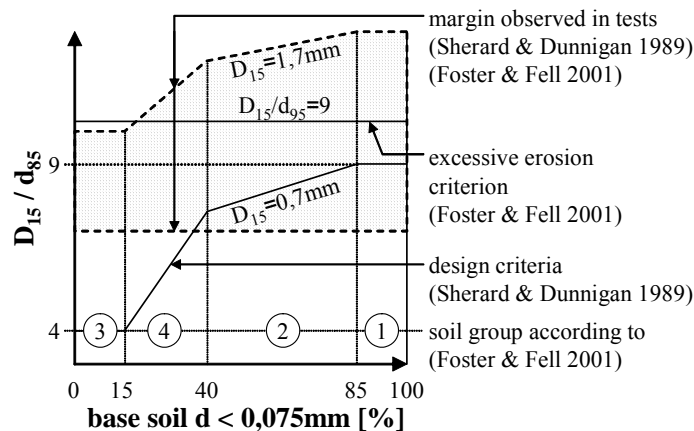


Figure 1: Critical filters and filter design criteria

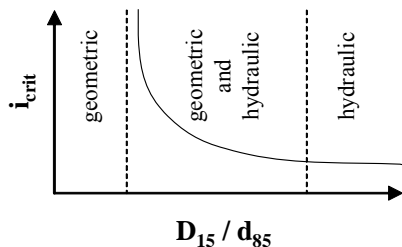


Figure 2: Interaction of geometric and hydraulic influence

Generally, the flow to an unfiltered exit and the flow within a matrix of particles as it is the case with contact erosion or with suffusion have to be distinguished. In the second case the matrix of the coarse particles has an impact on the transport process to some extent, either to partially hinder the particle transport by influencing the particles drag force or by limiting the flow and, thus, the hydraulic load. Considering the flow to an unfiltered exit the inclination of the plane surface and the angle of the flow lines against this surface have to be regarded.

Looking at the soil on a macro scale as a uniform homogeneous porous medium, hydraulic gradients causing zero stress condition known as heave or blow out can be derived. It is known that internal erosion and suffusion may initiate at gradients lower than this. This can be explained by assessing the process on a micro scale where the hydraulic load on single particles in cross flow exceeds their drag force.

2 Hydraulic Criteria for Erosion and Suffusion

2.1 Backward Erosion at an Unfiltered Exit

To assess the likelihood of internal erosion to initiate at an unfiltered exit of seepage, hydraulic criteria are the only option unless the problem is solved by putting a drainage filter on top. In cohesionless soil heave occurs when seepage pore pressure is such that the effective stress becomes zero. Likewise, the hydraulic fracture in cohesive soil is related to the effective stress. The critical gradient becomes

$$i_{\text{crit}} = \frac{(1-n) \cdot (\gamma_s - \gamma_w)}{\gamma_w} , \quad (1)$$

γ_w being the specific weight of the water and $(\gamma_s - \gamma_w)$ that one of soil under uplift. For a porosity $0.25 \leq n \leq 0.48$ and a specific weight of the particles γ_s of 26 kN/m^3 the critical gradient i_{crit} ranges between $0.83 \leq i_{\text{crit}} \leq 1.2$.

Hydraulic criteria for backward erosion are strongly interlinked with the process of piping, which is only one step beyond initiation. Hydraulic criteria for backward erosion and piping empirically derived from the experience of a large number of dams and weirs built on alluvial foundation are known from Bligh (1912), Lane (1935) and Chugaev (1962) as presented in Table 1. For cases without subsoil sealing elements the average critical hydraulic gradients after Bligh (1910) seem to contain an different factor of safety than those after Lane (1935) that only account for one third of the horizontal flow path ($L = L_{\text{vert}} + L_{\text{hor}} / 3$). Considering the range for critical gradients according to Chugaev (1962) it must be said that only the lower limit is reliable, because the upper limit contains 1.3 as a “future factor”, taking expected future gain of insight into account. Furthermore, 8 of the 162 evaluated structures collapsed due to piping, 5 of which had gradients smaller than the criterion. Thus, for an adequate estimation based on this criterion a reduction of the critical gradient is proposed in Table 1.

Table 1: Critical average gradients to initiate backward erosion and form a pipe

soil	gravel	coarse sand	med. sand	fine sand
i_{crit} Chugaev ¹	0.25	0.25	0.15	0.12
i_{crit} Chugaev reduced ²	0.25	0.25	0.11	0.10
i_{crit} after Bligh ³	0.11	0.083		0.067
i_{crit} after Lane ⁴	0.095	0.067	0.056	0.048
i_{crit} after Müller-Kirchenbauer ⁵ :				
lower limit		0.12	0.08	0.06
upper limit		0.17	0.10	0.08
i_{crit} after Weijers & Sellmeijer ⁶ :				
$C_u = d_{60} / d_{10} = 1.5$	0.28	0.18	0.16	0.09
$C_u = 3$	0.34	0.28	0.24	0.14

¹ Chugaev (1962) after Davidenkoff (1970) without „future coefficient 1.3“

² Chugaev (1962) including failed examples

³ medium sand and gravel corresponding to tables after Bligh (1910) in Mallet et al. (1951)

⁴ no vertical flow path and L/3 for horizontal flow path after Lane (1935) in Mallet et al. (1951)

⁵ for layered alluvium after Saucke (2006)

⁶ after Weijers & Sellmeijer (1993) with D: thickness of aquifer 10 m; L: length of flow path; D/L = 0.1; n = 0.39; gravel and coarse sand out of the area of validity; d₇₀: gravel 4 mm; coarse sand 1 mm; medium sand 0.6 mm; fine sand 0.1 mm

The criterion after Weijers & Sellmeijer (1993) allows for calculating a critical average hydraulic gradient taking soil parameters as well as the geometry of the aquifer into account. Similar to the other criteria listed in Table 1, which show comparable results even though Weijers & Sellmeijer (1993) limit the validity of their criterion to fine and medium sands, this gradient refers to complete piping from downstream to upstream. Müller-Kirchenbauer et al. (1993) and Schmertmann (2000) point out the possibly negative impact of a layered foundation.

After Schmertmann (2000) the critical gradient for backward erosion in cohesionless soil is influenced by the coefficient of uniformity $C_u = d_{60}/d_{10}$. Uniform cohesionless soils of small particle size like fine to medium sands are especially susceptible to backward erosion. From flume tests Schmertmann (2000) derives critical point gradients which have to be exceeded continuously to initiate backward erosion and form a complete pipe from downstream to upstream. Correction factors are given that allow for transferring the test results to practical cases. Weijers & Sellmeijer (1993) discovered in their flume tests that backward erosion may initiate at 40 % of the gradients needed for complete piping. Recapitulating these two findings critical gradients for the initiation of backward erosion could be derived as shown in figure 3.

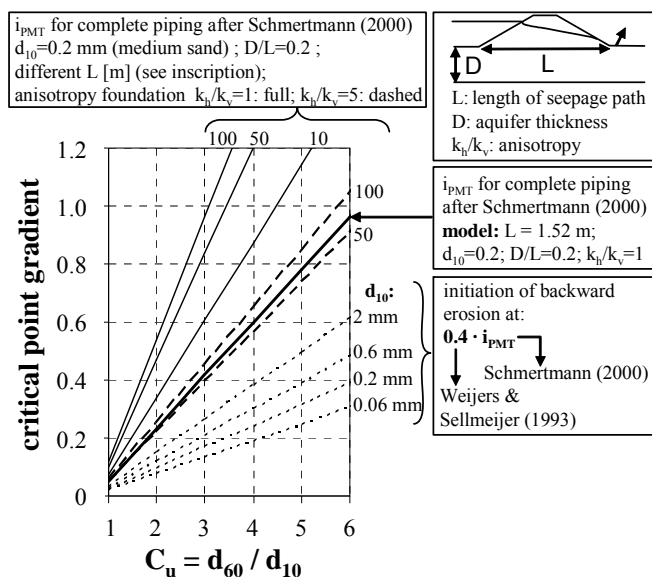


Figure 3: Critical point gradients to initiate backward erosion and form a pipe

Looking at backward erosion from an unfiltered exit at the downstream slope of a dam the geostatic local stability of the upper most layer with additional hydraulic load must be considered. Thus, for cohesionless fill without a vegetation layer on top the critical angle of the slope can be calculated as 1:4.5 to 1:3 from the friction angles 25° (sand) to 35° (gravel). Considering the flow lines parallel to the surface at the highest exit point of seepage and horizontal at the downstream toe after Davidenkoff (1964) the portion of the hydraulic gradient vertical to the sloped surface range from 0.05 to 0.11 referring to the cases described above. Comparing these gradients with those listed in Table 1 and figure 2, the initiation of backward erosion on the downstream shoulder seems to be unlikely in cohesionless soils, if geostatic local stability is given and no less permeable vegetation layer is existent. Collapse rather arises from slope instability or unravelling of the shoulder at extensive leakage. Only if a vegetation layer less permeable than the fill of the dam lies on the downstream shoulder, local gradients in voids of the vegetation layer might be high enough to initiate backward erosion.

2.2 Contact Erosion

For designing a filter for any kind of soil, which has to be protected from erosion, geometric criteria should be used as they are by far more reliable than hydraulic criteria. To assess filters that do not satisfy modern design criteria or soil interfaces in the foundation that have to be managed as they are, hydraulic criteria can be very helpful. In a sense, assessing the rate of erosion from a cracked clay core in cases where the filter is too coarse falls into the field of hydraulic criteria as well, however, this is not discussed here.

The critical gradient due to the zero stress condition can be lower than (1), if the porosity of the base is larger than that of the filter and flow concentrates at the interface. Local heave on the interface can occur from the base material into a pore of the filter at

$$i_{crit} = \{0.7 \text{ to } 0.8\} \cdot \frac{(1-n) \cdot (\gamma_s - \gamma_w)}{\gamma_w} \quad (2)$$

For the porosity $0.25 \leq n \leq 0.48$ and a specific weight of the particles of 26 kN/m^3 the critical gradient ranges between $0.58 \leq i_{crit} \leq 0.96$.

Some hydraulic criteria for contact erosion in cohesionless soil that have been derived from experimental data take both, the hydraulic load and the geometry of the filter into account. Ziems (1969) based his hydraulic criteria for a horizontal interface between a base soil ($C_u < 5$) and a filter lying on top with vertical upward flow on a filter base particle size ratio $A_{50} = D_{50}/d_{50}$. The critical gradient in the base soil decreases with increasing A_{50} . Compared to (2) the minimum critical gradients according to (3) seem to be too high for very coarse filters.

$$i_{crit} = 0.66 + \frac{6}{d_{10}^2 \cdot A_{50}^2} \quad (3)$$

Brauns (1985) developed a criterion for contact erosion on a horizontal interface between a base soil and a filter on top at parallel (horizontal) flow. He found out that for $\kappa = n_F \cdot D_{15}/d_{85}$ smaller than 3 geometrical stability is given, for κ between 3 and 10 geometric and hydraulic effects interact and for κ larger than 10 hydraulic effects dominate in such a way that the factor

between pressure and gravity forces reaches a constant value for critical flow velocities to move base soil particles.

$$v_{f,crit} = \{0.65 \text{ to } 0.7\} \cdot n_F \cdot \sqrt{(\gamma_s - \gamma_w) \cdot d_{50}/\rho_w} \quad (4)$$

The critical hydraulic gradients (between 0 and 0.6) derived from (4) take the nonlinearity of the flow through porous media after Forchheimer (1901) into account, considering d_w to be the characteristic particle diameter of the filter given as

$$d_w = \left(\sum_{i=1}^m \frac{F_i}{d_i} \right)^{-1} \quad (5)$$

d_i being the particle size of the fraction i and F_i the percentage by mass of the fraction i .

The hydraulic criterion after Bezuijen et al. (1987) for contact erosion on inclined surfaces under variably inclined flow conditions is derived from test results. The particle transport is assessed by the critical shear stress after Shields (1930). The influence of the inclined interface as well as the upward flow components are derived from equilibrium of forces. The resulting chart allows to estimate critical hydraulic gradients (between 0.05 and 0.8) depending on the soil parameters of base (d_{50}) and filter (D_{15} , n_F) as well as the inclination of the interface and the gradient vertical to the interface.

2.3 Suffusion

From Istomina (1957, in Busch et al. 1993) a hydraulic criterion for suffusion is known which gives acceptable gradients i_{zul} as a function of the coefficient of uniformity C_u , including a factor of safety of about two compared to underlying test results.

$$i_{zul} = \begin{cases} 0.3 \text{ to } 0.4 & \text{for } C_u < 10 \\ 0.2 & \text{for } 10 \leq C_u \leq 20 \\ 0.1 & \text{for } C_u > 20 \end{cases} \quad (6)$$

The critical hydraulic gradients to initiate suffusion in not gap graded soils after Busch et al. (1993) take into account the coefficient of uniformity C_u , the porosity n , the dry density ρ_d , the Darcian coefficient of permeability k_D , the dynamic viscosity of the fluid ν and the inclination of the flow against vertical downward α .

$$i_{crit} = 0.6 \cdot \left(\frac{\rho_d}{\rho_w} - 1 \right) \cdot (0.82 - 1.8 \cdot n + 0.0062 \cdot (U - 5)) \cdot \sin\left(30^\circ - \frac{\alpha}{8}\right) \cdot \sqrt{\frac{n \cdot g \cdot d_s^2}{\nu \cdot k_D}} \quad (7)$$

The largest particle subject to suffusion d_s is about 0.6 times the mean pore diameter after Pavicic in Wittmann (1980)

$$d_s = 0.27 \cdot \sqrt[6]{U} \cdot \frac{n}{1-n} \cdot d_{17} \quad (8)$$

where d_{17} is the particle diameter larger than 17 % by mass of the soil. Other hydraulic criteria for suffusion are known from Wittmann (1980) and Muckenthaler (1989) which are partly based on the theory described below.

However, due to the fact that dispersion of the underlying test results in general is very large, geometric criteria for suffusion are still rare unless they are very conservative. Accordingly, hydraulic criteria for suffusion still lack of preciseness even more.

2.4 General Appraisement

Many hydraulic criteria are based on tests with consistent soil samples or on analytical descriptions of the particle and pore geometry derived from characteristic parameters. Therefore, an intact and homogeneous soil texture has to be assumed for their validity. By contrast, most soil materials contain a certain variability of their characteristic parameters. Especially permeability, the parameter relevant to the transport of single particles transforming hydraulic gradients to local flow velocities, is known to have a large variability. Consequently, in modern filter design geometric stability is generally aimed at and safety factors for hydraulic design criteria in places are larger than for geometric design criteria (DWA in prep.). Schuler (1997) for instance suggests limiting the application of hydraulic filter design criteria to cohesive base material or to filters only affected temporarily or uncritical stability wise. However, some cases like backward erosion from an unfiltered exit can only be assessed using hydraulic criteria. In the scope of the framework for internal erosion where focus is rather on the probability of failure than on reaching adequate factors of safety strived for in design criteria, hydraulic criteria can be extremely helpful.

3 Further Remarks on Hydraulic Criteria

3.1 General

Some of the criteria described above are based on sediment transport theory, as the criteria from Brauns (1985) and Bezuijen et al. (1987). Hydraulic criteria aiming to physically describe the transport phenomena rather than to empirically evaluate test results in a limited area of validity should compare the hydraulic load on the particle with its drag force. Consequently, the effective flow velocity and the type of flow (Darcy, Forchheimer or turbulent) in the pores have to be compared with critical flow velocities for particle transport. Concerning the drag force free movement of the particles is assumed as the limit for any geometrical filter impact is exceeded.

From sediment transport it is known that very fine particles are affected by adhesion, which might influence particle transport in the scope of internal erosion as well. After Zanke (1982) adhesion can be incorporated by an apparent increase of the density $\rho_{s,A}$ of the fine particles.

$$\rho_{s,A} = \rho_s + \frac{9 \cdot 10^{-6}}{d^2} \text{ [kg/m}^3\text{]} \text{ with } d \text{ in [m]} \quad (9)$$

3.2 Non linearity of Flow through Porous Media

H. Darcy's experimental investigation of the flow through sand filled tubes in the year 1856 led to the well known linear correlation between Darcian velocity v_f and the hydraulic gradient i valid for one dimensional laminar flow.

$$v_f = i \cdot k_D \quad (10)$$

The Darcian coefficient of permeability k_D in [m/s] can be estimated from particle size distribution e.g. after Beyer (1964) for sand with $C_u < 20$

$$k_D = \left(\frac{268}{C_u + 3.4} + 55 \right) \cdot d_{10}^2 \cdot 100 \quad \left[\frac{\text{m}}{\text{s}} \right] \quad (11)$$

with d_{10} in [m] for $0.06 \text{ mm} < d_{10} < 0.6 \text{ mm}$. A universal formulation of (10) contains the intrinsic permeability K in [m^2], the vector of the pressure gradient $\text{grad } p$ and the kinematic viscosity η

$$-\text{grad } p = \frac{\eta}{K} \cdot v_f \quad (12)$$

The intrinsic permeability can be expressed as a function of the specific surface O_s of the porous media and its porosity

$$K = \frac{n^3}{O_s^2 \cdot (1-n)^2 \cdot \kappa'} \quad \text{with } O_s = \frac{A}{V} = \frac{\pi \cdot d_w^2}{\frac{1}{6} \cdot \pi \cdot d_w^3} = \frac{6}{d_w} \quad (13)$$

where A is the surface area of all particles in a volume V of the porous media. The value of the Kozeny-Karman constant $\kappa' = 5.34$ proposed by Fand (1987) results in an intrinsic permeability of

$$K = \frac{d_w^2 \cdot n^3}{192.24 \cdot (1-n)^2} \approx \frac{k_D \cdot \eta}{\gamma_w} \quad (14)$$

Since the dominance of viscosity is superposed by inertia effects with increasing flow velocity the linear correlation for the laminar flow regime is no more valid. Forchheimer (1901) postulated the following extension of (12) to account for the non linearity

$$-\text{grad } p = a' \cdot v_f + b' \cdot v_f^2 \quad (15)$$

where a' and b' are empirical constants to be determined for any combination of fluid and porous media. After Ergun (1952) the Forchheimer flow can be described using the particle Reynolds number

$$Re_d = \frac{v_f \cdot d_w}{v} \quad (16)$$

A clear description of Darcian, Forchheimer and turbulent flow can be achieved with the Ergun-constants A , B and A' , B' empirically determined by Fand (1987) according to the following expressions:

$$f' = \frac{-\text{grad } p \cdot d_w \cdot n^3}{\rho_f \cdot v_f^2 \cdot (1-n)} \quad \text{with } Re'_d = \frac{Re_d}{(1-n)} \quad (17)$$

Darcian flow ($10^{-5} < \text{Re}_d < 2.3$): $f' = \frac{36 \cdot \kappa'}{\text{Re}'_d}$

Forchheimer flow ($5 < \text{Re}_d < 80$): $f' = \frac{A}{\text{Re}'_d} + B$ with $A = 182$ and $B = 1.92$

Turbulent flow ($\text{Re}_d > 120$): $f' = \frac{A'}{\text{Re}'_d} + B'$ with $A' = 225$ and $B' = 1.61$

For a hydraulic gradient of 1 and a Darcian permeability estimated after (14) the Darcian law is valid for effective particle diameters after (5) smaller than 1.5 mm and turbulent flow starts at effective particle diameters larger than 20 mm.

3.3 Critical Flow Velocity derived from Particle Sink Velocity

The hydraulic load on a single particle of diameter d in cross flow of a velocity relative to the particle v_r can be expressed by the force F

$$F = c_D \cdot d^2 \cdot \pi \cdot \frac{\rho_w \cdot v_r^2}{8} \quad (18)$$

Muckenthaler (1989) proposes to use a drag force coefficient c_D valid for natural sediments after Kanzanskij (1981)

$$c_D = \frac{24}{\text{Re}_d} + \frac{5.6}{\text{Re}_d^{0.5}} + 0.25 \quad (19)$$

$$\text{for } \text{Re}_d = \frac{v_r \cdot d}{v} < 4300$$

If the force F forms equilibrium with the particle's weight and uplift, v_r is equal to the particle sink velocity v_s . Assessing the transport phenomena by setting the particle sink velocity v_s equal to the critical flow velocity in the pores $v_{p,crit}$ to start particle transport leads to (20). The particles are already loose and transported by an upward flow. Consequently, adhesion does not influence the drag force.

$$\left[\frac{24 \cdot v}{v_{p,crit} \cdot d} + \frac{5.6}{\sqrt{v_{p,crit} \cdot d/v}} + 0.25 \right] \cdot \frac{3}{4} \cdot \rho_w \cdot v_{p,crit}^2 - d \cdot g \cdot (\rho_s - \rho_w) = 0 \quad (20)$$

The actual mean pore velocity $v_{p,av}$ can be derived from the Darcian flow velocity v_f , the porosity n and the tortuosity T , which describes the ratio between the shortest distance of two points in flow direction and the effective length of the flow path following the winding pore channels quoted by Wittmann (1980) with $2/\pi = 0.6366$.

$$v_{p,av} = \frac{v_f}{n \cdot T} \quad (21)$$

This approach of the erosion process for instance can describe the effect of boiling at an unfiltered exit of seepage. A particle which partially blocks a pore of the soil at the surface is

lifted by the pore velocity. Once the particle is transported away from the surface, velocity reduces as porosity approaches 1 and the particle sinks back to the surface.

3.4 Critical Flow Velocity derived from Drag Force of Resting Particles

Assessing the transport phenomena by setting the hydraulic load F on a single particle after (18) equal to the friction force R (static friction) after Kezdi (1976) defined by the friction angle Φ

$$R = \frac{\pi \cdot d^3}{6} \cdot g \cdot (\rho_s - \rho_w) \cdot \tan\Phi \quad (22)$$

leads to a critical pore velocity $v_{p,crit}$ valid for horizontal transport of particles over a surface similar to the one for vertical upward flow in (20). With the Reynolds number according to (19) and adhesion forces as given in (9) the critical pore velocity $v_{p,crit}$ can be derived from (23).

$$\left[\frac{24 \cdot v}{v_{p,crit} \cdot d} + \frac{5.6}{\sqrt{v_{p,crit} \cdot d/v}} + 0.25 \right] \cdot \frac{3}{4} \cdot \rho_w \cdot v_{p,crit}^2 - d \cdot g \cdot \left(\rho_s + \frac{9 \cdot 10^{-6}}{d^2} - \rho_w \right) \tan\Phi = 0 \quad (23)$$

For a friction angle of 45° (23) is equal to (20) despite the influence of adhesion. A more realistic friction angle would be 30° . The influence of adhesion starts with d smaller than 0.2 mm and leads to almost constant critical pore velocities $v_{p,crit}$ for particles smaller than 0.02 mm.

3.5 Critical Flow Velocity derived from Sediment Transport

From the correlation between shear stress coefficient and Reynolds number Re^* based on the shear velocity v^* given in the Shields-diagram, Muckenthaler (1989) derived a critical flow velocity for sediment transport in which adhesion can be considered after (9). Furthermore, he transferred the findings of Bonnefille (1963), who plotted the correlation between a dimensionless sediment diameter D^* and the Reynolds number Re^* to a critical pore velocity for particle transport. He completed this approach considering the findings of Vollmers & Pernecker (1967) for very fine sediments leading to similar influence of adhesion as with the sediment transport after Shields (1930) and (9). The critical flow velocity remains almost constant for $d < 0.1$ mm due to adhesion and for larger particles increases with growing particle diameter. The crucial point of this derivation is probably the assumptions needed to quantify the ratio between the mean pore velocity and the shear velocity at the flow boundary layer around the particles.

3.6 Comparison

The critical velocities derived from the different approaches comparing the drag force of the particles and the hydraulic load deliver similar results as can be seen in figure 4. Taking adhesion into account, the critical flow velocities remain almost constant for particle diameters smaller than 0.1 mm and particle transport does not appear to be likely for flow velocities less than 10^{-3} m/s. Assuming that the critical flow velocity refers to a velocity in the pores, the resulting mean critical Darcian velocities should be 4 to 8 times smaller according to (21). In regards of the fact that the permeability due to the variability of the soil is not uniform, another factor of maybe 10 to 100 should be considered. Applying Muckenthaler's findings to practical cases still leaves the question which particle size to look at.

The critical flow velocities derived from the critical hydraulic point gradients for backward erosion and piping in uniform fine to medium sands after Schmertmann (2000) presented in figure 2 show good correlation with the criteria presented above, assuming the permeability at the wall (roof) of the flume test stand being 10 to 100 times larger than the average soil permeability e.g. after Beyer (1964) in (11) and considering d_{60} to be the relevant particle size representing these uniform sands (**Figure 5**). Furthermore, adhesion doesn't seem to limit critical flow velocity in the case of erosion initiating in a joint, as already proposed by Muckenthaler (1989).

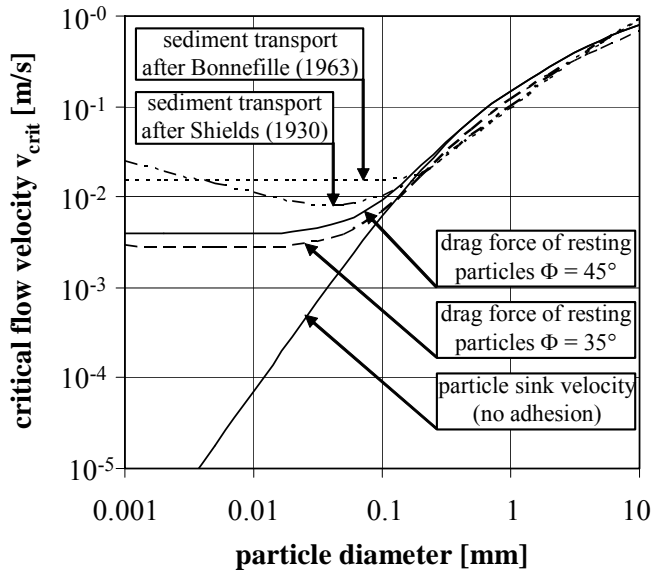


Figure 4: Critical flow velocity v_{crit} versus particle diameter according to different theories after Muckenthaler (1989)

The critical average flow velocities for contact erosion on a horizontal interface of a base soil with a filter lying on top at flow parallel to the interface after Brauns (1985) given in (4) show good correlation with the critical flow velocities derived in chapter 3. Brauns (1985) proposed d_{50} of the base to be the relevant particle size for the transport process and adhesion seems to have an influence (**Figure 5**).

The empirical criterion for contact erosion after Ziems (1969) given in (3) seems to take adhesion into account to some extent for small A_{50} . As long as the ratio between local permeability k_D and average permeability $k_{D,\text{av}}$ does not become too high the criterion appears comparable (**Figure 5**).

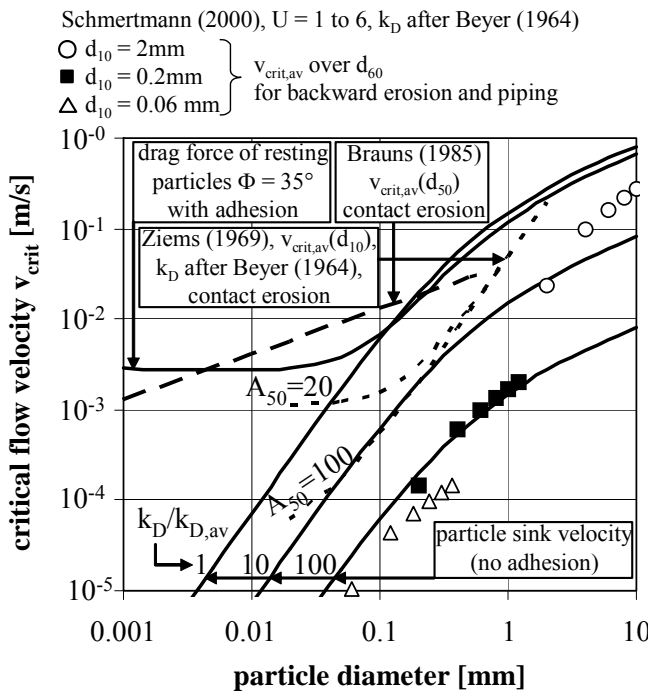


Figure 5: Mean pore velocity $v_{\text{crit,av}}$ after Schmertmann (2000), Brauns (1985) and Ziems (1969) for $n_F = 0.25$ and $T = 2/\pi$ compared to Muckenthaler (1989)

In the scope of their tests on the internal stability of silt sand gravel mixes Wan & Fell (2004) measured the hydraulic gradient and permeability at which loss of fines, extreme cloudiness and boiling started due to upward flow from a horizontal unfiltered exit. Unfortunately, the size of particles moved at different stages was not observed. Figure 6 shows the critical flow velocities calculated from the porosity, the tortuosity estimated by $2/\pi$, the gradient at which the first loss of fines and the permeability at which the first cloudiness was observed. It is assumed that the particles moved in this first phase somehow belong to the very fine fraction of the soil sample and, thus, d_5 is thought to be the critical particle size. The criteria after Muckenthaler (1989) not taking adhesion into account seem to form a lower boundary for the test results. The critical flow velocities for which extreme cloudiness was observed are higher and correlated with d_{10} seem to be influenced by adhesion. Furthermore, the critical flow velocities calculated from the gradient and the permeability where boiling was first observed are shown over the particle size d_{30} . As the tested soils are fairly uniform and some of them gap graded, d_{30} is meant to belong to the finer fractions of the coarse soil matrix, which has to be eroded to start boiling. The observed critical velocities for boiling are all in the order of 10^{-2} m/s. Correlated with d_{30} the critical flow velocities tend to be underestimated for larger particle diameters by the criteria presented. An explanation could be that the ratio between local permeability k_D and average permeability $k_{D,av}$ seems to increase once the zero stress condition is reached and preferential seepage paths are likely to be created.

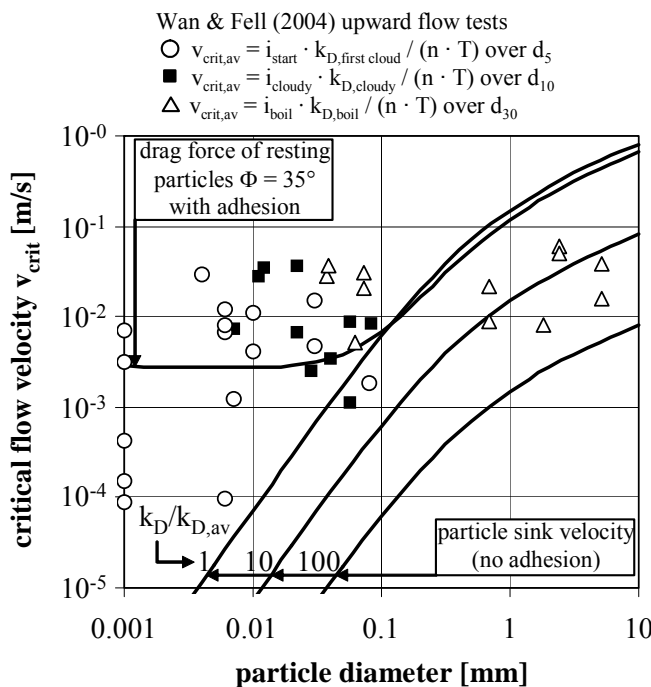


Figure 6: Mean pore velocity $v_{crit,av}$ in upward flow tests with unfiltered exit after Wan & Fell (2004) with $T = 2/\pi$ compared to Muckenthaler (1989)

Literature

- Beyer, W. 1964: Zur Bestimmung der Wasserdurchlässigkeit von Kiesen und Sanden aus der Kornverteilung. *WWT*, 14. Jahrgang, Heft 6.
- Bezuijen, A.; Klein-Breteler, M.; Bakker, K.J. 1987: Design criteria for placed block revetments and granular filters. *proceedings of the 2nd international conference on coastal & port engineering in developing countries*, Beijing.
- Bligh, W.G. 1910: The practical design of irrigation works. 2 ed. London.
- Bonnefille, R. 1963: Essais des synthèse des lois de début d'entrainement des sédiments sous l'action d'un courant en régime continu. *Bulletin du CREC* Nr. 5, p. 67-72.
- Brauns, J. 1985: Erosionsverhalten geschichteten Bodens bei horizontaler Durchströmung. *Wasserwirtschaft* 75, Nr. 9. 377-383.
- Busch K.-F.; Luckner, L.; Tiemer, K. 1993: *Geohydraulik, Lehrbuch der Hydrogeologie*. 3. neubearbeitete Auflage, Berlin; Gebrüder Bornträger.
- Chugaev, R. R. 1962: *Gründungsumriss von Wasserbauwerken* (in Russian). Moskau – Leningrad.
- Davidenkoff, R. 1964: *Deiche und Erddämme*. Werner-Verlag, Düsseldorf.
- Davidenkoff, R. 1970: *Unterläufigkeit von Staubaufwerken*. Werner-Verlag, Düsseldorf.
- DWA in prep.: *Merkblatt Deiche an Fließgewässern*. Deutsche Vereinigung f. Wasserwirtschaft, Abwasser u. Abfall e.V.
- Ergun, S. 1952: Fluid flow through packed columns. *Chem. Eng. Prog.* 48 1952, p. 89-94.

- Fand, R. M.; Kim, B. Y. K.; Lam, A. C. C.; Phan, R.T. 1987: Resistance to the flow of fluids through simple and complex porous media whose matrices are composed of randomly packed spheres. *Trans. ASME, J. Heat Transfer*, 109, S. 268 – 274, 1987.
- Fand, R. M.; Varahasamy, M.; Greer, L. S. 1993: Empirical correlation equation for heat transfer by forced convection from cylinders embedded in porous media that accounts for wall effects and dispersion. *Int. J. Heat and Mass Transfer* Vol. 36, No. 18, p. 4407 – 4418.
- Fell, R.; Foster, M.; Wan, C.-F. 2005: *A framework for assessing the likelihood of internal erosion and piping of embankment dams and their foundations*. Contribution to the Workshop of internal erosion and piping of dams and their foundations. Aussoise, France, April 2005.
- Forchheimer, Ph. 1901: Wasserbewegung durch Boden. *Zeitschrift Verband deutscher Ingenieure* 45 (1901), p. 1736-1741, 1781-1788.
- Foster, M.; Fell, R. 2001: Assessing embankment dam filters that do not satisfy design criteria. *J. Geotechnical and Geoenvironmental Eng.* ASCE, Vol. 127, No. 4, 398-402.
- Kanzanskij, J 1981: *Über theoretische und praxisbezogene Aspekte des hydraulischen Feststofftransports*. Mitteilungen des Franzius – Instituts für Wasserbau und Küstingenieurwesen der Universität Hannover, H. 52.
- Kezdi, A. 1976: *Fragen der Bodenphysik*. Verlag der Ungarischen Akademie der Wissenschaft, Budapest.
- Lane, E.W. 1935: *Security from under-seepage masonry dams on earth foundations*. Transaction American Soc. of Civ. Eng., Vol 100, 1233-1351.
- Mallet, C.; Pacquant, J. 1951: *Erdstaudämme*. Orig. Titel: *Les Barrages en Terre*. Übersetzt aus dem Franz.: H. Ferchland. VEB Verlag Technik, Berlin, DDR.
- Muckenthaler, P. 1989: *Hydraulische Sicherheit von Staudämmen*. Lehrstuhl und der Versuchsanstalt für Wasserbau und Wassermengenwirtschaft, TU München, Bericht Nr 61.
- Müller-Kirchenbauer, H.; Rankl, M.; Schlötzer, C. 1993: Mechanism for regressive erosion beneath dams and barrages. In: Brauns, Heibaum & Schuler (edt.): *Filters in Geotechnical and Hydraulic Engineering*, Balkema, 369–376.
- Sauke, U. 2006: Nachweis der Sicherheit gegen innere Erosion für körnige Erdstoffe. *geotechnik* 29, 2006 Nr. 1.
- Schmertmann, J.H. 2000: The non-filter factor of safety against piping through sands. *ASCE Geotechnical Special Publication No. 111, Judgement and innovation*. Edited by F. Silva and E. Kavazanjian, ASCE, Reston.
- Schuler, U. 1997: *Bemessung von Erdstoff-Filtern unter besonderer Berücksichtigung der Parameterstreuung*. Veröffentlichungen des Instituts für Bodenmechanik und Felsmechanik der Universität Fridericiana in Karlsruhe, Heft 143.
- Sherard, J.L.; Dunnigan, L.P. 1989: Critical Filters for impervious soils. *J. Geotech. Eng.* ASCE, Vol. 115, No. 7, 927-946.

- Shields, A. 1930: *Anwendung der Ähnlichkeitsmechanik und Turbulenzforschung auf die Geschiebebewegung*. Mitteilungen der Preußischen Versuchsanstalt für Wasserbau und Schiffbau, Berlin, H. 26.
- Vollmers, H.; Pernecker, L. 1967: Beginn des Feststofftransports für feinkörnige Materialien in einer richtungskonstanten Strömung. *Wasserwirtschaft* 6, p. 236-241.
- Wan, C.-F.; Fell, R. 2004: *Experimental investigation of internal instability of soils in embankment dams and their foundations*. UNICIV Report No. R-429. School of Civil and Environmental Engineering, The University of New South Wales. ISBN: 85841 396 5.
- Weijers, J.B.A.; Sellmeijer, J.B. 1993: A new model to deal with the piping mechanism. In: Brauns, Heibaum & Schuler (edt.): *Filters in Geotechnical and Hydraulic Engineering*, Rotterdam, Balkema, 345 – 355.
- Wittmann, L. 1980: *Filtrations- und Transportphänomene in porösen Medien*. Veröffentlichungen des Instituts für Bodenmechanik und Felsmechanik der Universität Fridericiana in Karlsruhe, Heft 86.
- Zanke, U 1982: *Grundlagen der Sedimentbewegung*. Springer – Verlag; Düsseldorf.
- Ziems, J. 1969: *Beitrag zur Kontakterosion nichtbindiger Erdstoffe*. Dissertation, Technische Universität Dresden.

Authors Name and Affiliation

S. Perzlmaier
 TIWAG – Tiroler Wasserkraft AG, Austria
 sebastian.perzlmaier@tiwag.at

P. Muckenthaler
 Ingenierbüro Dr. Muckenthaler, Germany
 ibmuck@t-online.de

A.R. Koelewijn
 GeoDelft / Deltares, Netherlands
 a.r.koelewijn@geodelft.nl

Criteria of Erosion for Cohesive Soils

S. Bonelli, D. Marot, F. Ternat, N. Benahmed

Abstract

This paper focus on three types of erosion: the suffusion, the backward erosion, and the piping erosion processes. A new triaxial device to quantifying suffusion and backward erosion, and a new model for interpreting the Hole Erosion Test, are presented. It is recommended to use these erosion tests in order to evaluate the erosion parameters on any sample of cohesive soil from a site.

1 Introduction

Erosion can only develop if two vital conditions are met: particles must be torn off and must be transported. Four types of erosion process, internal to the work, have been identified [Fell and Fry, 2007]: 1) suffusion, which affects the soil structure, 2) evolution of defects in the soil matrix (holes, cracks), 3) backward erosion, 4) contact erosion between two soils.

After exposing a new approach concerning the critical erosion shear stress for cohesive soil, the present paper presents some recent results concerning types 1), 2) and 3): the suffusion and backward erosion processes, internal to the soil, and the piping erosion process, external to the soil and internal to the work.

2 Critical Erosion Shear Stress for Cohesive Particles

Basically, the critical erosion shear stress of cohesive sediments depends on the granulometry (i.e. particle size and shape) and cohesive particle content whose diameter is finer than $2\mu\text{m}$ [Graf, 1984]. A strong dependence on the consolidation degree of the water/sediment mixture has also been highlighted [Mitchener, 1996]. This consolidation degree can be related to various experimental measurements such as porosity or water content measurements [Sunborg, 1956; Migniot, 1968]. The Atterberg limits are also useful, as featured on Table.1, but specific interpretation of this parameter is required to relate it to mechanical properties of the sediment. Particle whose diameter is smaller than $2\mu\text{m}$ are suggested to interact by the mean of the Van der Waals force. Its expression between two spherical particles of diameters d_1 and d_2 , separated with the distance d_i , [Israelachvili, 1985] can be written in the following way:

$$F_H = A_H / 12 * d_1 * d_2 / (d_1 + d_2) / d_i^2 \quad (1)$$

Recent work has tried to evaluate this particular cohesion force [Ternat, 2007]. The main difficulty remains in the determination of the interparticle distance d_i , which has been linked to the porosity n , considering a crystalline modelling of the particle network. This modelling provides, on the one hand, the expected link between interparticle distance and the porosity, but on the other hand, it also provides a multiplicative factor C_i , called coordination, that is used to account for multiple interactions. For instance, here is the expression of the interparticle distance between two same size particles:

$$d_i = d \left([(n_{\max} - n_{\min}) / (n_{\max} - n)]^{1/3} - 1 \right) \quad (2)$$

where n_{\max} and n_{\min} are respectively the maximum and the minimum values of the porosity, corresponding respectively to the most compacted and the loosest states of the sediment, n is the local porosity. The coordination factor is considered to vary like the cube of the ratio between the two particle sizes:

$$C_l \sim (d_1/d_2)^3 \quad (3)$$

Finally, the resulting cohesion force becomes:

$$F_C = F_H * C_l \quad (4)$$

Once determined, the cohesion force is included into the usual force balance considered to assess the critical shear stress [Dade, 1992; Graf, 1984; Wiberg, 1987]. The erosion criterion is expressed in the following form:

$$F_D = \tan \tilde{\Phi} (F_W - F_L + F_C) \quad (5)$$

Where Φ is the internal angle, F_D is the drag force of the flow, F_L is the lift force of the flow, F_W the buoyant weight of the particle and F_C the cohesion force. The drag force must account for the granulometry of the eroded surface, which is achieved in the drag coefficient [Graf, 1984]. The lift force is also described and can be accurately determined [Yalin, 1977; Saffman, 1965]. Note that hydrodynamic forces are valid in the viscous domain ($Re^* < 1$), determining thus the validity domain of the present model. The granulometry of the eroded surface is accounted by means of the α coefficient, characterizing the relative position of the particle related to the sediment/water interface. There is little controversy concerning the buoyant weight of the particle, which can be obtained by the product of the particle volume with its specific weight. All these contributions are adjusted with shape factors, related to each force: k_D for the drag force, k_L for the lift force, k_W for the buoyant weight. Gathering all those information leads to an expression of the critical shear stress for the erosion of a spherical cohesive particle, in terms of dimensionless Shields parameter τ^* in function of the particle Reynolds number Re^* :

$$\tau^* = \frac{k_W \frac{\tan \Phi}{\alpha k_D}}{a + \frac{k_L}{k_D} \tan \Phi \cdot Re^* + \frac{3 \cdot a \cdot \alpha}{16} \cdot Re^{*2}} \left(1 + \frac{F_C}{F_W} \right) \quad (6)$$

where a is a constant of the drag coefficient. This expression features the rule of the cohesion function $(1 + F_C/F_W)$ that increases the value of the erosion threshold since F_C becomes comparable to F_W . Let's note that the determination of the erosion threshold does not present any difficulty to be solved when F_C is null, but a numerical resolution must be done when not.

To illustrate these approaches, here are examples of possible results. Firstly, it is interesting to have a look over the cohesion function that features a critical diameter smaller than a few microns, where cohesion between two particles becomes efficient (**Figure 1**). When multiple interactions are accounted for, cohesion affects all the particle range present in the granulometry, revealing a kind of cementation of coarse particles by fine ones (**Figure 2**).

It is then possible to obtain the critical erosion velocity u^* (m/s), defined by $\tau^* = \rho_w \cdot u^{*2}$ in function of the particle diameter d (**Figure 3**).

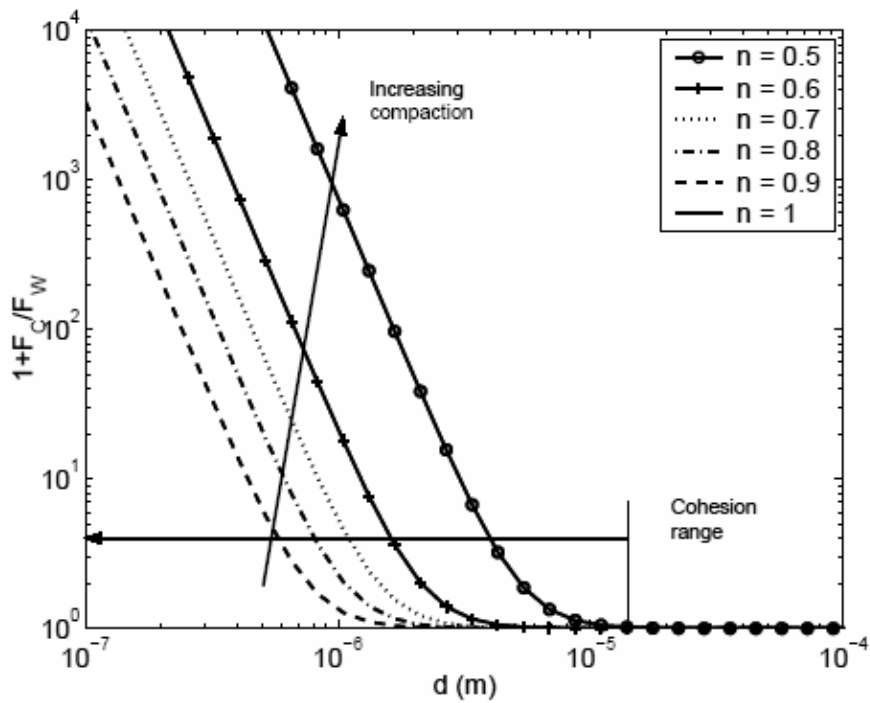


Figure 1: Evolution of the cohesion function $1+F_C/F_W$ vs. particle diameter d for different porosity values.

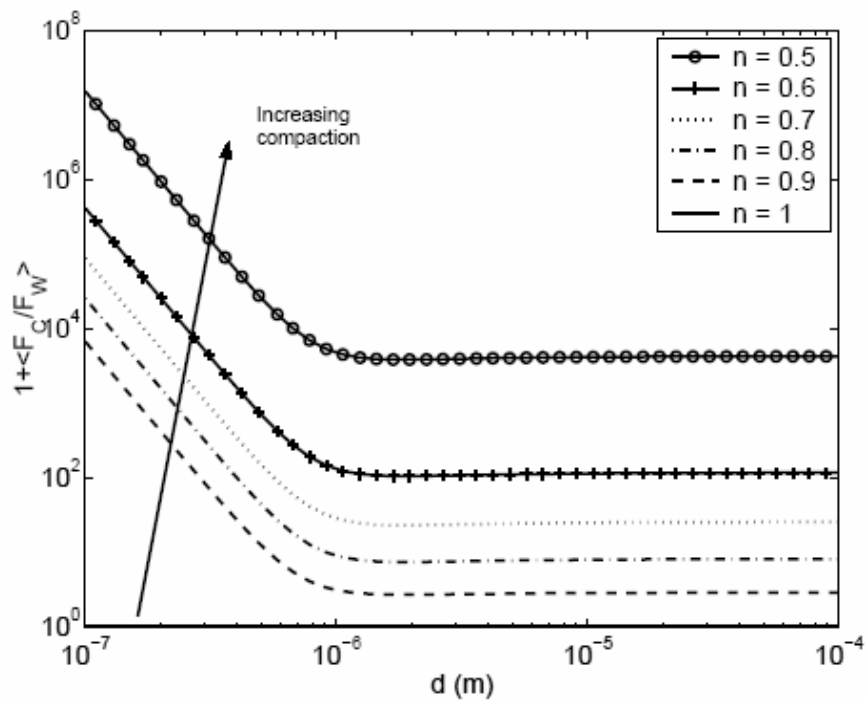


Figure 2: Evolution of the cohesion function $1+FC/FW$ vs. particle diameter d for different porosity values.

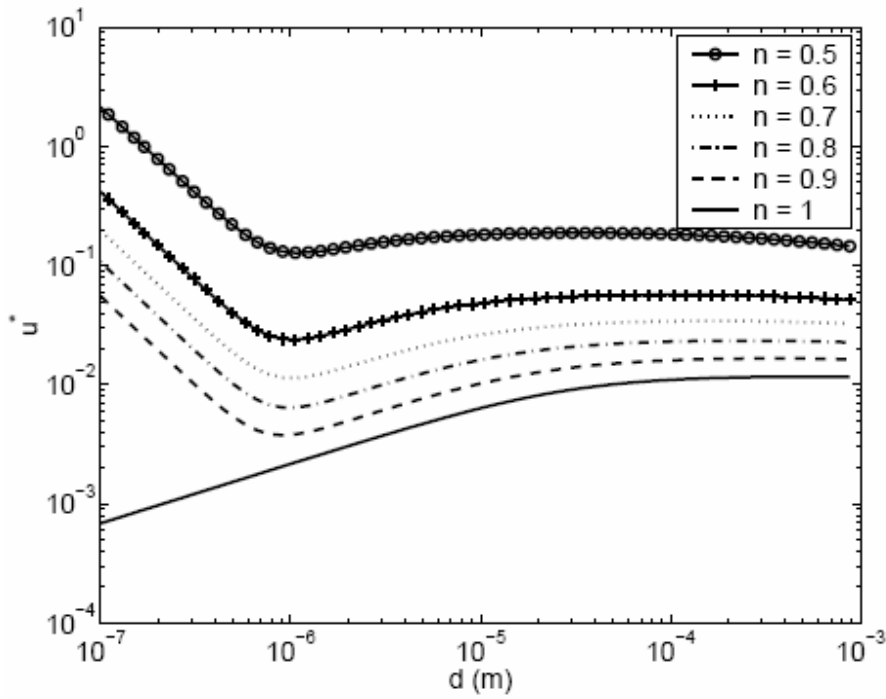


Figure 3: Evolution of the critical erosion velocity u^* vs. particle diameter d (m) for different porosity values.

All the parameters values required for the application of the presented modelling are given on Table 2.

This section reveals a first simple approach for assessing the critical erosion threshold of cohesive sediments. It is deduced from a force balance that includes the cohesion force, attributed to the presence of clay particles. This force, supposed to be the surface Van der Waals interaction, is directly dependent on the compaction degree and the particle size. The present model integrates all these declarations and introduces the porosity as a main parameter. Results reproduce well the main declarations of the literature: cohesion force appears to come from the presence of clay particles, and thanks to the coordination number, coarse particles are also affected. The usual critical shear stress magnitude is assessed in good agreement with the literature.

This model is interesting because of its simple parameterization by means of granulometry and porosity. The geometric factor including the unknown coordination appears also as a parameter, but whose value includes measurement and modelling errors. This original work results from the gathering of many models, which may be ameliorated. At the moment and to our knowledge, no modelling pretends to assess the coordination of such a wide range granulometric mixture. Moreover, cohesion is here attributed to the presence of clay particles, and is reduced to one of its components, the Van der Waals force. Other forces should also be incorporated to refine the results, such as double layer or chemical interactions.

Tab. 2: Numerical values of the parameters for the erosion threshold resolution

Symbol	Value	Units
ρ_s	2650	$\text{kg} \cdot \text{m}^{-3}$
ρ_w	1000	$\text{kg} \cdot \text{m}^{-3}$
G	10	$\text{m} \cdot \text{s}^{-2}$
Φ	52,5	°
A_H	10^{-20}	J
α	0,16	[\cdot]
A	37,49	[\cdot]
k_D	0,4	[\cdot]
k_L	30	[\cdot]
k_w	1	[\cdot]
n_{\max}	1	[\cdot]
n_{\min}	$1 - \square/6$	[\cdot]

3 Internal Erosion in Cohesive Soils without Crack

The two main phenomena responsible for erosion of particles in uncracked soils are backward erosion and suffusion. In backward erosion particles are detached from the downstream surface by the outward seepage. The suffusion process is similar but the coarse particles form a matrix and erosion is only of the finer particles in the pore space between the larger particles.

3.1 Criteria

Soil structure can be analyzed into two groups: a primary structure and a secondary structure [Kenney and Lau, 1985]. The primary structure consists of grains, which are in contact with each other and provide primary resistance to erosion, compressibility and shear strength. If these grains are eroded there are changes to the soil resistance and this may cause collapses. The secondary structure, on the other hand, is composed of grains, which are in the spaces between the primary grains and, which may be displaced under the action of mechanical (vibration) or hydraulic (flow) stresses.

On the assumption that bigger grains can hinder the erosion of smaller grains, Kenney and Lau [1985] have developed a method for assessing whether soils are internally unstable based on the shape of the coarse or the fine low-content grading curve. However, the method does not apply to clay soils.

In order to characterize the initiation of internal erosion for cohesive soils, Reddi et al. [2000] have developed an expression of the hydraulic shear stress τ :

$$\tau = \frac{\Delta p}{L} \sqrt{\frac{2\lambda}{n}}, \quad \lambda = \frac{\eta_w k}{\gamma_w}, \quad (7)$$

where $\Delta p/L$ is the average pressure gradient, λ is the intrinsic permeability, n is the porosity, k is the engineering hydraulic permeability, η_w and γ_w are the water viscosity, and specific weight, respectively.

3.2 The Triaxial Device

The developed experimental device can be used to study the initiation of suffusion and backward erosion for sandy-clay samples (**Figure 4**).

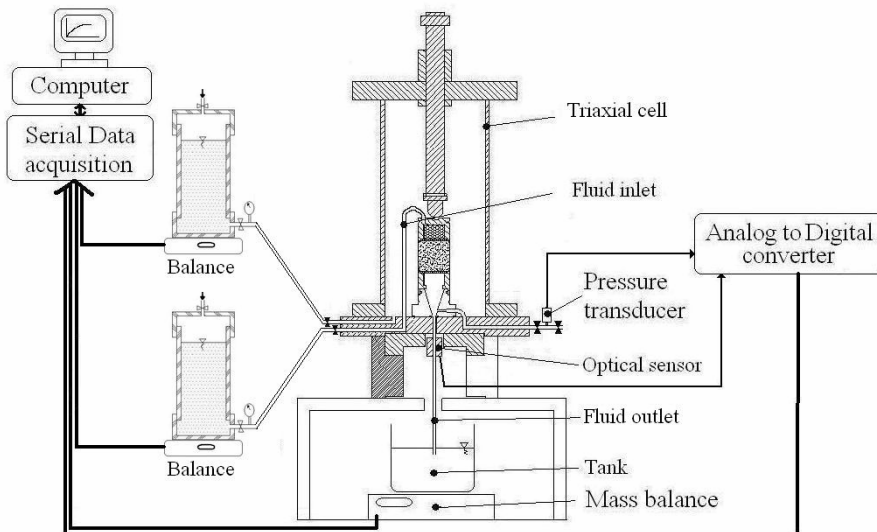


Figure 4: Schematic representation of the experimental triaxial cell equipped with the two controllers, effluent weight measurement and optical sensor mechanism (GeM).

The device placed in a temperature-controlled chamber ($20 \pm 0.5^\circ\text{C}$) consists of three modified triaxial cells. These cells have been modified to let the flow come through up to the core of the sample. So as to avoid all unwanted disturbances on the samples, saturation, consolidation, hydraulic and mechanical test stages are carried out inside the same cell without deconfining the samples. The carrying out of long-lasting tests is possible thanks to the automation of both the monitoring and the data acquisition. The use of three cells simultaneously makes it possible to reduce the duration of the test program.

The detection of erosion in the effluent is performed using optical aids and by weighing the amount of grains in the eroding fluid. The internal erosion critical gradient can be assessed from the effluent instantaneous optical analysis. In order to address internal erosion development, injection volume flow rates and obtained mass flow measurements are compared. A detailed description is given by Bendahmane et al. [2006].

3.3 Results

The material used is a washed Loire sand (grain density: 26 kN/m³) with a grain size distribution within the range 80µm-1mm ($d_{50} = 440\mu\text{m}$, uniformity coefficient: 3.125). The clay consists of kaolinite, with liquidity and plasticity limits are 55% and 22%, respectively.

In order to improve understanding of the phenomena, a distinction is made between the tests during which only clay particle migration is initiated, and the tests during which the transport of both clay particles and sand grains is observed. Maximum erosion rates per sample sections are preferred to some cumulative eroded mass information because the erosion rate here reaches its maximum value very quickly, which therefore means that it does not depend on the test duration.

3.3.1 Clay Erosion

From the beginning of the test, the mass flow increases until reaching a maximum value, $q_{s\max}$. It then decreases asymptotically toward zero. The permeability remains constant when no erosion occurs, but it decreases where erosion has been initiated. The erosion occurring within the clay fraction does not affect the size analysis nor the volume of the samples significantly. Consequently, according to the previously defined terminology, this phenomenon, characterized by some diffuse mass losses can be called suffusion.

The impact of three different parameters on the initiation of suffusion has been examined:

- kaolinite content: 5, 10, 20 and 30%;
- hydraulic gradient ranging between 5 and 160 m/m;
- confining pressure σ_3 : 100, 150, 200 and 250 kPa.

The range of hydraulic gradient was chosen relatively large to include the possible reduction of flow path in an earth structure by backward erosion phenomena. In this case, the local gradient can be much higher than the global one. The rate of suffusion increases according to the hydraulic gradient as follows:

$$q_{s\max} = 16.6 (10^{0.02(i-5)} - 1) \quad (8)$$

where $i = \Delta p / (\gamma_w L)$ is the hydraulic gradient.

Obtained results show that, depending on the hydraulic gradient, the erosion of the soils studied decreases as a function of the clay content according to:

$$\text{for } i = 20\text{m/m} : q_{s\max} = -0.06 \% \text{clay} + 1.28 \quad (9)$$

$$\text{for } i = 60\text{m/m} : q_{s\max} = -0.13 \% \text{clay} + 2.85 \quad (10)$$

$$\text{for } i = 100\text{m/m} : q_{s\max} = -0.17 \% \text{clay} + 5.15 \quad (11)$$

In a general way, the erosion rate doubles when the clay content changes from 20 to 10%.

Figure 5 represents the evolution of the maximum erosion rate according to the hydraulic shear stress Eq. (7) for $\sigma_3=100$ kPa.

The initial porosity depending on the consolidation, studying the effects of the confining pressure is essential. For sand specimens subjected to oedometer confinement conditions, Papamichos et al. [2001] observe that the maximum erosion rate growth according to the axial pressure applied is destabilizing. The present tests conducted under isotropic confinement with a 20 m/m hydraulic gradient and a 10 % clay content, reveal some opposite results (**Figure 6**).

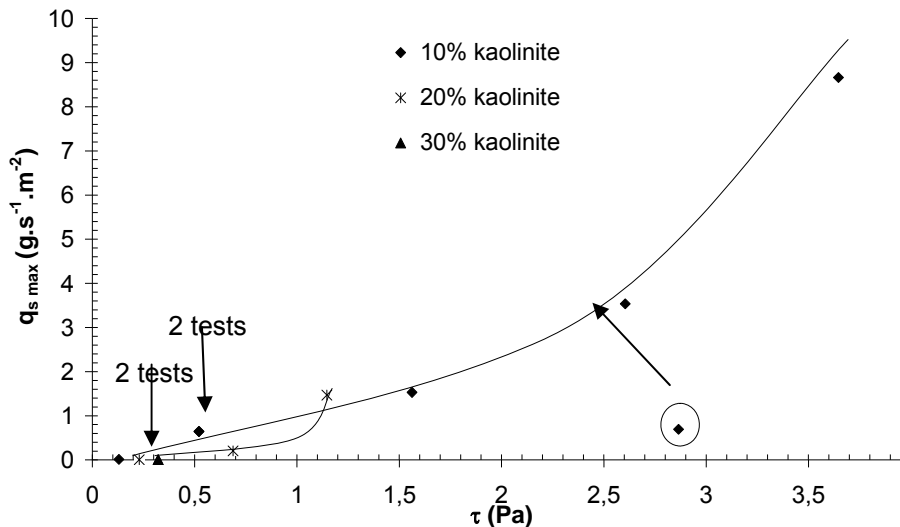


Figure 5: Maximum erosion rate v.s. hydraulic shear stress according to clay content ($\sigma_3 = 100 \text{ kPa}$).

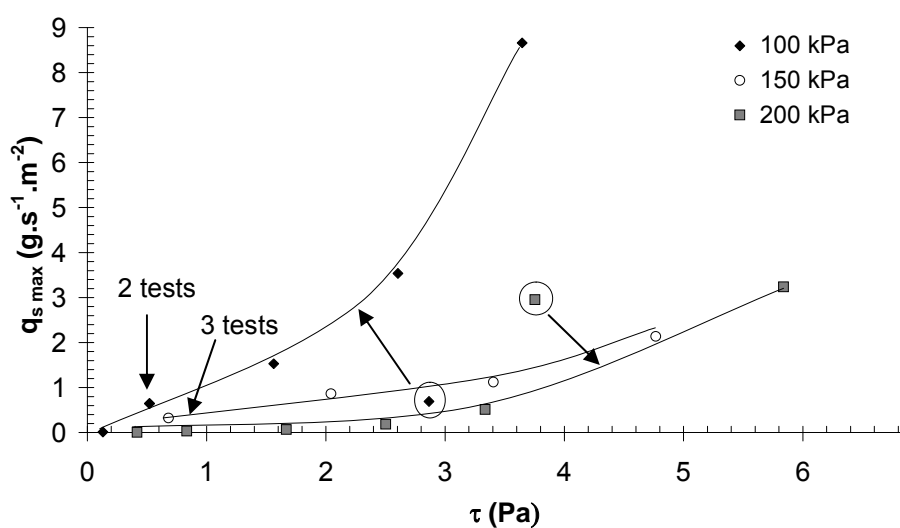


Figure 6: Maximum erosion rate v.s. hydraulic shear stress according to confining pressure (10% clay content)

Depending on the hydraulic gradient value, the linear decrease of the maximum erosion rate according to the confining pressure as follows:

$$\text{for } i = 20 \text{ m/m : } q_{s\max} = -0.006\sigma_3 + 1.256 \quad (11)$$

$$\text{for } i = 60 \text{ m/m : } q_{s\max} = -0.013\sigma_3 + 2.877 \quad (12)$$

To obtain the same maximum erosion rate, the hydraulic shear stress has to increase as a function of the confining pressure.

This approach makes it possible to identify the minimum stress levels, which depend on both clay contents and confining pressures and below which suffusion will not occur for the soils tested. For example, we obtained for $\sigma_3=100$ kPa

$$\tau_{cr} = 0.13 \text{ Pa with a 10 \% clay content};$$

$$\tau_{cr} = 0.23 \text{ Pa with a 20 \% clay content};$$

$$\tau_{cr} = 0.32 \text{ Pa with a 30 \% clay content.}$$

For $\sigma_3=200$ kPa and a 10 % clay content, τ_{cr} is approximately 0.42 Pa.

These values are several orders of magnitude greater than those in the case of surface erosion experiments, referring notably to the results from tests done in rotating cylinders [Arulanandan and Perry, 1983] or HET [Reddi et al., 2000]. However these values are four times smaller than those from Reddi et al. [2000]'s measurements in the case of internal erosion experiments. The direct application of our results and Reddi et al. [2000]'s seems to be difficult for the moment. The result difference observed between the samples tested here, and the Ottawa sand + kaolinite mixtures tested by Reddi et al. [2000] can be accounted for by many reasons. First the characteristics of the filter can either be open or be a porous stone may be responsible for these differences. The sand itself could also play a role, as grain sizes and grain angularities were different in our and their experiments.

The result difference observed between the samples tested here and Papamichos et al. [2001]'s specimens can be accounted for by many reasons: the characteristics of the pressure first, which can be isotropic or axial, of the samples, which can be made of a sandy-clay mixture or composed of sand only, then of the phenomena examined which are interpreted to be suffusion or backward erosion, and the sand grain angularity.

3.3.2 Clay and Sand Erosion

Considering two samples, both with a 10 % clay content and consolidated at 150 kPa. The first sample subjected to the action of a hydraulic gradient of 60 m/m suffers some clay erosion, whose extent is measured using the optical sensor, which gives a clay eroded mass of 60 mg. The second sample, on the other hand, subjected to a 140 m/m hydraulic gradient, gives a weighed eroded mass (clay and sand) of approximately 40 g.

The quantity of effluents achieved here (17% of the sample initial volume) produces a substantial volume variation within the sample, which finally collapses revealing then a significant change in the erosion mechanisms. Clay and sand particles are discharged from the soil downstream and along the upstream line through a backward erosion mechanism occurring within the sample.

Figure 7 shows the effects of the confining pressure on the maximum erosion rate (determined by weighing regarding sand erosion). This confirms that when the confining pressure rises, sand erosion within the samples tends to increase.

Backward erosion critical gradient values are very high, and, like suffusion, depend on both clay content and confinement stress. For clay contents higher than 10%, no backwards erosion effect is observed whereas, with a 10 % clay content, the backward erosion critical gradient is

90 m/m with $\sigma_3 = 200$ kPa ;

100 m/m with $\sigma_3 = 150$ kPa ;

140 m/m with $\sigma_3 = 100$ kPa.

The backward erosion increase as a function of confining pressure confirms conclusions of Papamichos et al. [2001] achieved with specimens made of sand only.

This experimental study opens up many new research prospects to address the problem of suffusion and backward erosion processes while demonstrating the importance of confinement effects on internal erosion. As the relationships between internal erosion processes and geotechnical or chemical properties of the soils remain unknown, it is recommended to use this test in order to evaluate the suffusion parameters on any sample of cohesive soil from a site.

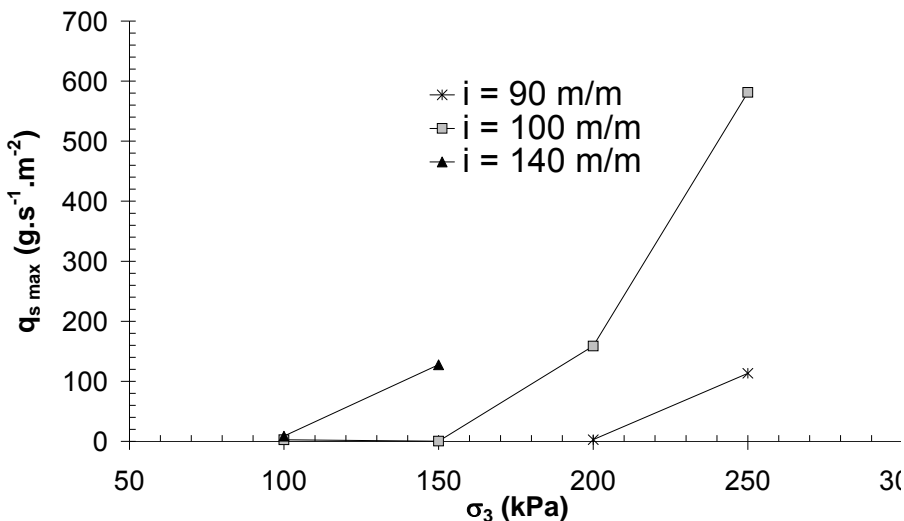


Figure 7: Maximum erosion rate v.s. confining pressure (10% clay content)

4. Piping Erosion in Cohesive Soils

Piping erosion is internal to the work, but external to the soil: this is a surface erosion. A large literature on surface erosion exists in the field of hydraulics and river engineering [Graf, 1984], [Yalin, 1977] and in the field of poromechanics and petroleum engineering [Papamichos et al., 2001]. In the field of geomechanics, several experimental methods have been developed for simulating the piping erosion process experimentally, with particular attention focussed on the hole erosion test. The experience acquired on more than 200 tests on several soils has confirmed what an excellent tool this test can be for quantifying the rate of piping erosion in a soil.

4.1 Criteria

Piping occurs if $P_0 > \tau_c$ where P_0 is the initial tangential shear stress exerted by the piping flow on the soil, and τ_c is the critical stress. The scaling law of radius time evolution is [Bonelli et al., 2006]

$$R(t) = R_0 \left[\frac{\tau_c}{P_0} + \left(1 - \frac{\tau_c}{P_0} \right) \exp \left(-\frac{t}{t_{er}} \right) \right], \quad (13)$$

with

$$P_0 = \frac{R_0 \Delta p}{2L}, \quad t_{er} = \frac{\rho_d R_0}{C_e P_0},$$

where t_{er} is the characteristic time of piping erosion, R_0 is the initial radius, Δp is the pressure drop, L is the hole length, ρ_d is the dry soil density, and C_e is the Fell coefficient of soil erosion. The later is similar to the Temple and Hanson [1994] coefficient of erosion k_d , as $k_d = C_e / \rho_d$. The Fell erosion index is $I_e = -\log(C_e)$ (C_e given in s/m).

4.2 Influence of Soil Properties

All test results - Temple and Hanson [1994] jet tests, Briaud EFA [2006] tests or Wan and Fell [2002] hole erosion tests - give a interesting relationship between the critical stress and the coefficient of erosion, or equivalently between the critical stress and the erosion rate index: I_e is proportional to $\log(\tau_c)$. The greater the critical stress, the greater the erosion rate index (the slower the erosion).

It is well known fact that different soils erode at different rate. Attempts were made to correlate erosion parameters - critical stress and coefficient of erosion - to common geotechnical or chemical soil properties in hope that simple equations could be developed for everyday use.

As a matter of fact, the erosion strength has been found to increase with: 1) the dry density of the soil, 2) the percent clay. This is illustrated by the following correlation [Temple and Hanson, 1994]:

$$I_e = 2 + 0.052 \left(\rho_d / \rho_w \right)^{3.1} (\%clay)^{0.406}. \quad (14)$$

However, for others parameters like the plasticity index, the liquid limit, the percent fines, the shear strength or the salinity, the situation is not clear. Due to the interdependence of these properties, however, it is clear that erosional strength of a soil cannot be represented accurately by the algebraic sum of the contribution of each of its properties. All attempts failed to reach a reasonable correlation coefficient value [Briaud, 2006]. It is strongly recommended carrying out hole erosion tests rather than using correlations [Wan and Fell, 2002].

4.3 The Hole Erosion Test

The hole erosion test was designed to simulate piping flow erosion in a hole. This test is not new [Lefebvre et al., 1985]. An eroding fluid is driven through the soil sample to initiate erosion of the soil along a pre-formed hole (**Figure 8**).

The results of the test are given in terms of the flow rate versus time curve with a constant pressure drop. Therefore, the flow rate is used as an indirect measurement of the erosion rate. For further details about this test, see [Wan and Fell, 2002].

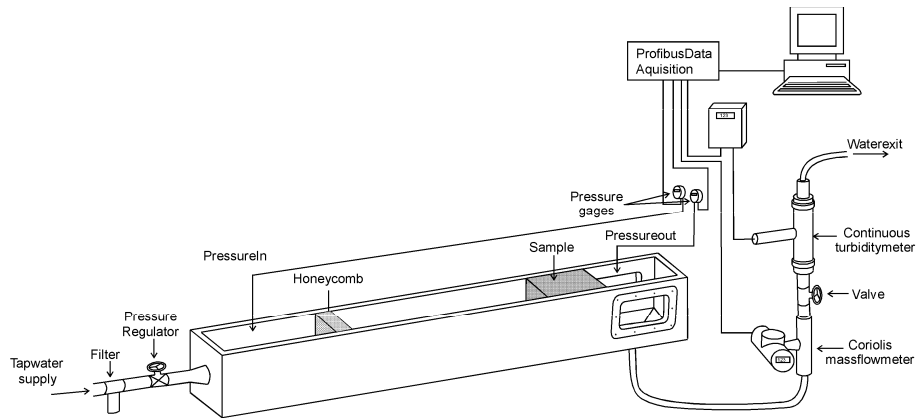


Figure 8: Schematic representation of the hole erosion test apparatus (Cemagref)

4.4 Results

The scaling law is now compared with previously published data [Wan and Fell, 2002]. Analysis were performed in 18 tests, using 9 different soils (clay, sandy clay, clayey sand or silty sand). The initial radius and the length of the pipe were $R_0=3$ mm and $L=117$ mm. Table 1 contains particle size distribution, and critical stress and Fell erosion index.

Figure 9 gives the effect of erosion process as the flow rate in relation to time, and shows that the use of t_{er} leads to efficient dimensionless scaling. Without this scaling, multiple graphs would be necessary to provide clarity of presentation. Scaled radius are plotted as a function of the scaling time in Figure 10. Nearly all the data can be seen to fall on a single curve. This graph confirms the validity of the scaling law (13).

Therefore, it is recommended to use hole erosion tests and the scaling law in order to evaluate the piping erosion parameters on any sample of cohesive soil from a site.

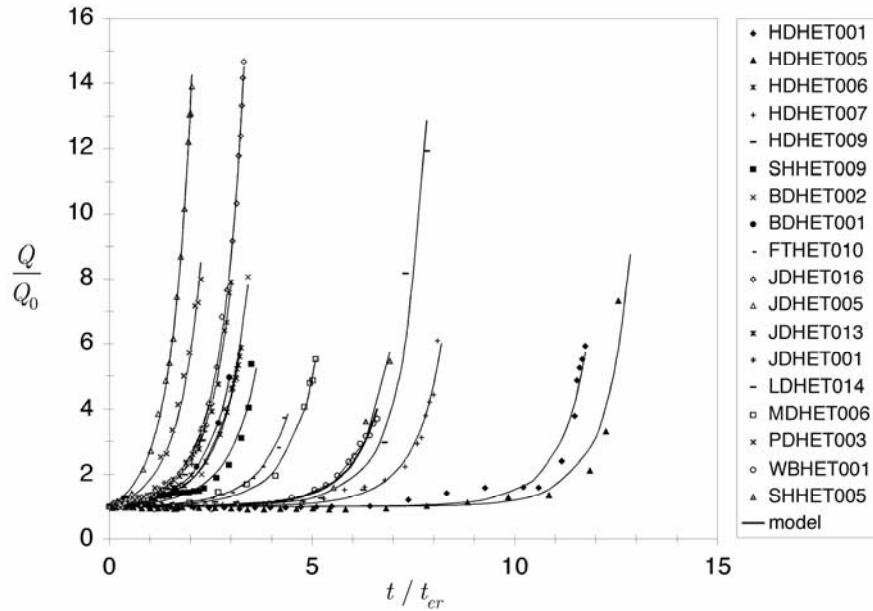


Figure 9: Hole Erosion Tests (symbols) versus scaling law (continuous lines). Dimensionless flow rate is shown as a function of dimensionless time.

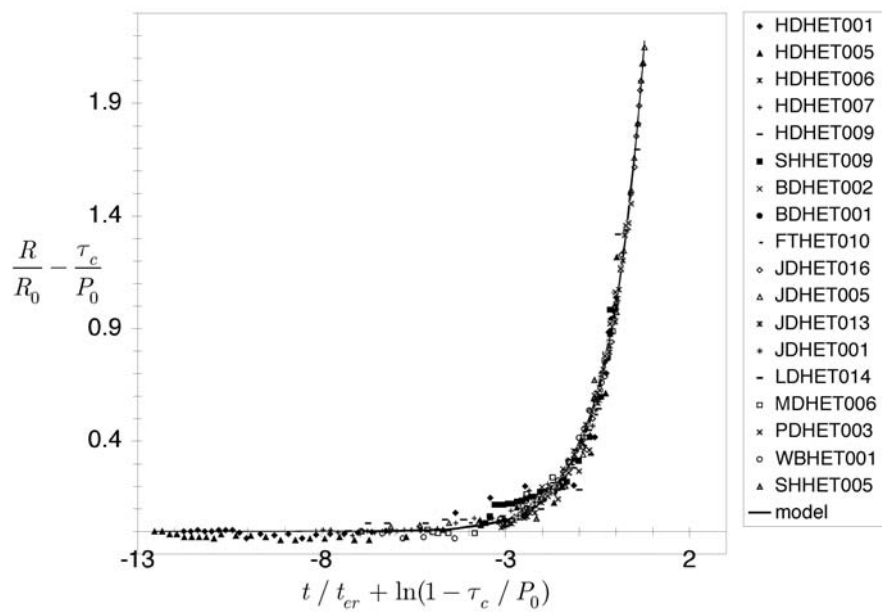


Figure 10: Hole Erosion Tests (symbols) versus scaling law (continuous lines). Dimensionless radius is shown as a function of dimensionless scaling time.

Table 1: Properties of soils samples, critical stress and Fell erosion index

Soil		% Gravel	% Sand	% Fines	% <2µm	τ_c (Pa)	I_e
Lyell	silty sand	1	70	29	13	8	2
Fattorini	medium plasticity sandy clay	3	22	75	14	6	3
Pukaki	silty sand	10	48	42	13	13	3
Jindabyne	Clayey sand	0	66	34	15	6 - 72	3 - 4
Brady's	high plasticity sandy clay	1	24	75	48	50 - 76	4
Shellharbour	high plasticity clay	1	11	88	77	99 - 106	4
Waranga	Low plasticity clay	0	21	79	54	106	4
Matahina	Low plasticity clay	7	43	50	25	128	4
Hume	Low plasticity sandy clay	0	19	81	51	66 - 92	4 - 5

Acknowledgement

This research project is sponsored by the French National Research Agency (ERINOH).

Literature

- [1] Arulanandan, K. and Perry, E.B. 1983. Erosion in relation to filter design criteria in earth dams. *Journal of Geotechnical Engineering*, 109(5), 682-696.
- [2] Bendahmane, F.; Marot, D.; Rosquoët, F.; Alexis, A. 2006. Characterization of internal erosion in sand kaolin soils. *European Journal of Civil Engineering*, 10(4), 505–520.
- [3] Bonelli, S.; Brivois, O.; Borghi, R.; Benahmed, N. 2006. On modelling of piping erosion. *Comptes Rendus de Mécanique*, 8-9(334), 555-559.
- [4] Bonelli, S.; Brivois, O. The scaling law of the hole erosion test with constant pressure drop, *International Journal for Numerical and Analytical Methods in Geomechanics*, to appear.
- [5] Briaud, J.-L. 2006. Chapter 9 - Erosion tests on New Orleans levee samples, in Investigation of the performance of the New Orleans protection systems in Hurricane Katrina on August 29, 2005. Final report July 31.
- [6] Dade, W.; Nowell, A.; Jumars, P. 1992. Predicting erosion resistance of muds. *Marine Geology*, 105, 285-297.
- [7] Fell, R.; Fry, J.-J. 2007. Internal erosion of dams and their foundations, Taylor & F.
- [8] Graf, W. H. 1984. *Hydraulics of Sediment Transport*. Water Resources publications, LLC.
- [9] Israelachvili, J. N. 1985. *Intermolecular and surface forces*. Academic Press.
- [10] Kenney, T.C.; Lau, D. 1985. Internal stability of granular filters. *Canadian Geotechnical Journal*, 22, 215-225.

- [11] Lefebvre, G.; Rohan, K.; Douville, S. 1985. Erosivity of natural intact structured clay : evaluation, Canadian Geotechnical Journal, 22: 508-517.
- [12] Migniot, C. 1968. A study of the physical properties of different very fine sediment and their behaviour under hydrodynamic action. La Houille Blanche, 7, 591-620.
- [13] Mitchener, H.; Torfs, H. 1996. Erosion of mud/sand mixtures. Coastal Engineering, 29, 1-25.
- [14] Papamichos, E., Vardoulakis, I., Tronvoll, J. and Skjærstein, A. 2001. Volumetric sand production model and experiment. International Journal for Numerical and Analytical Methods in Geomechanics, 25, 789-808.
- [15] Reddi, L.N., Lee, I. and Bonala, M.V.S. 2000. Comparison of internal and surface erosion using flow pump test on a sand-kaolinite mixture. Geotechnical Testing Journal, 23(1), 116-122.
- [16] Saffman, P. 1965. The lift force on a small sphere in a shear flow. Journal of Fluid Mechanics, 22, 385-400.
- [17] Sundborg, A. 1956. The River Klaralven: A study of Fluvial Processes. Esselte Aktiebolag.
- [18] Temple, D.M.; Hanson G.J. 1994. Headcut development in vegetated earth spillways. Applied Engineering in Agriculture. 10(5): 677-682.
- [19] Ternat, F. 2007. Erosion of self-weight consolidated cohesive sediments. Ph-D Thesis, Aix-Marseille II Mediterranean University.
- [20] Wan, C.F.; Fell, R. 2002. Investigation of internal erosion and piping of soils in embankment dams by the slot erosion test and the hole erosion test. UNICIV Report No R-412, The University of New South Wales Sydney ISSN 0077 880X.
- [21] Yalin, M. 1977. Mechanics of Sediment Transport. Pergamon Press.

Authors Name and Affiliation

S. Bonelli

Cemagref, Hydraulics Engineering and Hydrology Research Unit, France
stephane.bonelli@aix.cemagref.fr

D. Marot

Institute GeM, Interactions Water - Geomaterials Team, France
didier.marot@iutsn.univ-nantes.fr

F. Ternat

Irphe - CNRS - Universités d'Aix-Marseille, France
fternat@gmail.com

N. Benahmed

Cemagref, Hydraulics Engineering and Hydrology Research Unit, France
nadia.benahmed@cemagref.fr

Current Practice and new View on Granular Filters

Jean-Jacques Fry

Abstract

The first purpose of this paper is an attempt to bring up to date experience compiled on filters. A summary of the current specifications of filters in dams is presented. The second purpose is to underline the hydraulic condition of the retention function. The role of permeability of the filter is crucial. For instance, based on the results of hydraulic modelling, prevention of internal erosion and repair along a conduit in a zoned dam is provided by a filter permeability around 10^{-5} m/s.

1 Functions of Filter

1.1 Proposal for a Classification of the Functions of the Filter

The design functions are numerous. They depend on the location in the structure and the stresses created by the environment. According to Functional Analysis, they are of two types:

- **flow functions**, which concern particles transport, water transfer and load transfer ;
- **contact functions**, which guarantee the proper functioning of the filter whatever the physical, chemical or biological loading cases exerted by the external environment, during each phase of its lifetime.

Flow functions characterise the role of the filter, and the main functions are:

- **retention**: the filter limits the transport of particles of the base soil;
- **self-filtration (or stability)** : the filter is stable and limits the transport of its particles ;
- **drainage**: the filter transports and evacuates the pore water ;
- **Strength**: the filter transfers the stresses without being crushed.

The **contact functions** must be defined for all of the main two phases of a dam's life: installation and operation. In total, the contact functions can be grouped into three families:

- **Cohesionless (or self-healing)** in the operating phase: ability to collapse not to cement.
- **integrity** during the construction phase: making sure there is no deterioration or segregation during its application;
- **durability** resistance to in-service weathering and attrition throughout the targeted project lifetime.

In conclusion, the application of a filter in a dam requires defining seven types of functions for the construction and operation phases.

1.2 The Properties to be Specified

The functional specifications are based on the type of function to be respected and the type of filter to be used. The standards guarantee the associated characteristics and guarantee the quality of the functional specification. Conversely, the lack of standards may indicate new solutions or a lack of knowledge. Table 1 presents a list of descriptors for the functional specifications and their associated standards, based on the seven design functions.

Table 1: Design functional specifications related to the different authors

Function	Functional specifications	Authors or standards
Retention	Fine silts or clays more with $85\% > 0,074\text{mm}$: $D_{15} < 9 \text{ d85}$	Sherard [1], Fell
	Sandy clays or silts $40\% < 0,074\text{mm} < 85\%$: $D_{15} < 0,7 \text{ mm}$	Sherard [1], Fell
	Silty or clayey sand or gravel : $15\% < 0,074\text{mm} < 39\%$ $D_{15} < (40-A)/25^*(4d85-0,7)+0,7\text{mm}$	Sherard [1], Fell
	Silty or clayey sand or gravel $0,074\text{mm} < 15\%$: $D_{15} < 4d85$	Sherard [1], Fell
	Fine dispersive clay or silt : $K_F(\text{m/s}) < 6,7 \cdot 10^{-6} \delta r^{1,52}$ δr floc size in microns	Vaughan and Soares [2],
Self-filtration	Minimum passing between $4D$ and D is 15% $H/L > 1$	Terzaghi, Lowe Kenney and Lau
Drainage	$D_{15} > 5d_{15}$	Terzaghi, USACE
Strength	$UCS > 120 \text{ MPa}$	Rock Manual 2006
No cohesion	No plastic fines $PI=0$ Maximum % passing $0,074\text{mm} < 5\%$ Siliceous particles in acid environment $D_{15} > 0,1 \text{ mm}$	Sherard US SCS Sherard US SCS ICOLD 94 USDA SCS
Integrity	Los Angeles $< 25-30$ $D_{90} < 20\text{mm}$ $Cu < 6$ (filter bands) and $D(\text{upper band})/D(\text{lower band}) < 5$	EN 1097-2 1998 USBR USDA SCS USDA SCS
Durability	Water absorption $< 2\%$ Mass density $> 2,6$ $MgSO_4$ soundness $< 10\%$ Freeze-Thaw loss $< 0,5\%$	EN 13383-2 2002 EN 13383-2 2002 EN1367 EN 13383-2 2002

2 Hydraulic Condition of Criteria

2.1 Permeability Filter Requirement from Delgado

Delgado related filtering capability to permeability, a hydraulic criterion, as this appears to relate more truly to filter behaviour than geometric grading criteria alone. From successful laboratory hole erosion tests, those in which the filter trapped the base soil particles and prevented erosion from continuing, Delgado [3] derived the relationship shown on Figure 1, linking the percentage of the base soil passing the 0.075 mm sieve to the filter permeability required to filter it.

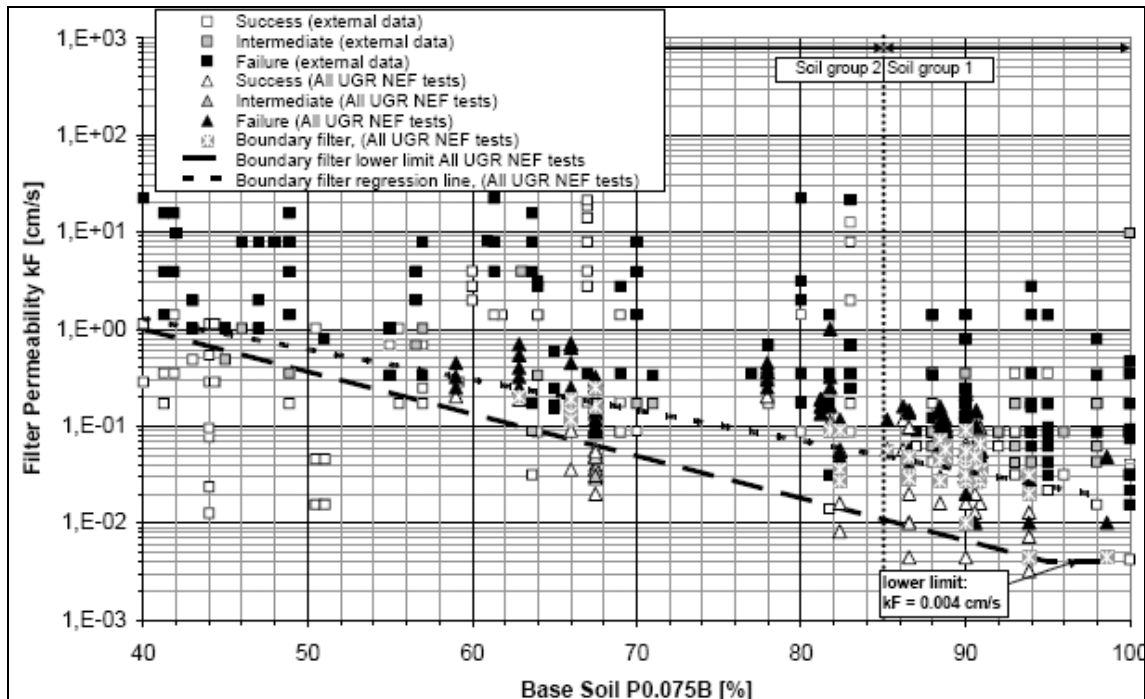


Figure 1: % of base soil passing the 0.074 mm sieve to the filter permeability required to filter it.

2.2 Importance of Hydraulic Condition of Internal Erosion in a Zoned Dam

2.2.1 The Hydraulic Model

Two conditions are required to initiate internal erosion : the geometrical criterion and the hydraulic criterion. Most research efforts were concentrated on geometric criterion (i.e. retention function). Not enough attention was paid on the hydraulic criterion. Without retention, eroded particles can be deposited following the drop of drag force according to the hydraulic criterion.

A very simple model has been developed in a view to demonstrating the influence of the hydraulic criterion [4]. This model, coupling the flow in a concentrated leak in the core to the porous flow in the filters and shoulders, assesses the hydraulic condition of internal erosion under the following assumptions :

- erosion initiation is erosion along a crack ;
- the dam is a zoned dam with core between two shoulders ;
- a 2 mm crack is at the base of the core ;

- At t=0, the full service water level H_w is on the upstream side and no water on downstream side, $H=0$.

The equations are :

- Mass Conservation : the discharge flow rate Q through the upstream shoulder is the flow rate through the core and the downstream shoulder.
- Energy Conservation (Bernoulli theorem) through the upstream shoulder, the core and the downstream shoulder :

$$\Delta H_{US}(Q) + \Delta H_{CORE}(Q) + \Delta H_{DS}(Q) = H_w(Q) - 0 \quad (1)$$

- The head ΔH loss in the core occurred in the pipe at the bottom of the core with the linear friction coefficient λ , deduced from Haaland relationship : $\lambda=f(R_e, d_{100}, D_h)$, the crack length L , the flow velocity V and the hydraulic diameter D_h :

$$\Delta H_{CORE} = \lambda \cdot \frac{L}{D_h} \cdot \frac{V^2}{2g} \quad (2)$$

- The head loss ΔH in the shoulders is computed by 2D flow net entering an horizontal crack or by a simple analytical 3D relationship flow coming into the void around half the perimeter of a conduit (radius R_0):

$$\text{Upstream shoulder : } \Delta H_{US}(Q) = H_w - H_a = \frac{Q}{2\pi K_m} \left(\frac{1}{R_0} - \frac{1}{H_w} \right) \quad (3)$$

$$\text{Downstream shoulder : } \Delta H_{DS}(Q) = H_b - 0 = \frac{Q}{\pi K_v} \left(\frac{1}{R_0} - \frac{1}{H} \right) \quad (4)$$

- The erosion law is governed by the solid erosion rate given by Gregory J. Hanson [5] :

$$\varepsilon = K_d \cdot (\tau_e - \tau_c) \quad (5)$$

Where ε is the volume erosion rate, K_d the erosion coefficient measured by Gregory J. Hanson, taken from 0,003 cm³/N/s for a very resistant clay to 2 cm³/N/s for a dispersive clay (figure 2), τ_c the critical shear stress, τ , the flow shear stress $\tau = \rho_w R_h J$, is the product of the specific mass, the hydraulic diameter and the hydraulic gradient and can be written :

$$\tau = \rho_w \cdot \frac{\lambda \cdot V^2}{8g} = \frac{1}{8} \rho_w \lambda \cdot \frac{V^2}{g} \quad (6)$$

- The eroded solid flow rate is the product of the eroded surface S and the erosion rate :

$$Q_s = \varepsilon S \quad (7)$$

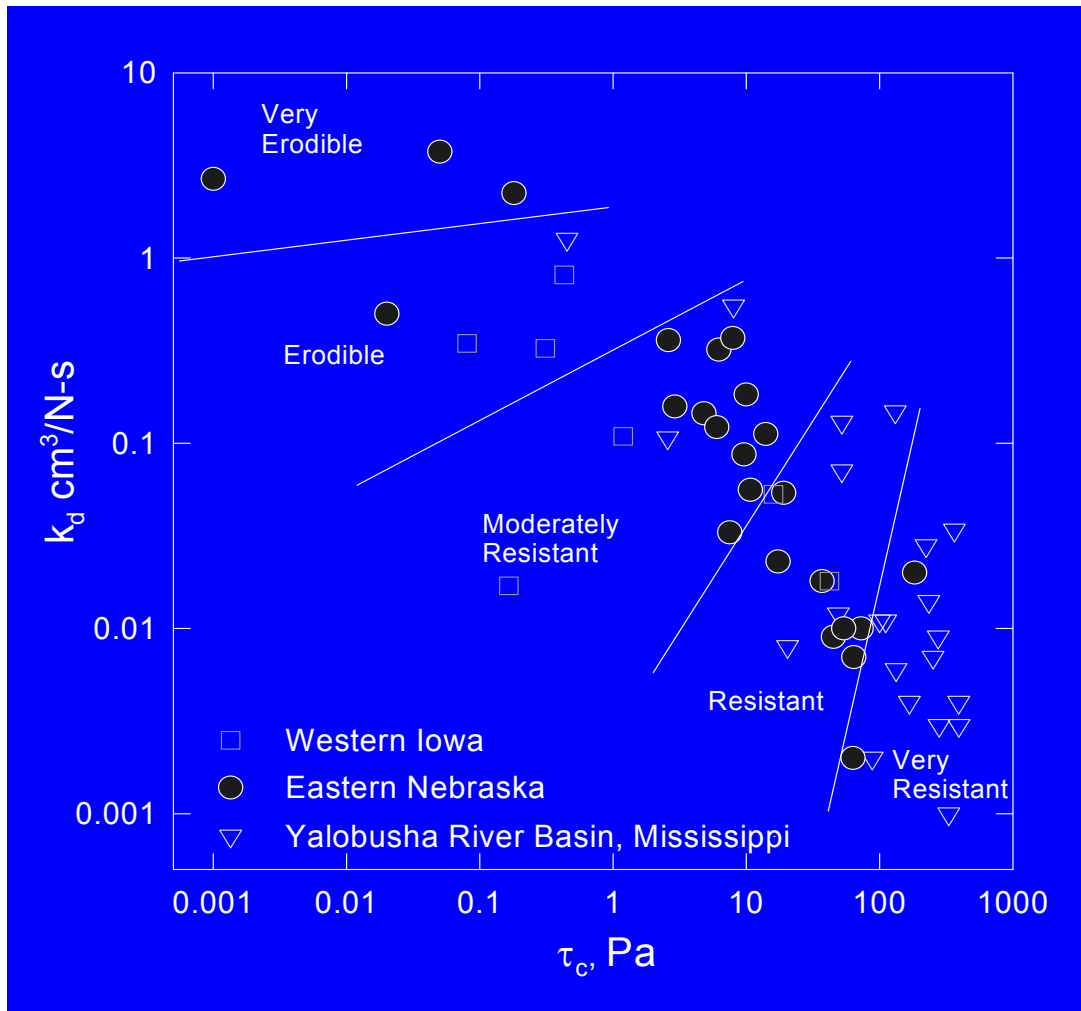


Figure 3: Clay categories from Greg Hanson

- The increase of the thickness e at $t+dt$ of a crack around the lower part of a conduit whose the radius is R_0 , within dt is :

$$e(t+dt) = \frac{Q_s dt}{\pi(R_0 + e(t)).V} \quad (8)$$

- The reservoir capacity C is the water volume, depending on H , the water height H behind the dam, by :

$$C(t) = cH_m^{2.5} \quad (9)$$

The shoulder is characterised by the permeability only, whose the range is 10^{-5} to 10^{-1} m/s.

The core is characterised by the resistance to erosion only. Table 2 presents the values used in the parametric survey.

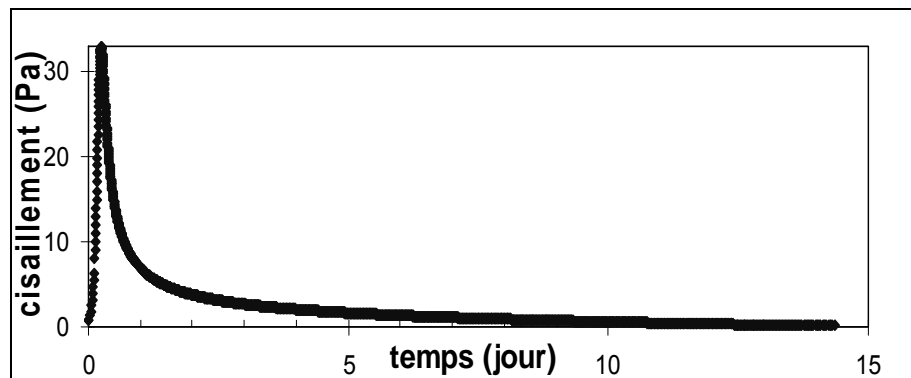
Table 2: the 5 core categories of the parametric survey

Core material	d_{100} (μm)	K_d ($\text{cm}^3/\text{N}\cdot\text{s}$)	τ_c (Pa)	Core category
(1)	2	2	0.01	very érodable
(2)	20	0.3	0.1	érodable
(3)	50	0.1	3	normal
(4)	50	0.01	20	resistant
(5)	50	0.003	200	very resistant

2.2.2 Application to a Zoned Dam without Filter

An application was driven through a typical zoned dam : dam height :50 m, Full Water Supply Level : 45m, core crest width : 6m, core H/V=1/4, permeable shoulder (H/V=2) and a crack along the lower part of a conduit at the base of the core. The results show 3 basic behaviours :

- The shear stress is below the critical stress of the core : internal erosion does not occur;
- At the beginning the shear stress increases and is larger than the critical stress, therefore the downstream head increases (figure 3), the upstream head decreases, in consequence the shear stress drops and becomes lower than the critical stress : i.e. the Internal erosion starts and stops in the core without big consequences ;

**Figure 3:** Example of shear Stress (Pa) change versus time (days) in the crack

- The shear stress is so high than internal erosion starts and drops the reservoir (Fig. 4).

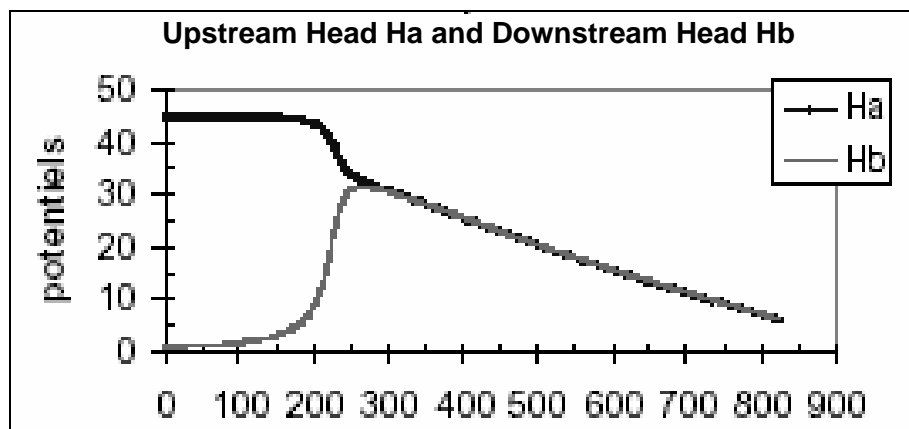


Figure 4: Example of change of head upstream and downstream of the pipe through the core

The results are summed up in the tables 3 to 6.

Table 3: Thickness of the crack in a zoned dam with cohesionless shoulders and no filter

Core category	Dispersive	erodable	average	resistant	Very hard
K=1E-1m/s	1,21 m	0,69 m			
K=1E-2m/s	0,53 m	0,23 m			
K=1E-3m/s	0,11 m	0,037 m			
K=1E-4m/s	0,016 m	0,005 m			
K=1E-5m/s	0,0025 m				

Table 4: Loss of reservoir head in a zoned dam with cohesionless shoulders and no filter

Core category	Dispersive	erodable	average	resistant	Very hard
K=1E-1m/s	-36 m	-30,1m			
K=1E-2m/s	-15,1 m	-7,9 m			
K=1E-3m/s	-1,3 m	-0,4 m			
K=1E-4m/s	-0,04 m	-0,01 m			
K=1E-5m/s	-0,01 m				

Table 5: Final discharge flow rate at end of erosion in a zoned dam

Core category	Dispersive	erodable	average	resistant	Very hard
K=1E-1m/s	1,5 m ³ /s	2,4 m ³ /s			
K=1E-2m/s	0,5 m ³ /s	0,6 m ³ /s			
K=1E-3m/s	70 l/s	70 l/s			
K=1E-4m/s	7 l/s	7 l/s			
K=1E-5m/s	0,7 l/s				

Table 6: Time required to stop internal erosion in a zoned dam

Core category	Dispersive	erodable	average	resistant	Very hard
K=1E-1m/s	24 days	22 days			
K=1E-2m/s	122 days	67 days			
K=1E-3m/s	118 days	37 days			
K=1E-4m/s	37 days	9 days			
K=1E-5m/s	9 days				

2.2.3 Interpretation and Conclusion of the first Results

The calculation with simple hypothesis should be confirmed by more sophisticated model based on more realistic assumptions. Whatever the shortcomings of this simple model, two main conclusions appear:

The resistance of the clay is a main parameter in the dam design : internal erosion does not occur in hard or very hard clay. This property cannot be ignored so far. The jet erosion test or hole erosion test should be mandatory in any new dam project.

The shoulder or filter permeability surrounding the core is a key factor : filter permeability strictly lower than 10^{-2} m/s controls the discharge rate, lower than 10^{-4} m/s prevents repair, and lower than 10^{-5} m/s impedes erosion for any kind of clay. This result supports the experimental evidence of the key role of permeability (Delgado, figure 1).

Other remarks are erosion time is quick and justify that most of incidents occur during first filling. With permeable shoulder whose the material cannot hold a roof, piping in the core is slowed down and time remediation is enough to take safety measures. However, the failure by instability or sloughing may occur. Cohesive and semi-pervious shoulders may threat piping.

2.2.4 Model with Pipe Plugging

The previous model has been developed to modelling the filling of the crack by the upstream material. The new hypothesis is as the void thickness is higher than a critical dimension

(diameter of particles of upstream shoulder pushed in the pipe) + 0,001m, pipe filling occurs and the thickness of the crack is reduced from that dimension. With that new hypothesis, the results are not deeply changed. Some discontinuities appear in the process : these instabilities remind the sequences of changing discharge flow rate at the exit of collectors of some eroded dams. The time of erosion stabilization can be in some cases 10 times larger than that without crack filling. The main difference with the previous results is that the full draw down of the reservoir occurs with the most erodible category (or dispersive soils) and permeability $\geq 10^{-2}$ m/s only.

2.2.5 Modelling of Zoned Dam with Filters

The hydraulic model was developed again to consider a zoned dam and a core wrapped in an 2m upstream and downstream filter. One more time, results show similar tendency than the first case. No erosion occurs in middle, hard and very hard clays. The permeability of the filter controls the final discharge through the crack (table 7).

Table 7: Final discharge flow rate at end of erosion in a zoned dam

K Filter	K=1E-1m/s	K=1E-2m/s	K=1E-3m/s	K=1E-4m/s	K=1E-5m/s
K Shoulder					
K=1E-1m/s	1,5 – 2,4 m³/s	0,9 -1,3 m³/s	0,25–0,28 m³/s	30 l/s	3l/s
K=1E-2m/s		0,5 –0,6 m³/s	0,2–0,22 m³/s	29 l/s	3l/s
K=1E-3m/s			70 l/s	28 l/s	3l/s
K=1E-4m/s				7 l/s	2 l/s
K=1E-5m/s					0,7 l/s

Permeability lower than 10^{-4} m/s does not prevent repair but strongly limits the discharge to 30l/s, and uniform permeability lower than 10^{-5} m/s prevents repair by impeding erosion for any kind of clay. This result confirms the key role of permeability (Delgado, figure 1).

It is noteworthy to interpret these results as pessimistic results. No natural clogging of the upstream face of the upstream filter has been considered. In reality internal erosion can be stopped by filter clogging for higher filter permeability.

3 Conclusion

The permeability of the filter is a key parameter. A simple hydraulic model simulating the erosion along a void at the base of the core of a 50 m zoned dam has been developed and used to compute the increase of the leak. The model is pessimistic as no natural clogging has been considered at the upstream face of the filter. Based on the first results, it appears that homogeneous permeability lower than 10^{-4} m/s controls the discharge, and homogeneous permeability around or lower than 10^{-5} m/s prevents repair by impeding erosion in any kind of clay.

New developments are required to confirm these conclusions. Complementary studies on other type of initiation are welcome. Consequences of all phenomena in terms of mechanisms of failure need to be analysed.

Literature

- [1] Sherard J L & Dunnigan L P 1989. Critical filters for impervious soils. ASCE Journal of Geotechnical Engineering Division, January, Vol 115 (GT7) 927-947.
- [2] Vaughan P R & Soares H F 1982. Design of filters for clay cores of dams. ASCE Journal of Geotechnical Engineering Division, January, Vol 108 (GT1) 17-31. [2] Sherard J L & Dunnigan L P 1989. Critical filters for impervious soils. ASCE Journal of Geotechnical Engineering Division, January, Vol 115 (GT7) 927-947.
- [3] Delgado F, Huber N P, Escuder I, & De Membrillera M G 2006. Revised criteria for evaluating granular filters in earth and rockfill dams. Transactions of the 22nd Congress, International Commission on Large Dams, Barcelona, Vol III, Q86 R29, 445-456
- [4] Fry J-J & Blais J-P 2006. Assessment of internal erosion risk of embankment or rockfill dams. Transactions of the 22nd Congress, International Commission on Large Dams, Barcelona, Vol III, Q86 R69, 1131-1141

Authors Name and Affiliation

Dr. Jean-Jacques Fry
EDF CIH Centre d'Ingénierie Hydraulique, France
jean-jacques.fry@edf.fr

Internal Erosion: Continuation and Filtration: Current Approaches Illustrated by a Case History

Rodney Bridle, Fernando Delgado and Nils P Huber

Abstract

The vulnerability to internal erosion of a 100-year old typical British embankment dam without filters has been examined using currently available methods. The methods used were the Sherard grading criteria, the Vaughan permeability criteria, the Delgado permeability criteria, and the Foster & Fell probability-based criteria. Attempts were also made to assess whether sufficient tractive forces would be available to initiate and continue erosion, including the Fry hydraulic condition approach. None of the methods give entirely re-assuring results, contrary to the apparently satisfactory performance of the dam, and suggestions are made for improved methods to confirm that the development of erosion at a rate that would lead to rapid failure is unlikely.

1 Safety Investigations

A 2003 dam safety report recommended investigations of the permeability and grading of the shoulder fill and foundations and investigations of the properties of the clay core of the dam, with the objective of checking the capacity of the fill to prevent erosion of the core, making use of the following:

- Vaughan and Soares' [1] 'perfect' filter relationship between a filter's permeability and its filtering capacity and the
- Sherard and Dunnigan's [2] 'critical' filter relationship between a filter's grading and its filtering capacity.
- Delgado's [3] approach linking the percentage of the base soil passing the 0.075 mm sieve to the filter permeability.
- Foster & Fell's [4] [5] approach using logistic regression method in order to replace deterministic no-erosion criteria by a probability-based approach

2 The Dam

The dam was completed in 1904. It is 22.5 m high in earthfill with a puddled clay core 2.7 m wide at the crest with side slopes of 1 to 12 above a clay filled cut-off trench.



Figure 1: Puddled clay fill placed in cut-off trench up to level of dam foundation

The upstream slope is 3 to 1 and the downstream slope is 2 to 1. The embankment fill is glacial till. Photographs (**Figures 1, 2 and 3**) show the puddled clay at the top of the cut-off trench, a steam driven face-shovel excavating the till, and the site railway that transported the till to the dam embankment, where it was placed on the dam shoulders by side-tipping from the railway wagons.

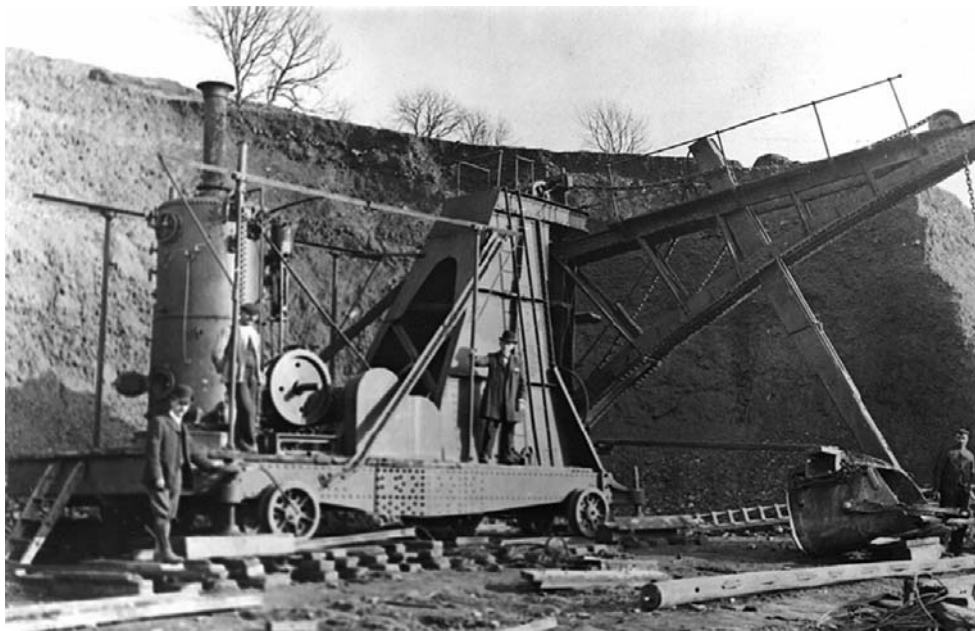


Figure 2: Steam face shovel excavating glacial till for shoulder fill in dam



Figure 3: Fill placed on shoulder of the dam by side tipping from railway wagons

No in-situ tests of the fill's permeability or density have yet been completed, but the photographs indicate that although there is some segregation of the fill, the method of placing may have produced dense fill of varying grading and permeability.

3 Laboratory Permeability Testing of Glacial till Shoulder Fill

The permeability of the fill in the shoulders of the dam has been established by tests in the large-scale TRL permeameter (**Figure 4**). This permeameter is 0.3 m square and 1.0 m long. The samples are placed in layers. Water is introduced under pressure at one end and flows along layers of fill, as it would from an opening in a core into the adjoining shoulder fill, and flows out at the other end of the permeameter.



Figure 4: TRL (formerly Transport and Road Research Laboratory) 0.3 m square by 1.0 m long permeameter.

The till is stony with many fines (**Figure 5**). The samples tested necessarily omitted particles larger than 37.5 mm, about 20% of a typical sample, as Figure 6 shows.

The permeability varies with density as shown in Figure 7.



Figure 5: Sampling glacial till used for shoulder fill

Vaughan & Soares [1] derived the following relationship between permeability and filtering capability:

$$\delta_R = 2.54 * 10^3 (k)^{0.658} \quad (1)$$

δ_R in microns, size of floc trapped;

k, permeability of filter in m/s

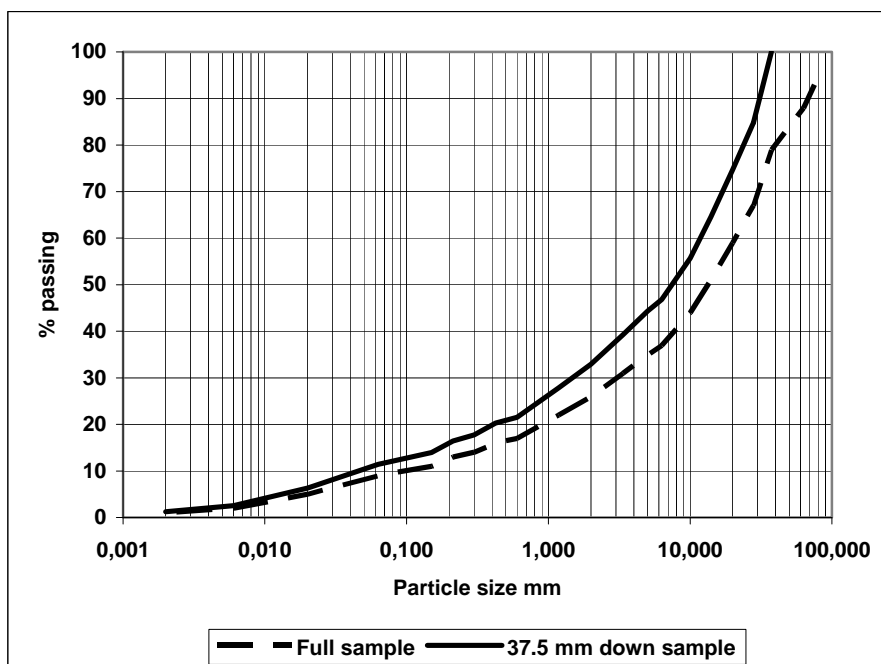


Figure 6: Grading of glacial till used as shoulder fill

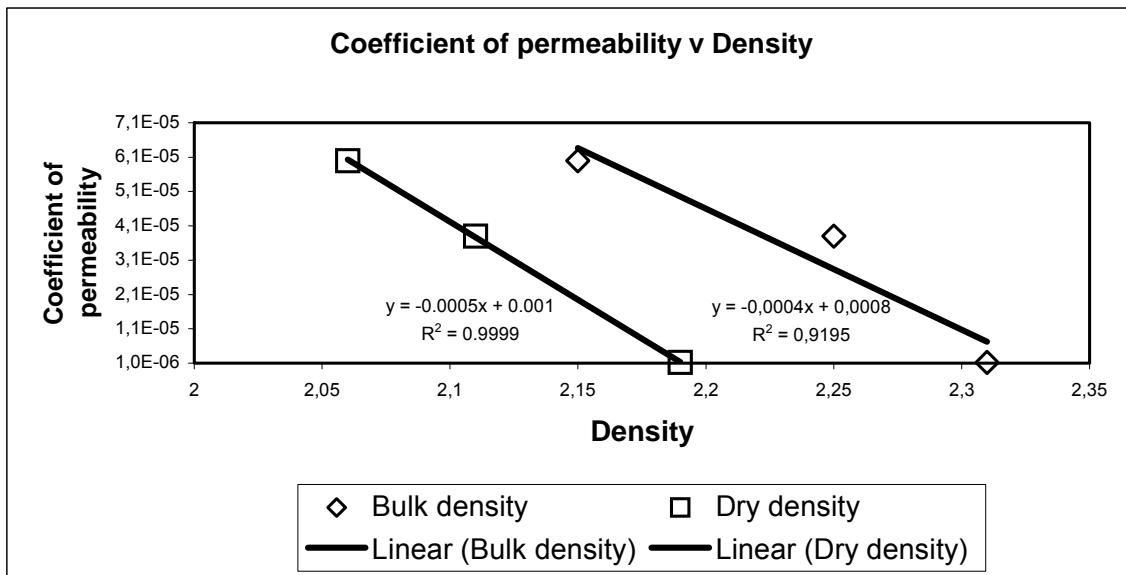


Figure 7: Permeability (m/s) v density (Mg/m³), glacial till shoulder fill. The till is non-cohesive, showing as non-plastic in index tests and in the 'sand castle' test. Using [1] fill would filter flocs between 0.3 microns (high density) and 4.2 microns (low density). Laboratory tests gave a minimum dry density of 1.84 Mg/m³ and a maximum dry density of 2.30Mg/m³. The standard optimum dry density was 1.87 Mg/m³ at 15% moisture content.

Using the relationship, the fill could trap flocs or particles from 0.3 to 4.2 microns, depending on its density.

4 Tests on Core Samples

The grading of the core was determined from conventional dispersed samples and from undispersed samples. The objective was to determine the smallest floc size present in the core because the Vaughan and Soares 'perfect' filter approach requires that there is no movement of the soil into the filter.

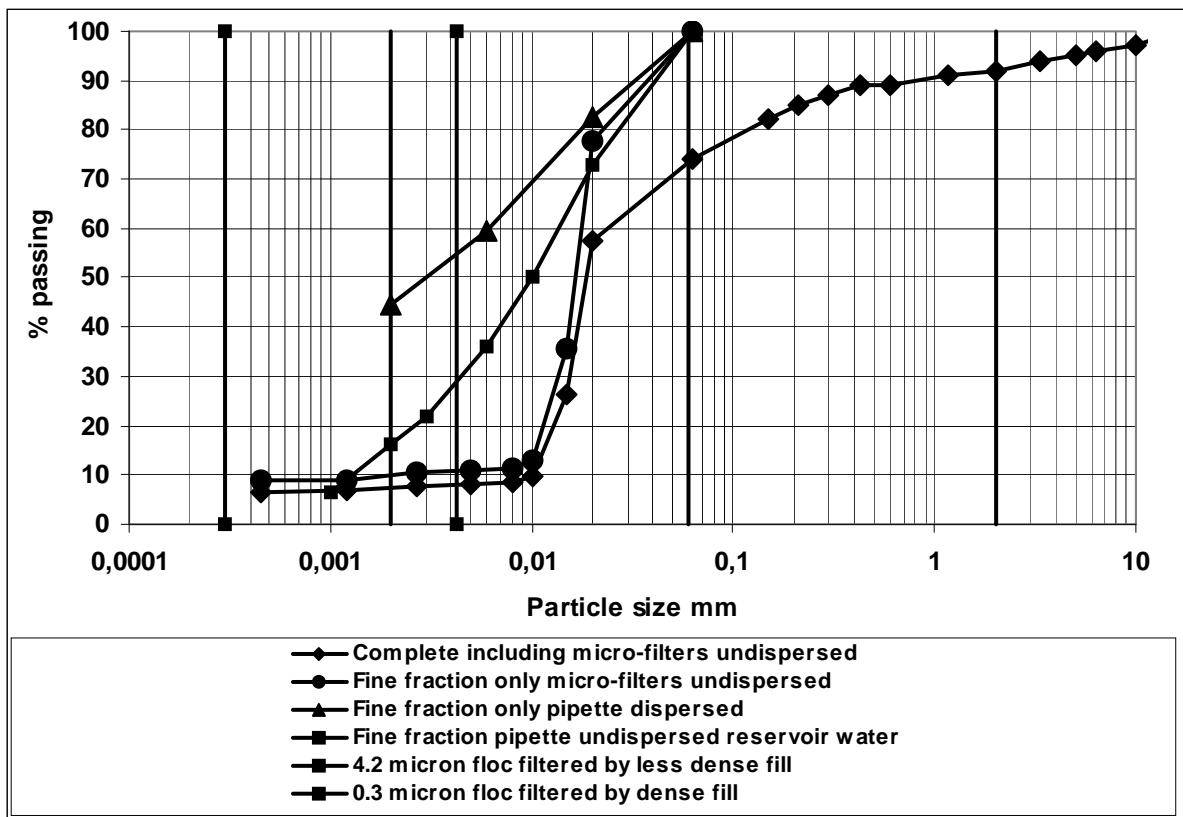


Figure 8: Complete grading core fill including use of very fine cellular micro sieves and glass fibre filters from 0.063 mm down to 0.00045 mm (0.45microns). Note micro-sieve samples very small (about one gram) and when compared to the larger samples tested by pipette apparently poorly represented all the grain or floc sizes present. Note apparent high clay (0.002 mm) content of dispersed sample (45%), lower clay content (17%), high silt content (83%) of undispersed sample. Filter capacity of fill also shown.

The core samples proved to be very 'murky' [6], making it impossible to assess the smallest floc size present using Stokes' Law tests because the falling front was not visible through the 'murk' and the velocity at which it was falling could not therefore be measured. The 'murk' was investigated particularly by 'sieving' on very fine cellular micro-sieves and glass fibre filters able to retain particles (or flocs) down to 0.45 microns, smaller than the usual minimum of 2 microns (0.002 mm) measured by pipette in standard soil mechanics laboratory tests. The tests showed that (at this dam, at least) the 'murk' cannot be ignored as colour or other property without physical substance. It was not possible to determine the size of the smallest floc or particle present, but about 7% passed the 0.45 micron 'sieve', as the grading curve on Figure 8 shows.

5 Filtering Capability of Glacial till Shoulder Fill using Vaughan and Soares Permeability Criteria

Tests on the core show that it may be particularly vulnerable to erosion because, as Figure 8 shows, it may be up to 83% silt and therefore behave as silt, and erode at a lower seepage velocity than cohesive clay.

The glacial till fill is capable of acting as a filter, trapping, when dense, particles or flocs as small as 0.3 microns. The particle size of the smallest particle present was not determined, but it was

proved to be smaller than 0.45 micron and could have been smaller than 0.3 micron, in which case about 7% of the weight of the core could be eroded into the fill, causing some damage. If the fill near the core were less dense, it would trap particles or flocs above 4.2 microns equivalent diameter, but as flocs smaller than these comprise somewhere between 8% and 29% of the weight of the core, the damage could be serious.

6 Filtering Capability of Glacial till Shoulder Fill using Sherard Grading Criteria

The results of considering the glacial till fill as a filter to the core following ‘critical’ filter rules [2] [7] are shown on Figure 9. The fill would be too coarse in the larger sizes and too fine in the smaller sizes to be the Category 2 filter required. However, the important D_{15} size is 0.4 mm, below the recommended maximum of 0.7 mm and above the recommended minimum of 0.1mm.

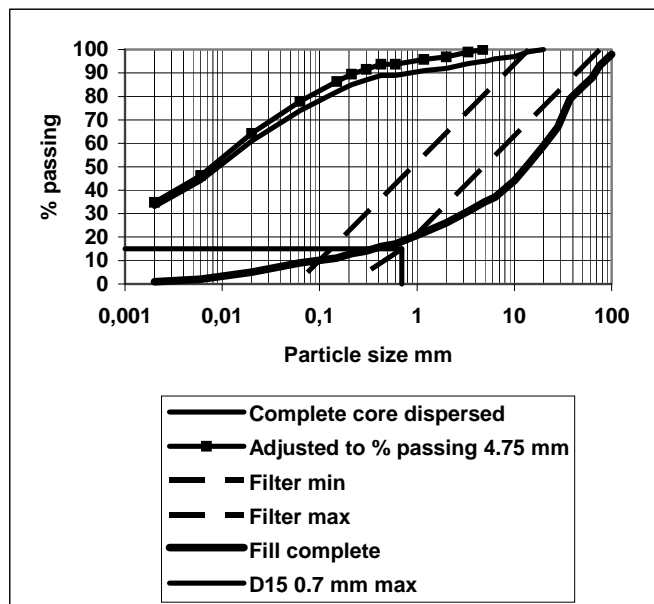


Figure 9: Considering glacial till shoulder fill as ‘critical’ Category 2 filter to core [2] [7]. Fill too coarse in larger sizes and too fine in smaller sizes, but meets $0.1 \text{ mm} < D_{15} < 0.7 \text{ mm}$ criterion

The dispersibility of the core was assessed using the pinhole test. It was a non-dispersive, ND2, soil. The fill’s capability as a filter was checked using the no-erosion filter test, which showed that no erosion occurred and that the sides of the 1.0 mm hole through the till had not been eroded. It could be said that this is the conclusive test to demonstrate that the fill provides an adequate filter to the core.

7 Filtering Capability of Glacial till Shoulder Fill using the Delgado Permeability Criteria

Delgado [3] re-examined 340 laboratory tests by others and carried out 348 tests further tests. From the successful tests, those in which the filter trapped the base soil particles and prevented

erosion from continuing, he derived the relationship shown on Figure 10, linking the percentage of the base soil passing the 0.075 mm sieve to the filter permeability required to filter it.

It should be noted that the objective was to relate filtering capability to permeability, a hydraulic criterion, as this appears to relate more truly to filter behaviour than geometric grading criteria alone. The 348 Delgado tests show the filtering capacity against a permeability assessed from density through specific regression formulae. Permeabilities were not measured in most of the 340 other tests, and the permeabilities were estimated by applying the Sherard relationship between permeability and D_{15} filter size, as follows:

$$k_{\text{filter}} = 0.35 * (D_{15})^2, \text{ k in cm/s, } D_{15} \text{ in mm} \quad (2)$$

This relationship gives permeability values markedly higher (nearly three times) than the Delgado regression formulae.

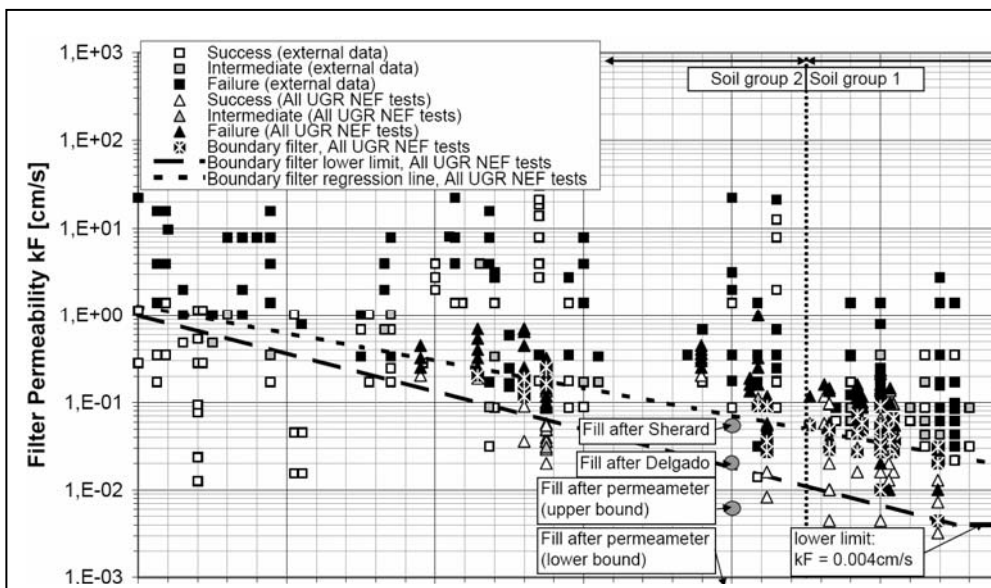


Figure 10: Delgado relationship between % base soil passing 0.075 mm sieve and filter permeability [3]

Using the Delgado line on Figure 10, the required permeability of the filter to trap the core with 80% (of the below 4.75 mm grading) passing 0.075 mm is 2.0E-02 cm/s (2.0E-04 m/s). The permeability of the fill calculated by the Sherard formula with D_{15} of 0.4 mm is 5.6E-02 cm/s, more than twice as high as required and the 'simple' approach suggests that the fill would be too permeable to filter the core. Using the Delgado regression curve for a compacted filter (**Figure 11**) shows that the permeability is 2E-02 cm/s, exactly the required value of 2.0E-02 cm/s, indicating that the fill would filter the core. The permeability of the fill measured in the permeameter was between 1.2E-04 and 6.0E-03 cm/s, again indicating that the fill would filter the core.

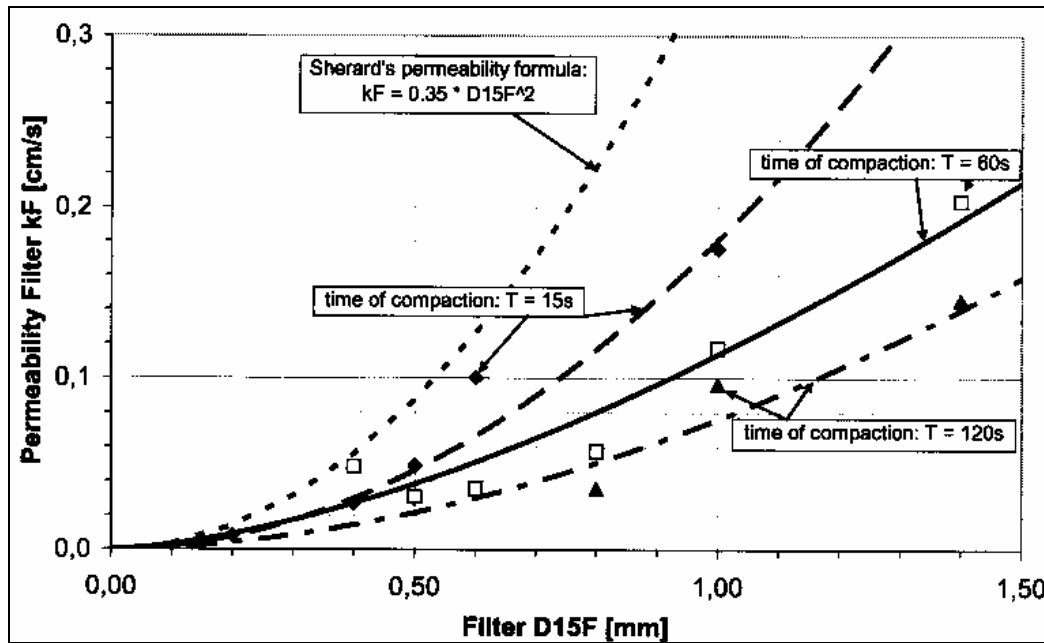


Figure 11: Delgado relationship between D_{15} and permeability of filters [3]

8 Estimated Probability of Erosion using Foster & Fell's Method

Foster & Fell [4] [5] use the method of logistic regression, already applied by Honjo & Veneziano [8], to replace deterministic no-erosion criteria by a probability-based approach. This allows for state-of-erosion criteria being viewed as gradual rather than strict. According to this methodology, the conditional probability of a data point which is characterized by a vector of parameters x_i for showing some defined property C, is defined as follows:

$$P(C | x_i) = \frac{e^Z}{1+e^Z}, \quad (3)$$

where e is Euler's number and Z is the general function $Z = \omega_0 + \sum_{i=1}^n \omega_i x_i$. ω_i are weighting factors

which are calibrated using available data.

In the present case, C is the "showing of erosion" in filter tests, e.g. the NEF test which is used by Foster & Fell [4] in order to extend existing data bases.

The core material in the present study shows a $pp_{0.075B}=80\%$, i.e. the percentage of grains of the base soil finer than a particle size of 0.075 mm. According to Foster & Fell [5], this soil is classified as being in Soil Group 2A, ranging from $pp_{0.075B}=35\%$ to $pp_{0.075B}=85\%$, for which no apparent relationship between the base-filter interaction and grain-size characteristics of the base soil can be identified (see also Sherard & Dunnigan [2]). Therefore, Z in the logistic regression function is only dependent on D_{15F} of the filter. As Foster & Fell [4] do not give the mathematical definition of Z for soil group 2A, it has to be approximated from the graphical representation in [4] and the given information that $P(\text{failure}|D_{15F}=0.82 \text{ mm})=0.5$. This approximation gives the function $Z \approx 3 \cdot (D_{15F} - 0.82)$. Introducing the $D_{15F}=0.2 \text{ mm}$ to $D_{15F}=0.4 \text{ mm}$ of the dam investigated in this paper (**Figure 6**), the probability of erosion is calculated as $P(\text{erosion}|D_{15F}=0.2 \text{ mm})=0.13$ to $P(\text{erosion}|D_{15F}=0.4 \text{ mm})=0.22$. The probabilities

are in both cases not insignificant but low. It is important to note that the probability here is the general probability that the till shoulder fill is able to filter the core soil without any, or at maximum with a very small, loss of mass of core material. The expressed uncertainty concerning the ability of filtration stems from the multitude of additional influencing and partially unknown parameters which cannot be included into a profound quantitative probabilistic regression equation yet. Local deviations in the characteristic parameters of core and fill may still occur and lead to some local erosion. These effects are not covered by the probabilistic assessment. But overall, for the soils present in the dam a potentially critical continuation of erosion leading to failure could occur at an even lower probability than 0.13 to 0.22.

9 Seepage Velocities to Initiate Erosion

The initiator of internal erosion is the energy available from the velocity of seeping water to erode soil particles from the walls of seepage channels. Both the upstream and downstream shoulders of the dam are in glacial till fill of low permeability which may limit quantity and velocity of water reaching any flow channels through the core. However, the core may behave as non-cohesive silt, and seepage velocities as low as 0.012 m/s may be sufficient to initiate erosion [9]. Very approximate flownet analysis examining flow towards a 10 mm high crack at about one-third height of the core into which water flows from the isotropic upstream shoulder and escapes 'freely' along a shorter flowpath through the isotropic downstream shoulder into a downstream drain, gave the results in Table 1, suggesting that initiation may occur.

However, calculation of the hydraulic condition of the filter, as presented by Fry [12], leads to the conclusion that tolerable erosion will occur if the permeability of the fill is 6.0E-05 m/s or less. The hydraulic head through the core will decrease as the discharge flow increases, in consequence the flow velocity will decrease down to the critical value and internal erosion will stop associated to a maximum value of total discharge flow around several litres/second, indicating that should initiation occur, the fill would filter the core.

Table 1: Velocity and potential to cause and continue erosion through 0.01 m high opening through core assuming measured permeabilities of fill in upstream and downstream shoulders

Density of fill (from Figure 6)	Permeability (m/s) (from Figure 6)	Velocity through 0.01 m high opening (m/s)	Outcome
Low	6.0E-05	0.13	Ten times greater than 0.012 m/s, erosion likely to be initiated
Medium	3.8E-05	0.085	Seven times greater than 0.012 m/s, erosion may be initiated
High	1.2E-06	0.0027	Less than 0.012 m/s, erosion not likely to be initiated

10 Conclusions to Date

Although its performance gives no reason for concern, the objective of the investigations is to assess the dam's ability to resist internal erosion. As it is old, it can be assumed that no large openings exist through which flow could occur at a velocity high enough to initiate erosion and lead to piping and failure. The mechanism envisaged is erosion in a (possibly new) discontinuity through the core, and the question is whether the adjoining glacial till fill would act as a filter, restricting velocity and trapping eroded particles to prevent initiation and continuation of erosion.

There are four absolutely re-assuring results to date:

- Two of the Delgado permeability results: for permeability assessed from the Delgado curves and from the permeability measured in the large-scale laboratory tests
- The Sherard no erosion filter test showed the fill to act as a filter to the core.
- Although the grading of the fill was not entirely within the limits required for a Category 2 Sherard filter, it did satisfy the important D_{15} filter criteria.
- Fry's [12] approach, which by analysis reaches a conclusion that engineering intuition would reach, namely that fine non-cohesive low permeability fill seems unlikely to be eroded.

The Foster & Fell [4] [5] probability-based approach is moderately re-assuring. It suggests probabilities of initiation of erosion of 0.13 to 0.22. But in general, the Foster & Fell [4] [5] method gives an indication of the probability of erosion without allowing any conclusions to be made concerning its development. Particularly it does not indicate a failure of the filtration process in a way that erosion or an increase in seepage may reach critical values concerning the stability of a whole dam. Foster & Fell [4] [5] introduce additional deterministic criteria in order to prevent 'excessive' and 'continuing' erosion. Excessive erosion means that the loss of core material through the filter pores is significant but the erosion comes to an end which is defined by some stable crack or erosion pipe in the core. Between no-erosion and excessive erosion infinite states of successful filtration and thus finite erosion are possible. For the soils investigated in the present paper the criterion for excessive erosion is defined as $D_{15F}=9 D_{90B}$, the criterion for continuing erosion as $D_{15F}=9 D_{95B}$. From $D_{90B}=0.25$ mm it can be concluded that the investigated base-filter-system is probably far away from showing even 'excessive' erosion. This statement is supported by the fact that, as the dam is over 100-years old, has shown no sign of any erosion.

The results from the Vaughan and Soares 'perfect' permeability approach are not re-assuring. The approach requires that the floc sizes are determined. Samples are not dispersed as in the conventional 'critical' filter approach. In this case, it appears that very small flocs or particles (smaller than 0.45 microns) are present. The undispersed properties of the fill show it to be predominantly silt-sized, and consequently more erodible than the clay it appears to be when dispersed conventionally. The permeability of the fill is low and, where dense, could trap particles or flocs with an equivalent diameter of only 0.3 microns. However, the permeability may not be low enough to trap between 7% and 29% of the core, the loss of which would cause considerable damage to the dam. No such losses have occurred, suggesting that no discontinuities through the core have developed and/or that the fill in-situ is generally sufficiently dense to filter the core. If the core behaves as non-cohesive silt it could not sustain an open

crack when saturated, a further factor explaining the satisfactory performance of the dam to date.

11 Suggestions for Further Work

The Sherard approach, the Delgado approach and the Foster & Fell approach rely on the no-erosion filter test to confirm the efficacy of the grading or permeability of filters. This recognises that in critical situations some movement (i.e. erosion) of fine particles occurs from the base soil into the filter thereby modifying the grading of the filter in-situ to change it to the grading required to prevent any further movement from the base soil. This process is called 'self-filtering'. The Vaughan and Soares approach seeks a perfect filter, one that will not permit any losses from the base soil. Kleiner [10] [11] quotes Sherard as recognising that his filters are successful because of self-filtering, and that he regarded this as sufficiently conservative because silt sized relatively mobile particles would be present and available to make a perfect filter before conditions leading to accelerating and catastrophic erosion could become established. Fry's [13] analysis links the two approaches.

As the crucial question for dam safety engineers is not whether internal erosion could occur but whether after initiation it would accelerate and proceed to failure too rapidly to take evasive action, further evidence should be found to support Sherard's conclusion. This could include analysis of the performance of similar types of embankment dams, including assessment of incidents, to develop an ability to quantitatively assess the probability of failure from internal erosion as has proved possible in Britain [13]; from case studies, from laboratory work, and by analytical methods, such as those of Fry [12] and of Bonelli, Steeb, Perzlmaier and their co-workers [14].

Acknowledgments

Thanks go the dam's owners for allowing publication of this paper and to the many members of the dam owner's staff and our professional colleagues for their support and assistance in carrying out this work.

Literature

- [1] Vaughan P R & Soares H F 1982. Design of filters for clay cores of dams. ASCE Journal of Geotechnical Engineering Division, January, Vol 108 (GT1) 17-31. [2] Sherard J L & Dunnigan L P 1989. Critical filters for impervious soils. ASCE Journal of Geotechnical Engineering Division, January, Vol 115 (GT7) 927-947.
- [2] Sherard J L & Dunnigan L P 1989. Critical filters for impervious soils. ASCE Journal of Geotechnical Engineering Division, January, Vol 115 (GT7) 927-947.
- [3] Delgado F, Huber N P, Escuder I, & De Membrillera M G 2006. Revised criteria for evaluating granular filters in earth and rockfill dams. Transactions of the 22nd Congress, International Commission on Large Dams, Barcelona, Vol III, Q86 R29, 445-456

- [4] Foster, M.A.; Fell, R. (1999): Assessing Embankment Dam Filters which do not Satisfy Design Criteria. Sydney, Australia: The University of New South Wales (Report / UNICIV; R-376). - ISBN 85841-343-4
- [5] Foster, M.A.; Fell, R. (2001): Assessing Embankment Dam Filters That Do Not Satisfy Design Criteria. In: Journal of Geotechnical and Geoenvironmental Engineering, Vol. 127, No. 5, pp. 398-407. - ISSN 1090-0241
- [6] Vaughan P R & Bridle R C 2004. An update on perfect filters. Long-term benefits and performance of dams. Proceedings 13th conference of the British Dam Society and European Club of ICOLD, University of Canterbury, UK, 22-26 June 2004, Thomas Telford, London, 516-531 (the 'original' paper, corrected in the version above. Please contact rodney.bridle@damsafety.co.uk for additional copies of the corrected paper if required).
- [7] USDA Soil Conservation Service 1986. Guide for determining the gradation of sand and gravel filters. Soil Mechanics Note No 1 210-VI. United States Dept of Agriculture, Soil Conservation Service, Engineering Division, Washington
- [8] Honjo, Y.; Veneziano, D. (1989): Improved Filter Criterion for Cohesionless Soils. In: Journal of Geotechnical Engineering, Vol. 115, No. 1, pp. 75-94. - ISSN 0733-9410
- [9] Bridle R C 2005. Assessing the vulnerability of dams to internal erosion. Symposium on Internal Erosion in Dams, Aussois, France, April 2005, in print.
- [10] Kleiner D E 2005. A review of filter criteria for embankment dams. Technologies to enhance dam safety and the environment, 25th Annual USSD Conference, Salt Lake City, Utah, June, 1-12, 631-644
- [11] Kleiner D E 2006. A review of filter criteria – embankment dams. Transactions of the 22nd Congress, International Commission on Large Dams, Barcelona, Vol III, Q86 R39, 565-580
- [12] Fry J-J & Blais J-P 2006. Assessment of internal erosion risk of embankment or rockfill dams. Transactions of the 22nd Congress, International Commission on Large Dams, Barcelona, Vol III, Q86 R69, 1131-1141
- [13] Brown A J & Gosden J D 2004. Interim guide to quantitative risk assessment for UK reservoirs. Thomas Telford, London. ISBN 0 7277 3267 6.
- [14] Preparation of the Final Report, European Working Group on Internal Erosion, Aix-les-Bains, France, 16-17 April 2007

Authors Names and Affiliations

Rodney Bridle
Consulting Civil Engineer, United Kingdom
rodney.bridle@damsafety.co.uk

Dr Fernando Delgado
Associate Professor
Faculty of Civil Engineering
University of Granada, Spain
fdelgado@ugr.es

Nils P. Huber
Senior Research Engineer
Institute of Hydraulic Engineering and Water Resources Management
RWTH Aachen University, Germany
huber@iww.rwth-aachen.de

Clogging Evaluation Opermeable Soil Filters

A. Benamar, A. Elkawafi, A. Alem, H. Wang

Abstract

The clogging of the void spaces within the permeable soil filters by eroded fine particles can severely reduce its drainage capacity. This will, in turn, reduce the service life of the permeable soil filters within dams and dykes. This study is devoted to deposition of kaolinite clay in sand and glass beads filters at various flow rates and different particle concentrations. The reduction in the vertical permeability of several soil filters as a result of clogging is investigated, and the depth of particle penetration is also analysed. The research results clearly show under what conditions soil clogging occurs and how to mitigate this problem. Maximum clogging occurs only in the upper lay of the bed and is dependent on the suspension concentration, pore structure and flow rate. The reduction in permeability of the filters is expressed as an equation of the initial permeability of the filters, porosity, amount of clogging material retained, and an experimental coefficient. Experimental data indicate exponential depth dependence of particle accumulation. The theoretical predictions of an analytical model have been compared with experimental results, with good agreement. The results describe the increased clogging that is always observed in the top of a filter.

1 Introduction

Detachment and mobilization of fine particles are important considerations both in soil erosion and in transport and fate of colloidal contaminants. The phenomenon of induced fines migration is of concern of both scientific and industrial fields. It finds application in flow in porous media when severe formation damage occurs, in the migration of wastes, in the ineffective regeneration of filter beds, and in the failure of earthen dams and dykes. Internal erosion involves detachment of fine particles whose the subsequent mobilization and transport is related to the clogging occurrence. Permeability reduction caused by particle deposition (physical clogging) in porous media is important in filter beds. Soil filters, which are commonly used to provide stability and drainage in dams and dykes, are prone to long-term accumulation of fine micron-sized particles. This causes reduction in the permeability, which in turn may lead to intolerable decreases in their drainage capacity and uplift pressures in the core. The flow of suspended particles through a filter is a complex phenomenon owing to define two mechanisms in deep filtration: a mechanical filtration for large particles and a physicochemical filtration for small particles (Herzig et al, 1970). When flowing through porous medium, the particles are brought in contact with retention sites; they stop there or are carried away by the stream. The deep filtration is therefore the result of several mechanisms: the contacting of particles with the retention sites, the fixing of particles on sites, and eventually the breaking away of previously retained particles. During the flow of the suspension through a porous medium, particle transport and capture result from several forces and mechanisms, depending on particle size. The flow results obtained by Khilar et al. (1987) elucidate the interaction of colloid chemistry and hydrodynamics in entrapment and release of fine particles. The release occurs below a critical

salt concentration and above a critical flow velocity. The capture of fines at the pore constrictions is partly due to direct interception and partly due to size exclusion. Several studies have noted that, for a given mass of deposited material, experiments conducted at greater fluid velocity show greater permeability (Mays et al., 2005). Previous researchers have recognized the importance of deposit morphology during long-term particle retention in saturated porous media. The different mechanisms leading to permeability damages due to particle deposition were analysed under various situations by Nabzar et al. (1997). They noted the influence of hydrodynamic forces and the effects of the location where the particles are deposited on permeability. Piping in hydraulic structures occurs when seepage gradients are high enough to produce erosive discharge velocities in the base soil. Filters are placed in embankments zones of hydraulic structures in order to prevent the erosion of soil particles by water passing through the openings. The most generally accepted retention criteria was proposed by Sherard et al.(1989) and based on D_{15F} and d_{85B} which are the diameters of filter and base particles for which 15% and 85% of the entire mass is finer, respectively. Almost engineers agree with the idea that D_{15F}/d_{85B} represents the effective criteria to design granular filters, but compaction and permeability of the filter is also very important. Delgado et al, (2006) concluded to a significant influence of filter compaction and permeability, and the most representative diameter is the d_{70B} . He also noted that hydraulic gradient has an important and negative influence on filtration. In Sherard and Dunnigan (1989) tests, the concentration of particles and the flow rate were not controlled and many parameters were varied. Khilar et al. (1987) used a capillary model for clay particle dispersion (detachment) in porous media to study piping and plugging mechanisms in earthen structures. They do not distinguish between size distributions of particles in suspension, and assume that particle trapping does not occur until the concentration of clay particles in suspension reaches a certain threshold value. The physicochemical filtration of colloidal particles in saturated porous media was studied by Tufenkji et al. (2004) and a new equation for predicting the single-collector contact efficiency is presented. The correlation equation is developed using the sum of the contributions of the transport mechanisms. Frey et al. (1999) focused on physico-chemical effects which were shown to drive not only deposit distribution in the porous medium but also the clogging process.

In this experimental study, a sandy soil or glass beads, used as a filter, was subjected to pore fluids containing kaolinite particles. Experimental flow tests were performed at various flow rates and different particle concentrations. This work identifies the main phenomena that control the transport and deposition of clay particles in a sand core. The reduction in the vertical permeability as a result of clogging has been studied. Under constant flow conditions, clogging is observed through a head loss and the amount of deposited particles. The concentration of particles in the pore stream affected the rate at which the permeability reduced. We demonstrate there is a consistent relationship between head loss data and imposed flow velocity. Most laboratory experiments are conducted under constant flow conditions while many situations operate under constant head conditions, which would suggest that deposit morphology changes with time as the velocity decreases. The objectives of this study are the investigation of the conditions under which clogging occurs, the identification of the parameters governing the particle retention, and the modelization of permeability reduction in the filter. To prevent any pore bridging, dilute suspension of Kaolinite particles having a size much smaller than that of pore throats were injected at low Peclet number (from 24 to 64). Clay particles are

progressively deposited onto pore surface, reducing pore size and thus permeability. Preferential particle deposition occurs in the upper part of the column. Permeability damage is observed to occur mainly at low velocities. A model is used to predict both deposition kinetics and subsequent permeability reduction.

2 Experimental Device and Permeameter Tests

Laboratory flow tests were performed in a vertical column under constant flow conditions in the first part and under constant head conditions in the second part. The column is 400 mm length and 40 mm diameter and packed in 5 cm increment by pouring the material (glass beads, sand) into the pre-filled column with fresh water. Six piezometers are installed along the column in order to carry out the permeability reduction during the filtration tests. The column is fed by two reservoirs containing water (pH of 6.8 ± 0.1) and suspended particles, using a peristaltic pump. As the porous medium is saturated the flow toward the column is switched to particle suspension. Figure 1 shows the configuration of the experimental device under constant flow conditions. The detection system consists of a Fisher Instrument turbidity meter which determines the turbidity level by measuring the amount of light scattered at 90° by the suspended particles. The particle concentrations in the effluent were determined with the help of correlations made a priori between suspended particles concentrations in water and turbidity. Four silica sands and glass beads are used as porous media, and their grain size distribution are presented on figure 2. The porosity obtained is close to 36%, except the coarser sand (number 4) which make a porosity of 40%. Suspended particles used are kaolinite clay whose 90 % of particles have a size less than 10 μm and D_{50} close to 1.2 μm . These clay particles are used because of their small size and their non-dispersive property and low electrochemical activity.

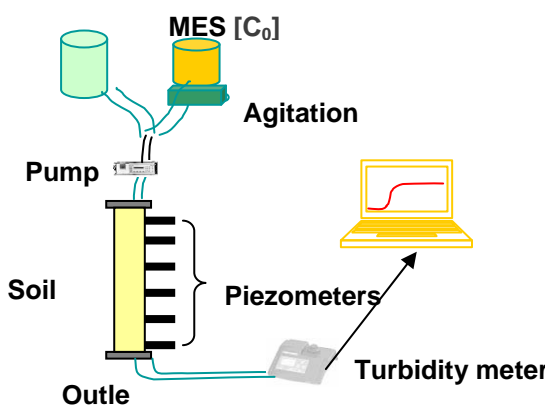


Figure 1: Schematic draw of experimental set-up

Different concentrations of suspended particles are used and particle retention is determined through the concentration reduction at the outlet of the column. After each test, the soil sample is extracted carefully from the column in slices and analysed to determine the mass particle retained during filtration at a given location from the top of the column. During these experiments, the main operating parameters, i.e. particle concentration, flow rate and soil filter permeability were systematically varied.

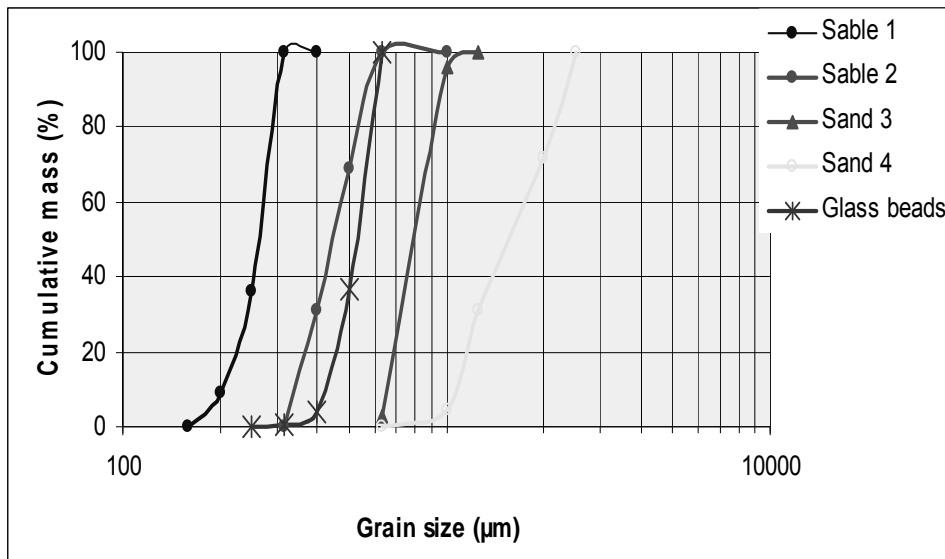


Figure 2: Grain size distribution of used materials

3 Filtration Process and Permeability Reduction

The objective of this section is to outline the influence of clogging in permeability variations during the flow in the soil filter of particle suspension. As pointed out before, the deposition process is governed by two kinetic phenomena: 1) the transfer of the suspended particles from the bulk phase to the interfacial zone and 2) the attachment to the collector surface. The suspension flowing within the filter makes the particles to be retained in the soil porosity, dealing to the permeability damage process. This permeability reduction caused by the in-depth retention of small particles is analysed. This analysis leads to the definition of deposition kinetics in the soil filter, which depends on both the flow rate and the mechanism determining permeability damage. As a consequence of deep-bed filtration process, fluid pressure (measured through water head) increases (**figure 3**). Pressure increase concerns the top part of the filter (4 cm), as observed in the two first piezometers. Hydraulic gradient increases strongly in this first part, reaching a value of 1.8 after a flow time more than 5 hours. The pressure evolution along the filter shows that the major clogging occurs at the front of the filter and even at high particle concentration the filter reminds operating without infinite increase of pressure. We can also observe in figure 3 the particle deposition kinetics which shows the overpressures moving in time from the front of filter to the toe with several decreasing in magnitude.

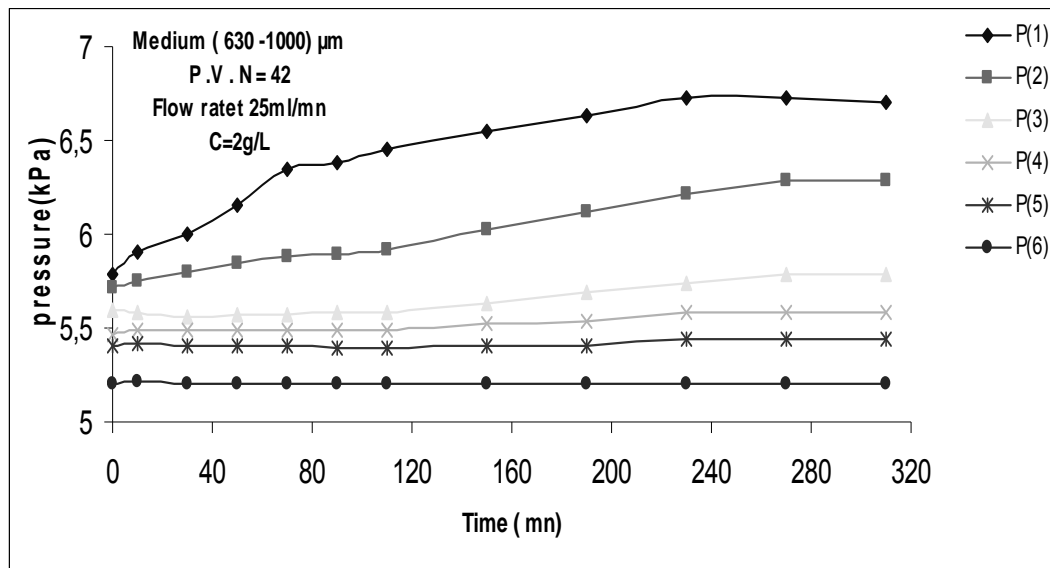


Figure 3: Evolution of uplift pressures along a soil filter during time

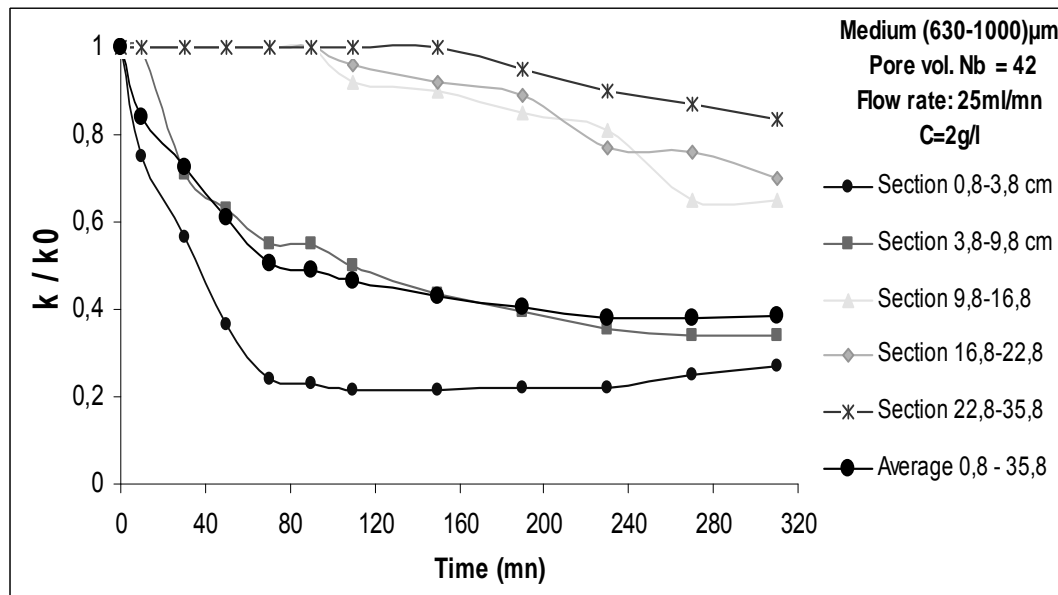


Figure 4: Permeability reduction along a soil filter during filtration test

The corresponding permeability reduction, subsequent to the pressure increase, is shown in figure 4. All available data indicate the non linear distribution of permeability reduction along the soil column, and the drastic reduction occurs in the up thin layer. The results (figure 4) shows 80 % reduction in the first section and 60 % reduction in the following one, and the permeability is slightly modified over this up layer. Data available with various concentrations of suspended particles show that permeability reduction increases with particle concentration but such parameter does not affect the distribution of permeability reduction along the soil filter. The influence of granular size distribution on permeability reduction is not evident. Experimental results indicate a same magnitude of reduction at the first slice of the filter, except for the finer sand (160 – 315 μm) where the reduction is higher, reaching more than 90 % of the initial permeability. The above results show that the filtration and clogging are controlled by the thin up layer of the soil filter.

The flow rate has a considerable influence on the permeability reduction in the first layer of the soil filter. Figure 5 shows the variation of the permeability in the upper slice (3.8 cm thickness) of the filter with a several decrease during the first phase (until 10 pore volumes), particularly for the lowest flow rate (25 ml/mn). As flow rate decreases, permeability reduction increases, showing the effect of particle velocity in the filtration process. For the lowest flow rate, permeability reduction operates quickly and then the filter permeability remains constant, while for higher flow rate the permeability reduction operates progressively. This reduction, inversely proportional to the flow rate, is nonlinear, describing an exponential permeability reduction.

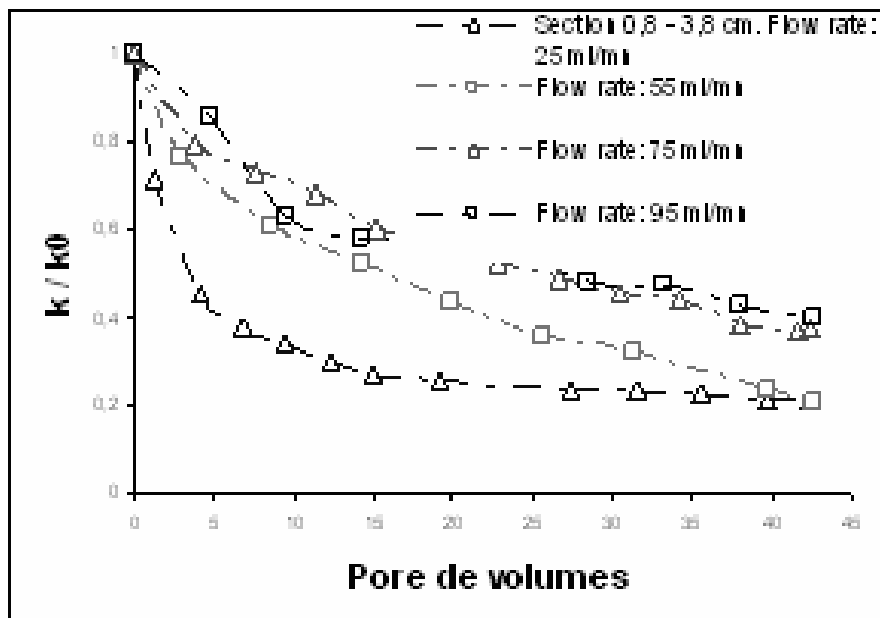


Figure 5: Influence of the flow rate on the permeability reduction

From the observed dependence of clogging on velocity we can propose that fluid velocity controls mainly deposit morphology, rather than the depth of particle penetration. This result shows that the upstream part of the filter controls the permeability reduction.

4 Deposit Distribution in Clogging Filters: Depth Dependent Filtration

Filtration theory predicts an exponential distribution of particles only in the initial phase of deposition, but an exponential deposit is more realistic than a uniform deposit. All the available data indicate no uniform particle distribution, even for low particle concentration. After each test, the soil sample is extracted carefully from the column in slices and analysed to determine the mass particle retained during filtration at a given location from the top of the column. The variation of filter porosity is then deduced slice by slice. Figure 6 below shows porosity reduction in the finer soil filter along the column for the larger concentration and the lowest flow rate. Particle deposit distribution is exponential and the porosity reduction operates mainly in the first 10 cm of the soil filter, leading to the drastic permeability reduction observed above. The depth of particle penetration is important because clogging is non linear with mass deposit. Other

things being equal, a filter with a double mass deposit in the top half and zero in the bottom half will be less permeable than a filter with a simple mass deposit throughout.

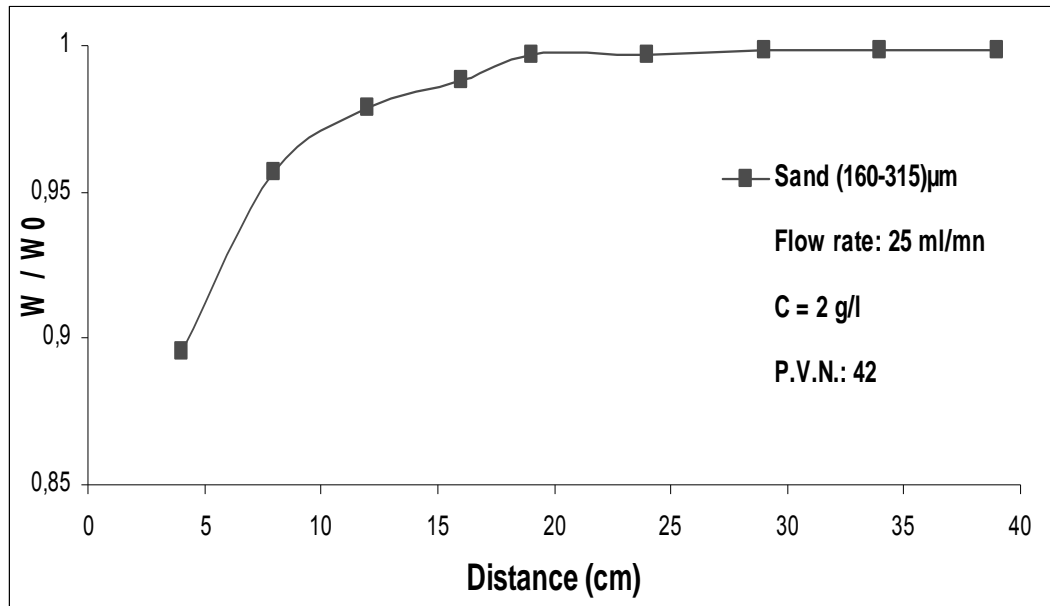


Figure 6: Porosity reduction and particle deposit along the soil filter

5 Modelization of Permeability Reduction and Particle Deposit

Particle deposition and deposit morphology depend on the characteristics of the porous media, the depositing particles and the fluid flow field. To model particle penetration quantitatively, permeability data and deposit mass taken at intermediate points along the filter will be analyzed to suggest a simple functional relationship for the deposit distribution.

To highlight the influence of particle deposit and porosity reduction on the permeability reduction, the approach similar to that presented by Ochi (1994) is used. Equation 1 below modelizes the average permeability reduction in the filter as a power function of mass deposit.

$$\frac{k}{k_0} = (1 - a \cdot \delta_{dp})^m \quad (1)$$

where m and a are positive parameters depending on experimental conditions, and δ_{dp} is the particle mass deposit within the filter.

For these data, $m = 3$ and $a = 0,014/(2,45 \cdot D_{50})$

This simple formula does not include explicitly the hydrodynamic effect on clogging. Analytical results obtained are matched with experimental data and figure 7 shows a good agreement, leading to a good representation by equation 1 of the average permeability reduction in the filter. This model allows the use of global parameters like total mass deposit to describe the permeability change at every time during suspension flow within the filter.

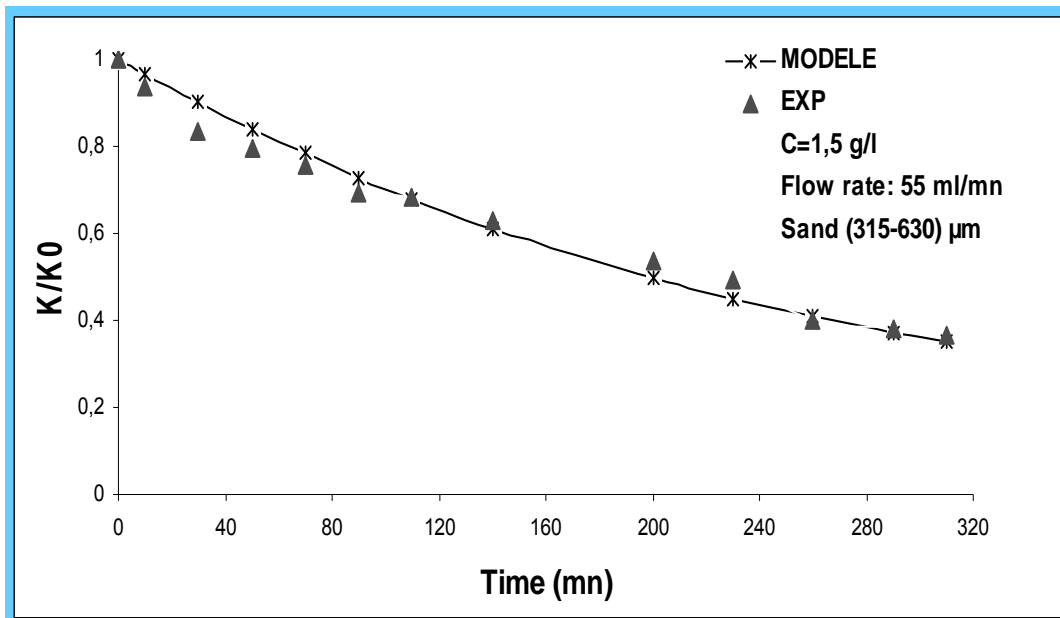


Figure 7: Adjustment of experimental data by analytical model

6 Granulat Size Selection by the Filtration Under Constant Head

As in field conditions filtration in hydraulic structures the water head is constant rather than flow rate constant, filtration tests under constant head conditions are carried out. The built up pressures in the up layer of the filter are more important than under constant flow conditions. This leads to a severe permeability reduction, more important clogging and large reduction of flow rate. The effects of the water head on the outlet concentration of particles present a linear dependency. The analysis of the size distribution of the particle recovery at various times allows determining the size selection operated by the filter on the suspended particles. Figure 8 shows the results obtained by means of a multisizer analyzer. It is clear that the important part of recovered particles occurs in the first step time of the filtration process. When the porous medium is “clear” (no deposit occurs yet), a large part of fine particles travel through the soil filter and reach the outlet of the column, and so the major part of large particles are retained within the filter. As the filtration process progresses, the porosity damage and the pore pressures increase, making the pore velocity higher and dealing to the mobilization of large particles. The size distribution of recovered particles shows curves approaching the initial distribution during time. This filtration process makes us thinking about the auto-filtration process where the large particles are retained at first in the front section of the soil filter, and then transported later under higher pore velocities.

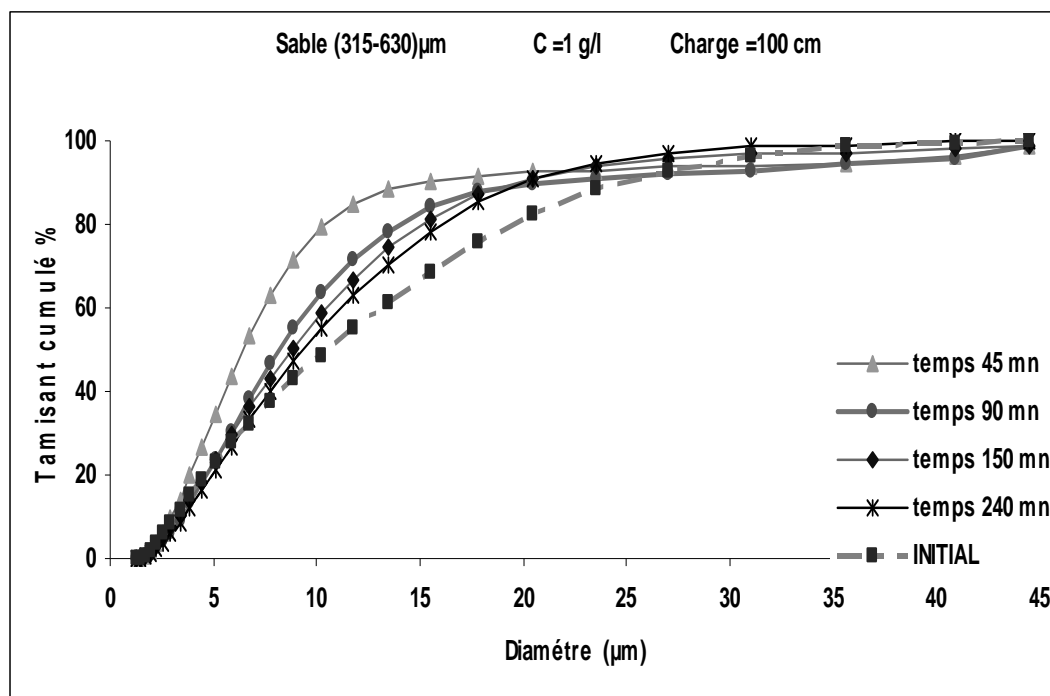


Figure 8: Granular size distribution of transported particles during filtration.

7 Conclusions

Both solution chemistry and hydrodynamics are known to alter the permeability of porous media during particle suspension flow. Few studies have been devoted to the effects of hydrodynamics. Filters must be fine enough and then the pore spaces between the filter particles should be small to hold some of the larger particles flowing through it. But filters must also be coarse enough to allow seepage flow to pass through the filter, preventing built up of high pressures. The finer filter experimented can fail according to Sherard criteria. The results obtained show that filtration and clogging depend on concentration and flow rate. For a given mass of deposited particles, experiments conducted at greater fluid velocity show greater permeability. Maximum clogging occurs only in the upper lay of the bed and is dependent on the suspension concentration, pore structure and flow rate. The reduction in permeability of the filters is expressed as an equation of the initial permeability of the filters, porosity, amount of clogging material retained, and an experimental coefficient. Experimental data indicate exponential depth dependence of particle accumulation. The theoretical predictions of an analytical model have been compared with experimental results, with good agreement.

A new step in dam filter design would be the formulation of a new criterion taking into account parameters which have significant effect on filtration process.

Literature

- [1] Delgado F., Huber N.P., Escuder I., de Membrillera M.G., (2006), Revised criteria for evaluating granular filters in earth and rockfill dams, 22ème Congrès des Grands Barrages, CIGB, Barcelona (Spain), june.
- [2] Frey, J. M., Schmitz, P., Dufreche, I., Gohr Pinheiro, I. (1999) Particle deposition in porous media: analysis of hydrodynamic and weak inertial effects. *Transport in porous media*. 37, 25-54.
- [3] Herzig J.P, Leclerc D.M., Le Goff P. (1970), Flow of suspensions trough porous media, application to deep filtration. *Ind. and Eng. Chem*, Vol. 62, N°5,pp.8-35.
- [4] Khilar K.C., Fogler H.S., (1987), Colloidally induced fines in porous media, *Review in chemical engineering*, vol. 4 N° 1 & 2.
- [5] Kufenkji N., Elimelech M., (2004), Correlation equation for predicting single-collector efficiency in physicochemical filtration in saturated porous media, *Environ. Sci. Technol.*, N° 38, pp. 529 – 536.
- [6] Mays D.C., Hunt J.R. (2005), Hydrodynamic aspects of particle clogging in porous media, *Environ. Sci. Technol.*, N° 39, pp. 577-584.
- [7] Moghadasi J, Müller-Steinhagen H., Jamialahmadi M., Sharif A. (2004). Theoretical and experimental study of particle movement and deposition in porous media during water injection, German Aerospace centre (DLR), Pfaffenwaldring 38-40, D-70550 Stuttgart, Germany.
- [8] Nabzar L., Chauveteau G., (1997), Permeability damage by deposition of colloidal particles, *Society of Petroleum Engineers N° 38160*.
- [9] Sherard J.L., Dunnigan L.P., (1989), Critical filters for impervious soils, *J. of Geotechnical Eng. ASCE*, july.

Authors Name and Affiliation

Benamar Ahmed
 L.M.P.G. Université du Havre, France
 benamar@univ-lehavre.fr

A. Elkawafi
 L.M.P.G. Université du Havre, France

A. Alem
 L.M.P.G. Université du Havre, France

H. Wang
 L.M.P.G. Université du Havre, France

Probabilistic Aspects of Geomechanical Filter Design

A. Wörman, U. Saucke, E.O.F. Calle, J.B. Sellmeijer and A.R. Koelewijn

1 Introduction

Earthfill structures like dikes, embankment dams, coastal revetments and breakwaters generally consist of several sections or zones of granular materials. Differential settlements or deficiencies in the construction procedure often give rise to local defects or anomalies in the filter layers. This means that even structures that are designed according to filter criteria can be susceptible to internal erosion and instabilities. For planning of extra design precautions and possible emergency actions it is sometimes suitable to be able to perform reliability analyses.

An objective of this paper is to provide a state-of-the art summary of selected design approaches that considers probabilistic aspects in filter design. These approaches cover the initiation mechanisms due to both piping in an inhomogeneous soil and internal erosion along interfaces of coarser and finer soil volumes, i.e. the filter-base problem. While the statistics of the hydraulic load is also an important issue, this paper deals mainly with the heterogeneities of the soil strata. The long-term erosion evolution along a heterogeneous filter-base interface is discussed as an aspect of aging and maintenance of erosion protections.

At times the engineer faces the task of evaluating a subsoil area below an embankment structure consisting of fluvial sediments with regard to the susceptibility of erosion under a given hydraulic load. In such context the analysis should focus on a limited area of the subsoil considered as a whole and should explore the spatial heterogeneity in detail on the basis of drillings with great care. This procedure would seem to be more appropriate for the assessment of the susceptibility to erosion than the analyses of discrete interfaces between two samples of a drilling.

Piping, or backward erosion, at the top of a sand layer underneath a clay dike along a river can be a serious threat to the safety against flooding, as recently shown in the Dutch Floris study (DWW, 2005). Early design rules, for instance by Bligh (1910) and Lane (1934), have faced much criticism, see e.g. Harza (1934) or the discussion section of Lane (1935). Much later, more sophisticated models emerged, among which Sellmeijer's design rule, which is based on hydro morphologic equilibrium of sand particles in a backward developing erosion pipe (Sellmeijer, 1988). To account for (random) soil variability induced parameter uncertainties, a probabilistic version of this model has been presented in 1989 (Calle et al., 1989). In Sellmeijer's original model the assumption of a uniformly permeable aquifer is an awkward limitation. Therefore, a more general approach will be presented and illustrated in this contribution.

2 Heterogeneities in Soil

Even carefully prepared soil exhibits spatial variations in its properties that can be characterised using geostatistical methods (Webster and Oliver, 1998). Figure 1 shows the porosity variations appearing in a rockfill prepared in a laboratory metal container in a several cubic metres large

volume. Even a careful preparation of the rockfill using a minor power shovel leads to both a depth-dependent separation of the soil and more stochastic deviations of the porosity from the trend. The stochastic deviations can be characterised in terms of the semi-variogram that indicates that neighbouring sampling points are likely to have more similar porosities than distant points.

The heterogeneities in soil suggest that soil structures can be susceptible to internal erosion even if designed according to filter rules and that this possibility might be essential to consider both in the design stage and for emergency planning.

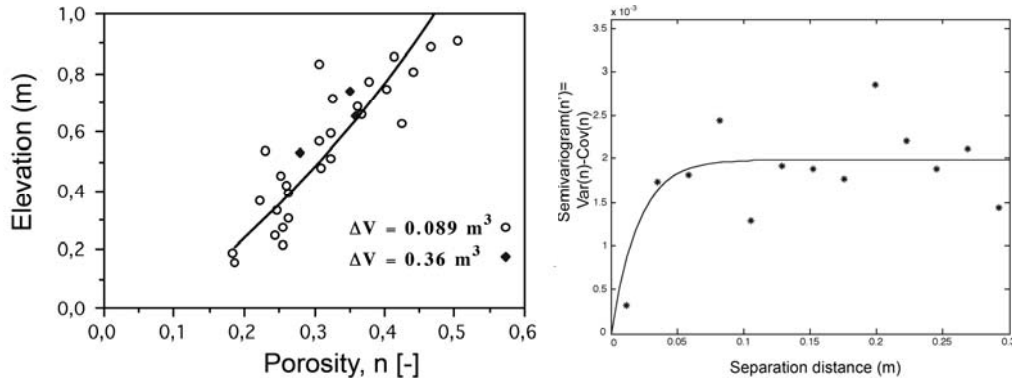


Figure 1: Left-hand side shows porosity variations in a rockfill from the same material as used in the Suorva rockfill dam in Northern Sweden. The material was prepared in a laboratory container with a horizontal area of 2.98 m^2 and the porosity was measured by stepwise rising the water level with 3 cm and 12,5 cm in two series, respectively (black circles and blue diamonds). The right-hand diagram shows the semivariogram for the spatial variations of porosity from the trend.

3 Various Mechanisms of Internal Erosion

3.1 Filter Stability

Internal erosion can occur either as a selective erosion process in a stratified material or as a fluidized channel of the soil. The traditional filter test assumes a fine-grained base material placed on top of the coarser filter material and a very high hydraulic gradient is applied perpendicular to the filter phase. In such tests with non-cohesive and narrow graded soils it has been found that stability versus instability is relatively well-defined by

$$\frac{D_{15}}{d_{85}} = a \quad (1)$$

where D_{15} is the 15%-percentile of the filter grain (sieve) size [m], d_{85} is the 85%-percentile of the base grain size [m] and a is an empirical factor. For a geometrical closed filter, a value of $a = 9$ can be taken (Sherard et al., 1984a). Alternatively, a geometrical open hydraulically stable filter may be applied, with a lower value for a but with additional criteria (den Adel et al., 1994). Similarly, it was found that cohesive base soil is closed and resists internal erosion up to a ratio of 56 (Sherard et al., 1984b).

In most design situations, the filter layer is placed either on-top of the base or the interface between the materials are oriented more or less vertically (**Figure 2**). Several investigations with non-cohesive soil show that initiation of erosion can occur when the D_{15}/d_{85} -ratio is below about 8, but the ratio depends on the hydraulic load applied (Graauwe, 1983, Brauns, 1985). It has also been found that the rate of permissible erosion can be an important factor for the long-term fate of this criterion (Wörman and Olafsdottir, 1992).

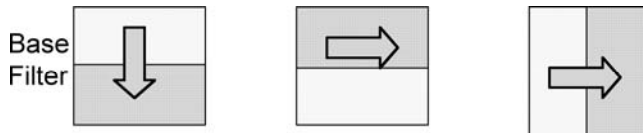


Figure 2: Different possible orientation of the base and filter material as well as different hydraulic load

3.2 Heave

Heave is generally associated with fluidization of the soil and the local fluidization occurs if the pressure gradient in the vertical direction z exceeds the weight of the submersed soil, i.e.

$$\frac{\partial p}{\partial z} > (1-n)(\rho_s - \rho_w)g \quad (2)$$

in which p = water pressure [Pa], n = soil porosity [-], g = acceleration due to gravity [m/s^2], ρ_s = density of solids [kg/m^3] and ρ_w = density of water [kg/m^3]. The fluidization of an entire soil channel depends on the conditions for backward piping and the entire flow domain geometry.

3.3. Piping

Piping is a similar mechanism as heave, but horizontally oriented. This erosion process occurs below water retaining structures due to seepage from the high head to the outflow point. Usually, this outflow point is a ditch or a crack in the impervious layer covering the aquifer (see **Figure 3**). In order to deal with too high outflow seepage pressures, pipes are formed below the embankment. This eases down the seepage pressures in the aquifer.

The length of the pipes corresponds to the hydraulic head across the structure. If the head increases, the length and thickness of the pipes will increase. A new equilibrium will be reached. The particles at the bottom of the pipes are in a state of limiting equilibrium. However, beyond a critical hydraulic head no longer equilibrium is found. The dike will collapse by progressive erosion.

The mechanism of piping is described in *Engineering tools for piping – neural networks created using FEM* of this European workgroup report. A FEM based computation model is available to predict the critical hydraulic head, as a function of subsoil geometry and soil properties of the aquifer. Yet, the use of such model in probabilistic reliability analyses would involve unacceptable computational burden. In order to reduce computation effort for such analyses, the numerical prediction model has been factorized, as shown in equation (3):

$$\frac{\Delta H_{crit}}{L} = \lambda F(\text{scaled geometry, permeability contrast})$$

where

$$\lambda = \frac{\pi}{3} \eta \frac{\gamma_p - \gamma_w}{\gamma_w} \frac{\sin(\theta + \alpha)}{\cos(\theta)} \sqrt[3]{\frac{g}{k\nu} \frac{d^3}{h}}$$
(3)

Further, ΔH_{crit} = critical (i.e. allowable) fall of potential head across the dike or dam [m], h = thickness of granular layer susceptible to piping (m), F = function of, H = hydraulic head across structure [m], L = width of structure [m], d = particle diameter of the granular layer potentially susceptible to piping [m], g = gravitational acceleration [m/s^2], k = hydraulic permeability [m/s], α = channel slope [DEG], γ_p = unit weight of particle material [N/m^3], γ_w = unit weight of water [N/m^3], θ = granular bedding angle [DEG], η = White's constant [-] and ν = kinematical viscosity [m^2/s].

The factor λ is the resistance against erosion in the pipe. It is an invariance in the process and depends only on the soil properties of the sand layer susceptible to piping.

The other factor in equation (3), $F(\cdot)$, is a function of the scaled geometry and the contrast of the hydraulic permeabilities of the soil layers (see **Figure 3**). Basically, the evaluation of this factor is computationally complex and can only be achieved by numerical (FEM) analysis. For this part, the technique of artificial neural network has been applied to provide a fast solution.

A numerical computation can be made arbitrary complex by considering every geometrical detail of the subsoil. In a probabilistic analysis, however, the key influences only should be involved in order to determine a suitable bandwidth of the risk. Therefore, smart geometries with a minimum of characteristic dimensions must be sought. For piping such geometries always consist of two layers. A top layer, where the pipe develops and a sublayer, which controls the water flow to the top layer.

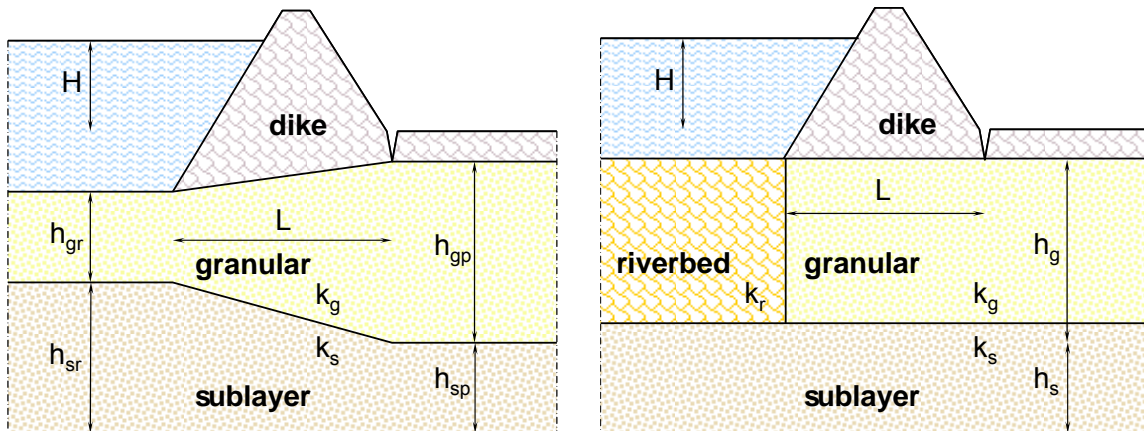


Figure 3: Geometry with sloping dike (left-hand side) and geometry with riverbed (right-hand side)

Examples of suitable geometries are presented in figure 3. The figure on the left shows a geometry of 2 layers. Their heights at the riverside and at the polder side are different. This

geometry requires 5 characteristic dimensions only; 4 scaled heights and the permeability contrast. Formula (3) reduces to:

$$\frac{\Delta H_{crit}}{L} = \lambda F\left(\frac{h_{gr}}{L}, \frac{h_{gp}}{L}, \frac{h_{sr}}{L}, \frac{h_{sp}}{L}, \frac{k_s}{k_g}\right) \quad (4)$$

$$\lambda = \frac{\pi}{3} \eta \frac{\gamma_p - \gamma_w}{\gamma_w} \frac{\sin(\theta + \alpha)}{\cos(\vartheta)} \sqrt[3]{\frac{g}{k_v} \frac{d^3}{h_{gp}}}$$

The figure on the right in figure 3 shows a geometry of 3 layers. Here, a separate riverbed is distinguished. The heights of the layers are constant. This geometry requires 4 characteristic dimensions only; 2 scaled heights and 2 permeability contrasts. Formula (3) reduces to:

$$\frac{\Delta H_{crit}}{L} = \lambda F\left(\frac{h_g}{L}, \frac{h_s}{L}, \frac{k_s}{k_g}, \frac{k_r}{k_g}\right) \quad (5)$$

$$\lambda = \frac{\pi}{3} \eta \frac{\gamma_p - \gamma_w}{\gamma_w} \frac{\sin(\theta + \alpha)}{\cos(\vartheta)} \sqrt[3]{\frac{g}{k_v} \frac{d^3}{h_g}}$$

The function F of any selected geometry may be specified by an Artificial Neural Network (ANN). Such a network consists of nodes. There are three types:

- input nodes for every input variable
- hidden nodes for transformation
- output node with the result

In order to transform input into output, a large number of calculations is carried out for a proper range of input cases. These results are used to train the network. The degrees of freedom of the hidden nodes are moulded such, that the network yields the proper result corresponding to the pre-calculations. An ANN is accessible as fast and easy as a database.

For the probabilistic analysis appropriate use may be made of schematised solutions as (4) and (5). The sensitivity of the involved parameters is available at a finger snap. Important features only play a role, which assures transparency of the problem at hand. It is recommendable to develop a few simplified geometries, rather than one complicated one.

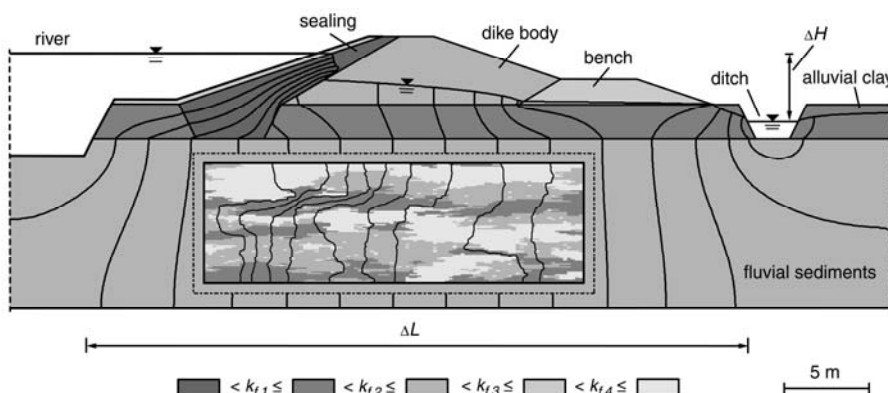


Figure 4: Flood protection dike under hydraulic load with resulting distributions of the hydraulic potential, illustrated for a homogenous (uniformly grey shaded) and for an inhomogeneous (detail inside dotted box) hydraulic permeability distribution.

4 Statistical Analysis of Initiation of Internal Erosion

4.1 Spatially Variable Patches of Coarse and Fine Material

The distribution of the hydraulic potential in a flood protection dike under the condition of a raised water level in the river is shown in figure 4. Areas shaded uniformly grey indicate a homogenous distribution of the hydraulic permeability. Frequently, as a first approximation, the hydraulic design gradient i_0 is defined by the quotient of the hydraulic potential ΔH and an existing seepage distance ΔL . Contrary to the homogenous case, an inhomogeneous hydraulic permeability distribution leads to an irregular distribution of the hydraulic potential which is considerably different from a homogenous one (see detailed image inside the dotted box in **Figure 4**). The irregular distribution of the hydraulic potential results in partly raised hydraulic gradients which could activate erosion processes at the interfaces.

With regard to particle movements parallel to interfaces over longer distances, there are subsoil structures which are regarded as being more susceptible than others because of the type of structure. In particular, irregularly layered structures are more susceptible because of locally increased hydraulic gradients as compared to the hydraulic design gradient i_0 .

This problem led to subsequent research into a method to evaluate subsoil structures as described above with respect to particle movement (Saucke 2004a, 2004b). The method is valid for sediments which consist of uniform sands (B) and gravels (F), separated by lens and layer structures. On the basis of a wide range of numerical simulations and the erosion criterion of Brauns (1985) an evaluation diagram was derived which is presented in figure 5. Use of the diagram requires determination of the geostatistic variability number V_z . The value C_z represents the sill of a semi-variogram in the vertical direction z , calculated on the basis of hydraulic permeability values derived from drilling samples. The value k_B represents the hydraulic permeability of the finer material B. For calculation of the normalized hydraulic permeability in the horizontal direction, k_h can be taken from classic pumping test. Drawing on these values, a critical hydraulic design gradient $i_{0,crit(irreg)}$ can be determined using the plotted curves in figure 5.

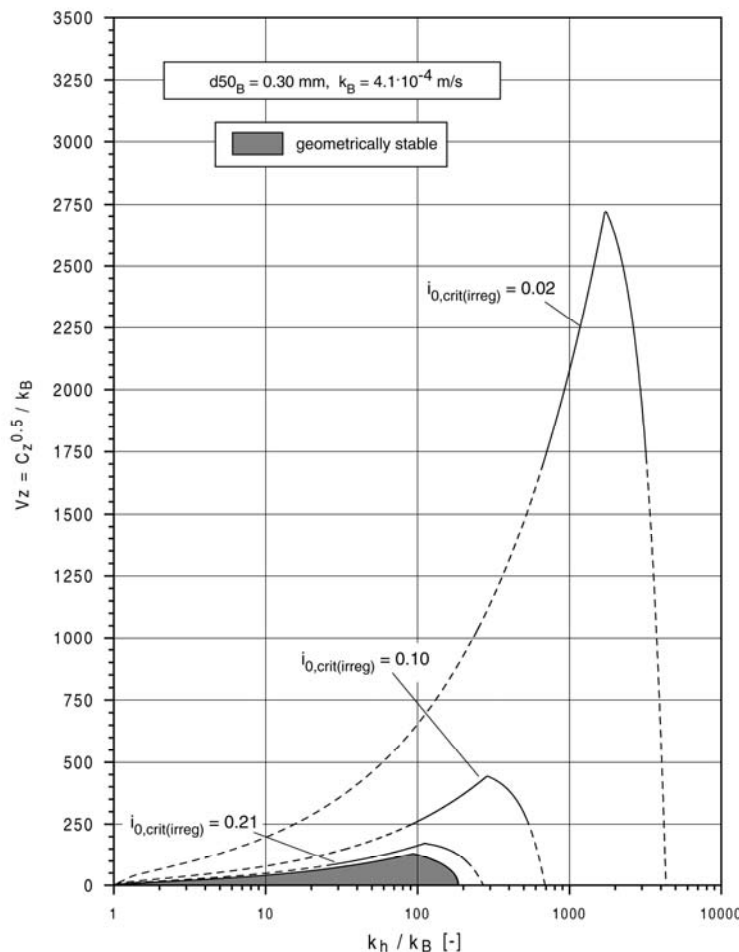


Figure 5: Evaluation diagram for irregularly layered structures for $d50_B = 0.3$ mm with $k_B = 4.1 \cdot 10^{-4}$ m/s

4.2 Probability of Dike or Dam Failure due to Piping

Equations (4) and (5) express the so called critical fall of potential head across the dike or dam. Effectively, this represents the resistance against failure due to piping. Both geometrical as well as physical parameters are subject to random spatial variability, originating from the nature of the processes of sedimentation and erosion in the course of its genesis. Therefore estimations of these parameters may involve considerable uncertainty, thus inducing uncertainty of the predicted critical head fall. Uncertainty of critical head fall may be characterized in statistical terms, i.e. expected mean value and variance, based on statistical characterization of the involved soil parameters.

The extreme head fall across a dike or dam, actually occurring in the course of some specific period of time, usually one year, may be uncertain too in the case of river dikes or sea dikes, and should also be characterized by (extreme event) statistics.

Usually the probability of initiation of piping is conceived as the probability that the actually occurring extreme head fall across the dike, the load ΔH_L , exceeds the critical head fall. It should be noted that the occurrence of extreme head fall relates to a process in time, whereas the critical head fall relates to a more or less time independent state of the dike or dam. The probability of piping can be expressed mathematically as:

$$P_{piping} = P(\Delta H_L > \Delta H_{crit}) = \int \int U(\xi - \eta) f_{\Delta H L}(\xi) f_{\Delta H crit}(\eta) d\xi d\eta \quad (6)$$

where $f_{\Delta H L}(\xi)$ and $f_{\Delta H crit}(\eta)$ denote the probability density functions (p.d.f.) of the extreme load and the critical head respectively, $U(\xi - \eta) = 1$ if $\xi > \eta$ and $U(\xi - \eta) = 0$ otherwise and the integration extends over the full domains of the p.d.f.'s. Equation (6) yields the probability of failure due to piping in the period of time for which $f_{\Delta H L}(\xi)$ is valid, so in our case the probability of failure per year.

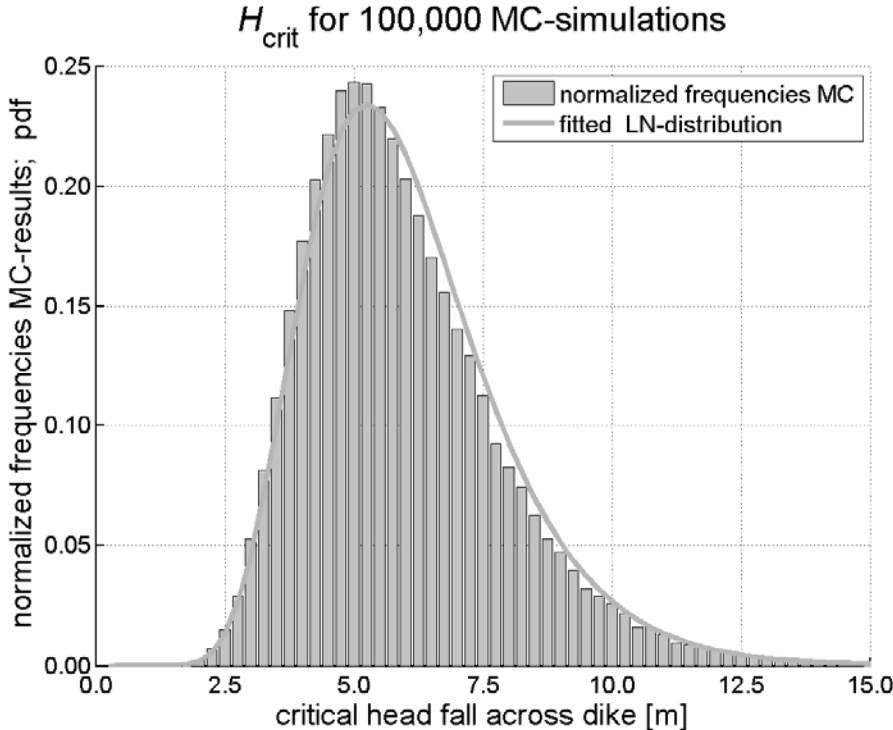


Figure 6: Evaluation of the frequency distribution of critical head fall ΔH_{crit} , based on 10^5 MC simulations

The p.d.f. $f_{\Delta H crit}(\eta)$ is a composite function of the geometrical and physical soil parameters, the associated p.d.f.'s which characterize its uncertainties and the relations (4) or (5). It can be evaluated using one of the computation methods of reliability theory, e.g. by Monte Carlo (MC) simulations or First Order Second Moment approaches. As an example, figure 6 resembles the results of 10^5 MC simulations of the critical head, showing the experimental frequency distribution, based on eq. (5), corresponding with figure 6. The assumed statistics for the geometrical and physical soil parameters are shown in Table 1.

Figure 6 clearly illustrates the compound effect of uncertainties of the soil parameters on the range of uncertainty of the critical head. Just for curiosity reasons a log normal distribution has been fitted, based on estimates of the expected mean value $E[\Delta H_{crit}] = 6.06 \text{ m}$ and of the standard deviation $\sigma(\Delta H_{crit}) = 1.92 \text{ m}$, determined from the MC-simulations. In order to determine the probability of failure due to piping the MC-simulation procedure should be applied directly to the performance function:

$$Z = \Delta H_{crit} - \Delta H_L \quad (7)$$

where $Z < 0$ means piping failure and $Z > 0$ means non failure. Then $P_{piping} = P(Z < 0)$, which can be evaluated from the MC-procedure as the fraction of the total number of simulation runs giving a negative performance function. Merely for illustration the frequency distribution of simulation results for the performance function has been displayed in figure 7, based on the soil parameters in Table 1 and assuming a Gumbel type of p.d.f. for the hydraulic load. The corresponding annual probability of piping is 1/2000. Just for the purpose of reference, the corresponding overall safety factor, expressed as the ratio of expected mean strength $E[\Delta H_{crit}]$ and a design load with annual probability of exceedence of 1/200, equals 2.0 in this computation example.

Table 1: Assumed statistics in the MC-simulation analysis

Variable (see Figure 2 and eq. 3)	Distribution type	Expected mean value	Standard deviation
Seepage length L [m]	LN	50	2.5
Thickness top sand layer h_g [m]	LN	15	0.75
Thickness second sand layer h_s [m]	LN	25	1.25
Volume weight sand particles γ_p	Det	26.5	-
Volume weight water γ_w	Det	9.81	-
Sand grain size d [m]	LN	$1.5 \cdot 10^{-4}$	$1.5 \cdot 10^{-5}$
Permeability top sand layer k_g [m/s]	LN	10^{-4}	10^{-4}
Permeability river bed layer k_r [m/s]	LN	10^{-5}	10^{-5}
Permeability sub sand layer k_s [m/s]	LN	$5 \cdot 10^{-4}$	$5 \cdot 10^{-4}$
Kinematic viscosity ν [m^2/s]	LN	$1.33 \cdot 10^{-6}$	0
Bedding angle ϑ [$^\circ$]	LN	40	4
White's constant η [-]	LN	0.3	0.03
Hydraulic load ΔH_L [m] $F_{\Delta HL}(\xi) = \exp(-\exp(-a(\xi-u)))$ ($u=1.41$, $a=3.28$)	Gumbel (max)	1.6	0.4
Design load (1/200 annual probability of exceedence):		3.04	-

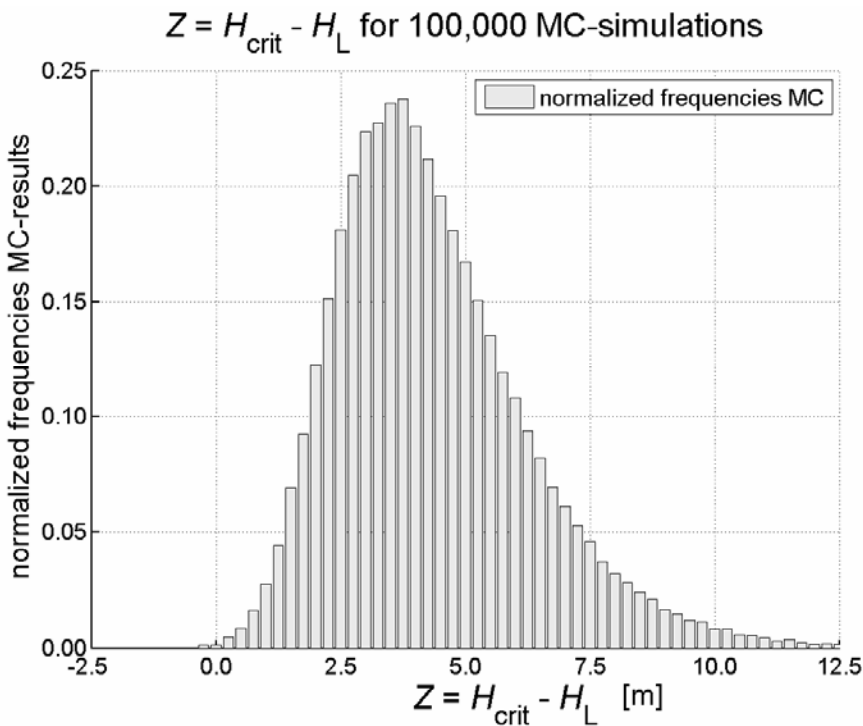


Figure 7: Frequency distribution of random realisations of the performance function (parameters c.f. Table 1). Number of MC-simulation runs: 10^5 . The estimated probability of failure equals the number of MC-runs, returning $Z < 0$, divided by the total number of MC-runs.

The MC procedure described is known as the Crude Monte Carlo approach, which is simple and very robust. However, it may be computationally heavy since it requires many simulation runs to obtain a reasonable accuracy of the estimation of the probability of failure. As a rule of thumb, to obtain a probability of failure with relative error of 10 percent (with 95 percent reliability), the number of simulation runs needed equals approximately $400/P_f$ (Vrijling & Vrouwenvelder, 1984). So, in case of a probability of failure of 1/2000, like in our computation example, the required number of simulations would be $8 \cdot 10^5$. Figures 6 and 7 are based on 10^5 simulation runs, which yields a relative error of the computed probability of failure of approximately 25 percent.

In case of a numerically complex performance function and small probability of failure, the required number of simulation runs may be prohibitive from the point of view of computational burden involved. Therefore a variety of computationally more efficient methods has been developed through the past decades. For an overview the reader is referred to the literature, a.o. (Beacher and Christian, 2003).

5. Long-term Evolution of Erosion Status in Heterogeneous Soil

The evolution of internal erosion in heterogeneous stratified soils can be analysed by combining existing methods used to study sediment transport in canals, filtration phenomena and stochastic processes. The erosion process in a canal is described by the equation of motion for the flow, the continuity equation of water – known as Saint Venant equations – a constitutive equation for erosion and the continuity equation reflecting the change in bed elevation (Wörman

and Xu, 2002). For instance, the desiltation of sediment in a water reservoir at a dam site can lead to a transport constraint below the dam and degradation in the downstream canal, also below a riprap layer with sufficiently coarse pore spaces. Heterogeneities in the riprap layer can often be significant and this leads to a heterogeneous erosion process in the canal.

Figure 8 shows how the expected value solutions to the bed elevation z_B depends on a specific erosion parameter K_1 (see below), the bed slope F (also slope of energy line), distance x below the dam, elapsed time t and the spatial variation in the K_1 -parameter. $E[\dots]$ denotes expected value, $CV[\dots]$ denotes the coefficient of variation and $I =$ is correlation length from the so called exponential semivariogram model. The empirical coefficient K_1 is defined as

$$K_1 = \frac{1}{1-n} \frac{\partial G}{\partial F} = \frac{12.5 G}{(1-n)F} \quad (8)$$

where G = volumetric transport rate of sediment mass per unit width [$m^3/(m s)$].

As can be seen in the figure, increasing the heterogeneity of a defective filter layer in a canal retards the propagation of the expected bed degradation. An implication is that the heterogeneity of the riprap in this respect prolongs the expected degradation process and the expected life-span of the structure. On the other hand, the increased variance and decreased correlation length of the riprap reduces the confidence of the mean value solution. The stochastic analysis is therefore suitable as a part of risk analyses of extreme events for which empirical observations are rare such as failure of embankment dams.

6. Potential use of Probabilistic Reliability Analyses

Analysis of the probability of failure may serve various purposes. Codes for design of dikes or dams often adopt the LRFD concept (Load and Resistance Factor Design), for which load and resistance factors are usually determined on the basis of some specific probability of failure which is considered acceptable. Such code development requires extended series of probabilistic failure analyses to determine partial safety factors for the load and strength parameters. For the principles of code development the reader is referred to (Ciria, 1977), and for reliability based code calibration to (Faber et. al., 2003).

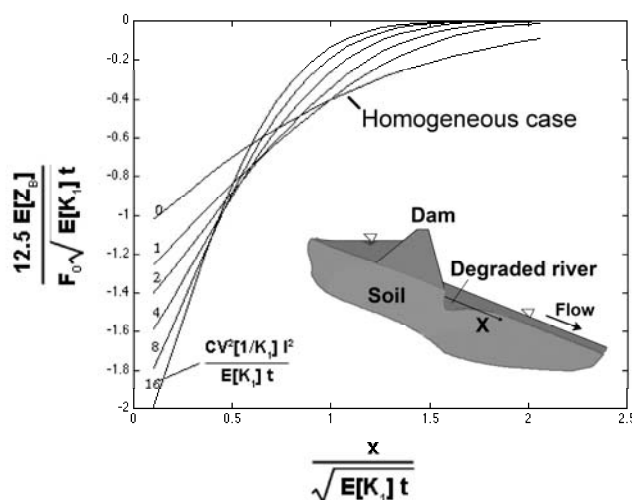


Figure 8: Long-term evolution of erosion below a riprap layer in a canal downstream of a desilting reservoir.

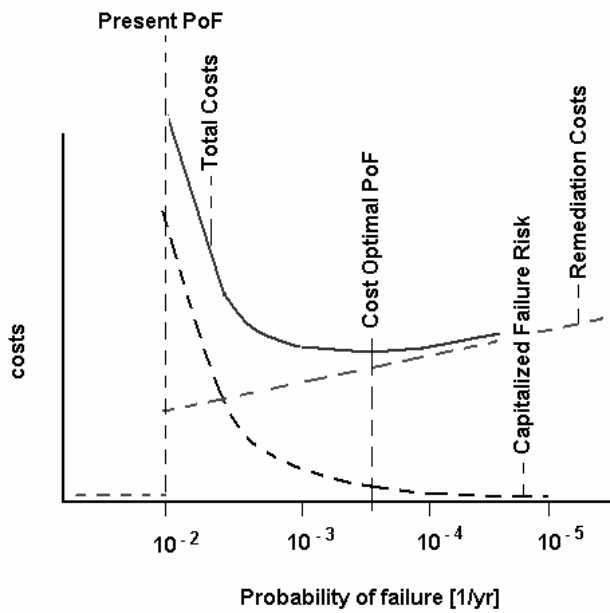


Figure 9: Outline of cost-benefit analysis of risk mitigating measures (Vrijling and Vrouwenvelder, 1984)

Acceptable probabilities of failure may follow from a failure risk analysis, or better a failure risk management analysis. The rationale for such analysis is that the costs of remedial measures to mitigate the risk of failure, e.g. to reduce the probability of failure, and capitalized failure risk after remediation, the so-called residual risk, should be minimized.

Optimal cost effective measures reduce the probability of failure to such extent that sum of costs of remedial measures and the (capitalized) residual costs of failure risk to a minimum. This has been illustrated in outline in figure 9. The horizontal axis shows decreasing probabilities of failure, which may potentially be achieved by some risk mitigating measure. In this figure it is supposed that in the present state the probability of failure is 10^{-2} . The vertical axis represents the costs of remediation, as a function of the reduced probability of failure (red dashed line), and the cost of residual failure risk (black dashed line), capitalized over the intended lifetime of the remediation measure. The sum of both (the blue line) gives the total costs, which reaches a minimum for a probability of failure of, say, $3 \cdot 10^{-4}$, meaning that from a cost optimization point of view, this probability of failure is most desirable in this example.

7. Design Recommendations

The following recommendations seem useful for the evaluation of fluvial structured sediments regarding their susceptibility to erosion:

The quality of the assessment of erosion susceptibility depends mainly on the quality of the analyses of the subsoil. It is recommended to take core drillings in order to derive a detailed profile in vertical direction of the hydraulic permeability and specific grain size diameter respectively. Consider the statistics in soil properties and evaluate the autocovariance in properties.

Yet, the horizontal distances between the core drillings are normally too large to obtain correct information on whether the subsoil is mainly consisting of layers or lens structures. It is therefore useful to perform the pumping test. High values of k_h indicate the presence of highly permeable layer structures (highly permeable joined lenses) leading to a high risk of erosion.

Due to extreme heterogeneities of the subsoil combined with resulting uncertainties in the distribution of the hydraulic gradients an exact formulation of a probabilistic filter design is hardly possible. But in practice, substantial certainty about erosion susceptibility can be gained by 6 drillings evenly spread over a distance of 50 m in lateral direction.

A possibility is to perform a probabilistic filter design according to section 4. A smaller risk for erosion requires more strict criteria for filter design or design of mitigating measures regarding piping . One can also evaluate the long-term erosion behaviour as part of the risk perspective as well as maintenance plans.

Probabilistic reliability analyses can be helpful in the process of optimization of the design of a dike or a dam. It enables prior evaluation of costs and benefits of design options for mitigation of erosion related risk of failure, or further soil investigation efforts to reduce subsoil related uncertainties. In analyzing design options for risk mitigation, the long term erosion behaviour as well as maintenance plans (and costs) should be taken into account.

Literature

Adel, H. den, Koenders, M.A., Bakker, K.J., 1994, "The analysis of relaxed criteria for erosion-control filters", Canadian Geotechnical Journal, 31, 829-840.

Beacher, G.B and J.T. Christian, 2003, "Reliability and Statistics in Geotechnical Engineering", Wiley, West Sussex, England. ISBN 0-471-49833-5

Bligh, W.G., 1910, "Practical design of irrigation works", Second edition, Constable, Edinburgh

Brauns, J., 1985, "Erosionsverhalten geschichteter Bodens bei horizontaler Durchströmung", Wasserwirtschaft, 75, 10, 448-453.

Calle, E.O.F., Best, H., Sellmeijer, J.B., Weijers, J., 1989, "Probabilistic analysis of piping underneath water retaining structures", Proc. 12th Int. Conf. Soil Mech. Found. Eng., Rio de Janeiro, 819-822.

Ciria, 1977, "Rationalisation of safety factors in structural design", Ciria Report 63, Ciria London

de Graauw, A., van der Meulen, T., van der Does de Bye, M., 1983, "design criteria for granular filters", publication No. 287, Delft Hydraulics.

DWW, Ministerie van Verkeer en Waterstaat, 2005: "Flood Risks and Safety in the Netherlands (Floris)", ISBN 90-369-5604-9, Delft

(<http://www.projectvnk.nl/html/download.php?file=publicatie.137.strUpload.HoofdrapportVNKEngels.pdf>, last accessed on June 7, 2007).

Faber, M.H., O. Kübler and J. Köhler, 2003, "Tutorial for the JCSS Code Calibration Program", ETH-Zürich (www.jcss.ethz.ch)

- Harza, L.F., 1934, "Uplift and seepage under dams on sand", Proc. Am. Soc. Civ. Eng., September.
- Lane, E.W., 1934, "Security from under-seepage masonry dams on earth foundations", Proc. Am. Soc. Civ. Eng., September.
- Lane, E.W., 1935, "Security from under-seepage masonry dams on earth foundations, with discussion by Creager, W.P., Harza, L.F., Justin, J.D., Ayres, L.E., Griffith, W.M., McKenzie Taylor, E., Hebert, D.J., Casagrande, A., Davis, C.V., Eiffert, C.H., Burroughs, E.H., Potter, A., Kennedy, R.E., Khosla, A.N., Streiff, A., and Lane, E.W.", Trans. Am. Soc. Civ. Eng., 1236-1351.
- Saucke, U., 2004a, "Bewertung der Erosionsanfälligkeit strukturierter körniger Sedimente", Veröffentlichungen des Instituts für Bodenmechanik und Felsmechanik der Universität Fridericiana in Karlsruhe.
- Saucke, U., 2004b, "The Susceptibility to Erosion of Structured Fluvial Sediments", in: Fourie, A. (Editor): Geofilters 2004, South Africa.
- Sellmeijer, J.B., 1988, "On the mechanism of piping under impervious structures", Ph.D. thesis, Delft University of Technology.
- Sherard, J.L., Dunnigan, L.P., Talbot, J.R., 1984a. "Basic properties of sand and gravel filters", J.Geotech.Engng, ASCE, 110(6).
- Sherard, J.L., Dunnigan, L.P., Talbot, J.R., 1984b, "Critical filters for silts and clays", J.Geotech.Engng, ASCE, 110(6).
- Vrijling, J.K. and A.C.W.M. Vrouwenvelder, 1984, "Probabilistic Design in Civil Engineering", Lecture notes, Delft University of Technology, Civil Engineering Faculty. (in Dutch)
- Webster, R., Oliver, M.A., 1998. "Geostatistics for environmental scientists", Wiley, New York.
- Wörman, A., Olafsdottir, H., 1992, "Erosion in a Granular Medium Interface", Journal of Hydraulic Research, Vol. , No. 5, pp 1-17.
- Wörman, A., Xu, S., 2001. "Stochastic Transport Analysis of Internal Erosion in Stratified Soil Structures – Implications to risk Assessments", Journal of Hydraulic Engineering, 2001: 127(5), 419-428.

Authors Name and Affiliation

A. Wörman
 The Royal Institute of Technology, Dept. Land and Water Resources Engineering, Sweden
 worman@kth.se

U. Saucke

Universität Karlsruhe, Institut für Bodenmechanik und Felsmechanik, Germany

ulrich.saucke@ibf.uni-karlsruhe.de

E.O.F. Calle, J.B. Sellmeijer and A.R. Koelewijn

GeoDelft/Deltares, Netherlands,

J.B.Sellmeijer@geodelft.nl

Engineering Tools for Piping – Neural Networks Created using FEM

J.B. Sellmeijer & A.R. Koelewijn

Abstract

The design and safety assessment of dams and embankments against failure by piping calls for practical tools. After a description of the mechanism, several of these tools to determine the critical hydraulic head are described: the old empirical rules of Bligh and Lane, the more recent analytical rule of Sellmeijer, a stable finite element model (FEM) and finally a neural network, which bypasses the FEM in speed, ease, availability and accuracy.

1 Introduction

Progressive failure of dams and embankments by piping is of concern both around reservoirs and along other water bodies like rivers, estuaries and seas with low-lying hinterland which needs to be protected. Both the design of new protective measurements or improvement of existing protection works and the safety assessment of these constructions calls for practical tools. This contribution describes several of these tools, focussing on the present state-of-the-art on embankment design and safety assessment in the Netherlands.

As the word piping tends to be used for a variety of phenomena, first some terminology is presented. Here, the word *piping* is used for the formation of erosion pipes in a granular layer directly underneath a cohesive layer or a construction, which serves to maintain a difference in the hydraulic head (e.g. a clayey embankment on a sandy subsoil, see **Figure 1**). When the head difference increases, these pipes may grow progressively from the area with a lower hydraulic head towards the higher head. This is often called *backward erosion*. In case of a cohesive top layer, this process can only start after *hydraulic fracturing*, i.e. the cracking of the top layer as a result of a high water pressure. Subsequently, *seepage erosion* takes place, i.e. the wash away of the particles. In case of a vertical construction like a wall or skirt penetrating into the granular layer, first *heave*, being the uplift of the granular layer, needs to occur.

During high water levels in the rivers in the Netherlands very often sand boils (see **Figure 2**) have been noticed. An old countermeasure is to build a small dam of sand bags around a boil, to reduce the head difference (see **Figure 3**). Although this has often proven to be effective, in the early 1970s a research program was started in the Netherlands to arrive at a sound risk assessment of the safety of embankments with sand boils. Two decades later, this research program resulted in the so-called design rule of Sellmeijer, which is commonly used in Dutch engineering practice and guidelines [TAW, 1999].

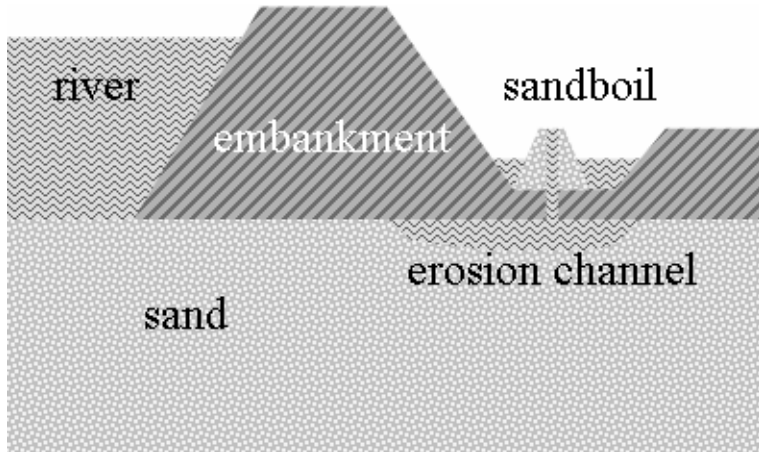


Figure 1: Principal sketch of embankment geometry with erosion zone.

This research is described in Section 2. In Section 3 this design rule is presented, along with some other design rules which are often applied in practice.



Figure 2: Sand boil behind a river embankment.

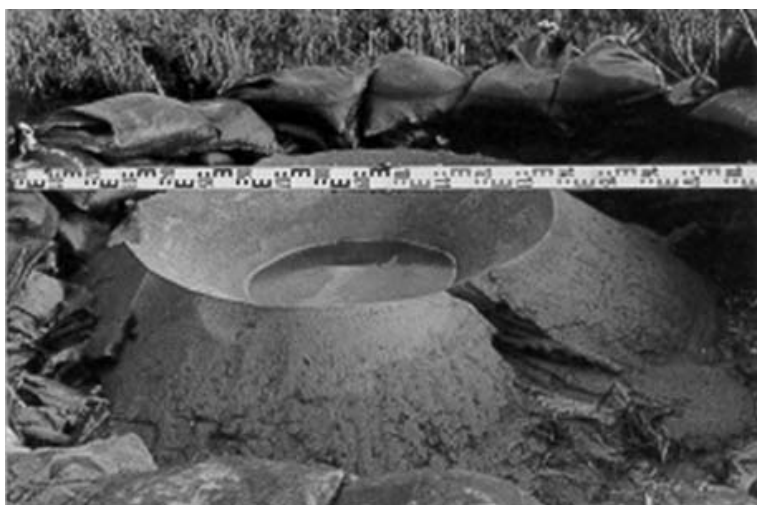


Figure 3: Small dam of sand bags around sand boil of Figure 2, after retreat of high water.

In 2002 a large risk assessment study started to quantify the safety level of the main embankments in the Netherlands. This 'Flood Risks and Safety' study resulted in a non-expected dominant contribution of the piping mechanism in the total risk of flooding. In fact, piping was found to be even a greater risk than overtopping, i.e. the mechanism deemed to be dominant [DWW, 2005]. This triggered a new attention for research into the piping mechanism. Questions like the influence of multiple sand layers, partial cut-offs of sheet piles and the inclination of a foundation triggered the need for a finite element approach. A finite element model including backward erosion has been completed in 2006. This is presented in Section 4. The results obtained by this model give more insight and are yet to be validated in a large research program involving field experiments. This program called 'IJkdijk' will run from 2007 to 2009.

The main challenge in the FEM-approach was to find a calculation algorithm giving stable results for design situations. After all, it requires quite some knowledge to perform a reliable calculation. In order to help engineers with their calculations, an artificial neural network has been created. This neural network is described in Section 5. It can be used as a quickly applicable, yet reliable engineering tool for daily practice. Apart from this application, it can be used as a quick check on results from other methods and it can be applied for more general risk assessment studies on piping in general.

2 Piping Mechanism

2.1 Observations in Visual Tests

Field observations during the first decades of the 20th century, mainly in India and the United States, led to the well-known empirical rules of Bligh [1910a,b] and Lane [1934], described in Section 0. Similar rules and methods by others, e.g. Griffith [1913-14] and Harza [1934], received less attention.

Only in the early 1970s new experimental studies have been started to get better insight into the fundamentals of the piping phenomenon under river embankments. Around 1972, De Wit started a series of tens of laboratory tests in Delft, one of which is shown in Figures 4 and 5.

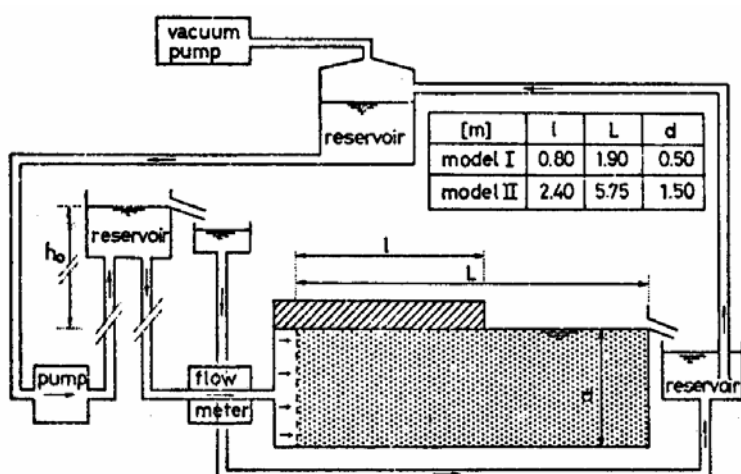


Figure 4: Set-up of piping experiments by De Wit [Wit, de et al., 1981].



Figure 5: Result of piping test showing erosion pattern [Wit, de et al, 1981]

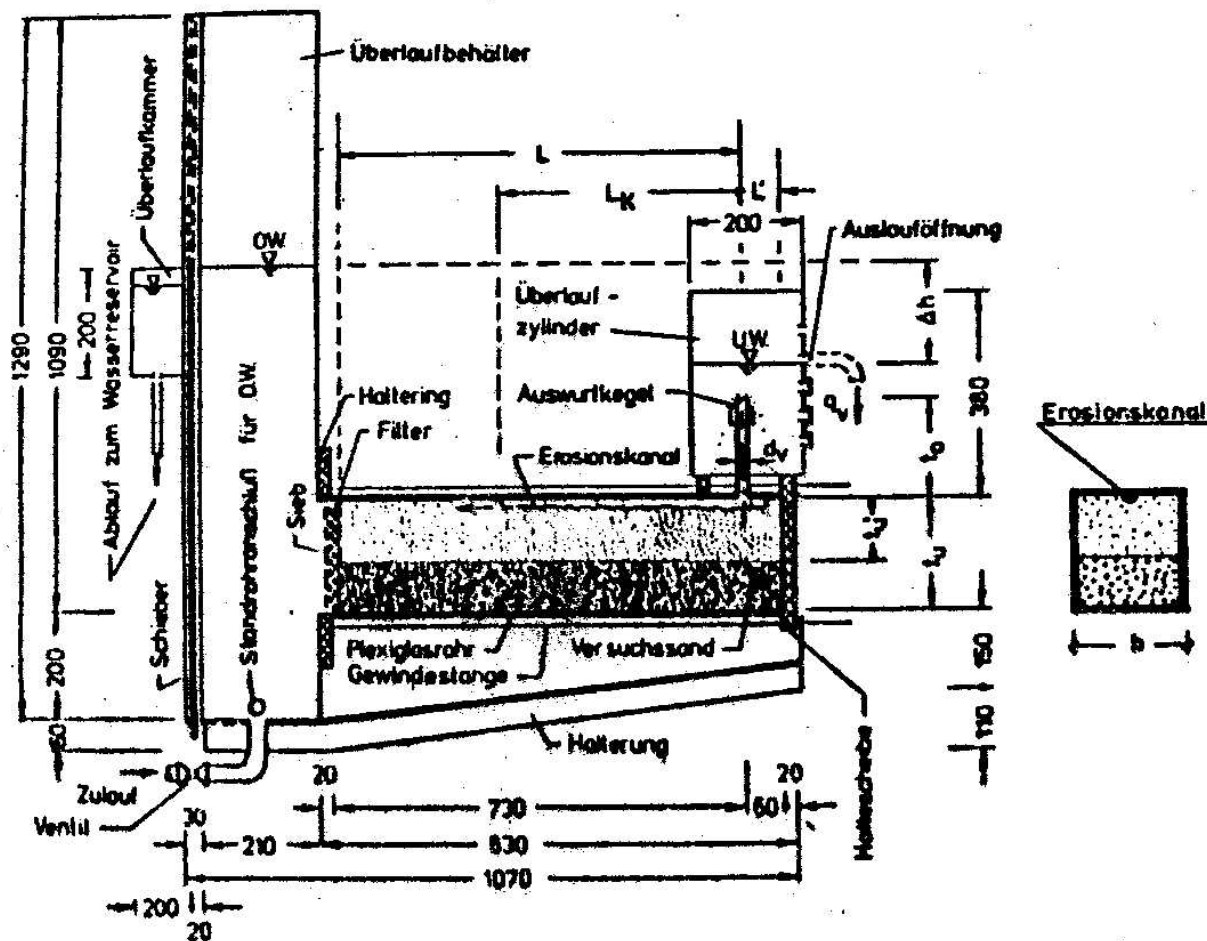


Figure 6: Experimental set-up with double-layered test bed [Müller-Kirchenbauer, 1978].

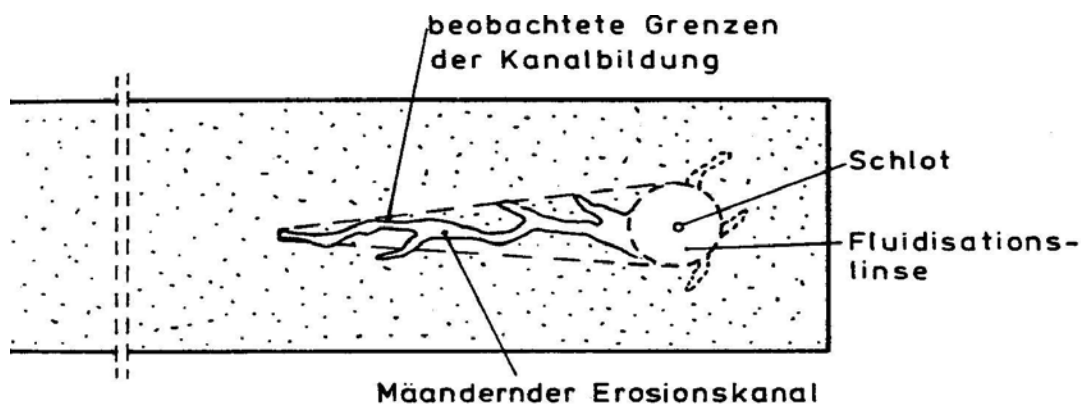


Figure 7: Development of erosion channel [Müller-Kirchenbauer & Hanses, 1981].

Not much later, Müller-Kirchenbauer, Miesel and Hansel [Miesel, 1978; Müller-Kirchenbauer, 1978; Müller-Kirchenbauer & Hanses, 1981] carried out similar tests in Berlin, but with a double-layered composition of the test bed, as shown in Figure 6. A similar meandering pattern of the erosion channels was found, as shown in Figure 7.

Similar findings were reported by Kohno et al. [1987] from tests in Okayama. They also looked into the time-dependent failure process. The set-up of some of their tests and typical results are reproduced in Figures 8 and 9.

In the Netherlands, research was continued with three large scale tests in the Delta Flume of Delft Hydraulics in De Voorst. Figure 10 shows the top and side views of these tests. In Figure 11 the progression of the erosion channels during one of the tests is reproduced.

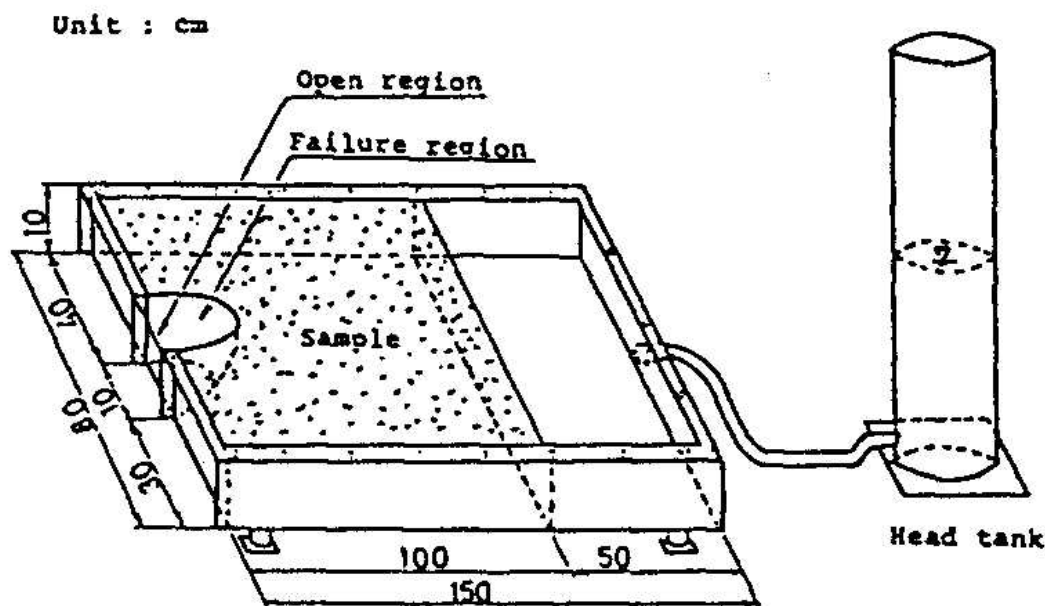


Figure 8: Experimental apparatus used to measure horizontal two-dimensional erosion [Kohno et al., 1987].

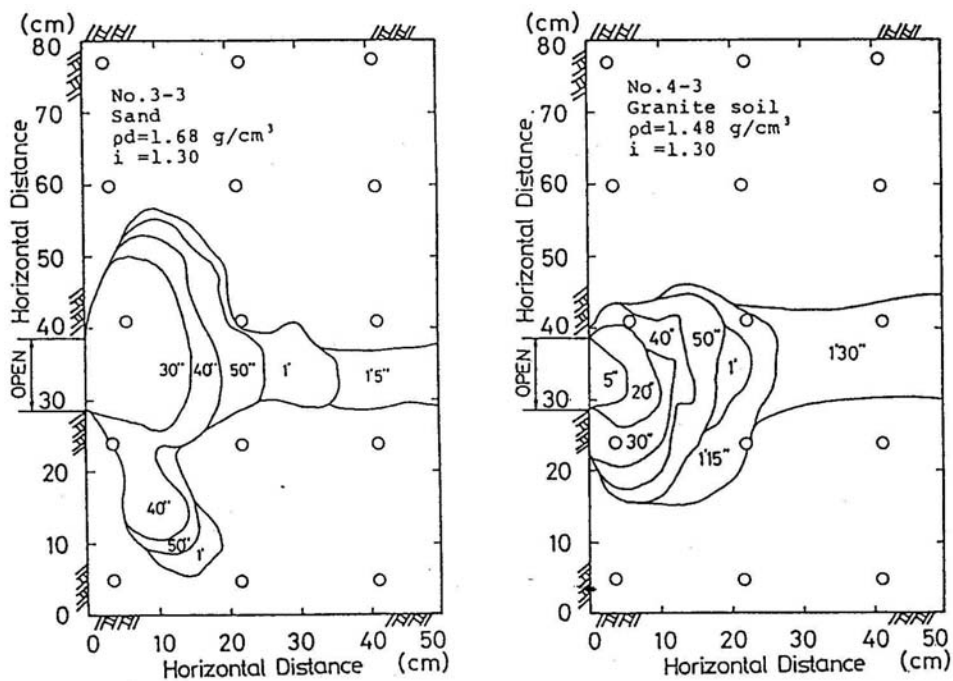


Figure 9: Horizontal erosion patterns in time for sand (left) and granite soil (right) [Kohno et al., 1987].

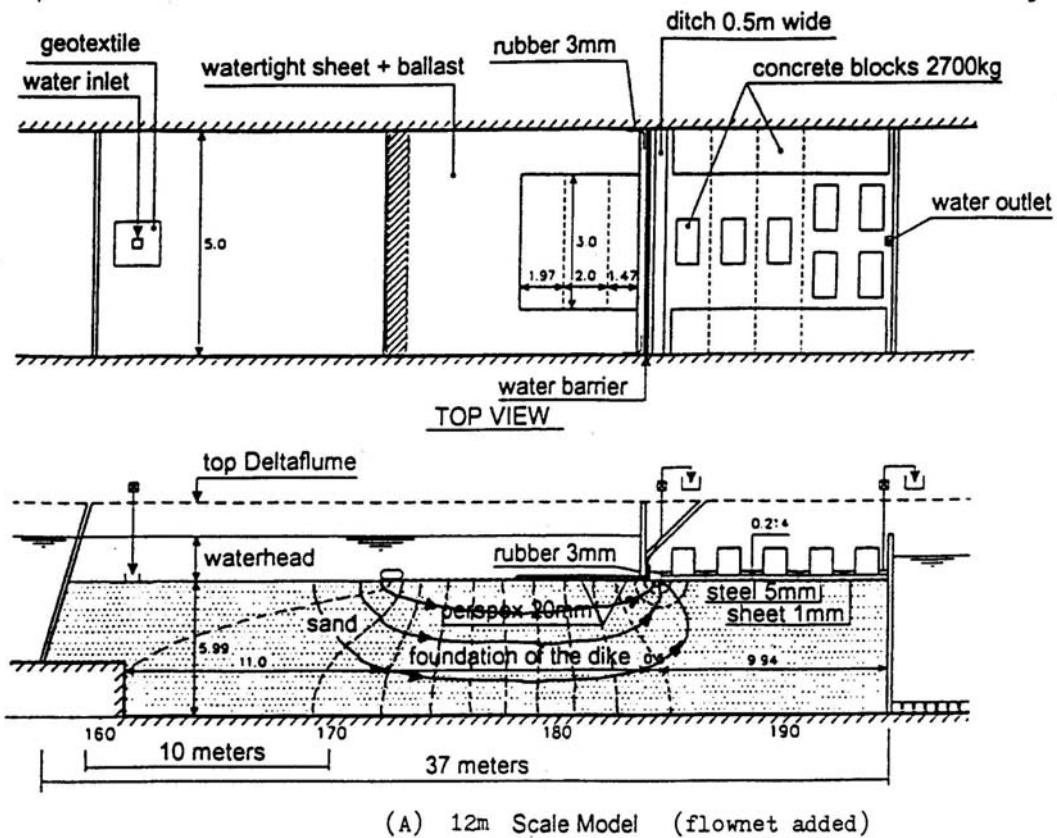


Figure 10: Set-up of Delta Flume tests.

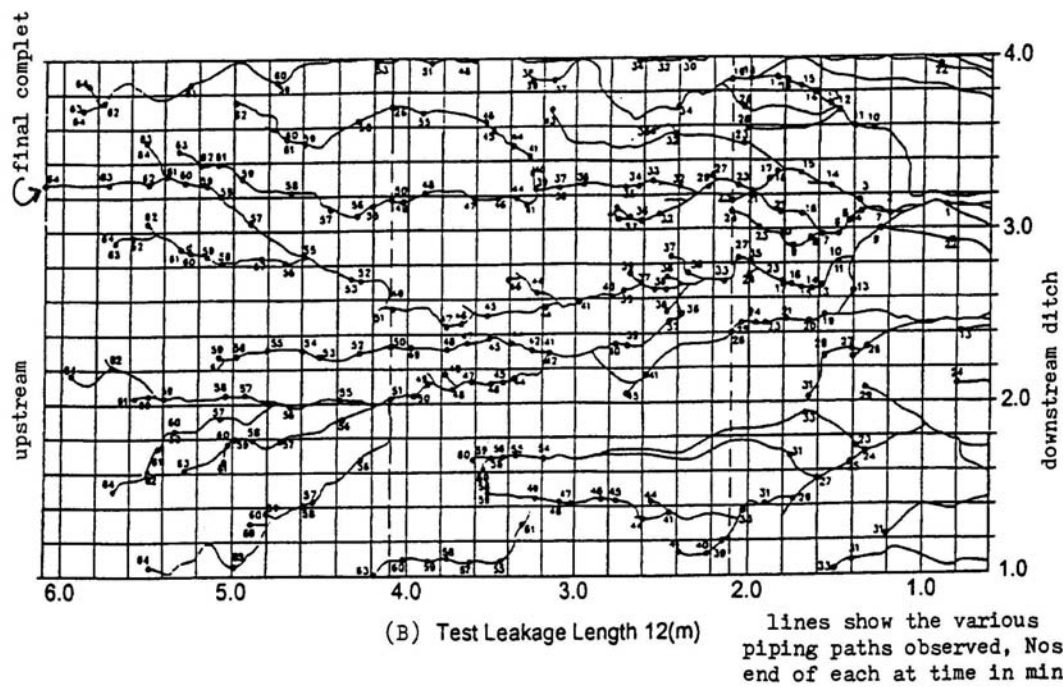


Figure 11: Progression of erosion channels in time during one of the Delta Flume tests.

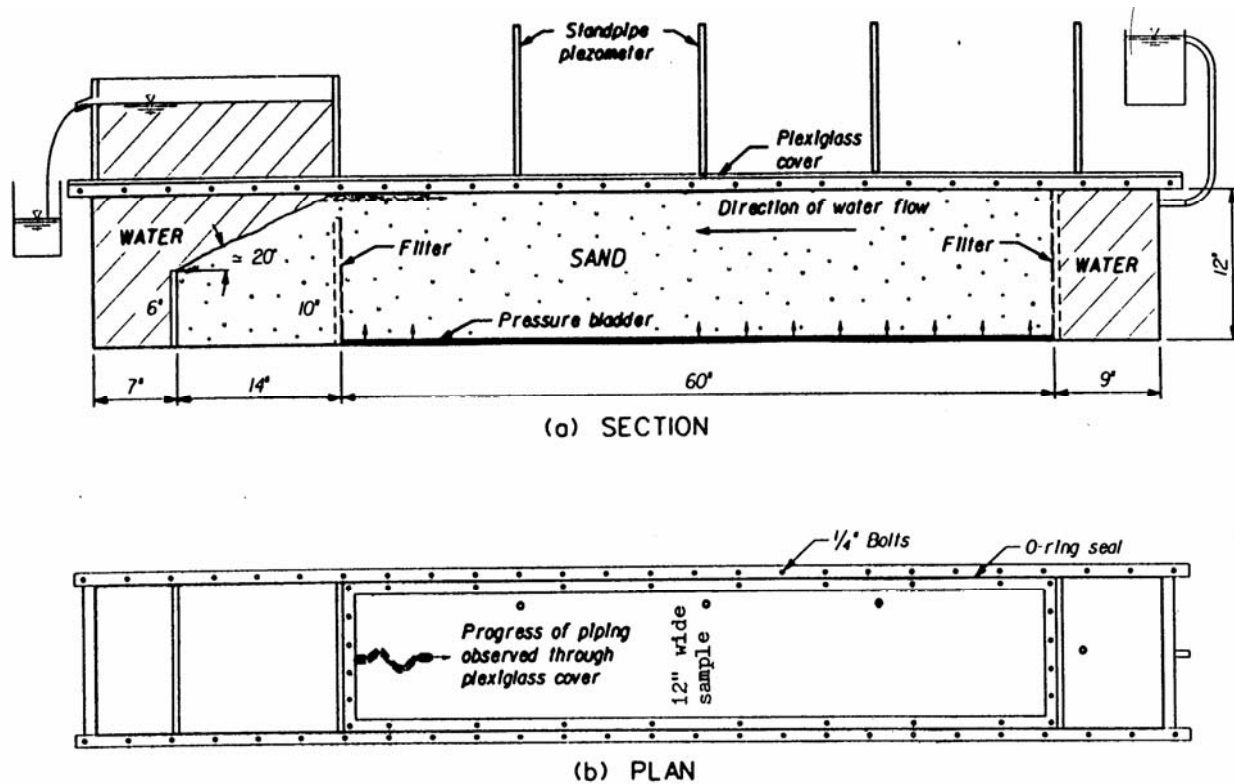


Figure 12: University of Florida piping flume [Schmertmann, 2000]

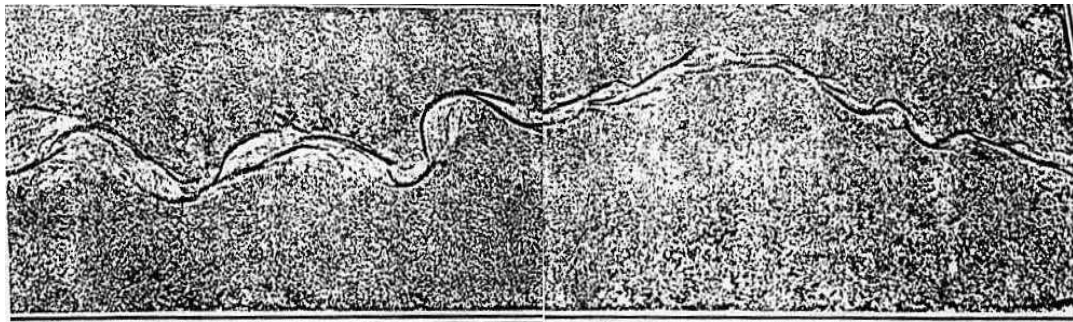


Figure 13: Distorted top view of part of one the University of Florida piping flume tests, showing meandering pipepaths [Schmertmann, 2000].

Partly ignorant of the other research, in Florida similar tests were carried out with similar findings, as reported by Schmertmann [2000], see Figures 12 and 13.

In the described visual tests, it was observed that in the presence of high seepage gradients sand is transferred from underneath the structure to the outflow region, while the weight of the cover is irrelevant. This process results in the appearance of an irregular pattern of erosion channels and sand boils at the downstream end. It was noticed that equilibrium state conditions are possible as long as the channels and sand boils restrict the seepage gradients below a critical value. This critical value is believed to coincide with the point of failure of the sand. Beyond this point progressive erosion begins and leads to the collapse of the geotechnical structure.

In reality, the problem is three-dimensional. However, to achieve the primary goal - a description of the mechanism of piping - a two-dimensional approach is presented. Such a description is believed still to capture the main mechanical features and not to invalidate the quality of the results. This implies that it will be impossible to include the braiding of the slits in the investigation. Braiding is due to the search for weak links in the granular structure of the sand. It is associated with the non-homogeneity of the sand properties and is therefore not an essential but an added feature of the piping problem.

The sand boil in the outflow region is a result of the outflow of material from underneath the structure. This erosion process is associated with the formation of a channel. As the channel becomes longer, locally the permeability increases and the gradients reduce. Eventually, for a given overall hydraulic head equilibrium is restored. The particles at the bottom will then be in limit equilibrium. Already in Figure 1 an outline of an embankment geometry with an erosion zone was shown. Note that in this figure the depth of the erosion channel is exaggerated to view it properly.

2.2 Modelling Based on Physical Principles

The steady state is modelled. In the model the transient effects are ignored so that no information can be achieved about the duration of the process. For a certain length of the erosion channel the corresponding hydraulic head over the structure is fixed. According to the visual tests there appears to be a maximum possible hydraulic head. This head is the critical one, where progressive erosion begins.

The model will contain three essential components. First, the groundwater flow in the sand. This connects the hydraulic head to the condition in the erosion channel. Next, the channel flow. This connects the groundwater flow to the flow forces in the channel. Finally, the state of limit equilibrium of the particles at the bottom of the channel. This connects the flow forces to the interparticle forces.

The groundwater flow can be dealt with if the boundary conditions are known. These conditions involve potential lines like the river bottom, flow lines in case of impermeable layers and phreatic surfaces, where available. In the erosion channel the boundary condition depends on the erosion process. In fact, the channel flow and the state of limit equilibrium will act as boundary condition for the groundwater flow.

In the following parts these aspects will be elaborated upon and unified into one mathematical model to describe the phenomenon of piping.

2.2.1 Groundwater Flow

The groundwater flow problem may be solved if all boundary conditions are specified. The condition in the channel is not elaborated yet. Even if it were, a direct solution would not be possible. This condition is non-linear and dependent on the state in the entire channel location. Only by iteration a proper solution may be obtained.

The problem is now how to incorporate the erosion condition in the flow calculations. The following iterative scheme proves to be fruitful:

- Indicate the value of the head in the erosion channel by a variable, then solve the groundwater flow;
- At the same time solve the flow in the erosion channel and connect it to the groundwater flow by the conditions of continuity for the head and discharge;
- Finally, define the flow forces on a sand particle at the bottom of the channel. These forces are related by the condition of limit equilibrium for the particles.

During iteration an estimate for the head in the erosion channel is made and improved in order to fit to the erosion criterion. For a fixed head a groundwater flow computation is readily made. The flow model may be:

- Numerical: the erosion channel consists of a number of nodes, where the head is adjustable during iteration;
- Analytical: along the erosion channel a distribution is placed. The strength of the distribution is changed every iteration step.

The numerical approach is more versatile to use, the analytical one is more flexible to apply.

2.2.2 Channel Flow

The character of the flow in the slit, either laminar or turbulent, depends on the Reynolds number. The channel depth is very small. The Reynolds number is then expressed as the ratio of discharge per unit width Q and the kinematical viscosity v : $Re = Q / v$. If $Re < 2300$ the flow is laminar. In practice this is often true. For large permeabilities and/or large structures the

Reynolds number may go beyond this range. However, here only the laminar flow condition is analysed.

A steady state laminar flow in general is governed by the Navier-Stokes equations [Batchelor, 1983]. A careful solution of these equations for the erosion channel results in a formula not unlike the one for flow in a pipe [Sellmeijer, 1988]. It reads:

$$a^3 \frac{\partial \varphi}{\partial x} = 12 \frac{v}{g} Q \quad Q = \int k \frac{\partial \varphi}{\partial y} dx \quad (1)$$

a is the depth of the slit; g is the gravitational acceleration; k is the permeability; x is the horizontal coordinate; y is the vertical coordinate; φ is the hydraulic head.

The main use of equation (1) is to express the depth of the channel. Note that the conditions of continuity for head and discharge are met. The head φ corresponds to the groundwater flow head at the erosion channel. The discharge Q is composed of the contributions of the specific discharge from the groundwater flow.

Besides the pipe flow relation, the Navier-Stokes equations supply an expression for the drag force on the particles which is exerted by the flow. It reads:

$$\tau = \frac{1}{2} \gamma_w a \frac{\partial \varphi}{\partial x} \quad (2)$$

γ_w is the unit weight of the water.

This force plays a major role in the interparticle forces, which define the limit equilibrium of the particles.

2.2.3 Limit Equilibrium of Sand Particles

The question of limiting stability at the interface of soil and water cannot be solved by regarding the soil as a continuum. This is due to the fact that continuum mechanics allow the effective vertical stresses to vanish near the bottom of the slit. The shearing stress which is associated with the near parabolic velocity profile in the slit itself therefore cannot be dealt with in a Coulomb manner. Failure phenomena due to vanishing skeleton stresses need not be taken into account, since the vertical gradient is of minor importance.

To find a single particle force balance for a grain at the top of the interface, two distinct forces must be considered. The horizontal one is the drag force due to the channel flow. The vertical one is the weight of a particle. In Figure 14, where d is the particle diameter, α is the channel slope, γ_p is the unit weight of the particles, v is the bedding angle of sand and η is White's constant [White, 1940], these interparticle forces are shown. Note that the channel may slope gently. The condition of limiting equilibrium must be imposed; this yields a connection for the forces for a given mode of motion.

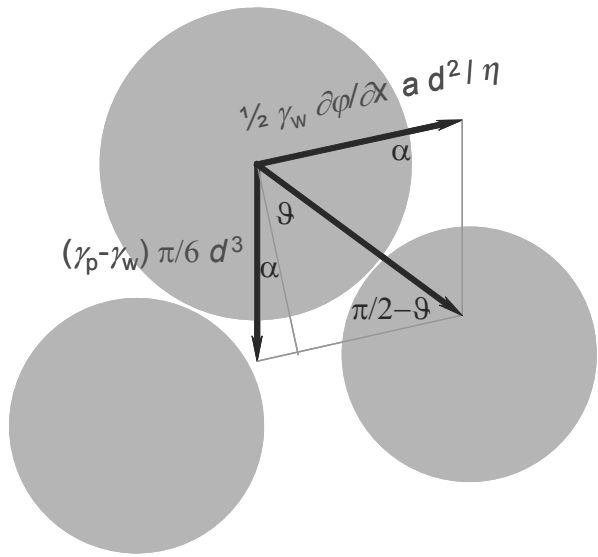


Figure 14: Interparticle forces

A heterogeneous mixture in steady state shows a landscape where the large grains stick out and the small ones are well buried. The treatment of the single particle stability analysis can be made arbitrarily complex by taking into account an increasing number of geometric features of the packing and variety in particle shapes. Engineering interest however must focus on a relatively simple criterion for limiting stability.

Essential features in the interparticle force balance are:

- A preference for the rolling mode of motion [Koenders, 1987];
- An approach with spherical particles, facilitating the use of the bedding angle;
- Employment of Whites constant, to take account of the density of the top particles.

The result is a rule not unlike a Coulomb criterion:

$$\frac{\gamma_p - \gamma_w}{\gamma_w} \frac{\sin(\theta + \alpha)}{\cos(\vartheta)} = \frac{\frac{3}{\pi}}{\eta} \frac{\partial \varphi}{\partial x} \frac{a}{d} \quad (3)$$

2.2.4 Piping Condition in the Erosion Channel

With equation (3) a relation for the interparticle forces is obtained. Before, the pipe flow formula (1) characterizing the flow in the erosion channel was already given. These results may be combined to provide the missing boundary condition for the groundwater flow.

The depth of the erosion channel is eliminated from equations (1) and (3), which results in the piping condition:

$$\begin{aligned} \left(\frac{\partial \varphi}{\partial x} \right)^2 \frac{Q}{kL} &= \left[\frac{\pi}{3} \eta \frac{\gamma_p - \gamma_w}{\gamma_w} \frac{\sin(\theta + \alpha)}{\cos(\vartheta)} \right]^3 \frac{1}{12} \frac{g}{k\nu} \frac{d^3}{L} \\ Q &= \int k \frac{\partial \varphi}{\partial y} dx \end{aligned} \quad (4)$$

Note that this relation a division is made by a length unit, for instance the width of the embankment L , in order to obtain a dimensionless expression.

The right-hand side of the piping condition is constant during the flow computation. It may vary by position due to the channel slope or properties. The left-hand side depends on the flow. It is a non-linear expression.

Groundwater flow computations may be carried out now for a certain length of the erosion channel. These computations are performed in an iterative fashion. The result of computation is a corresponding hydraulic head over the structure, such that the particles at the bottom of the channel are in a state of limit equilibrium. The critical head is the maximum hydraulic head obtained in the entire range of channel lengths, as is shown in Figure 15.

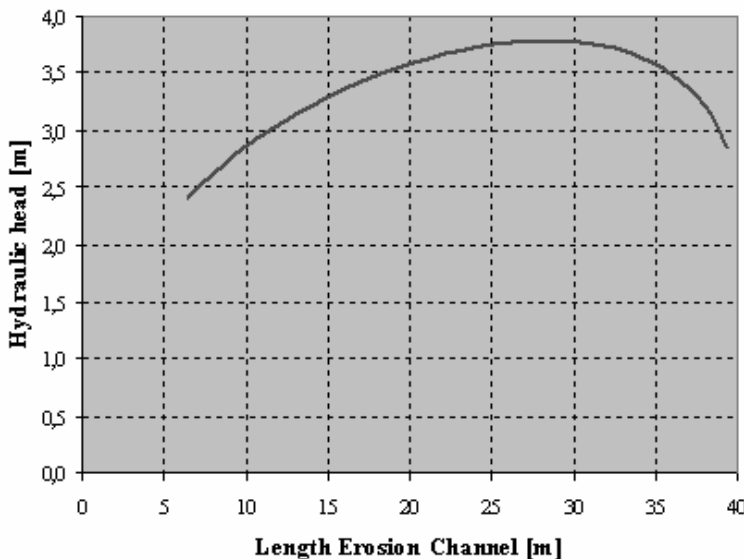


Figure 15: Critical head.

3 Empirical and Analytical Rules

3.1 Bligh

Bligh [1910a,b] formulated a linear relationship between the head across the structure and the length of structure. Although it is unusual to do so, this relationship may be written as:

$$\frac{H}{L} = \frac{1}{C_{\text{Bligh}}} \quad (5)$$

C is the so-called creep ratio, where ‘creep’ refers to the line-of-creep, i.e. the line along the bottom of the structure. Originally, Bligh only considered structures with a horizontal bottom. Based on field experience in India, he suggested the soil-dependent values for C_{Bligh} given in Table 1.

Table 1: Creep coefficients C according to Bligh [1910a,b]

Fine silty sand	18
Moderate fine sand	15
Course sand	12
Fine gravel	9
Course gravel	4

3.2 Lane

Lane [1934] provided an empirical rule similar to the one by Bligh, taking account of vertical constructions like skirts below weirs. This rule is based upon data from 200 structures. The relationship he gave may be written as:

$$\frac{H}{L_h} = \frac{\frac{1}{3} + \frac{L_v}{L_h}}{C_{Lane}} \quad (6)$$

h stands for ‘horizontal’, *v* for ‘vertical’. Values for C_{Lane} are given in Table 2.

Table 2: Creep coefficients C according to Lane [1934]

Fine silty sand	8.5
Moderate fine sand	7
Course sand	5
Fine gravel	4
Course gravel	3

A quick comparison of both rules indicates that in case of absence of vertical pathways, for which Bligh’s rule is applicable only, Lane’s rule is more conservative than Bligh’s rule.

Sellmeijer

In the Dutch guideline for design against piping [TAW, 1999], Sellmeijer’s rule is formulated as:

$$\frac{H}{L} = \frac{1}{C_{Sellmeijer}} = G R S F \quad (7)$$

$$G = \left(\frac{D}{L} \right)^{\frac{0.28}{\left(\frac{D}{L} \right)^{2.8} - 1}} \quad R = \frac{\gamma'_p}{\gamma_w} \tan \vartheta \quad S = \eta \frac{d}{\sqrt[3]{\kappa L}} \quad F = 0.68 - 0.1 \ln(S)$$

G is the geometry factor, *R* is the rolling equilibrium factor, *S* is the sand properties factor, *F* is the force factor. This special case of Sellmeijer’s formulation is valid for a single horizontal sand layer of finite thickness underneath a rigid construction, as indicated in Figure 16.

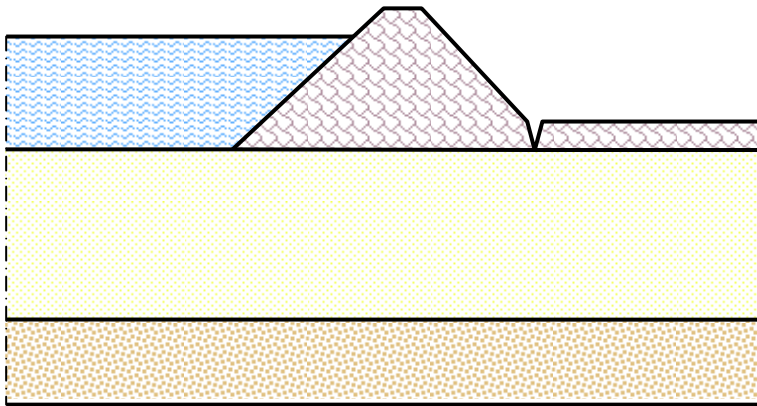


Figure 16: Geometry for Sellmeijer's rule.

4 Finite Element Model for Piping

4.1 Modeling of Groundwater Flow

In Section 0 the mechanism of piping has been illustrated. It appeared that the erosion channel provides a special kind of boundary condition for the groundwater flow in the layers. Any groundwater flow programme is appropriate to be used in piping calculations. It may range from the simplest Laplacean type to advanced unsaturated transient encoding.

The head in the erosion channel is defined by the non-linear piping condition. It must be computed by iteration. Thereto, variations of the head in the channel are considered and used to assess the degree of adaptation. Thus, the deviation from the piping condition may be decreased.

In general the groundwater flow variations are non-linear of nature. They need to be determined during every iteration step. This is a time consuming activity. A linearized approach is preferred. Then the groundwater flow variations are determined beforehand. They may be applied during the entire iteration process.

Simple Laplacean flow is often linear. However, the influence of phreatic surfaces is not linear. Advanced unsaturated transient flow certainly is not linear. In case of moderate non-linearity a stepwise linear approach is recommended. The variations are determined by stepwise approaching the actual flow pattern.

4.2 Piping Condition

The condition of limiting equilibrium in the erosion channel has been derived in Section 0. This led to equation (4). This equation quantifies the degree of deviation from the piping condition for a certain estimate of the head in the channel. This head may be composed of shape functions. Examples of such functions are polynomials, Fourier functions or triangular nodal contributions. The magnitude of these shape functions must be determined in such a way that the closest match of equation (4) is found.

This is accomplished by minimizing the residual f of equation (4). This reads:

$$f = \left(\frac{1}{\beta} \frac{\partial \varphi}{\partial x} \right)^2 \frac{1}{\beta} \frac{Q}{kL} - 1 \quad \beta = \frac{\pi}{3} \eta \frac{\gamma_p - \gamma_w}{\gamma_w} \frac{\sin(\theta + \alpha)}{\cos(\theta)} \sqrt[3]{\frac{1}{12} \frac{g}{k\nu} \frac{d^3}{L}} \quad (8)$$

The magnitude of the shape functions is indicated by S_i , with $i = 1 \dots I$. Discrete positions along the erosion channel are indicated by the index $j = 1 \dots J$. Then minimizing straightforwardly the following incremental scheme may be applied:

$$\Delta f_j = \left(\frac{1}{\beta} \frac{\partial \varphi}{\partial x} \right)_j^2 \frac{1}{\beta kL} \left[\frac{Q_j}{Q_j} \left(\frac{1}{Q_j} \frac{\partial Q_j}{\partial S_i} \Delta S_i + \frac{1}{Q_j} \frac{\partial Q_j}{\partial H} \Delta H + 2 \left(\frac{\partial \varphi}{\partial x} \right)_j^{-1} \frac{\partial}{\partial S_i} \left(\frac{\partial \varphi}{\partial x} \right)_j \Delta S_i \right) \right] \quad (9)$$

Note that the discharge also depends on the hydraulic head across the structure. For the index i the summation convention is applied.

It appeared that this scheme does not converge. This is caused by the inverse relationship between discharge and horizontal gradient. If the discharge increases, the gradient will decrease and vice versa. By implication, the iteration process is slow and interrupted by jumps.

The rate of convergence is strongly improved by fixing the relation between the hydraulic head and the shape functions. This is achieved by setting the discharge at the entrance point explicitly to naught. Everywhere outside the channel the net discharge vanishes. It is subtle to demand explicit vanishing at the entrance. Apparently, it is required to ease down the jumping effects. The discharge at the entrance is characterized by:

$$\Delta Q_j = \frac{\partial Q_j}{\partial S_i} \Delta S_i + \frac{\partial Q_j}{\partial H} \Delta H = 0 \quad (10)$$

This equation is applied to eliminate the influence of the hydraulic head in equation (9), which leads to:

$$\Delta f_j = \left(\frac{1}{\beta} \frac{\partial \varphi}{\partial x} \right)_j^2 \frac{1}{\beta kL} \left[\frac{Q_j}{Q_j} \left\{ \frac{\partial Q_j}{\partial S_i} - \frac{\partial Q_j}{\partial H} \frac{\partial Q_j}{\partial S_i} \right\} + 2 \left(\frac{\partial \varphi}{\partial x} \right)_j^{-1} \frac{\partial}{\partial S_i} \left(\frac{\partial \varphi}{\partial x} \right)_j \right] \Delta S_i \quad (11)$$

With this scheme, the iteration process converges well.

4.3 Numerical Piping Design

The numerical piping programme MSeep is developed to design against piping. Here, a range of lengths of the erosion channel is considered. For each length equation (11) is applied to fix the head in the channel. The hydraulic head across the structure follows from equation (10). This hydraulic head corresponds to the length of the erosion channel. The maximum computed hydraulic head is critical. An example is shown in Figure 15.

5 Neural Networks for Piping

With MSeep a wide variety of geometries may be taken into account. The programme is easy to apply, although the geometry input may require some time and a calculation may take dozens of minutes. If the goal of piping design is probabilistic of nature, this takes too long. Also consultancy prefers ready made approaches. For both applications a simplified approach is sought. An example is Sellmeijers rule. This rule is valid for geometries consisting of a single layer of constant height, see Figure 16. It is determined by simplification of the analytical solution and curve fitting of parts of the results. It is a strong tool which may easily be applied in everyday consultancy.

However, in more critical problems the accuracy of the rule is insufficient. An advanced rule of two layers with diverse properties is required. An appropriate means to facilitate this is the use of an Artificial Neural Network. In principle, neural networks are meant for pattern recognition. The pattern to be recognized could be a handwriting or a fingerprint, but also results of computations. The advantage is that results of laborious computation are available at a fingersnap.

In the following, it will be illustrated how a neural network functions and how it can be applied successfully to the piping problem.

5.1 Principles of Neural Networks

In this contribution only a brief introduction into the theory of neural networks is given. An elaboration on artificial neural networks is beyond the scope of this paper, but can be found in Bishop [1995].

Artificial neural networks (ANNs) were developed in the Artificial Intelligence community to simulate the learning abilities of the human brain. By now, the technique has proven to be very useful in other scientific disciplines as well and nowadays it is used in many complex multi-dimensional regression and classification applications.

ANNs are constructed from interconnected ‘neurons’ or ‘nodes’. In each node a numerical transformation is applied to all input values. Then the results are summed, creating a new output value. The number of nodes, the numerical transformation and the topology of the interconnections define the problem solving capabilities of the ANN. A schematic visualization of a common topology, viz. that of a feed forward backpropagation ANN, is displayed in Figure 17.

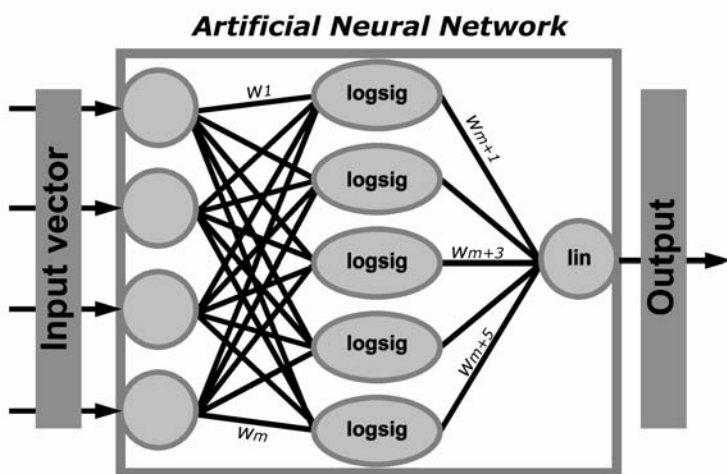


Figure 17: Sketch of the main components of a feed forward backpropagation artificial neural network.

The figure shows a schematic visualization of a feed forward backpropagation artificial neural network with nonlinear transfer functions in the (single) hidden layer and a linear transfer function in the output layer. By modifying the weights w on the connections between the neurons, the network can ‘learn’ to transfer input into output.

ANNs are capable of learning from examples or observations in various ways. For the type of applications described in this paper, feed forward backpropagation neural networks are quite suitable, see e.g. Bishop [1995] or Sarle [2002].

In McKay [1992] learning in these networks is described as ‘finding a set of connections w which gives a mapping which fits the training set well, i.e. has small error.’ For learning, a set of examples of input and corresponding output are presented to the network. The network will make a prediction of the output for these examples. The errors of these predictions are used to change the weights w .

The dataset used in training is often divided in two parts: a training set and a test set. The training set is used to change and improve the network weights as described before. The data in the test set is not directly used in learning, but is used to evaluate how well the network performs on new data. Neural networks can be trained to approximate arbitrarily complex functions, so the test set is required to check the performance of the network.

5.2 Choice of Characteristic Dimensions

To set up a proper network the degrees of freedom must be limited as much as possible. Every freedom multiplies the required number of data by a factor depending on its complexity. Therefore, the piping parameters are first grouped together into meaningful clusters. Moreover, the geometry must be chosen in such a way, that only a minimum of parameters are added to the flow problem. Local refinements are ignored.

An example of an appropriate network is outlined in Figure 18. Two layers of varying height with a minimum of characteristic dimensions are considered. Four layer heights and the width of the structure are sufficient to represent a sloping embankment on top of two layers with varying height.

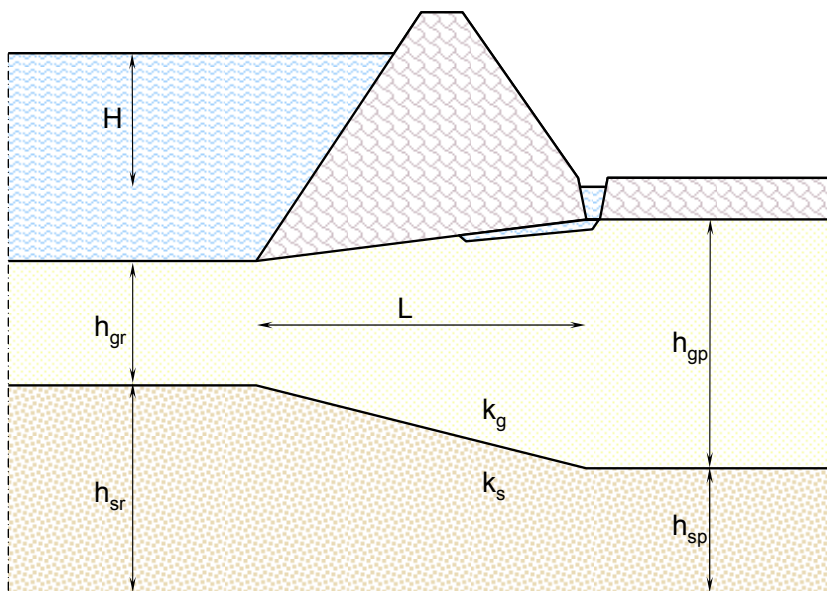


Figure 18: Typical embankment geometry applied for the training of the neural network.

The clustering of parameters is defined by the piping condition of equation (4). This condition is copied here in an adapted fashion:

$$\begin{aligned} \left(\frac{\partial \bar{\varphi}}{\partial \bar{x}} \right)^2 \frac{\bar{Q}}{kL} &= 1 & \bar{\varphi} &= \frac{1}{\beta} \frac{\varphi}{L} & \bar{x} &= \frac{x}{L} \\ \beta &= \frac{\pi}{3} \eta \frac{\gamma_p - \gamma_w}{\gamma_w} \frac{\sin(\theta + \alpha)}{\cos(\theta)} \sqrt[3]{\frac{1}{12} \frac{g}{kv} \frac{d^3}{L}} & \bar{Q} &= \int k \frac{\partial \bar{\varphi}}{\partial \bar{y}} dx & \bar{y} &= \frac{y}{L} \end{aligned} \quad (12)$$

The geometry is scaled by the seepage length L . The head is scaled by the cluster β and the seepage length L . The scaled head satisfies the steady state Laplacean equation for groundwater flow. By implication, the result for the scaled head depends on scaled geometry and permeability contrast of the layers alone.

It turns out that there are five characteristic dimensions in the neural network. The critical head is defined by:

$$\frac{1}{\beta} \frac{H}{L} = F \left(\frac{h_{gr}}{L}, \frac{h_{sr}}{L}, \frac{h_{gp}}{L}, \frac{h_{sp}}{L}, \frac{k_s}{k_g} \right) \quad (13)$$

F indicates ‘function of’. The arguments are input to connect the corresponding critical head.

A single piping computation determines the critical head as function of the geometry and soil parameters. The result, however, may be interpreted as the critical width of the embankment as function of the head across the embankment. Therefore, two useful types of neural networks may be derived: one for the classification of the critical head, represented by equation (13), and one for the critical width of the embankment. The latter is defined as:

$$\beta \frac{L}{H} = G \left(\beta \frac{h_{gr}}{H}, \beta \frac{h_{sr}}{H}, \beta \frac{h_{gp}}{H}, \beta \frac{h_{sp}}{H}, \frac{k_s}{k_g} \right) \quad (14)$$

Engineers usually prefer the last one, since the head occurs as a given according to the river discharge, while the width of the embankment may be designed. G indicates ‘function of’, which represents, of course, a different network than F .

A total number of five characteristic dimensions appear to be in the geometry of Figure 18. Arbitrary geometries would contain a lot more dimensions. If proper training requires N computations per dimension, then N^5 computations would be required for the geometry of Figure 18. This means that 16807 computations are required if $N = 7$. It will be clear that random geometries are out of the question for a neural network analysis. Geometries should be limited to the basic patterns required. It makes sense to develop different neural networks for different simple geometries to investigate a particular geometrical influence.

5.3 Development and Performance of a Neural Network for Piping

The next step in the process is training a neural network. Thereto, a sufficient number of computations for the chosen geometry is made. In this case ‘sufficient’ corresponds to between 10,000 and 20,000 computations. The number of hidden nodes in the network is free. Few nodes provide a smooth straightened result, while many nodes allow sharp bends in the result.

Experience shows that a number equal to the square root of the number of computations suits well in this case.

Training is performed by the standard procedures available in the MatLab neural network toolbox. The major part of the computations is used for training. 10% of the computations is set aside to check the accuracy of the trained neural network. In Figure 19 the obtained accuracy is shown. The horizontal axis represents the results of computation. The vertical axis is the result of a prediction with the neural network. A perfect agreement would show a 45° degree straight line, indicated in green. The blue dots show the actual results. The red dotted lines reflect the standard deviation.

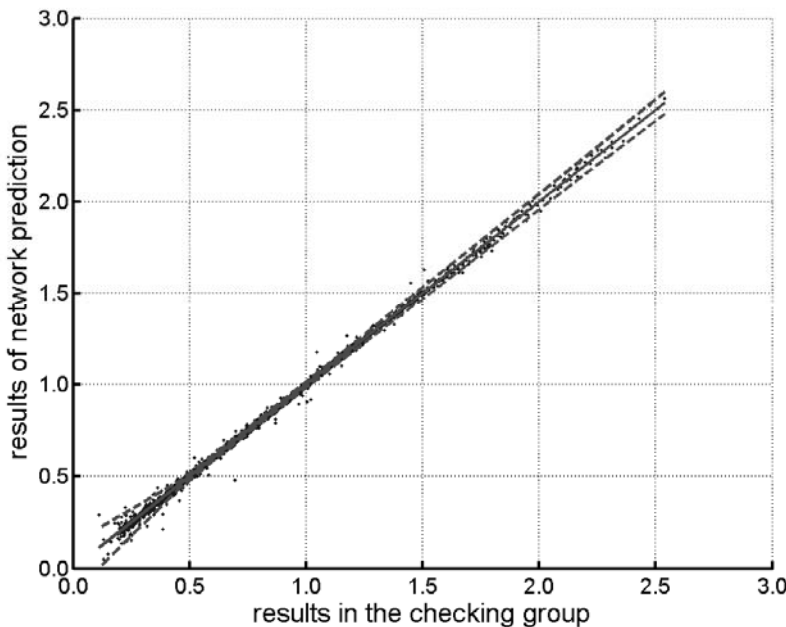


Figure 19: Accuracy of the neural network for the test set.

The agreement is good. There are a few declinations. These are concerned with extremely thin layers. There, the flow mesh is very thin and consequently only one row of finite elements high. This hampers a proper single computation and should be improved in the applied numerical tool. However, the neural network has a smoothing effect on this inconvenience. This may be observed in Figure 20. Here, both derived neural networks (related to equations (13) and (14)) are applied to the standard geometry of Figure 14. This is a special case of Figure 18. The results are shown as blue and green lines. The red dots represent direct computations. The agreement is so close, that the lines partly coincide. Computation around $h / L = 0.01$ is inaccurate, but the neural network predictions seem to be proper.

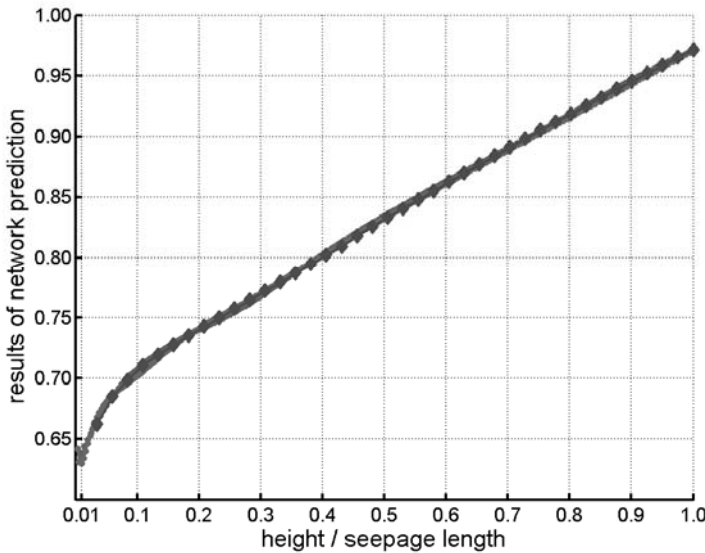


Figure 20: Accuracy of the neural networks for the standard geometry of Figure 14.

5.4 Applicability of Neural Networks for Piping

The application of neural networks to design against piping erosion and for safety assessments has a clear potential. With a proper set up of the model with respect to the implemented theory and geometrical limitations/possibilities, an advanced model can be made accessible for engineers who would otherwise easily restrict themselves to simple rules like the ones published long ago by Bligh or Lane.

Compared to finite element models, the major added values of neural networks are:

- *Speed.* A numerical computation requires dozens of minutes for an average mesh. Much more time is required for fine meshes. For probabilistic analyses this is too long. Also for common engineering practice this appears to be too long. A neural network yields results in a fraction of a second.
- *Ease.* Experience is required to operate a numerical programme properly. Using a neural network is much simpler.
- *Availability.* A neural network may be accessed from a PDA or a mobile phone, while a finite element model requires at least a laptop to run.
- *Accuracy.* Computations for very thin erodible layers suffer from badly shaped meshes. This causes inaccuracies, especially at the entrance of the piping channel, since the state of limit equilibrium is very sensitive here. In a neural network this effect is smoothed down. Moreover, the computations which form the basis for the training of the neural network are performed by an expert and therefore of a high quality. Finally, the consistency of the output range is better.

Literature

- [1] Batchelor, G.K. 1983. *An introduction to fluid mechanics*. Cambridge University Press, Cambridge.
- [2] Bishop, C.M. 1995. *Neural networks for pattern recognition*. Oxford University Press, Oxford.
- [3] Bligh, W.G. 1910a. *Practical design of irrigation works*, Second edition, Constable, Edinburgh.
- [4] Bligh, W.G. 1910b. Dams, barrages and weirs on porous foundations, *Engineering News*, December 29, p. 708.
- [5] DWW, Ministerie van Verkeer en Waterstaat, 2005: *Flood Risks and Safety in the Netherlands (Floris)*, *Floris study – Full report*. DWW-2006-014, ISBN 90-369-5604-9, Delft [available at http://www.projectvnk.nl/html/download.php?file=publicatie.137.strUpload.Hoofdrapport_VNK_Engels.pdf (last accessed on April 5, 2007)].
- [6] Griffith, W.M. 1913-14. The stability of weir foundations on sand and soil subject to hydrostatic pressure, *Minutes of proceedings*, Inst. Civil Eng., Volume 197, Part III, p. 221.
- [7] Harza, L.F. 1934. Uplift and seepage under dams on sand, *Proc. American society of civil engineers* [republished with discussions in 1935 in *Transactions American society of civil engineers*, paper no. 1920, Volume 100, pp. 1352-1406].
- [8] Koenders, M.A.; Meulen, T. van der 1987. *Hydraulic criteria for protective filters*. Unpublished report, Kingston on Thames/Emmeloord.
- [9] Kohno, I., Nishigaki, M., Takeshita, Y. 1987. Levee failure caused by seepage and preventive measures, *Natural disaster science*, Volume 9, Number 2, pp. 55-76.
- [10] Lane, E.W. 1935. Security from under-seepage masonry dams on earth foundations, *Proc. American society of civil engineers* [republished with discussions in 1935 in *Transactions American society of civil engineers*, paper no. 1919, Volume 100, pp. 1236-1351].
- [11] McKay, D.J.C. 1992. A practical Bayesian framework for backprop networks. *Neural Computation* 4:448-472.
- [12] Miesel, D. 1978. Rückschreitender Erosion unter bindiger Decksicht [in German, „Backward development of erosion under a cohesive top-layer“], *Proc. Baugrundtagung*, Deutsche Gesellschaft für Erd- und Grundbau E.V., Berlin.
- [13] Müller-Kirchenbauer, H. 1978. Zum zeitlichen Verlauf der rückschreitenden Erosion in geschichtetem Untergrund unter Dämmen und Stauanlagen [in German, „On the development in time of backward erosion in stratified soils under dams and barrages“], *Proc. Talsperrensymposium*, Munich.

- [14] Müller-Kirchenbauer, H., Hanses, U. 1981. Neuere Erkenntnisse zum Ablauf des Erosionsgrundbruches [in German, „New findings on the development of soil fracturing by erosion“], *presentation held on January 6, 1981* [further information unavailable].
- [15] Sarle, W.S. 2002. Neural Network FAQ, <ftp://ftp.sas.com/pub/neural/FAQ.html> (last accessed on April 13, 2007). Cary.
- [16] Schmertmann, J.H. 2000. The no-filter factor of safety against piping through sands, *Judgment and innovation – the heritage and future of the geotechnical engineering profession*, ASCE, Reston, pp. 65-132.
- [17] Sellmeijer, J.B. 1988. *On the mechanism of piping under impervious structures*. Ph. D. thesis Technical University Delft, LGM Mededelingen no. 96, Delft.
- [18] TAW, Technische Adviescommissie voor de Waterkeringen 1999: *Technisch Rapport Zandmeevoerende Wellen* [in Dutch, draft English translation *Technical Report on Sand Boils (Piping)* available at <http://www.tawinfo.nl/engels/downloads/TRSandBoilsPiping.pdf> (last accessed on April 5, 2007)]. Delft.
- [19] White, C.W. 1940. *The equilibrium of grains on the bed of a stream*, Proc. Royal Soc. London, Vol. 174A, London.
- [20] Wit, J.M. de, Sellmeijer, J.B., Penning, A. 1981. Laboratory testing on piping, *Proc. 10th Int. Conf. on Soil Mech. and Foundation Engineering*, Stockholm, paper 3/29, pp. 517-520.

Authors Name and Affiliation

J.B. Sellmeijer & A.R. Koelewijn
GeoDelft / Deltares, Netherlands
j.b.sellmeijer@geodelft.nl

Introduction to the Detection of Internal Erosion

Jean-Jacques Fry, Jean-Paul Blais, Sebastian Perzlmaier, Markus Aufleger and Matthias Goltz

Abstract

This report gives an introduction to the detection of internal erosion. The goal is to give guidance whether to monitor or not against this mode of failure and if monitoring is performed guidance in choosing the most suitable method. Clear distinction is made between remedial, preventive and routine maintenance. Emphasis is put on the cheapest and most effective investigation techniques used today for rapid diagnosis, and to long term monitoring techniques capable of detecting the potential hazard of internal erosion. The criteria for a risk based decision making process are defined.

1 Surveillance Based on Internal Erosion Risk

1.1 Internal Erosion is the First Mode of Failure to Control

Throughout the world, but mainly in Europe, a lot of existing water retaining structures are old and are of uncertain design and are more likely to be susceptible to internal erosion failure than more modern structures. The potential exists therefore that piping may breach the dam before repair measures can be instigated. Current literature does not give enough attention to this threat, despite the fact that failure by internal erosion is 10 times more frequent than failure by sliding. The common cause of damage to the integrity of the dam is through erosion.

This report develops a framework for assessing internal erosion in order to reduce the chances of failure. Once the hazard is evaluated, the owner can then investigate the most economical way to control the risk.

1.2 Internal Erosion may Jeopardize Current Surveillance

Piping could suddenly occur without significant warning beforehand. For instance, homogeneous dykes can be breached in a few hours by piping triggered by animal holes or shrinkage cracks. The frequency of visual inspections may be ineffective. Piezometers in the lower portion of a dyke often indicate low water levels whilst leakage is apparent at higher elevations. Piezometers spaced at 200m intervals will not be sufficient to guarantee no leakage. Dirty water on the surface of a dyke is a sign of on going internal erosion, however turbid water flowing in the foundation will not be seen.

1.3 Special Strategy is required for Controlling Internal Erosion

There are two important factors with internal erosion that in turn dictate the type of preventative measures to adopt.

- The danger is very localised.
- The danger can increase very quickly.

In some cases upgrading the design is the only solution and in other cases remote control surveillance combined with the installation of instrumentation is the most efficient solution to control the risk.

2 Maintenance Strategy

2.1 Maintenance According to the Risk Assessment Evaluation

The first step in selecting the detection method is the risk evaluation carried out at the end of the periodical dam safety review or given in conclusion of the quick risk assessment required after an incident. The evaluation concludes if filtration is guaranteed or not in the dam and its foundation.

Assuming that filtration is not ensured, erosion may progress and the owner faces one of the following four situations (table 1):

Table 1: Maintenance related to the risk evaluation result

Probability of occurrence of progression	Rate of progression	Consequence of the failure	Type of maintenance
high	high	high	Empty reservoir
high	Low	Low and high	remedial
low	low	high	Preventive
low	low	low	Routine

2.2 Investigations for Rehabilitation: Remedial Maintenance

In this case, the objective is on the one hand to give a diagnosis on the causes of the problem and on the other hand to define the extent of the disturbed zone: location and dimensions of permeable or erodable layers in the soil or the presence of discontinuities, fracturing or cavities of an unstable nature in rock. The experience of EDF is that the most suitable methodology consists of 3 steps:

- undertaking global non-destructive investigations to detect whether weak zones exist,
- investigating in detail the suspected areas to define their extent,
- carrying out the geotechnical investigations to define soil properties.

Thus the diagnosis is based on a three phase programme:

2.2.1 Phase 1: Data Compiling

This phase consists in collecting all existing data:

- history of the work (bibliography, topography, monitoring...),
- the geology of the foundation work (geological context, materials,...),
- local hydrogeology as the morphodynamic analysis of the river.

This research is supplemented by a visual inspection identifying on site the locations of all the geological, geomorphological and hydrogeologic signs of seepages, like the erosion zones, the specific vegetation, gullies, the springs or oozing, and any other surface anomalies.

2.2.2 Phase 2: Investigation by Non-Destructive Methods (Geophysics)

At the end of this first phase, an investigation by non-destructive methods is adopted. It is prudent to use 2 methods in order to cross check any anomalies. The aim of the geophysical investigation is to define the internal characteristics of the dam body by studying the change of a physical field measured along longitudinal and/or transverse profile. This phase can be split into two sub-phases:

2.2.2.1 Phase 2.1. Quick Geophysical Investigation

The advantage of the geophysical investigation is that it is a relatively quick and cheap investigation tool (several km/day) that provides a representative picture of the structure (body of dyke and its foundation), the nature of the foundation and the distribution of materials, the dry zones and the wet zones, the repaired and heterogeneous areas, the important anomalies (buried pipes and cableways, ...). The evaluation of the results enables a preliminary zoning to be performed according to the measured physical parameters (for instance, resistivity or SP). The current methods used by EDF along parallel longitudinal profiles (crest, toe downstream) are:

- SP (measurement of the difference in potential between two points in the ground) is efficient to find the entry and exit of a leak
- Fast Electrical panels –*up method or roll along* -(or electrical profiling multidepth), of dipole-dipole type, multi-electrodes in D.C. (well suited for linear structures)
- Electromagnetic methods low frequency with moving transmitter: EM 31 – EM 34 (or Slingram methods for old or unknown dyke only),
- RMT, Radio- Magneto-Telluric method (dyke),
- GPR, Ground Penetrating Radar.

The selection of the method to be adopted depends on the site specific conditions and on the performance required: depth of investigation, operational limits (table 2):

Table 2: Main methods of quick investigation

Method	Depth investigation	Physical Parameter measured	Speed Acquisition (by day)	Required Conditions for use	Prohibited use	Observations
EM 31	0 → 7m	Conductivity	4 – 5 km	Existence of resistivity contrasts	Industrial, Urban environment	Close field Low frequency
EM 34	0 → 50m		4 – 5 km /h			
RMT	0 → > 50 m	Apparent resistivity +Phase E/M	4 – 5 km (even more)	Good reception of radio waves	Buried Metallic networks	No Experiment At EDF
GPR	0 → 8 m (depend antenna frequency)	Speed propagation waves EM	3 – 4 km / h	Comparatively resistive terrain	Very conductive medium. Metallic screen	Difficult Penetration in Silt and clay
Electrical panel Roll along Direct current	0 → 50 m (depend geometry of the system)	Apparent resistivity	2 km	Existence of vertical or oblique resistivity contrasts	Urban, industrial areas, pipes, high-voltages cables	Method in full evolution

2.2.2.2 Phase 2.2. Local Investigation

This phase is devoted to the deep investigation by geophysical methods of the eroded or deteriorated area previously detected (ranging from a few meters to a few hundred meters long). The objectives of this phase are firstly to improve the initial geophysical zoning carried out in phase 2.1 and secondly to quantify the structural damage: Definition of the inlet and erosion path, dimensions of the weak area and determination of the flow rate of the leak. Thermal soundings allow a precise extent of the anomaly to be obtained such that the area affected by leakage in the dam can be defined (efficient to detect leakage, in winter or in summer, leakage in low or average height structures with un cohesive soil). The other methods frequently used in this phase are mainly the relative electrical potential and electrical panels. The profiles are carried out in a longitudinal and transverse direction to the dam. Cross-hole seismic shear wave testing was successfully developed for sinkhole detection and evolution in large dam (S. Garner). Ground Penetrating Radar, acoustic methods and Ground Infrared Thermography may be a complementary investigation. The zones with identified leaks can then be tested using

brine tracers enabling the salt transport to be tracked by electrical panels. The results of this local inspection then makes it possible to rigorously establish the destructive investigations to be performed to enable validation of the geophysical anomalies.

Table 3: Methods for local inspection

Method	Depth investigation	Physical Parameter measured	Conditions of use	Prohibited use	Observations
Thermal sound	0 → 25 m (depend on gravel and cobbles)	temperature	Summer or winter	Homogeneous Clay material	Efficient to localise leakage and seepage
Electrical panel Direct current	0 → 50 m (depend geometry of the system)	Apparent resistivity	Existence of vertical or oblique resistivity contrasts	Urban, industrial areas, pipes, high-voltages cables	Method in full evolution
Self Potential	Few meters	Potential difference	Water flow or ions transport inducing an electrical current	Urban, industrial areas: pipes, buried electrical or telephone cables, heavy rain, high evaporation	Efficient and under development to quantify flow rate
GPR	0 → 8 m (depend antenna frequency)	Speed propagation waves EM	Comparatively resistive terrain	Very conductive medium. Metallic screen	Difficult Penetration: Silt, clay
Acoustic methods	Few meters	Acoustic signals generated by the seepage	Noise of seepage identified by its frequency spectrum	Very noisy zones	Very simple to use

2.2.3 Phase 3: Investigations by Destructive Methods

Geophysical methods have often been considered as an alternative to geotechnical methods, but in fact they complement each other and it is useful to calibrate them against each other and to correlate their data. Geotechnical measurements only give information along the drillhole, but it is possible to use the same drillholes to take geophysical measurements, and thus to test the ground between drillholes.

Main geotechnical investigations are:

- Core drillings with laboratory tests on samples, for instance the Hole Erosion Test should be now mandatory and should replace the pine-hole test
- Cone Penetrometers Tests
- Destructive drillings with data recording offers a couple of advantages on CPT: continuous measurement and ability to pass through all types of ground. Other advantages are speed, low cost, and easy to use.
- Permeafor: the permeafor is a new instrument specifically adapted to diagnose internal erosion. It has been developed to locate the weakest zones by cone penetration and to determine the flow rate versus depth by continuous water injection test (URSAT, 1995).

The final step of the process is the design of the repair. For rehabilitation works that do not repair the waterproof element, such as downstream toe weighting, preventive maintenance should be recommended to check for any further deterioration and if deemed necessary to repair the defect detected by DFOT.

2.3 Preventive Maintenance

2.3.1 Distributed Temperature Measurement

When performing a review of a structure internal erosion cannot be ruled out, especially in the foundations of old earthfill dams or long dykes where site investigations in the design and construction stages were of a limited extent. Should any sign indicating the occurrence of internal erosion be noted, the extent of the zone affected should be urgently assessed and repaired using the most efficient methods. If it is considered that there is a low probability that internal erosion may occur in the structure and then only after a long time the best solution to guarantee a tolerable level of safety and to save money is to improve the monitoring of the structure such that any signs of internal erosion can be detected. One of the major limitations when applying routine monitoring along several kilometres of a long embankment or a dyke is the fact that the measuring points are inevitably widely spaced and the time interval between readings are too long for the initiation of piping to be detected.

Thus a suitable method for detecting internal erosion should consist of taking a series of measurements in real time. The goal is to detect any kind of anomalies, interpret them in real time with the participation of experienced engineers and compare them to several safety criteria. Distributed Fibre Optic Temperature measurements are well suited to achieve these goals. Remote control monitoring of temperature by fibre optic is the only method available for practical application, which has been used during the last 10 years in Germany, Sweden and France.

This advanced preventative maintenance is well suited for uncohesive soil. However for homogeneous clay embankments, it may be incorporated as part of a structure redesign, for instance in the filter of a weighting berm (see remedial maintenance).

This method is suited to zones where suffusion is suspected and thus it is important that the condition of the structure is assessed by regular temperature measurements. Hourly, daily or

monthly measurements quantify the diagnosis for an annual evaluation. Unrecoverable trend may be detected and interpreted.

Remote control monitoring of the resistivity and SP are others methods under development in Sweden.

2.4 Routine Monitoring

For the low risk case of a water retaining structure with a low probability to be subject to piping failure, the owner relies on routine surveillance: frequent visual routine tours and a few global parameters like total seepage flow.

3 Method of Evaluation and Interpretation

3.1 Routine Maintenance

Internal erosion affects permeability and is therefore revealed by variations in leakage flow rate and pressures. Such changes are often limited to local areas and can generally be detected by visual inspection. Therefore the method of evaluation and interpretation is based mainly on visual inspection. So it is important that these inspections are performed according to well established procedures, by persons that have a background knowledge of the dam and who are then able to detect, check and interpret changes. Qualification of the personnel who carry out these inspections has to be defined and respected.

Concerning monitoring, statistical analysis may underline any abnormal change in real time. In such a case a comparison with the expected behaviour of the structure compared with threshold criteria should be performed for global parameters (total flow discharge) and some local parameters (pore pressure).

3.2 Preventive Maintenance

3.2.1 General

According to the particularities of internal erosion, the method of evaluation of the data must be done so as to:

- detect any possible dysfunction.
- inform the engineer in real time of the anomaly.
- result in guaranteed operability when required.
- Preset limits of data plausibility.
- clearly distinguish between the behaviour of the instrumentation and the real behaviour of the dam.

There are two types of interpretation: the statistical approach and the hydro-mechanical approach. The statistical approach is currently the most efficient : any new trend detected, after verification and correction is a sign of a physical change in the body of the dam. This approach is well suited to clayey soils. The physical approach is the most academic way however it is not so easy to interpret.

The method of interpretation must be done to enable:

- The relevant parameter to be defined.
- The influence of the environment and the behaviour of the dam to be clearly distinguished
- Any irrecoverable trend of the dam behaviour to be identified.
- The behaviour to be judged against preset criteria.
- The various measurement criteria to be compared and the alarm to be raised.
- Correlate chronological data to previous dam behaviour to check the calibration of the diagnosis.

3.2.2 Temperature

Interpretation of temperature measurements have been developed through 2 approaches:

- The passive approach, using natural temperature as a tracer
- The active method, inducing heat to evaluate thermal response.

The passive method has two backgrounds. The first one was proposed by Sam Johansson. The field of application is an area saturated by the water table, not too close to the surface and not too deep. The basic point is the seasonal variations of monitored temperature within a dam. Analysing the lag time and damping versus reservoir temperature can quantify leakage flows that can be quantified assuming simplified assumptions. The simplified model deduces discharge flow rate and permeability in the seepage based on the heat transfer equation. Johansson has defined two methods for determining permeability and discharge flow, which were successfully applied in a large number of case studies. The method is sensitive for seepage flow changes, in the order of 10^{-6} or $10^{-5} \text{m}^3/\text{s}/\text{m}$.

The second background of the passive method is a more sophisticate statistical approach. A joint team from EDF and CEMAGREF has recently developed it. The field of application is for both saturated and unsaturated soils using real time measurements. The analysis consists of testing the assumption that the anomaly between the new monitored temperature and a reference temperature induced by conduction from the surface at the measured point is significant or not. This new approach has been successfully applied to the leakage detection at Oraison canal. Quantification of leakage is under development by EDF. The method is sensitive for seepage flow changes, in the order of $10^{-5} \text{m}^3/\text{s}/\text{m}$.

Filter under downstream shoulder is a very effective location for cables (Nilsson and Bartsch, Johansson), if not under downstream toe (for homogeneous dam). The depth is linked to method of evaluation. Up to now, no extensive comparison has been done between the three methods of evaluation (two passive and one active). For critical structures, owner are advised to install a system ready to perform not one but at least two methods of evaluation.

3.2.3 Resistivity

Sjodahl and Johansson have demonstrated the feasibility of the resistivity method to be a new non-destructive method suitable for long term monitoring. The interpretation is under development. Inspection of the resistivity versus time plot is the simplest method of

interpretation. Irrecoverable trend is the main indicator. Back analysis by theoretical model of the resistivity field of the dam may be carried out until the calculated field of resistivity fits the observed data. Definition, improvement and justification of criteria and sensitivity are going on.

3.2.4 Self-Potential

Self potential is currently used for investigation. Data interpretation is a simple qualitative inspection of the plotted relative potential profile or of the plot contours from cross-profiles. Location of minimum potential in the upstream face may correspond to the entry point of seepage flow on the upstream face of the dam and the location of the maximum potential to the flow is likely to be exit point on the downstream face.

New 2D and 3D interpretation, with back-calculation of flow pattern are under development and look very promising. However monitoring by SP technique shall need several years to be fully calibrated.

4 Relevant Parameters for Internal Erosion

4.1 Routine Maintenance

Visual inspection will therefore prevent most potential failures by identifying:

- either traces of humidity (seepage, changes in colour, development of vegetation, springs),
- or traces of erosion (turbidity, deposits of eroded materials, particles in suspension).

Maintenance of the downstream face and the toe culvert is required to make surveillance easier.

Leakage flow rates and piezometer readings are mandatory elements in monitoring. Any variation in them must be rapidly analysed to detect signs of internal erosion triggered by ageing or accident.

4.2 Preventive Maintenance

The big advantage of the preventive maintenance is the monitoring of the basic parameters governing initiation of internal erosion:

- The flow velocity: it is the initiating parameter for particle detachment: the knowledge of –that parameter enables the grain size affected by internal erosion to be identified.
- The flow discharge integrating the different flows gives a global view of the seepage.
- The hydraulic gradient is another main parameter, governing not only the entrainment of particles by flow through the material but the stability as well.
- The permeability is an important parameter and may be compared to specifications and safety guidelines.
- The degree of saturation could be useful to interpret data since saturation is a local sign of evidence that seepage is passing through a particular point.

5 Criteria

5.1 Type of Criteria

Referring to preventive maintenance, it is useful to provide the owner with 4 hazard levels:

- Anomaly level: a sudden change higher than sensitivity level is noticed
- Alarm level: the initiation of internal erosion is very probable
- Intervention level: internal erosion development is no more tolerable
- Critical level: failure is probable, this level is fixed only to evaluate the margin of safety in terms of flow velocity, pore pressure, discharge flow rate,...

5.2 Alarm Level

They are 2 approaches of the alarm levels:

- The statistical approach is currently the most efficient: any new trend detected after verification and correction is a sign of a physical change in the dam body. This approach is well suited to clayey soils.
- The physical approach is the most academic way, not so easy to handle. 5 basic parameters should be checked:
 - Flow velocity
 - Flow rate
 - Hydraulic gradient
 - Permeability
 - Degree of saturation

S. Perzlmaier gives the physical threshold value for initiation for uncohesive soils. Thus it is possible in uncohesive soils to assign threshold values for preventive maintenance by geophysical remote-control methods, like fibre optic.

5.3 Intervention Level

The rule of thumb for dam repair is based on the average permeability K of the deteriorated sealing element:

- $K > 10^{-5}$ m/s: upgrading the watertightness is relevant
- $K < 10^{-6}$ m/s: downstream filter and drainage system is enough
- $10^{-6} \text{ m/s} < K < 10^{-5} \text{ m/s}$: special attention is needed.

According to stability analysis, hydraulic gradient may be correlated to safety coefficient. Therefore, the threshold value is the hydraulic gradient correlated to the critical safety factor.

From case studies of repairs performed on large dams the same type of conclusion may be drawn using global discharge rate Q:

- $Q > 0,01$ to $0,1 \text{ m}^3/\text{s}$: upgrading the watertightness is necessary.
- $Q < 0,001$ to $0,01 \text{ m}^3/\text{s}$: provision of downstream filter and drainage system is sufficient.
- In any case for $0,001 \text{ m}^3/\text{s} < Q < 0,1 \text{ m}^3/\text{s}$ a survey is needed.

For dykes repair, particularly on alluvial foundations, where deposits are horizontally stratified with high permeability, the critical flow velocity criteria, proposed by S. Perzlmaier is particularly relevant. For clay dyke on sandy foundation the hydraulic gradient criteria developed by Sellmeijer is recommended.

Local measurements are of the utmost importance. Fiber optic sensors with 0.5m distance measurement spots are theoretically able to detect sand boils.

For sandy gravel foundation of the Rhone and Rhine rivers, it is noticed that :

- $Q > 0,1$ to $1 \text{ m}^3/\text{s}/\text{km}$: upgrading of watertightness is usually decided.
- $Q < 0,01$ – $0,1 \text{ m}^3/\text{s}/\text{km}$: downstream filter and drainage system is often the solution.

In any case, criteria is checked and revised by engineer according to past behaviour, soil type in the dyke and type of mode of failure.

5.4 Critical Levels

Critical velocity is the through flow velocity able to remove particles of the downstream toe by erosion (internal or external erosion: see paper of Perzlmaier, Muckenthaler and al). For fine sand foundation, in Netherlands, the critical discharge and velocity thresholds computed by first theoretical application of the Sellmeijer model, for a 50 m width dike on a sandy foundation with a sand permeability 0.0001 m/s and particle diameter around 0.0002 m , at the exit point in the sand boil, just before the beginning of piping failure, turn out to be:

- Velocity: 0.0768 m/s .
- average specific discharge: $0.000171 \text{ m}^3/\text{s}/\text{m}'$ or $10 \text{ liter}/\text{minute}/\text{m}'$.

Critical discharge is deduced from the integration of the critical velocity along the deteriorated surface. The use of discharge is not appropriate to detect piping. From case studies, Fell and al, after collecting data on failures, showed that it is difficult to control leakage with discharge flow rate around $0,5 \text{ m}^3$.

Critical hydraulic gradient is assessed by stability analysis: it is the value correlated to a safety factor =1.00.

6 Conclusion

New methods of detection of internal erosion are now available. They have been developed to keep a high level of safety on dams where filtration is not guaranteed. If it is suspected that internal erosion may occur in the structure over a certain period of time, the best solution to guarantee a tolerable level of safety and to save money is to improve the monitoring of the

structure, and to apply surveillance based on the detection and interpretation of the progression phase of internal erosion.

Thus the adequate method for internal erosion detection should consist in taking distributed measurements in real time. Distributed Fibre Optic Temperature measurements are well suited to achieve these goals. Remote control monitoring of temperature by fibre optic is the only one method available for practical application and has been used for the last 10 years in Germany, Sweden and France.

Authors Name and Affiliation

Dr. J-Jacques Fry, Jean-Paul Blais

EDF, France

jean-jacques.fry@edf.fr

jean-paul.blais@edf.fr

Dipl-ing Sebastian Perzelmaier

TIWAG – Tiroler Wasserkraft AG, Austria

sebastian.perzlmaier@tiwag.at

Markus Aufleger

University of Innsbruck, Austria

Unit of Hydraulic Engineering / Institute of Infrastructure

markus.aufleger@uibk.ac.at

Matthias Goltz

University of Innsbruck, Austria

Unit of Hydraulic Engineering / Institute of Infrastructure

matthias.goltz@uibk.ac.at

Detection of Leakage by non Destructive Methods : EDF Experience

Jean-Paul Blais, Serge Gravelat, René Foillard

Abstract

Detection of leakage by non-destructive methods is the first step of dam safety diagnosis after incident. From EDF experience are presented here three methods: the high speed electromagnetic profiling, the ground penetrating radar and electrical panel with brine tracing. General principle, objective, equipment and procedures, field of application and method of evaluation are shortly described.

1 High Speed Electromagnetic Profiling

1.1 Principle

The electromagnetic method consists in measuring the ground response to an electromagnetic field. In practice, a primary field is emitted which is transformed into a secondary field under the influence of a conducting body, and measured by a receiving reel. The primary to secondary field ratio makes it possible to deduce the average ground conductivity. By the use of this method, the conductivity of the ground is measured in milliSiemens/m (or its reverse, resistivity, in Ohm.m). The strongest conductivities characterize clays (50 to 100 milliSiemens/m) whereas the lowest values (3 to 10 milliSiemens/m and less) correspond to the resistant layers such as sands, gravels or ground rock. The intermediate values denote the presence of resistive materials into more or less important quantity within the argillaceous layers.

1.2 Objectives

The aim of the method is to locate heterogeneities, zones of repair, in a dam body in order to establish a zoning of the work. Generally, two profiles are carried out: in peak and toe of downstream side of dams.

1.3 Equipment and Procedure

The equipment comprises two reels connected to a measuring device. One reel emits the electromagnetic field and the second receives the response signal. The two reels are maintained coplanar at a distance D of one another. Measurements can be taken according to 2 positions of reels: they are either horizontal or vertical, for the same reel spacing. The investigation depth is theoretically equal to 0.75 D when the reels are vertical, horizontal magnetic dipole, and 1.5 D when the reels are horizontal, vertical magnetic dipole.

The acquisition system is a high-output system of Fast EM® type (see photo below), equipped with an EM31 or EM34 device from Geonics and associated to an embarked DGPS. The reel-spacing is 3.6 m for EM31 and 10 m for EM34. An automatic acquisition system allows a measurement every second, that is to say, for a travel speed of 4 to 5 km/h, every 1.5 m.



Figure 1: Fast EM® investigation device with mounted EM34

1.4 Field of Application and shortcomings

The real investigation depth can sometimes be reduced when the surface grounds are electrically conductive. The electromagnetic waves will then circulate preferentially in this layer, without reaching the lower levels. The presence of metal fence, high-tension lines, sheeting piles... can disturb measurements.

1.5 Data Processing and Interpretation

The results are presented as profiles or iso-conductivities charts, for each of the two reel positions, if the number of profiles allows it. Anomalies are detected and investigated by a destructive investigation campaign (mechanical surveys).

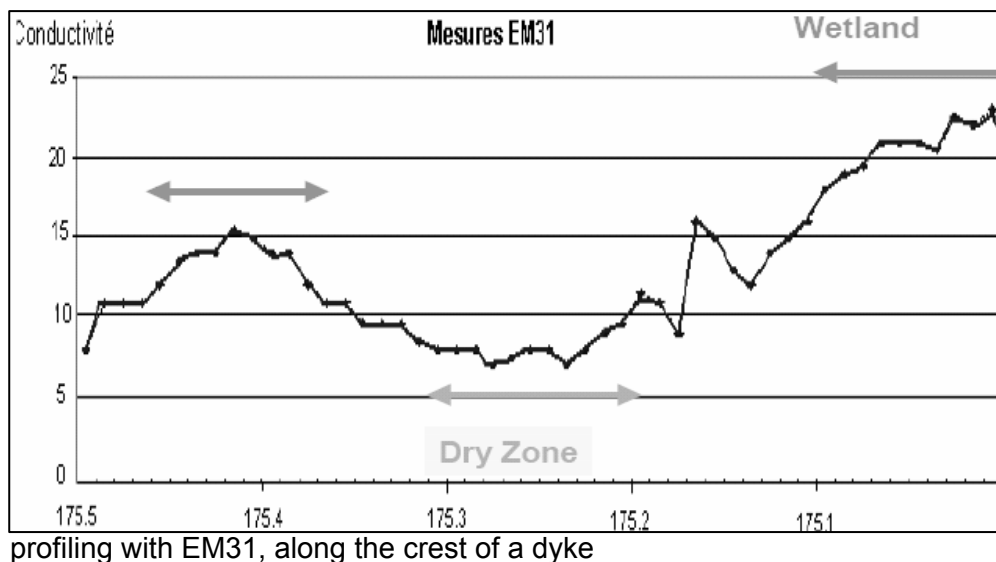


Figure 2:
Electromagnetic

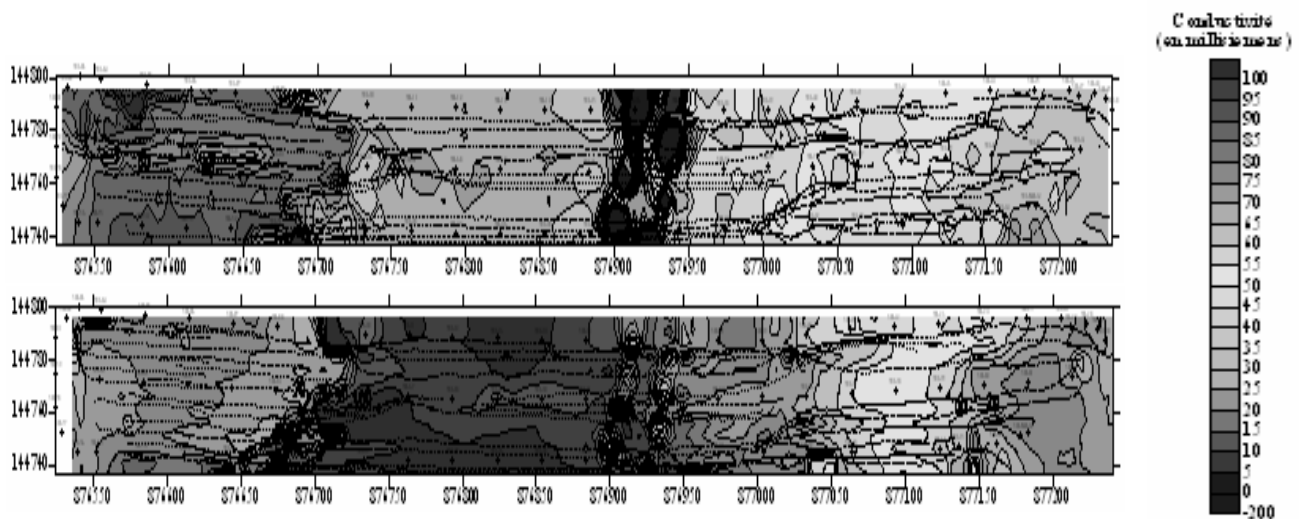


Figure 3: Iso-conductivity chart with two reel positions, with EM34.

2 Ground Penetrating Radar Methodology

2.1 Principle

Search of defaults in the internal structure of dams and its embankments such as presence of drains and water circulations, can be carried out by G.P.R. reflectometry from the sides and the top of the dam. This geophysical investigation is based on the detection and location of discontinuities within the constitutive materials of the embankment dam.

The technique of G.P.R. data acquisition has the advantage to be carried quite continuously and fast along the profiles of measurements, it is a non-destructive method with depth penetration reaching 5 to 15 meters. An electromagnetic impulse is radiated from the antenna and propagated in the material. As it encounters a change in the electrical properties of the media, part of the wave is reflected and part is transmitted. These changes in the dielectric properties correspond to discontinuities in the ground or other structures. As an example a void or the interface between two materials conducts to the reflection of part of the emitted energy to the reception antenna.

The detection and sampling of the radar echoes for a given time (from 20 to 1000 nsec) allows the reconstitution of the echoes trace to the shooting point. The number of selected traces per second is generally of 25 scans or traces per second. In exceptional cases, 256 scans/sec could be selected. The signal received is recovered in a screen or graphic recorder and over a magnetic recorder to enable the signal interpretations. It means information from underground or structures investigations are quite continuous, with more than one scan per centimetre. The data is presented as a "cross section" or radar profile.

The depth of investigation depends on the attenuation characteristics of the media and on the working frequency. The attenuation is mainly dependant on the resistivity of the material; the greater the resistivity, the lower the attenuation. The depth of investigation decreases for increasing frequencies and the absolute precision at the depth could reach the order of the centimetre. At greater depth the resolution (which means the minimum distance between two

discernible objectives) depends on the wavelength in the media. In the best cases it is of the order of a few centimetres.

The radar method applied to geophysical investigation of the dam's body is able to delineate any contrast of dielectric properties of the medium such as:

- loss material, heterogeneous or washed soils
- voids, cavities, pipes, drains.

2.2 Objectives

The purpose of G.P.R. data acquisition, operated from the top, or the sides of dam embankments along longitudinal profiles for high velocity data acquisition, and transversal profiles for complementary investigation, is to give an internal image of the dam such as:

- structural repartition and distribution of the materials in the body;
- detecting and locating anthropic works such as buried works, pipes, networks;
- locating natural drains or water flows;
- detecting probable presence of saturated medium in water content.

2.3 Field of Application: Advantages, Constraints and Limits

The advantages are:

- In comparison with other geophysical techniques, such as electromagnetic and electrical methods, GPR which is a dynamic method, permits to find anomalies or events with high accuracy in x, y and z location, less than 1 meter in x, y and 10 % of the depth z.
- The image of underground variations is continuously seen with its own geometry being interpreted in terms of naturalistic events.
- Data acquisition can be carried out at 5 to 10 kilometres of longitudinal profile per day.

The Constraints and limitations are:

- The penetration rate is reduced by the presence of clay content, and the dielectric contrast between two different media must be sufficient to generate wave reflections.
- The presence of water content reduces the wave velocity and increases the attenuation of the signal, decreasing the performances of the G.P.R.

The radar sections obtained from raw and processed data permits to detect and locate any dielectric contrast between two media or a medium and a particular event. G.P.R. investigations are able to detect with high precision and accuracy:

- buried objects such as pipes, bombs, buried structures as war constructions
- the different layers of whom the dam is made between 0 and 10 meters.
- Anomalies of these layers such as nature of the medium, homogeneous soils or heterogeneous soils such as washed soils, structural deformations of the interface between two layers linked to local saturated medium.
- Points of the dam structure such as drains or holes linked to water flow risks.



Figure 4: Radar equipment operating on the crest of a dyke

2.4 Equipments

Fast data acquisition required G.P.R. data with high sampling velocity. High penetration depth is linked to low transducer frequency, generally between 50 to 100 MHz high powers radar antennas in bistatic mode (separate transmitter and receiver with long offset ≥ 1.5 meters) top increases the ratio signal/noise. Monostatic 200 MHz transducer can also be used. Data must be linked to GPS measurements. The performances of the technique are summarised in table 1.

Table 1: performances of Radar

Acquisition velocity	10 to 15 km a day on surfaces without obstacles.
Depth of investigation	0 → 10 meters with bistatic 100 MHz antennas
Prohibited case	Conductive medium such as pure clay or salty medium application to relative resistive soils.

2.5 Processing of the Data and Interpretation.

The process of the data consists in using filters, deconvolution and migration operators according with G.P.R. software. The process is used to highlight the data. Interpretation is done from raw and processed radar sections edited and correlated from one profile to an other one after calibration of distance.

2.6 Case Studies

Recent results of several surveys on dykes of Grand Canal d'Alsace demonstrate the capability of the radar technique to investigate more than 10 kilometres of profile per day. Results can be seen on the following commented figure 4 (equipment), 5 and 6 (radar interpreted sections).

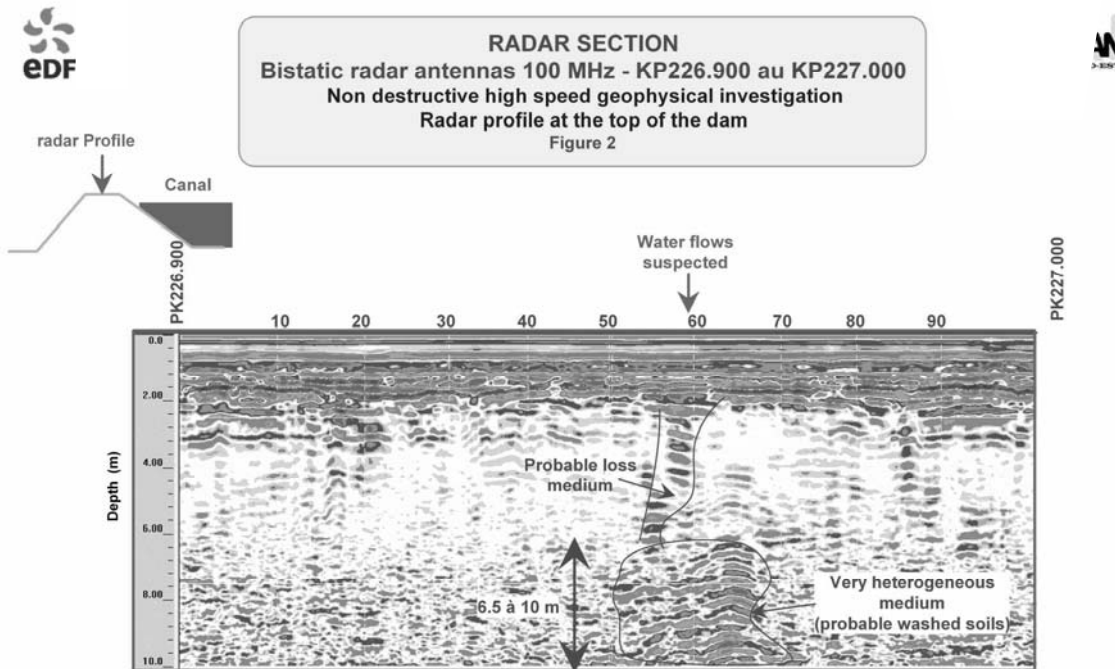


Figure 5: Example of interpretation of Radar profile at the dyke crest : bistatic radar antennas 100MHz

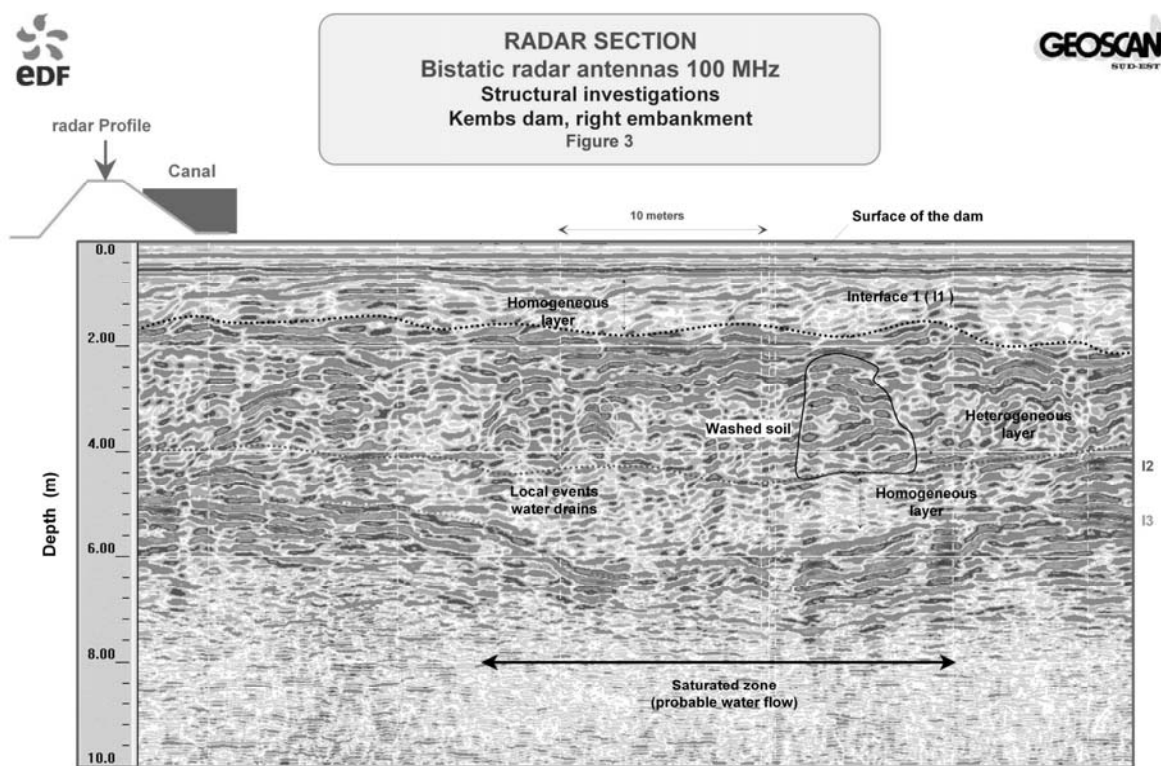


Figure 6: Example of interpretation of radar results

3 Brine Tracing with Electrical Panel

3.1 General Principles of Electrical Panel

The electrical panel is a geophysical method of investigation based on measures of earth resistivity in shallow subsurface for various depths using electrodes grounded directly in the soil. The 4-electrodes system gets 2 injecting electrodes (A and B) and 2 measuring electrodes (M and N). A current I is injected between A and B and the induced potential V is measured between M and N. The quadripole of measurement is widenend to increase the depth of investigation by combining the various electrodes of the panel to create new devices. The measured value is shifted compared to the previous quadripole of smaller size. The measurements taken at the ends of the panel are located on a diagonal whose lower end corresponds to the depth of maximum investigation.

3.2 Acquisition Device and Data Processing

The system of injection of current and acquisition used is the multi-electrode system associated to a resistivimeter (SYSCAL from Iris Instruments, LUND from Abem). The device includes 24 to 48 electrodes, or even more, with a 2,50m spacing. The acquisition's configuration used is of the Dipole-Dipole type, which offers a good definition for the side variations of resistivity. The data files are transferred and converted to be treated by an inversion process with the RES2DINV software developed by H. LOKE.

3.3 Brine Tracing

The used methodology is as follows:

- Before the brine injection, an electrical panel is done in order to get reference data of the work.
- The salted water is injected into reserve at the supposed infiltration zones with a system allowing an injection in the bottom of reserve (cf photography below figure 7) and according to the results of self potentials measurements
- At the same time, the measurement of the electrical panels is done, according to a predefined protocol and rhythm which depends on the speed of the salted flow in the work or the ground. Data treatment is carried out at the end of each acquisition in order to immediately detect the passage of the salted face.

Temperature measurements of water and ground near the dam are done every hour throughout operation in order to correlate if necessary the variations of resistivity and temperature.

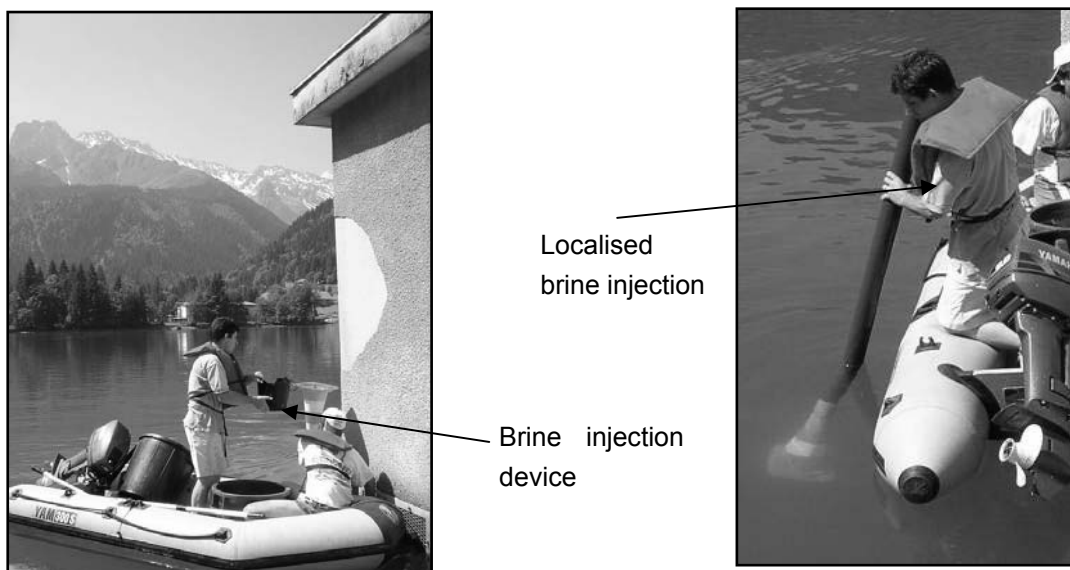


Figure 7: salt injection for electrical panel tracing

3.4 Results Analysis

Differential Analysis of Electrical Panel

The differential analysis of the apparent resistivities obtained for every panel compared to initial measurement is essential to the data processing. For every quadripole the difference in apparent resistivity between the reference and the concerned panel is calculated. This method makes possible to detect the weak resistivity variations which often characterize the circulation of the brine and which would not appear on the inversed sections because they will be smoothed by the treatment. Figure 8 presents the contours of initial resistivity measured in the initial panel and the results every hour of the differential analysis for detecting leakage paths in the vertical section along small dam axis Figure 2 presents horizontal detection on plan view from differential analysis with 4 panels: pink area is the brine flow 1h after injection, orange area is the progression of brine flow 3h after and green area is the progression of brine flow 5h after injection.

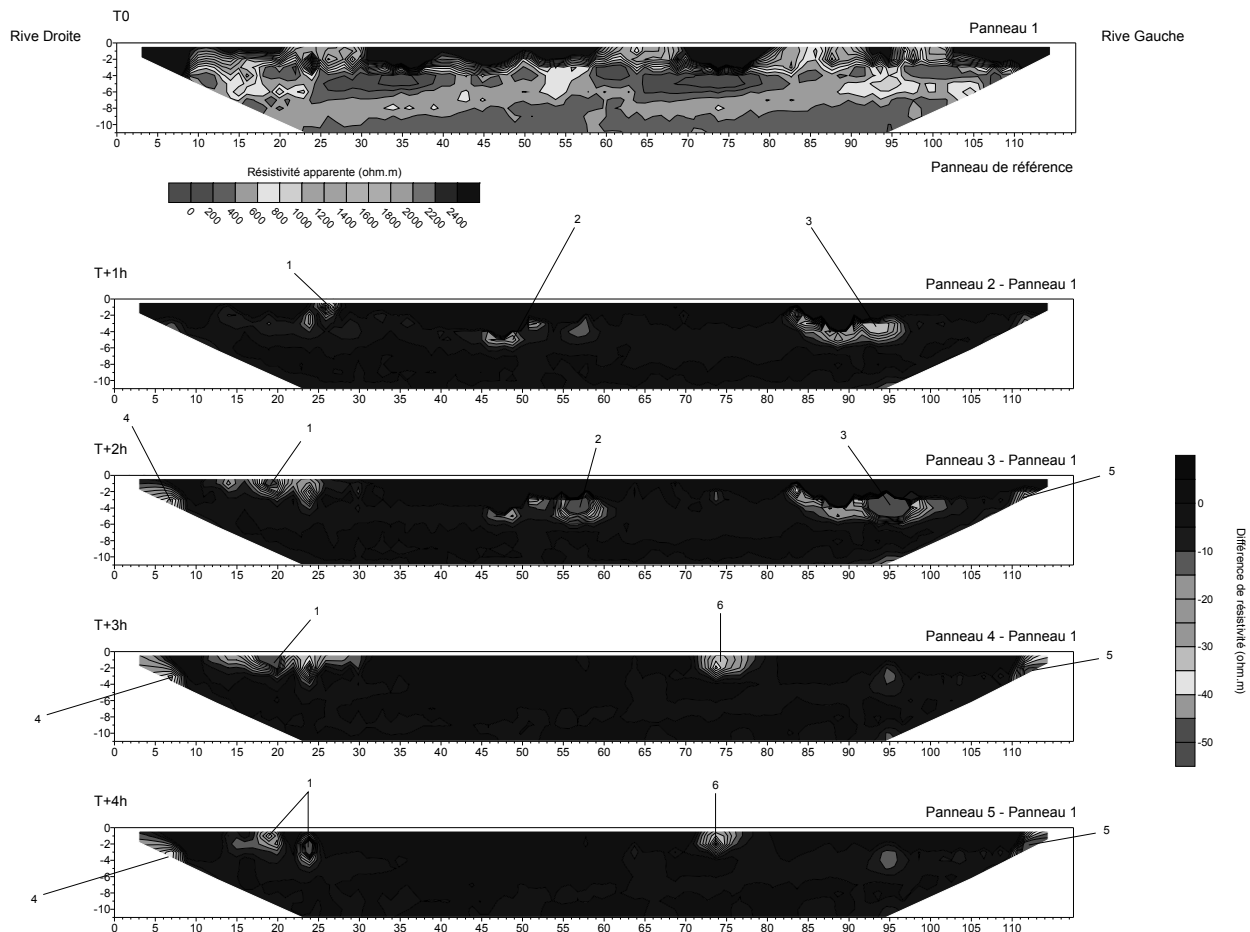


Figure 8: Detection of leakage paths in vertical section with differential analysis

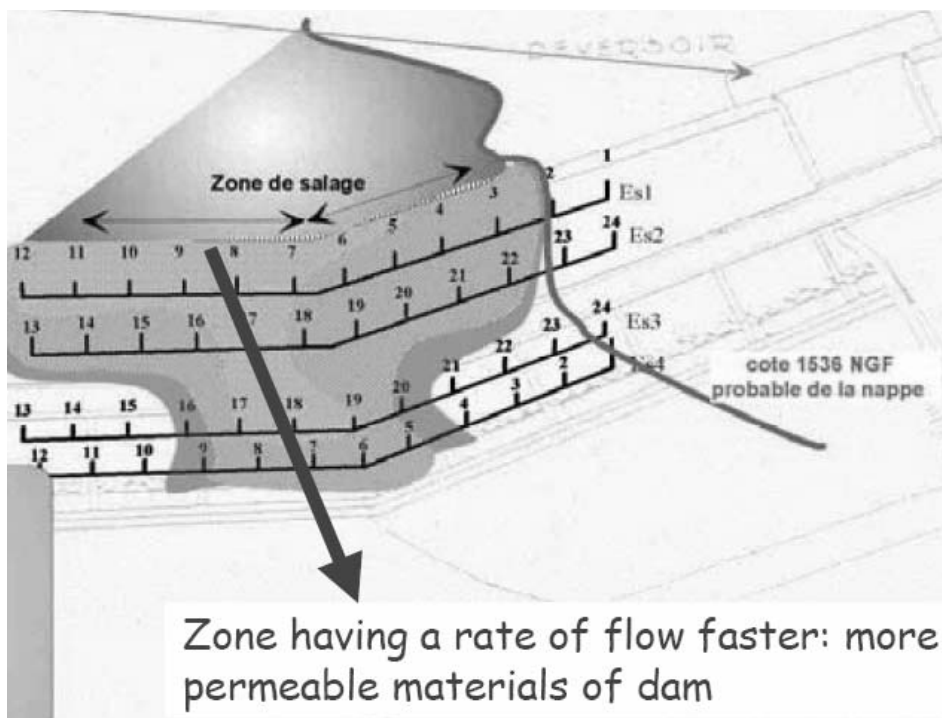


Figure 9: Example of leakage on a plane view of dam foundation

Authors Name and Affiliation

Jean-Paul. Blais ,
EDF, Geology & Geotechnical
jean-paul.blais@edf.fr

Serge Gravelat
SOBESOL
s.gravelat@sobesol.com

René Foillard
GEOSCAN
geoscansudest@geoscan.fr

Analysis of Conventional Monitoring and Cross-Hole Seismic Data for Detection of Internal Erosion in an Earthfill Dam

S.J. Garner, S. Vazinkhoo

Abstract

The process of internal erosion within earthfill dams can often take many years or decades before obvious symptoms manifest on or from the dam surface. Symptoms such as sinkholes, boils, sudden increases in seepage flows and pore pressures or the emergence of turbid water often occur at the final stages of an accelerating sequence, after the opportunity to proactively manage has long passed. However, subtle indicators and warnings of the developing failure process are often embedded in the historical surveillance data taken from conventional instruments such as piezometers and weirs or from well-established geophysical techniques such as cross-hole seismic.

This paper describes techniques used to analyze the past performance to help predict the future performance of an earthfill dam using conventional instrumentation data. Techniques discussed include: trends analyses, progressive seepage modeling, scenario modeling and repeat cross-hole seismic shear wave testing.

1 Introduction

The occurrences of sinkholes at several dam sites in British Columbia, Canada provided the opportunity for BC Hydro to carry out extensive field investigations and develop analytical processes in order to better understand the causes and to be capable of proactively, rather than reactively, managing any risks. The aim of the processes was to provide a method for determining early indications of developing failure modes. The earlier an indication, the earlier an informed risk management plan can be implemented. The plans can include:

- increasing instrumentation monitoring frequencies, including use of Automatic data Acquisition Systems (ADAS)
- adding instrumentation
- preparing detailed response plans
- implementing repairs

The process for identifying subtle indicators of internal erosion includes carrying out rigorous analyses of the past performance of the dam and comparing them to early performance. By comparing the analyses to actual measured performance data, rather than only to design expectations, minor deviations in performance due to benign design or construction variations can be identified and factored out as potential developing failure modes.

The process involves:

- carrying out trends analyses of all key performance indicators to identify any temporal deviations
- developing seepage models of the dam as expected during design (“Ideal Dam”)
- developing seepage models adjusted to match actual instrumentation data during the early years of operation (“Model Dam”)
- developing seepage models that are progressively adjusted to match changes in instrumentation data over time
- where the opportunity is available, carry out periodic cross-hole shear wave tests and compare measured velocities to expected velocities and to previous test results.
- using the trends analyses, progressive seepage modeling and shear wave velocity data, forecast future performance of the dam to determine whether there are any developing failure modes.

2 Trends Analyses

Trends analysis is a simple yet powerful tool that can analyze often random and infrequent data and determine whether actual performance changes are occurring around the instrument. The tool can be used for any routine surveillance measurement but is particularly useful for piezometric and weir flow data. The tool can be used to:

- determine instrument reliability
- determine whether reservoir operation is the key driver for instrument performance
- identify anomalous dam behavior or instrumentation readings
- determine instrument lag time (an important component for assessing dam performance)
- identify gradual changes in dam performance
- predict future expected instrument readings

As shown in Figures 1a and 1b, a trends analysis was carried out on data from a typical weir, using only weekly manual readings. Figure 1a shows a raw scatter plot where the weir data is plotted directly against reservoir readings. A manually applied bi-linear curve represents the best-fit correlation equation for this data. Keeping the correlation equations separate from the data is an important consideration, because other factors such as precipitation, run-off or instrument errors may skew the results. Figure 1b shows the same data but with the weir data correlated to reservoir data taken 9 days earlier. The R^2 correlation factors show that the best fit occurs when the 9 day lag is incorporated into the analysis.

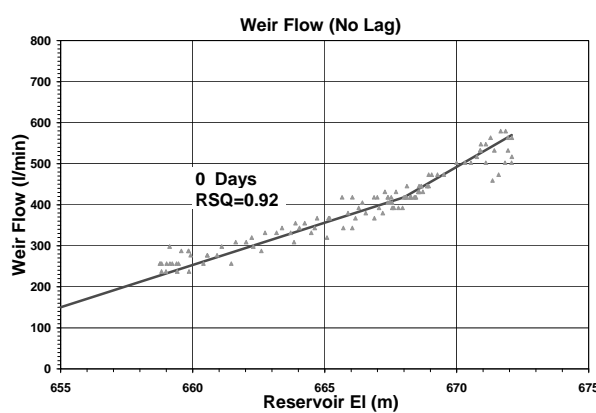


Figure 1a: Scatter Plot with No Lag Correction

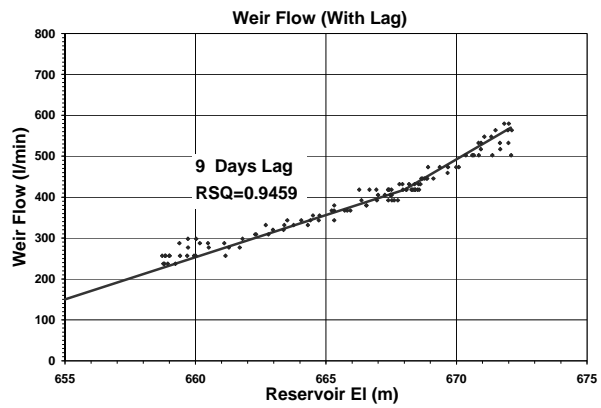


Figure 1b: Scatter Plot with Lag Correction

Figure 2 shows the weir data plotted against time for the years 2002 to 2004. Superimposed on the data points are the correlation curves developed from Figures 1a and 1b. The plots show that the weir is measuring flows that are directly related to the reservoir after about 9 days lag. The plot also indicates that this weir has been performing predictably with no changes in performance and that there is a flow spike every spring during the annual freshet.

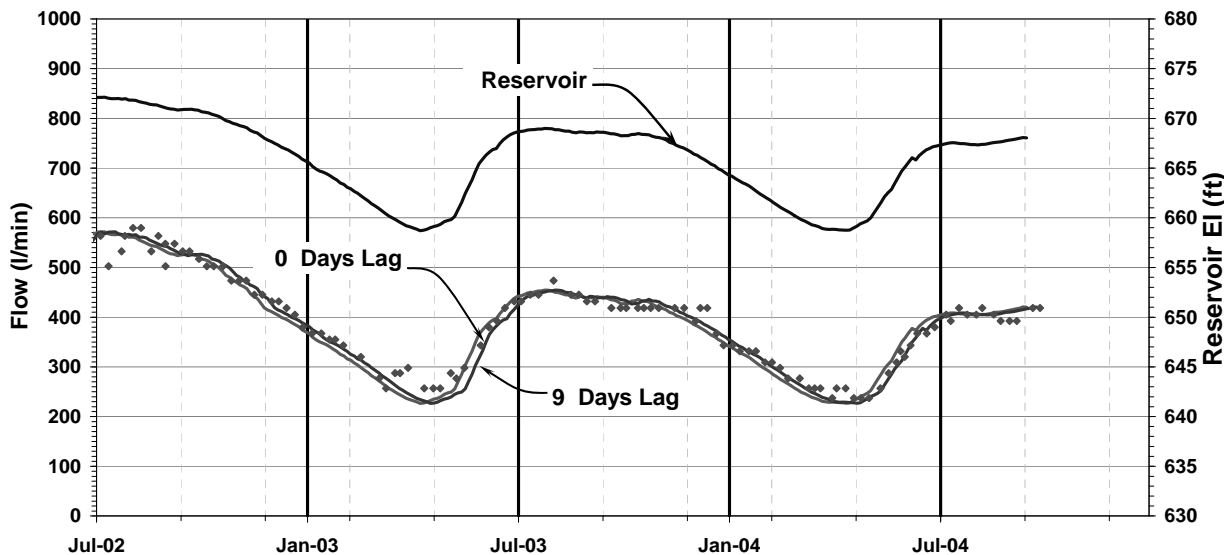


Figure 2: Weir Flow Corrected for Lag

This process can also be used to accurately identify and characterize unexpected or gradual changes in performance of a dam. Figure 3 shows historical pore pressure readings from a hydraulic piezometer, installed in the core of a large earthfill dam. Also shown are curves correlating the pre-1982 and post-1982 trends of the pore pressures. The pre-1982 curve shows that, starting in 1976, occasional unexpected high readings were read. The behavior of the piezometer clearly changed in 1982 when a declining trend commenced.

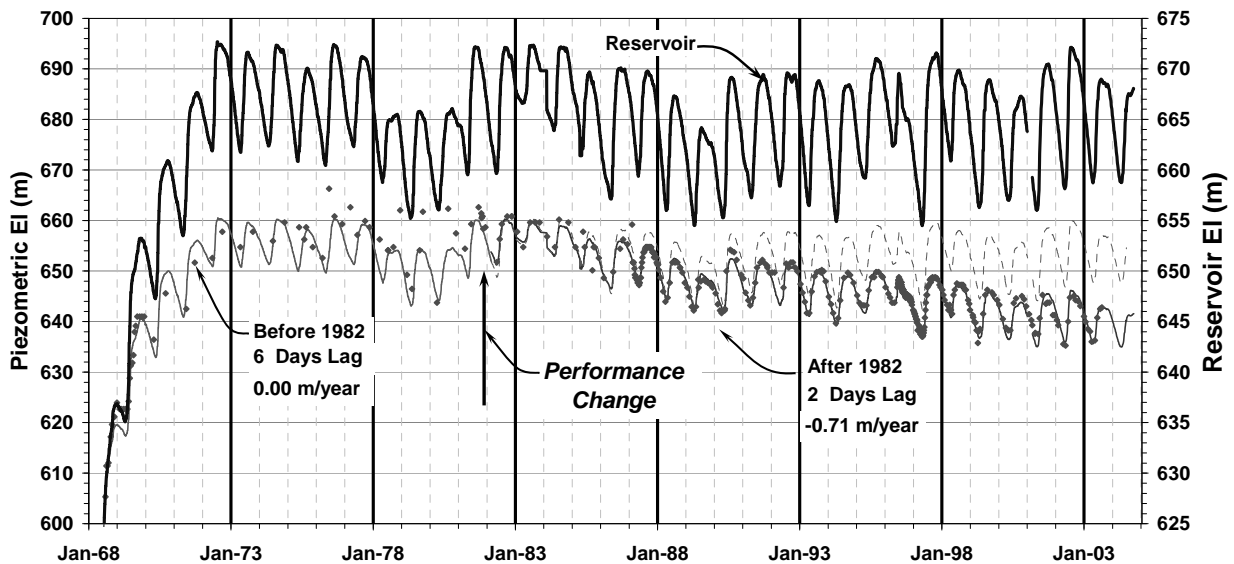


Figure 3: Trends Analysis of a Hydraulic Piezometer

Scatter plots, shown on Figures 4a and 4b show that a very good correlation can be achieved if post-1982 pore pressures are assumed to be dropping at a rate of 0.71 m per year. This rate of change is consistent with the entire group of 15 piezometers installed in the area. This slow, steady and predictable trend may be a signature of suffusion in materials downstream of the instruments or some other physical phenomena.

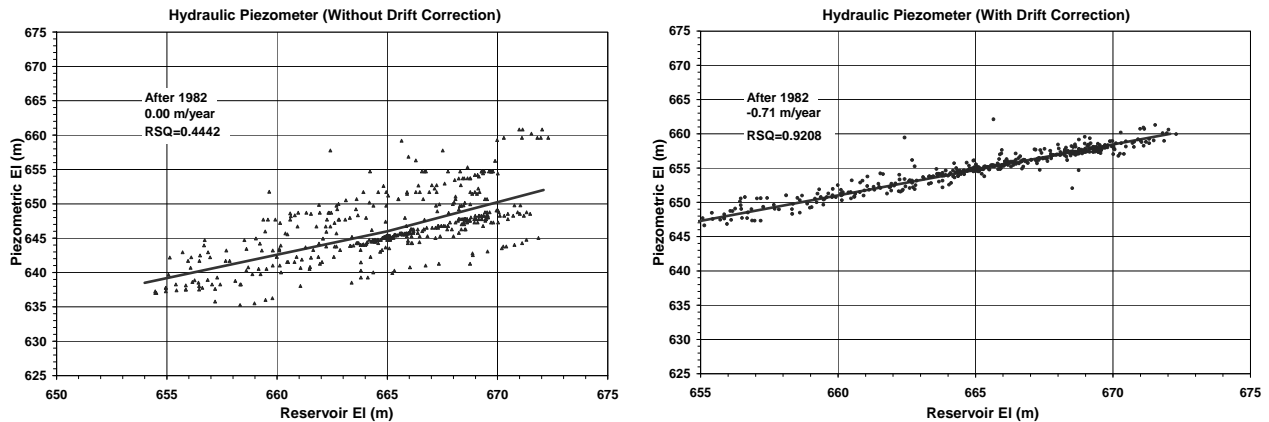


Figure 4a: Scatter Plot Without Drift Correction

Figure 4b: Scatter Plot With Drift Correction

3 Progressive Seepage Modeling

Progressive seepage modeling is the process of developing detailed seepage models of flow sections through the dam and comparing and adjusting the models to accurately depict the pore pressure and flow readings actually being read in a manner that is consistent with a working hypothesis. Any changes in the model required to match the readings would be deemed an indication of a change in performance and the working hypothesis needs to be assessed for its consistency with the performance change. Often, more than one working hypothesis can be developed that is consistent with the performance history.

The initial seepage model (“ideal dam”) is usually based on design expectations and construction information. A baseline performance model (“model dam”) is then developed to calibrate the model to actual performance data. Since the model is usually steady-state it should be calibrated to a time when steady-state conditions are expected to be approached. As well, the effects of lag should be considered in the calibration.

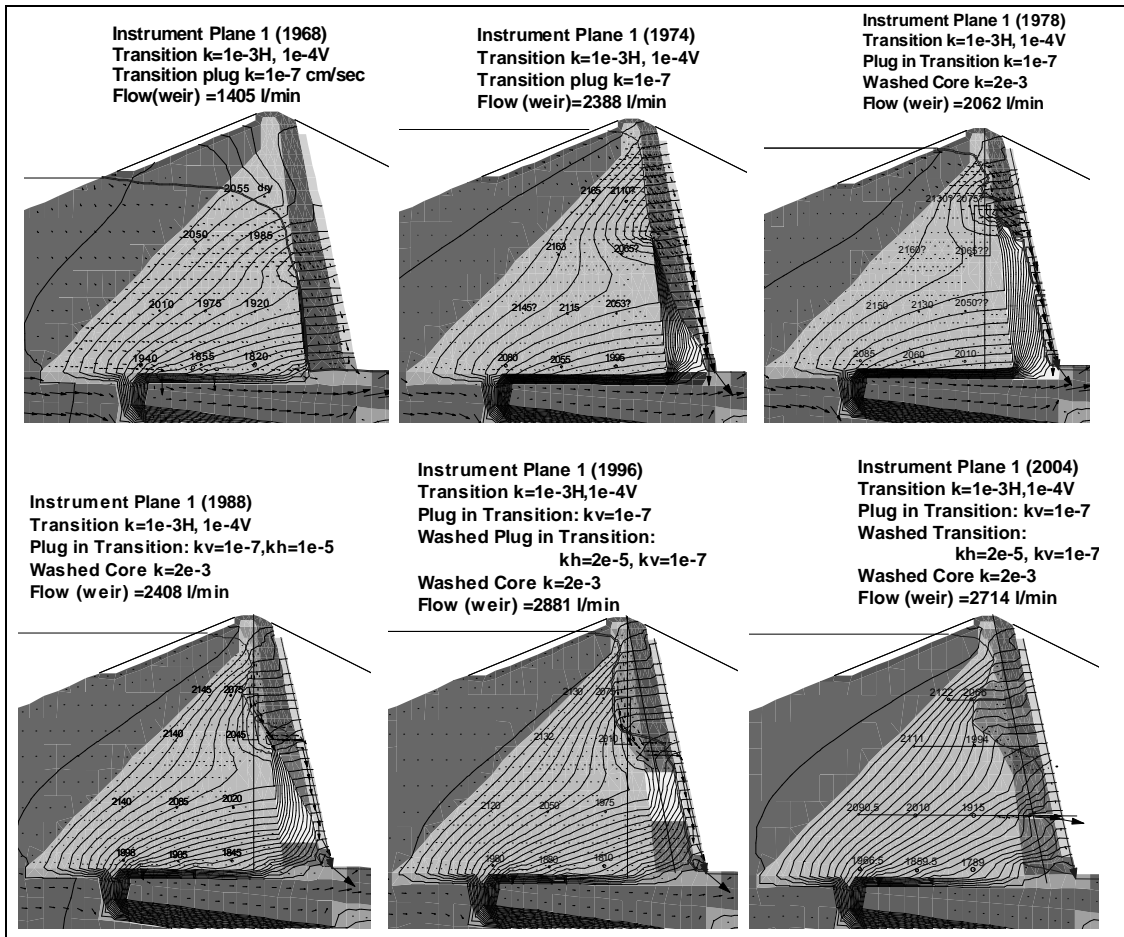


Figure 5: Progressive Seepage Modeling of a Working Hypothesis

The calibrated model is then tested against readings from later time periods. If the calibrated model does not match the measured data, then alternative hypotheses need to be developed to explain any deviations. Each hypothesis should be tested by modeling progressively against data from subsequent time periods to determine whether the hypothesis has merit. If adjustments to the model over one time period are not consistent with the hypothesis, the details of the entire modeling sequence may have to be readjusted. If the progressive seepage model cannot be reconciled with the data, the validity of the hypothesis may be in doubt.

Figure 5 shows an example of progressive seepage modeling of a flow section that contains the hydraulic piezometer shown on Figure 3. In this example, the hypothesis being modeled assumes the piezometers are acting as a group in response to the build-up and deterioration of a low permeability plug in the transition zone immediately downstream of the core. The entire sequence depicted is consistent with the recorded measurements. Other information, such as the presence of unusual volumes of fines in the transition, supports the hypothesis. The hypothetical model also suggests that the fines may have originated from the upper portions of the core.

4 Repeat Cross-Hole Seismic Shear Wave Testing

Cross-hole seismic shear wave testing has been used occasionally for identifying and characterizing defects within earthfill dams. Several dam owners have also attempted shear wave tomography in order to better define the damage around defects and sinkholes.

Extensive work carried out by BC Hydro since 1996 has determined that the repeat use of simple horizontal ray paths can be an effective means for identifying and monitoring low shear wave velocity zones around construction defects and sinkholes. The defects and sinkholes are centered on leaky vertical observation wells and survey benchmark tubes which were installed using several different manual compaction methodologies. The construction methodologies are interpreted to have caused varying degrees of arching and low stress zones (silo effect) around the instrument columns. The working hypothesis assumes that several of these zones have collapsed and formed sinkholes. Since low stresses appear to be one critical requirement for fines migration in internally unstable materials, the ability to monitor changes in stress in low stress zones may be extremely useful for predicting whether any additional sinkholes could develop.

The aim of cross-hole seismic testing is to identify low velocity zones related to low stresses around or near a defect, not necessarily to identify high void ratios at the defect itself. Since shear wave velocities are based on first arrival times, very localized low velocity defects may not be apparent since the shear wave will simply travel around it. However, if the zone around the defect was constructed at low stress or the defect has induced low stresses in the surrounding zone due to partial collapse, shear wave velocities will be affected.

The fundamental formula for shear wave velocity is:

$$V_s^2 = \frac{G^e}{\rho} \quad (1)$$

where: G^e = elastic shear modulus

ρ = mass density

V_s = shear wave velocity

This can be derived into the following formula:

$$V_s^2 = \frac{A}{\rho} F(e) P_A \left(\frac{p'}{P_A} \right)^m \quad (2)$$

where: p' = mean effective stress

P_A = atmospheric pressure

A = particle size and shape variable

$F(e)$ = void ratio function

m = modulus exponent, (typically 0.4 to 0.5)

From the formula, it can be seen that, since V_s is proportional to $(p')^{0.20}$ to $(p')^{0.25}$, changes to p' will generate subtle changes to V_s . Conversely, significant changes to V_s can be indications of very large changes to p' .

Bender testing indicates that the void ratio function proposed by Jefferies and Been provides a good correlation between void ratio and V_s over a large range of e .

$$F(e) = \frac{1}{e - e_{\min}} \quad (3)$$

* e_{\min} used by Jefferies and Been is lower than that determined by the ASTM test method.

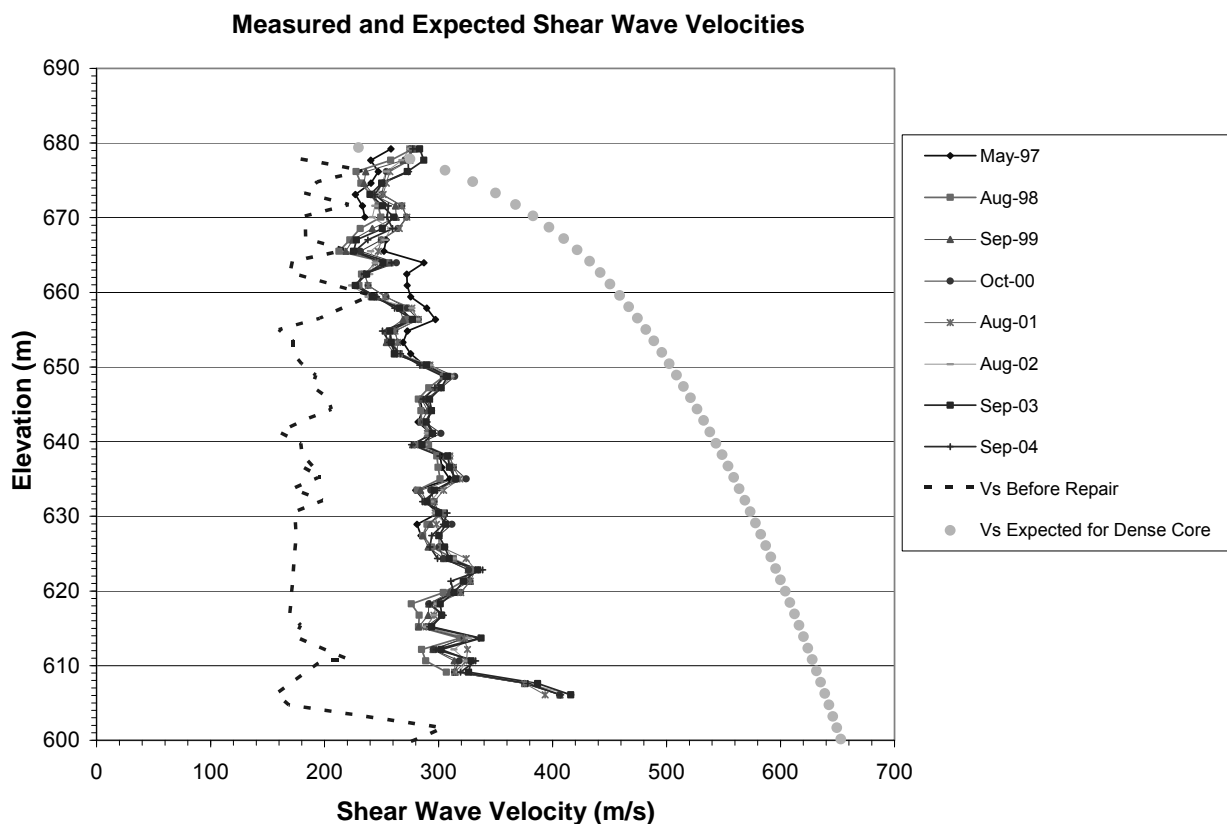


Figure 6: Measured and Expected Shear Wave Velocities Below a Sinkhole

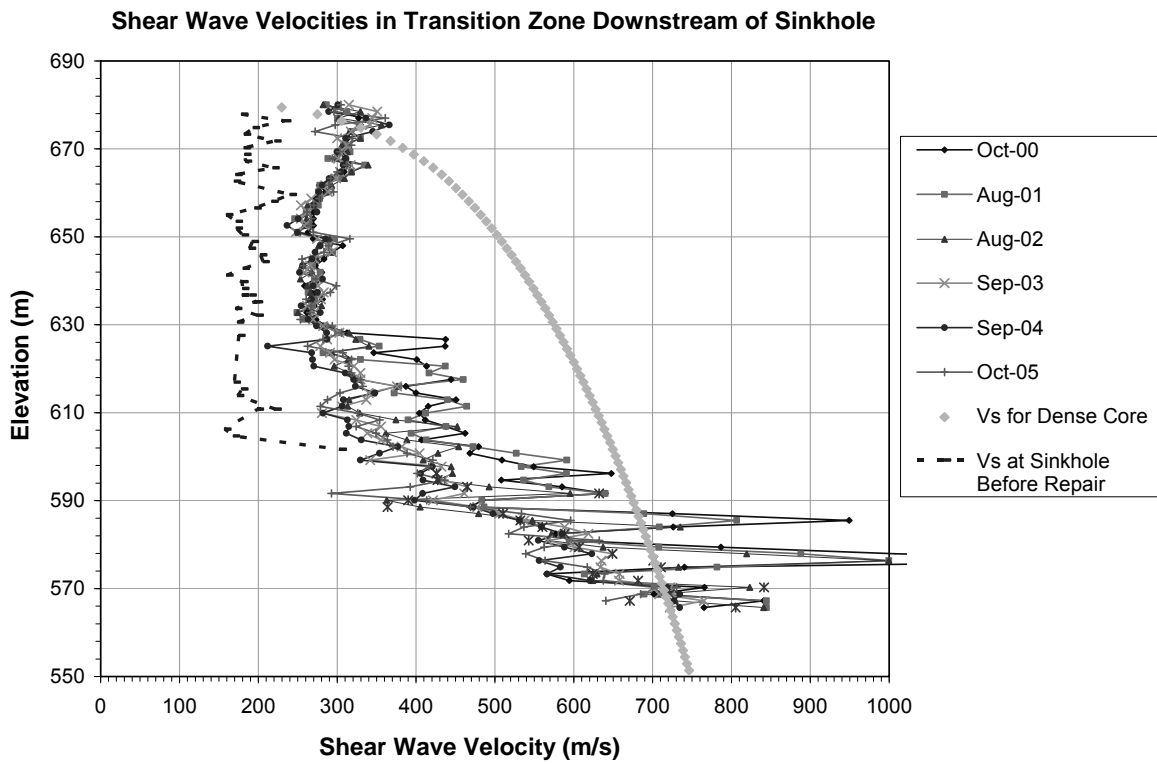


Figure 7: Changing Shear Wave Velocities in Transition Zone Downstream of Sinkhole

Combining [2] with [3] indicates that, since V_s is inversely proportional to $(e - e_{min})^{0.5}$, changes to e will also generate changes to V_s and, conversely, measured changes to V_s can be indications of large changes to e . Figure 6 shows results of repeat horizontal ray-path cross-hole seismic testing taken along a 5.8 m wide plane through a disturbed zone beneath a sinkhole which was repaired by compaction grouting in 1997.

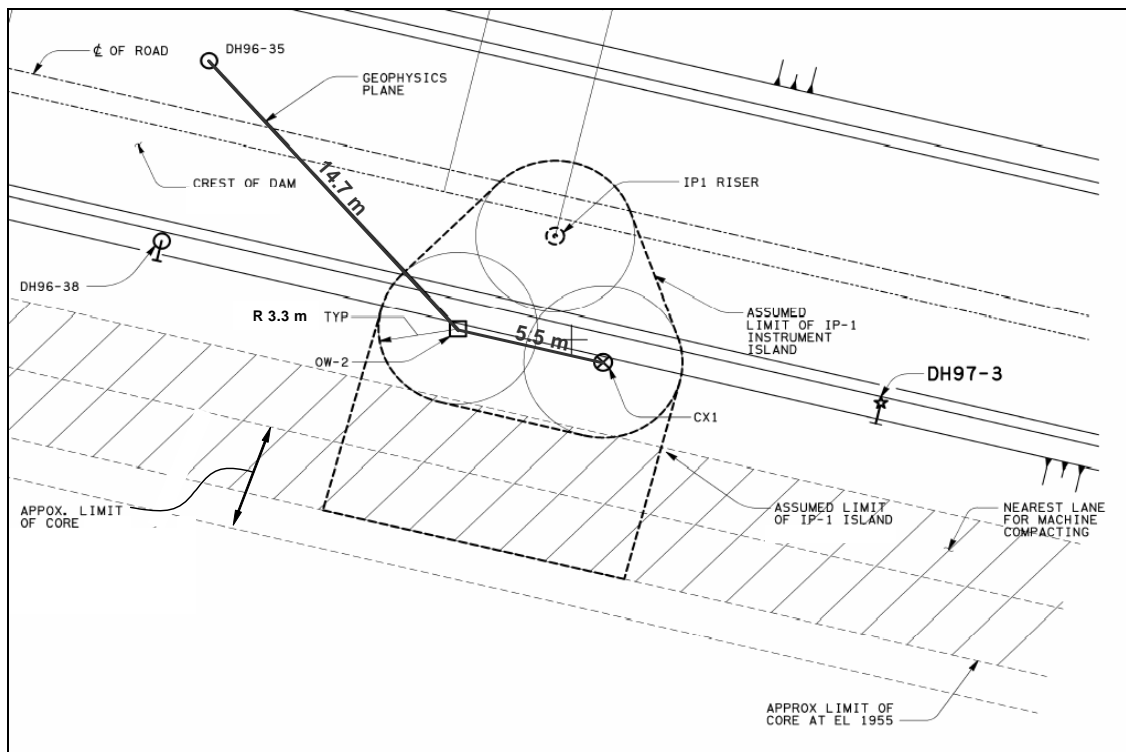


Figure 8: Instrument Island at Observation Well

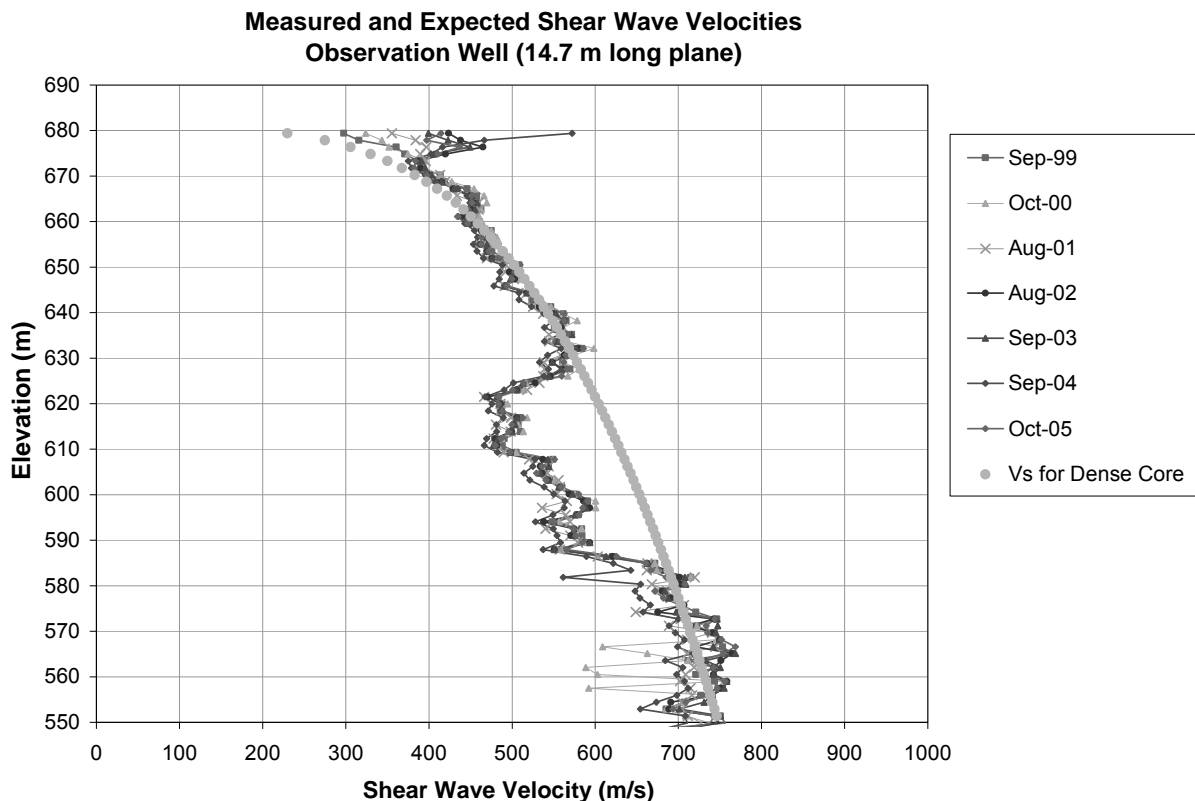


Figure 9: Observation Well Shear Wave Velocities (14.7 m plane)

The test results show that, on average, remediation significantly improved the disturbed ground. Importantly, the annual repeat cross-hole tests confirm that the remediated core remains stable, with no indication of re-initiation of internal erosion or stress release.

Figure 7 shows the results of cross-hole shear wave seismic testing performed along a sloping 5 m wide plane through the middle of a transition zone, downstream of the sinkhole. This zone was not treated in 1997. The repeat cross-hole shear wave seismic tests indicate that in this section, velocities are dropping to about 265 m/sec where they remain constant. One interpretation is that fines migration may be continuing in the downstream transition zone with fines being stripped out by downward seepage flows emerging from the upper portions of the core. If the interpretation is correct, the zone of stripped fines has moved from EI 628 in 2000 to EI 592 in 2005. The lower elevation zones may be continuing to lose fines at a diminishing rate.

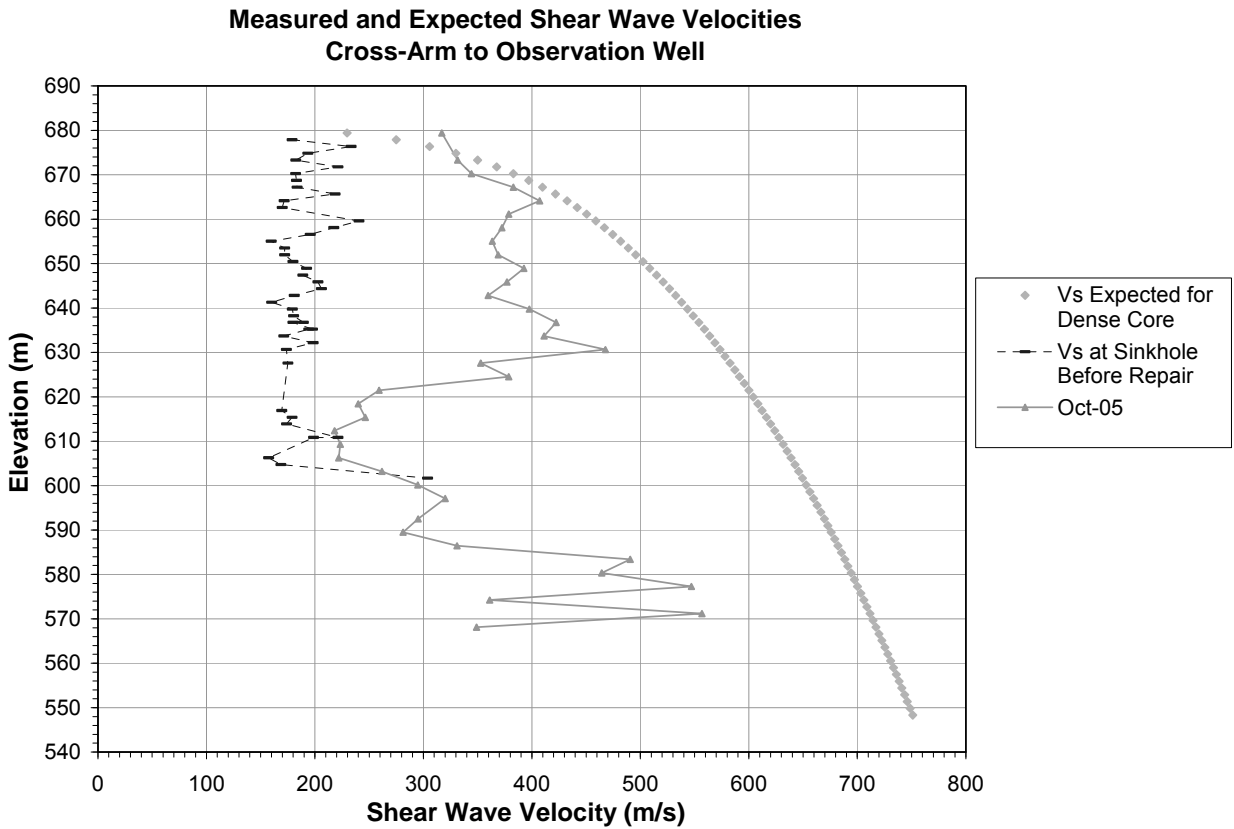


Figure 10: Shear Wave Velocities - Cross-Arm Device to Observation Well

Figure 8 is a plan view of the dam in the vicinity of three instrument columns around an observation well (OW-2), a cross-arm settlement device (CX-1) and a riser pipe connecting hydraulic leads. Between EI 580 and EI 630 the instruments were constructed in a single island and the surrounding fills were manually compacted.

Figure 9 shows results of repeat cross-hole shear wave seismic testing performed in the core of the dam along a 14.7 m wide plane between the observation well and a cased drill hole, where part of the plane extends into the manually compacted zone. The upper and lower portions of the plane have shear wave velocities that would be as expected for dense intact core. However, a low velocity zone is apparent in the central portion of the plane where the manual compaction took place.

Displayed in this conventional manner, the characteristics of the anomaly are difficult to interpret since the calculated velocities of the ray paths are blends of high and low velocity zones.

Figure 10 shows the results of crosshole seismic testing in the 5.5 m long plane between CX-1 and OW-2. The lowest velocities are approaching velocities measured in Sinkhole 1 prior to its repair. These velocities are likely more representative of the anomalous zones than the section analyzed on Figure 9. The velocities shown on Figure 10 are much too low to be caused by poor compaction and are likely due to low stresses and/or high void ratios caused by fines migration.

Figure 11 shows the same data as on Figure 10 but plotted as measured and expected arrival times. The arrival delay, the difference between measured and expected arrival times, is up to

16 ms in this example. Since delay time is a characteristic of the anomaly, not of the higher velocity intact core, this appears to be a useful way to depict the low velocity zone.

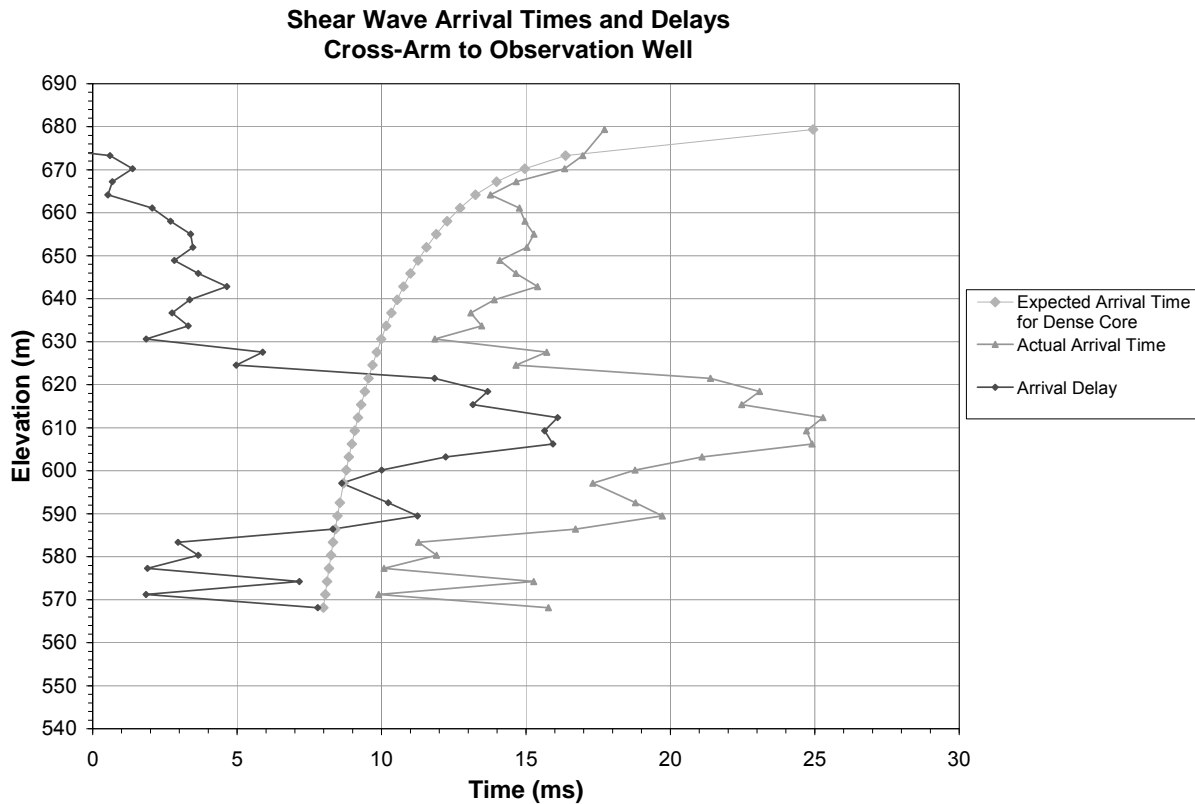


Figure 11: Arrival Times and Delays - Cross-Arm Device to Observation Well

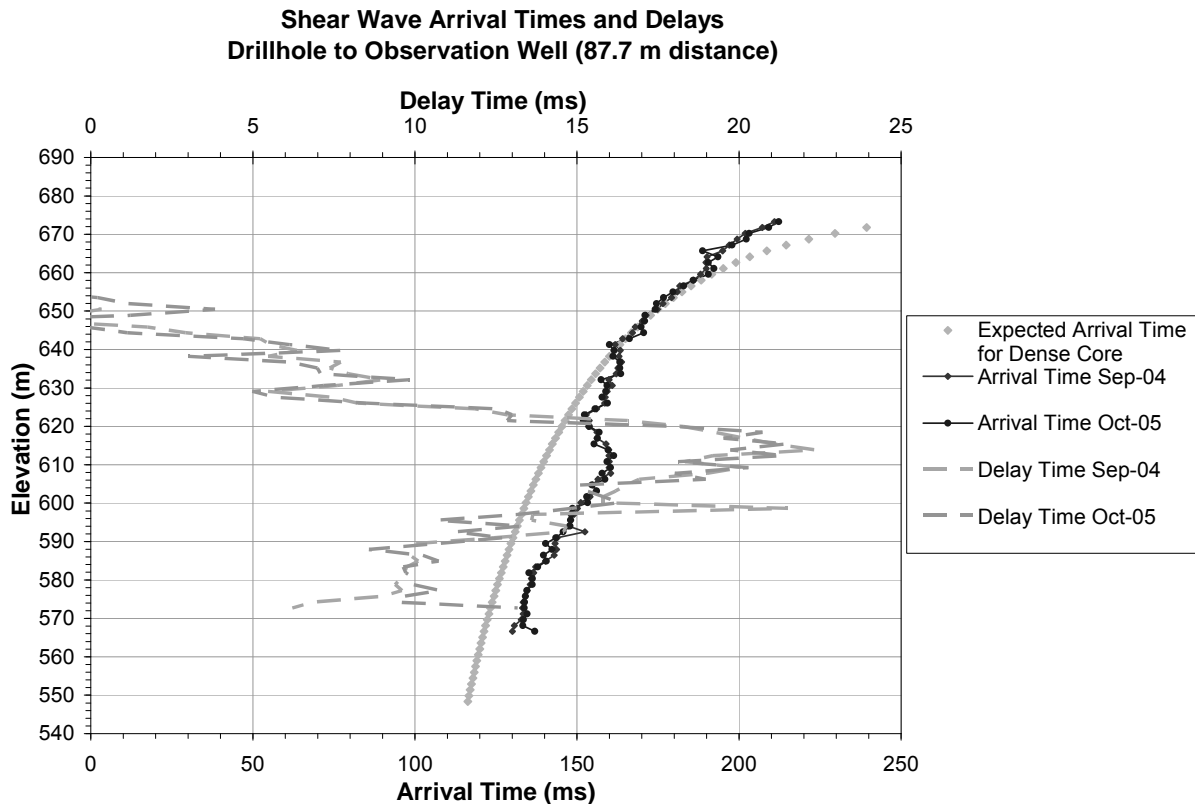


Figure 12: Arrival Times and Delays - Drillhole to Second Observation Well

Figure 12 shows arrival times and delays for a plane that bisects another zone in the dam, centered around a second observation well and a riser pipe (with no cross-arm device), which was constructed in a similar manner.

The plane between observation well and the nearest drilled-in geophysics hole is about 86.3 m long. A clear increase in arrival times appears below El 625. The calculated delay times, up to 22 ms, are very similar to the delay times determined between CX-1 and OW-2 indicating a similar condition at OW-4 and OW-2. The distance of the plane between source and receiver did not appear to affect the calculated delay time.

5 Conclusions

Rigorous analysis of conventional monitoring data can provide valuable insights into the changes in earthfill dams caused by internal erosion.

Methods are available for determining when and how quickly changes are occurring in the dam.

Progressive seepage modeling can be used to determine the reasonableness of hypotheses proposed to explain the performances of earthfill dams.

Annual cross-hole seismic testing has been used successfully for monitoring and assessing defective zones, likely associated with fines migration, around vertically installed instrumentation in a major earthfill dam.

Literature

- [1] Hartford, N.D and Baecher, G.B., *Risk and Uncertainty in Dam Safety*. CEA Technologies Dam Safety Interest Group. Thomas Telford, 2004.
- [2] Jefferies, M.G. and Been, K., 2000. *Implications for critical state theory from isotropic compression of sand*. Géotechnique 50, vol. 4, pp 419-429.
- [3] Stewart, R.A., Garner, S.J., Scott, D.L. and Baker, J.R., 2000. *Surveillance-The cornerstone of dam risk management*. Proc., 20th Congress on Large Dams, ICOLD, Beijing, China.
- [4] Stewart, R., Norstedt, U., Berntsson, S. and Hartford, N.D. *On the problem of managing the propensity for earth dams to fail through the process of internal erosion*. IREX-EDF Symposium 25-27 April 2005, Aussois, France.
- [5] Vazinkhoo, S. and Gaffran P., 2002. Crosshole seismic measurements to characterize and monitor the internal condition of embankment dams. Proc. 2002 CDA Conference, Victoria, B.C., Canada.
- [6] Yu and Richart, 1984. *Stress ratio effects on shear modulus of dry sands*. Journal of the Geotechnical Engineering Division, ASCE, Vol. 110, No. 3, pp 331-34.

Authors Name and Affiliation

Garner Steve
BC Hydro, Canada
steve.garner@bchydro.com

S. Vazinkhoo
BC Hydro, Canada

Self-Potential as a Detection Method to Evaluate Fluid Flow

A. Revil, A. Bolève

Abstract

The self-potential method is a passive geophysical method that can be used to detect electrical potential anomalies related to ground water flow. Indeed, the flow of the ground water generates a source current density in the conductive ground that acts a source term in the Maxwell equations to produce electromagnetic signals. The resulting electrical field can be measured with non-polarizing electrode at the surface of the investigated system or in boreholes. In the quasi-static limit, the electrical potential is solution of a Poisson's equation with a source term given as the divergence of the source current density. This equation can be easily solved with the finite element method. This equation can also be inverted to determine preferential ground water flow pathway from the measurements of the self-potential signals and the knowledge of the distribution of the electrical resistivity of the medium. The combination of self-potential tomography with temperature measurements appears as very promising combined approach to detect temporal variations in the flow pattern of the ground water in dams and embankments.

1 Introduction

Self-potential signals are electrical potentials passively measured at the ground surface of the Earth or in boreholes using non-polarizing electrodes and a voltmeter (Nourbehecht, 1963; Ogilvy, 1967; Corwin, 1990; Aubert and Atangana, 1996). Once filtered to remove anthropic signals and telluric currents (Corwin, 1990) and redox contributions (see Naudet et al., 2003; Rizzo et al., 2004), the residual self-potential signals can be associated with polarization mechanisms can be considered as the electrical signature of ground water flow (see Nourbehecht, 1963; Bogoslovsky, and Ogilvy, 1972, 1973; Kilty and Lange, 1991; Maineult et al., 2005). Indeed, one of the main polarization phenomena occurring in the ground is due to flow of the ground water, which drags the excess of electrical charge contained in the pore water (e.g., Ogilvy et al., 1969; Bogoslovsky, and Ogilvy, 1972;). The electrical field associated with the flow of the ground water is called the streaming potential (e.g., Ishido and Mizutani, 1981; Ernstson and Scherer, 1986; Wishart et al., 2006). The interpretation of streaming potentials measured during pumping or injection tests (see Bogoslovsky, and Ogilvy, 1972, 1973; Kilty and Lange, 1991; Maineult et al., 2005; Wishart et al., 2006) has been used recently to invert the transmissivity of a shallow aquifer (Straface et al., 2007). The analysis of streaming potentials has also been used in the study of landslides in combination with electrical resistivity tomography (Lapenna et al., 2003, 2005; Perrone et al., 2004; Colangelo et al., 2006) and in the study of leakages through dams (e.g., Bogoslovsky, and Ogilvy, 1973; Gex, 1980; Sheffer and Oldenburg, 2007). It has also been used in the study in the geohydrology of volcanoes (e.g., Aubert et al., 2000; Aizawa, 2004; Finizola et al., 2004; Ishido, 2004; Bedrosian et al., 2007).

In this review paper, we describe the physics of the hydroelectric coupling, we explain the type of equipment needed to achieve good measurements in the field, and we discuss quickly few

case studies, and both the forward and inverse problems in the interpretation of self-potential data.

2 Underlying Physics

All the minerals that are in contact with water develop a charge density over their surface. The fixed charge surface is counterbalanced by electrical charges located in the Stern layer of adsorbed counterions plus the mobile electrical charge located in the so-called diffuse layer located in the vicinity of the mineral surface, inside the pore water. The drag of this excess of electrical charge by the flow of the pore water generates an electrical current density. Indeed, a source current density is a net charge passing per unit surface area of the porous material per unit time. It follows that the source current density is equal to the excess of electrical charge of the pore water time the Darcy velocity (Revil and Leroy, 2004; Revil et al., 2005). An alternative model consists in describing the source current density in terms of zeta potential (a microscopic electrical potential of the electrical double layer coating the surface of the minerals) and the gradient of the fluid pressure or hydraulic head (e.g., Ishido and Mizutani, 1981). The model of Revil and Leroy (2004) was recently extended to unsaturated conditions (accounting for capillary effects) by Linde et al. (2007).

The key material property that describes the streaming potential is the streaming potential coupling coefficient. This material property can be measured very easily in the laboratory using the apparatus described in Figure 1. It consists simply of a Plexiglas tube with a permeable and electrically insulating membrane, placed at its bottom, with a mesh of 50 μm . The permeability of this membrane is always at least ten times larger than the permeability of the sample. To measure the streaming potential coupling coefficient, we use the following protocol. In some cases, a given hydraulic head is imposed on the cylindrical sample inside the tube by adding water to the water column in the tube in such a way that the hydraulic head is maintained constant. We use also for some experiments a falling head method during which the electrical potential is measured during the decrease of the hydraulic head in the tube associated with the flow of the water through the porous pack. The gradient of the fluid pressure is controlled by the hydraulic head in the tube and the length of the porous pack (typically between 1 to 60 centimeters). In both cases, the brine is flowing through the porous sample. The resulting electrical potential is measured with two non-polarizable Ag/AgCl₂ electrodes (Ref321/XR300, Radiometer Analytical) located in the vicinity of the end faces of the sample. The difference of the electrical potential measured between the end-faces of the porous pack divided by the length of the sample is the streaming electrical field associated with the flow of the brine through the pack. The voltages are measured with a data logger (Easy Log, internal impedance of 10 M Ω , sensitivity of 0.1 mV) or with a voltmeter (Metrix MX-20, internal impedance 100 M Ω , sensitivity of 0.1 mV). Both provided consistent measurements.

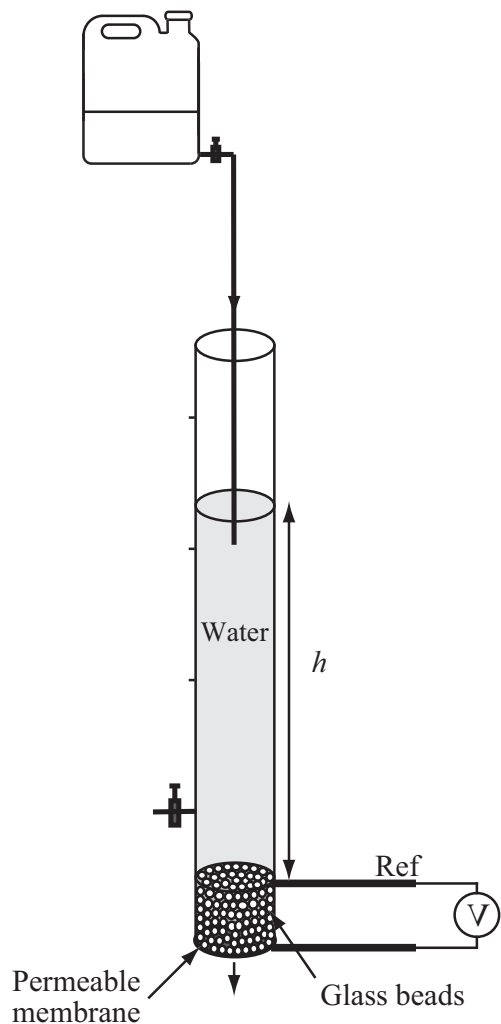


Figure 1: Sketch of the experimental setup. The sample is packed at the bottom of a Plexiglas tube and is maintained in the tube by a permeable membrane with a coarse mesh (the mesh is, however, finer than the diameter of the grains). The record of the self-potentials during the flow of the electrolyte through the sample is done with Ag/AgCl₂ electrodes ("Ref" is the reference electrode). The hydraulic heads are maintained constant at different levels and the streaming potentials are recorded at these levels at the end-faces of the sample (from Bolèvre et al., 2007).

Streaming potential data from a typical run are shown at Figures 2 and 3. In viscous laminar flow conditions, the differences of the electrical potential measured in the vicinity of the end-faces of the porous medium are proportional to the imposed hydraulic heads, as shown on Figures 2 and 3. The slope of the linear trend of streaming potential vs. head is the streaming potential coupling coefficient. From the measurement of the streaming potential coupling coefficient, the permeability, and the electrical conductivity of a porous sample, it is possible to determine the excess of electrical charge contained in its pore water using the model of Revil and Leroy (2004).

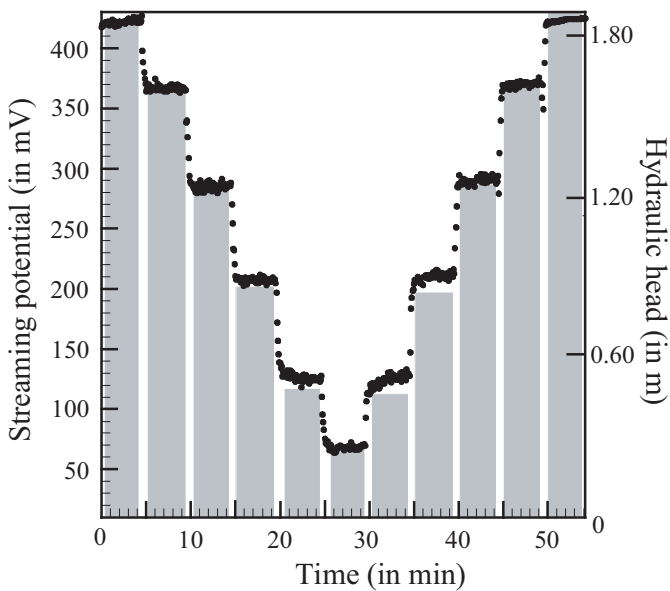


Figure 2: Example of a typical run for sample S3 (grain size of 150-212 µm) and a water conductivity of 10^{-3} S m $^{-1}$. The filled circles correspond to the measurements of the streaming potential at the two end-faces of the sample while the grey columns correspond to the measurement of the hydraulic heads. The streaming potentials are proportional to the imposed hydraulic heads. The results are reproducible. This means that there is no drift of the electrical potential of the electrodes during the duration of the experiment (from Bolève et al., 2007).

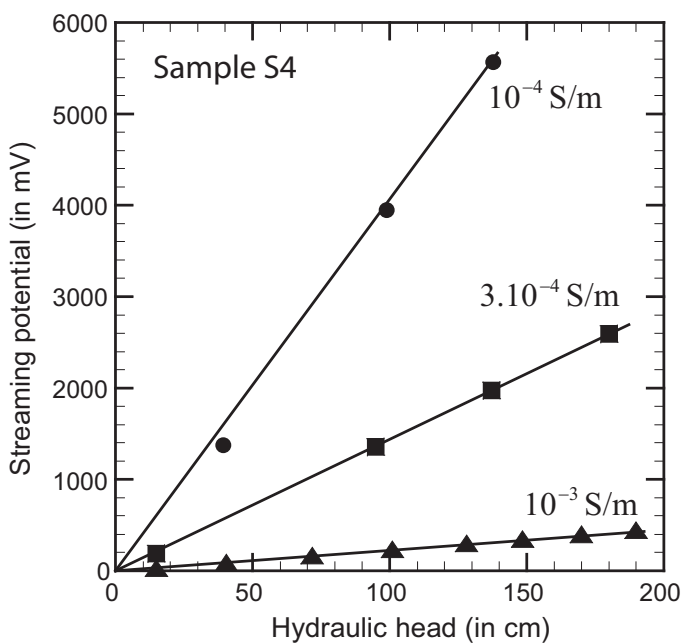


Figure 3: Example of typical runs for a granular material made of glass beads with a grain size distribution in the range 212-300 µm. the measurements have been performed at three water conductivities that are given on the plot. At each salinity, we observe a linear relationship between the streaming potential and the hydraulic head. At each salinity, the streaming potential coupling coefficient is equal to the slope of the linear trend (from Bolève et al., 2007).

3 Instrumentation

In the field, the self-potential signature of ground water flow can be evidenced with non-polarizing electrodes (typically Cu/CuSO₄, Ag/AgCl, or Pb/PbCl₂) and a high internal voltmeter (typically with internal impedance higher than 10 MΩ and a sensitivity of 0.1 or 0.01 mV). The high impedance of the voltmeter is necessary in order to prevent electrical current to flow through the voltmeter from the ground, which would disturb the potential reading and cause polarization of the electrodes. For monitoring purpose, the voltmeter can be a multichannel voltmeter (like the Keithley 2701 with 80 channels and an ethernet port, see Rizzo et al., 2004). It follows that both the sensors and the acquisition system are relatively cheap. This implies that a lot of sensors can be used in the field and connected to a multichannel system that can be used to scan the distribution of the self-potential in real time. Over the last decade, the development of very stable non-polarizing electrodes (e.g., Petiau, 2000) has been instrumental in the development of the self-potential method for applications in hydrogeophysics (see Perrier and Morat, 2000; Suski et al., 2007 and references therein). One of the most stable electrodes developed to date is the so-called Petiau electrode commercialized by SDEC (see Petiau, 2000). This electrode has a very small drift (less than 1 mV/year) and very small temperature dependence (0.2 mV/°C). The use of metallic electrodes should be avoided because they provide unstable readings. In a very recent study, Crespy et al. (2007) used a BioSemi apparatus, which is a very sensitive voltmeter developed initially for electroencephalography in medical imaging. With a new generation of non-polarizing electrodes, the level of detection was found to be equal to 0.1 microvolt.

4 Evaluation Method

There are two possible ways to do self-potential measurements. For mapping surveys, one electrode is used as a reference station and a second electrode is used to scan the electrical potential at the ground surface. The reference electrode is usually placed outside of the study area where self-potential anomalies are expected, in a spot where the self-potential values are constant. A map of the self-potential field can be created. Note that the electrical potential is relative to the electrical potential of the base (reference) station, so only the gradients of the electrical potential (the electrical field) has a physical meaning. The self-potential distribution can be also monitored over time using a network of electrodes and a multichannel voltmeter (see Rizzo et al., 2004, Suski et al., 2006) to detect preferential fluid flow pathways for example. This method is more and more used to determine the hydraulic properties of the ground during pumping and infiltration tests (see Suski et al., 2006; Straface et al., 2007). Because the shape of the electrical equipotentials are disturbed by the distribution of the electrical resistivity of the ground, it is important to determine the resistivity of the ground to interpret self-potential measurements (e.g., Suski et al., 2007 for an example). The distribution of the electrical resistivity can be obtained with an electrical resistivity tomography.

5 Numerical Modeling

The first numerical computation of streaming potentials due to ground water flow was performed by Sill (1983). Sill used a 2D finite-difference code and solved two semi-coupled constitutive

equations for the electrical current density and the seepage (Darcy) velocity. The forward simulation of self-potential data is done in three distinct stages. The hydraulic potential distribution in the ground is first determined based on the distribution of the hydraulic conductivity, the hydraulic driving forces (such as the pressure drop through an embankment dam), the storage coefficient, and an appropriate boundary conditions. Then, the geometry and magnitude of the source current density is computed based on the fluid flow and the excess of electrical charge per unit pore volume for each discretized element of the system. Finally the electric potential distribution is determined by solving the Poisson equation with a source term that depends on the divergence of the source current density, the distribution of the electrical resistivity (which can be obtained by electrical resistivity tomography), and appropriate boundary conditions for the electrical potential or the current density. An example of resulting self-potential distribution resulting from ground water flow through a dam is shown Figure 4.

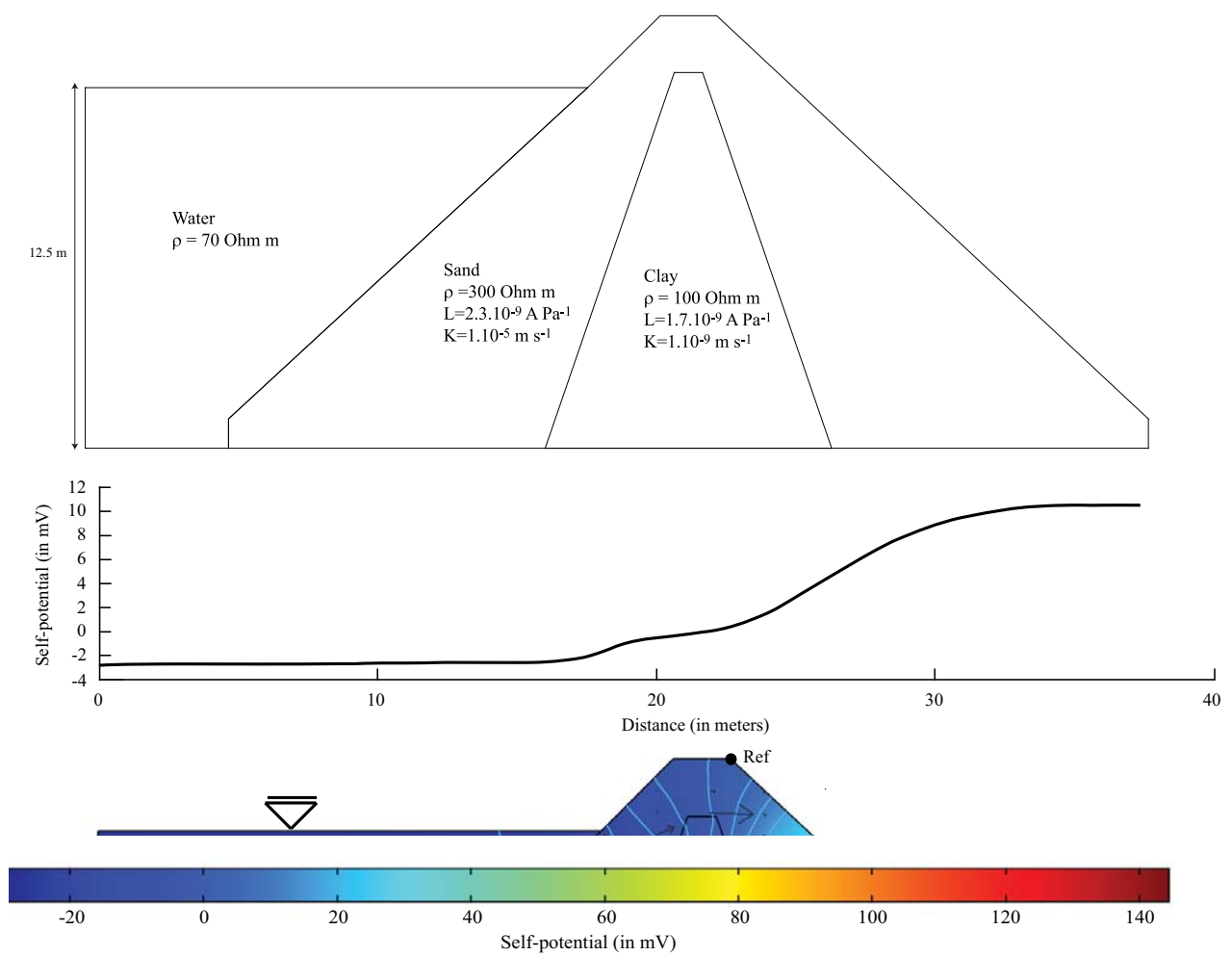


Figure 4: An example of the computation of the distribution of the self-potential associated with fluid flow through a dam. The upper plot shows the geometry of the system and the values of the critical parameters (ρ is the electrical resistivity, L is the streaming current coupling coefficient, and K is the hydraulic conductivity). The intermediate plot shows the computation of the self-potential at the ground surface. The lower plot shows that distribution of the electrical potential associated with the flow of the ground water (the arrows represent the seepage velocity).

6 Case Studies in the Study of Dams and Embankments

Examples of the detection of leakages in embankments and dams and the interpretation of the resulting self-potential signals in terms of seepage velocity can be found in various papers (Bogoslovsky and Ogilvy, 1970; Gex, 1980; Panthulu et al., 2001; Sheffer, 2002; Sheffer and Howie, 2001, 2003; Titov et al., 2005; Rozycki et al., 2006). An up to date paper for the computation of the self-potential field over dams was published recently by Sheffer and Oldenburg (2007). 3D numerical simulations were performed according to the methodology described above in Section 4 (see Sill, 1983). Examples are given with both sandbox experiments and field data obtained from an unspecified dam site in British Columbia. A fair comparison was obtained between the forward model and the field data. Bolève et al. (2007) extended recently the coupled hydroelectric equations to the case where the flow occurs at high Reynolds numbers, which is the case for leakages in fractured media even with model hydraulic heads. Figure 5 shows that both the apparent permeability and the apparent streaming potential coupling coefficient of granular porous media depends on the flow regime, and therefore on the value of the Reynolds number. Figure 6 to 8 show numerical simulations performed with Comsol Multiphysics 3.3 of the self-potential field resulting from preferential infiltration in a very permeable conduit.

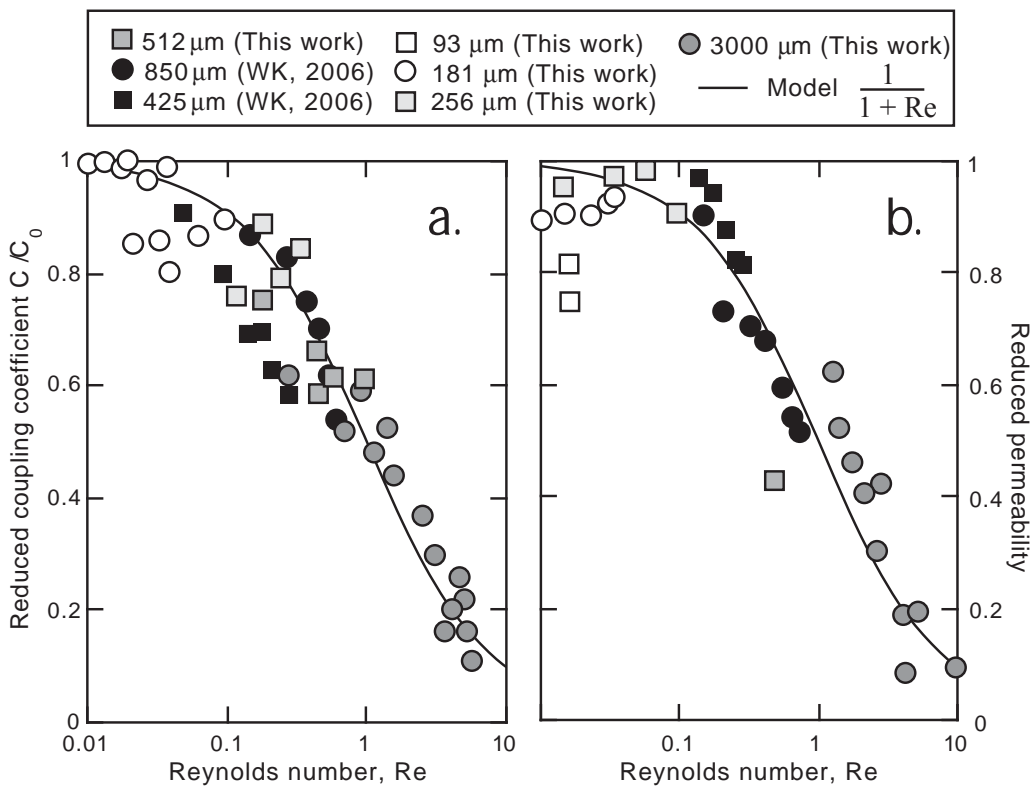


Figure 5: Influence of the Reynolds number upon the relative coupling coefficient and the relative permeability. The relative coupling coefficient is defined as the ratio between the measured apparent streaming potential coupling coefficient and the value of the streaming potential coupling coefficient in the viscous-laminar flow regime. The relative permeability is defined as the ratio between the measured apparent permeability (using Darcy's law) and the permeability measured in the viscous-laminar flow regime. These measurements have been made at different salinities showing the universal character of this trend (from Bolève et al., 2007).

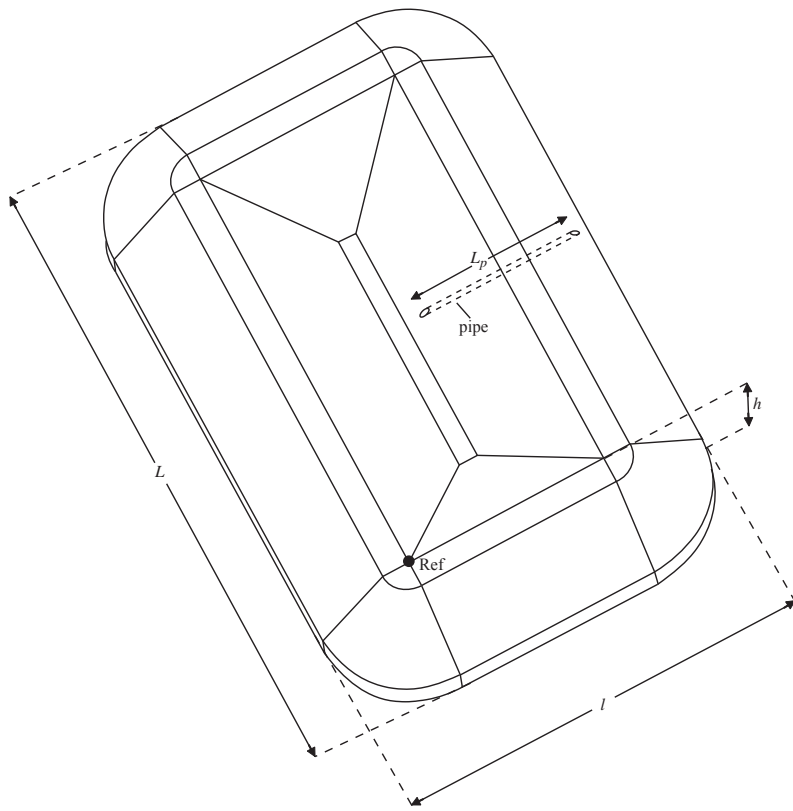


Figure 6: Geometry of water-filled basin with the position of the gravel-filled pipe, which constitutes the preferential fluid flow pathways for the water. The embankment is made of clay (permeability 10 mD). The reference for the electrical potential (position of the reference electrode where the electrical potential is taken equal to zero) is placed at the point Ref (ideally it should be located as far as possible from the self-potential anomaly resulting from the pipe).

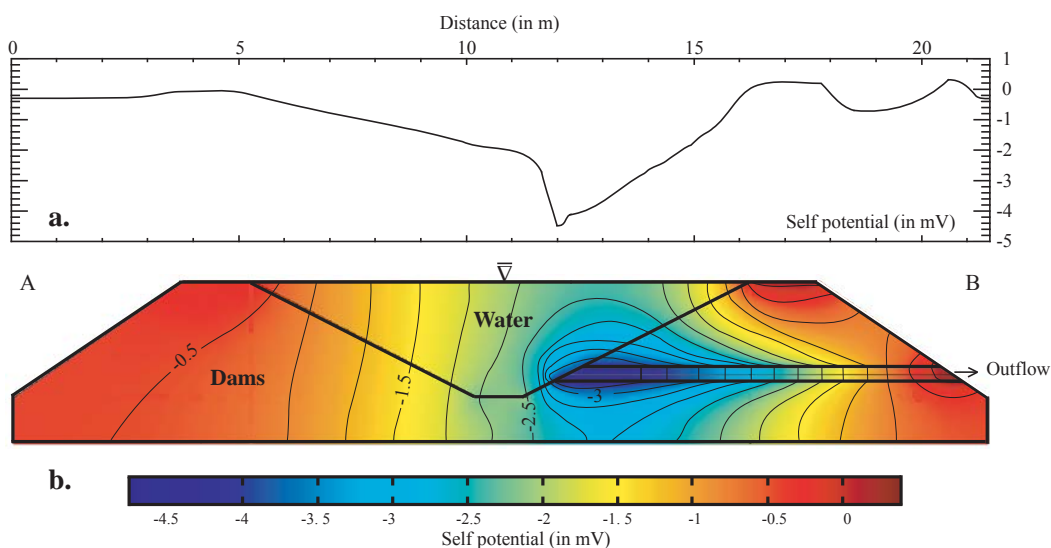


Figure 7: Plot showing the distribution of the electrical potential along a cross-section parallel to the pipe (the reference for the self-potential signals is shown on Figure 4). a. Distribution at the surface of the dams. The minimum of the self-potential distribution is located at the entrance of the pipe where a negative self-potential anomaly is observed (with an amplitude of few mV). Note that in water, the sensitivity of the measurements is typically 0.2 mV, which warranties a good signal-to-noise ratio. b. Distribution of the streaming equipotentials (from Bolèvre et al., 2007).

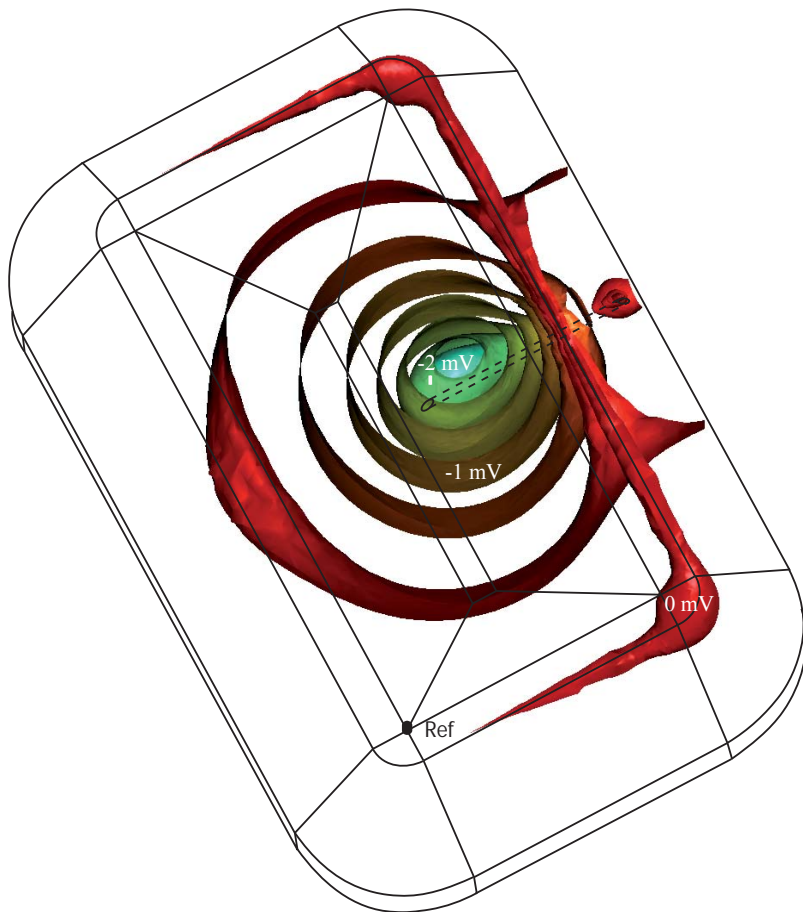


Figure 8: 3D-distribution of the electrical equipotentials in the basin due to the leakage of water through the pipe. The maximum intensity of the self-potential anomaly is 4 mV at the entrance of the leaking area (from Bolève et al., 2007).

7 Prospective

The new challenge in the use of the self-potential method is the inversion of the self-potential data in terms of ground water flow. An example of the self-potential distribution resulting from preferential infiltration through an idealized sinkhole is shown on Figures 9a and 9b. Jardani et al. (2007) have developed a new method invert self-potential data in terms of seepage velocities. This method is based on Tikhonov regularization of the inverse problem and incorporates the information related to the distribution of the electrical resistivity of the ground and the a priori information related to ground water flow. The inversion of the self-potential data shown on Figure 9b have been inverted in terms of velocity of the ground water flow and shown on Figure 9c. The comparison with the synthetic case demonstrates the usefulness of this approach in the reconstruction of the seepage velocity. In the near future, this inverse method will be coupled with the information related to thermal measurements to determine more precisely the pattern of ground water flow. Because of the natural complementary between the two fields (self-potential and temperature), it is expected that the joint inversion of self-potential and temperature measurements will represent a breakthrough to invert the pattern of ground water flow in Earth dams and embankments.

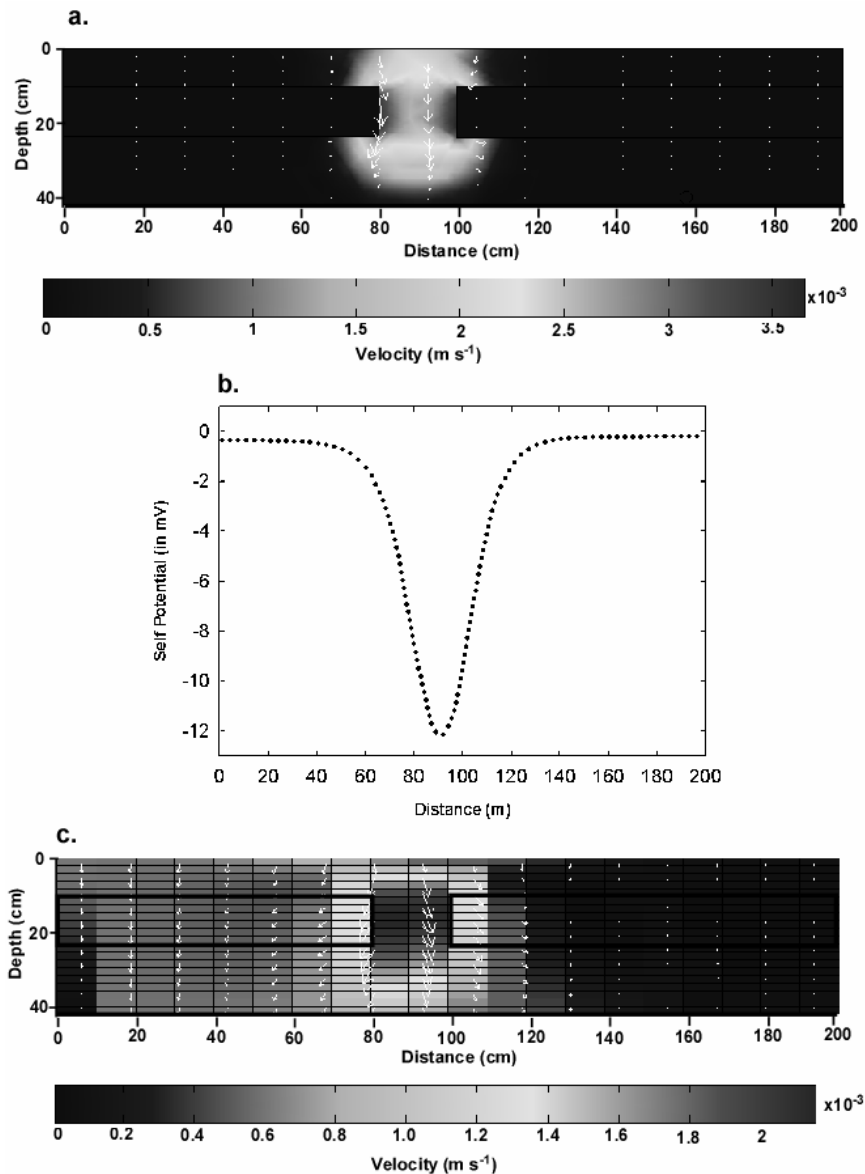


Figure 9: Inversion of self-potential data for a synthetic case corresponding to the 2D-infiltration of water in a sinkhole. a. The seepage velocity (in m s^{-1}) is modeled from the Darcy equation together with the continuity equation for the mass of the pore water (water is infiltrated from above). The flux of water is imposed at the upper boundary of the system corresponding to the ground surface. b. Distribution of the self-potential for the synthetic case. We assume that the « measurements » of the self-potentials are performed at the top surface. c. Distribution of the inverted flow velocity (in m s^{-1}) using a Tikhonov regularization of the inverse problem with a null a priori information (from Jardani et al., 2007).

Literature

- [1] Aizawa, K., 2004. A large self-potential anomaly and its changes on the quiet Mt. Fuji, Japan. *Geophys. Res. Lett.* 31, L05612. doi:10.1029/2004GL019462.
- [2] Aubert, M., Dana, I. N., Gourgaud, A., 2000. Internal structure of the Merapi summit from self-potential measurements. *J. Volcanol. Geotherm. Res.* 100(1), 337-343.
- [3] Aubert, M., Atangana, Q.Y., 1996. Self-potential method in hydrogeological exploration of volcanic areas. *Ground Water* 34, 1010–1016.
- [4] Bedrosian, P. A., Unsworth, M. J., Johnston, M. J. S., 2007. Hydrothermal circulation at Mount St. Helens determined by self-potential measurements. *J. Volcanol. Geotherm. Res* 160(1-2), 137-146.
- [5] Bogoslovsky, V.A., and V.A. Ogilvy (1970), Natural potential anomalies as a quantitative index of the role of water seepage from reservoir, *Geophysical Prospecting*, 18, 261-268.
- [6] Bogoslovsky, V.A., Ogilvy, A.A., 1972. The study of streaming potentials on fissured media models. *Geophys Prospecting* 51, 109–117.
- [7] Bogoslovsky, V.A., Ogilvy, A.A., 1973. Deformation of natural electric fields near drainage structures. *Geophys. Prospecting* 21, 716–723.
- [8] Bolève, A., A. Crespy, A. Revil, F. Janod, and J.L. Mattiuzzo, Streaming potentials of granular media. Influence of the Dukhin and Reynolds numbers, in press in *Journal of Geophysical Research*, 2007.
- [9] Colangelo, G., Lapenna, V., Perrone, A., et al., 2006. 2D Self-Potential tomographies for studying groundwater flows in the Varco d'Izzo landslide (Basilicata, southern Italy). *Engineering Geology* 88 (3-4), 274-286.
- [10] Corwin R.F. 1990. The self-potential for environmental and engineering applications. In *Geotechnical and Environmental Geophysics*, Ward SH(ed.). Society of Exploration Geophysicists, Tulsa, USA, *Investigations in Geophysics*, no. 5, p127–145.
- [11] Ernstson K, Scherer, H. U., 1986. Self-potential variations with time and their relation to hydrogeologic and meteorological parameters. *Geophysics* 51, 1967–1977.
- [12] Finizola, A., Lénat, J. F., Macedo, O., Ramos, D., Thouret, J. C., Sortino, F., 2004. Fluid circulation and structural discontinuities inside Misti volcano (Peru) inferred from self-potential measurements. *J. Volcanol. Geotherm. Res.* 135, 343-360.
- [13] Gex, P. (1980), Electrifiltration phenomena associated with several dam sites, *Bulletin of the Society Vaud Science and Nature*, 357(75), 39-50.
- [14] Ishido, T. Mizutani, H., 1981. Experimental and theoretical basis of electrokinetic phenomena in rock-water systems and its application to geophysics. *J. Geophys. Res.* 86, 1763-1775
- [15] Ishido, T., 2004. Electrokinetic mechanism for the "W"-shaped self-potential profile on volcanoes. *Geophys. Res. Let.* 31, L15616. doi:10.1029/2004GL020409.

- [16] Jardani A., A. Revil, A. Bolève, J.P. Dupont, W. Barrash, and B. Malama, Tomography of groundwater flow from self-potential (SP) data, submitted to *Journal of Geophysical Research*, 2007.
- [17] Kilty, K.T., Lange, A.L., 1991. Electrochemistry of natural potential processes in karst. In: *Proc 3rd Conf on Hydrogeology, Ecology, Monitoring, and Management of Groundwater in Karst Terranes*, 4–6 Dec 1991, Maxwell House, Clarison, Nashville, Tennessee. pp 163–177.
- [18] Lapenna, V., P. Lorenzo, A. Perrone, S. Piscitelli, E. Rizzo, and F. Sdao, 2003. High resolution geoelectrical tomographies in the study of the Giarrosa landslide (Potenza, Basilicata). *Bull. Eng. Geol. Environ.*, 62, 259-268.
- [19] Lapenna, V., P. Lorenzo, A. Perrone, S. Piscitelli, E. Rizzo, and F. Sdao, 2005. 2D electrical resistivity imaging of some complex landslides in the Lucanian Appenine chain, Southern Italy. *Geophysics*, 70(3), B11-B18.
- [20] Linde, N., D. Jougnot, A. Revil, S.K. Matthaï, T. Arora, D. Renard, and C. Doussan, Streaming current generation in two-phase flow conditions, *Geophysical Research Letters*, 34(3), L03306, doi: 10.1029/2006GL028878, 2007.
- [21] Maineult, A., Bernabé, Y., Ackerer, P., 2005. Detection of advected concentration and pH fronts from self-potential measurements. *J. Geophys. Res.* 110(B11), B11205. doi: 10.1029/2005JB003824.
- [22] Naudet, V., A. Revil, J.-Y. Bottero, and P. Bégassat, Relationship between self-potential (SP) signals and redox conditions in contaminated groundwater, *Geophys. Res. Lett.*, 30(21), 2091, doi: 10.1029/2003GL018096, 2003.
- [23] Nourbehecht, B., 1963. Irreversible thermodynamic effects in inhomogeneous media and their application in certain geoelectric problems. Ph.D Thesis, MIT Cambridge.
- [24] Ogilvy, A.A., 1967. Studies of underground water movement. *Geol Surv Can Rep* 26, 540–543.
- [25] Ogilvy A.A., Ayed, M.A., Bogoslovsky, V.A., 1969. Geophysical studies of water leakage from reservoirs. *Geophys Prospect* 22, 36–62.
- [26] Panthulu, T.V., C. Krishnaiah, and J.M. Shirke (2001), Detection of seepage paths in earth dams using self-potential and electrical resistivity methods, *Engineering Geology*, 59, 281-295, 2001.
- [27] Petiau, G., 2000. Second generation of lead-lead chloride electrodes for geophysical applications. *Pure Appl. Geophys.* 157, 357– 382.
- [28] Perrier, F., Morat, P., 2000. Characterization of electrical daily variations induced by capillary flow in the non-saturated zone. *Pure Appl. Geophys.* 157, 785-810.
- [29] Perrone, A., Iannuzzi, A., Lapenna, V. et al., 2004. High resolution electrical imaging of the Varco d'Izzo earthflow (southern Italy). *J. Applied Geophysics* 56(1), 17-29.
- [30] Revil, A. et P. Leroy, Governing equations for ionic transport in porous shales, *Journal of Geophysical Research*, 109, B03208, doi : 10.1029/2003JB002755, 2004.

- [31] Revil, A., P. Leroy, et K. Titov, Characterization of transport properties of argillaceous sediments. Application to the Callovo-Oxfordian Argillite, *Journal of Geophysical Research*, 110, B06202, doi: 10.1029/2004JB003442, 2005.
- [32] Rizzo, E., B. Suski, A. Revil, S. Straface, and S. Troisi, Self-potential signals associated with pumping-tests experiments, *Journal of Geophysical Research*, 109, B10203, doi: 10.1029/2004JB003049, 2004.
- [33] Rozycki, A., J.M.R. Fonticiella, and A. Cuadra (2006), Detection and evaluation of horizontal fractures in Earth dams using self-potential method, *Engineering Geology*, 82(3), 145-153.
- [34] Sheffer, M.R., and D.W. Oldenburg, Three-dimensional modeling of streaming potential, *Geophys. J. Int.*, 169, 839-848, 2007.
- [35] Sheffer, M.R. (2002), Response of the self-potential method to changing seepage conditions in embankments dams, M.A.Sc. Thesis, Dept. of Civil Eng., University of British Columbia, April 2002.
- [36] Sheffer, M.R., and J.A. Howie (2001), Imaging subsurface seepage conditions through the modeling of streaming potential, Proceedings of 54th Canadian Geotechnical Conference, Calgary, P. 1094-1101.
- [37] Sill, W.R., 1983. Self-potential modeling from primary flows, *Geophysics*, 48(1), 76-86.
- [38] Straface, S., C. Falico, S. Troisi, E. Rizzo, et A. Revil, Estimating of the transmissivities of a real aquifer using self potential signals associated with a pumping test, *Ground Water*, 45(4), 420-428, 2007.
- [39] Suski, B., Revil, A., Titov, K., Konosavsky, P., Voltz, M., Dagès, C., Huttel, O., 2006. Monitoring of an infiltration experiment using the self-potential method. *Water Resour. Res.* 42, W08418. doi:10.1029/2005WR004840.
- [40] Wishart, D. N., Slater, L. D., Gates, A. E., 2006. Self potential improves characterization of hydraulically-active fractures from azimuthal geoelectrical measurements. *Geophys. Res. Lett.* 33, L17314. doi:10.1029/ 2006GL027092.

Authors Name and Affiliation

Revil André Dr
CNRS-CEREGE Europôle, France
revil@cerege.fr

A. Bolève
LGIT, University of Savoy
SOBESOL, Savoie Technolac, France
boleve@cerege.fr

Detection of Internal Erosion and Seepage Evaluation using Resistivity Monitoring

By Pontus Sjödahl, Torleif Dahlin and Sam Johansson

Abstract

The resistivity method is well suited for dam monitoring as it is non-destructive and easily adapted for long-term monitoring. Measurements detect changes of material properties as well as anomalous variations, which may relate to internal erosion and seepage. However, applying the resistivity method on embankment dams can be challenging. This paper contends with practical use of the resistivity method on embankment dams, and presents two examples from Sweden.

1 Introduction

Resistivity surveying is a geophysical method widely used for a variety of engineering and environmental applications. In characterizing the subsurface the method makes use of the fact that earth materials have different ability to conduct electrical current. Being non-destructive the method may be attractive for installations on existing dams and it has been found useful for status control in dam safety investigations. Another more ambitious and more powerful approach is using the method for long-term monitoring of dams. In that case additional information is received from an analysis of the seasonal resistivity variations in the dam.

2 Fundamental Principles

The resistivity in an embankment dam varies seasonally, and depends mainly on the temperature and the ion content of the seepage water. Both these parameters vary seasonally, and their variation in the dam depends on the seepage flow. Areas in the dam with larger seepage may stand out as areas with larger seasonal variation.

2.1 Seepage Induced Variations

Seasonal temperature variations in an embankment dam has since long successfully been used for seepage detection. Seepage flow rates can be evaluated from temperature measurements without knowledge of hydraulic conductivity in the dam [1]. This is a great achievement, as the true in-field hydraulic conductivity is a difficult parameter to estimate. In a similar way resistivity can be used to evaluate seepage. Seepage causes resistivity variations in the dam that may be recorded by repeated measurements. Johansson and Dahlin [2] did some initial test on repeated resistivity measurements from the Lövön dam.

The basis for this principle is the relation between temperature and resistivity (**Equation 1**), where the resistivities, ρ_T , at different temperatures, T , relates to the resistivity, ρ_{18} , at a temperature of 18°C. The temperature coefficient of resistivity, α , is empirically found to be approximately $0.025^{\circ}\text{C}^{-1}$, and valid for temperatures above the freezing point [3].

$$\rho_T = \frac{\rho_{18}}{(1 + \alpha(T - 18))} \quad (1)$$

2.2 Effects from Internal Erosion

Internal erosion is the reason why weak zones can take the form of high-resistive anomalies.

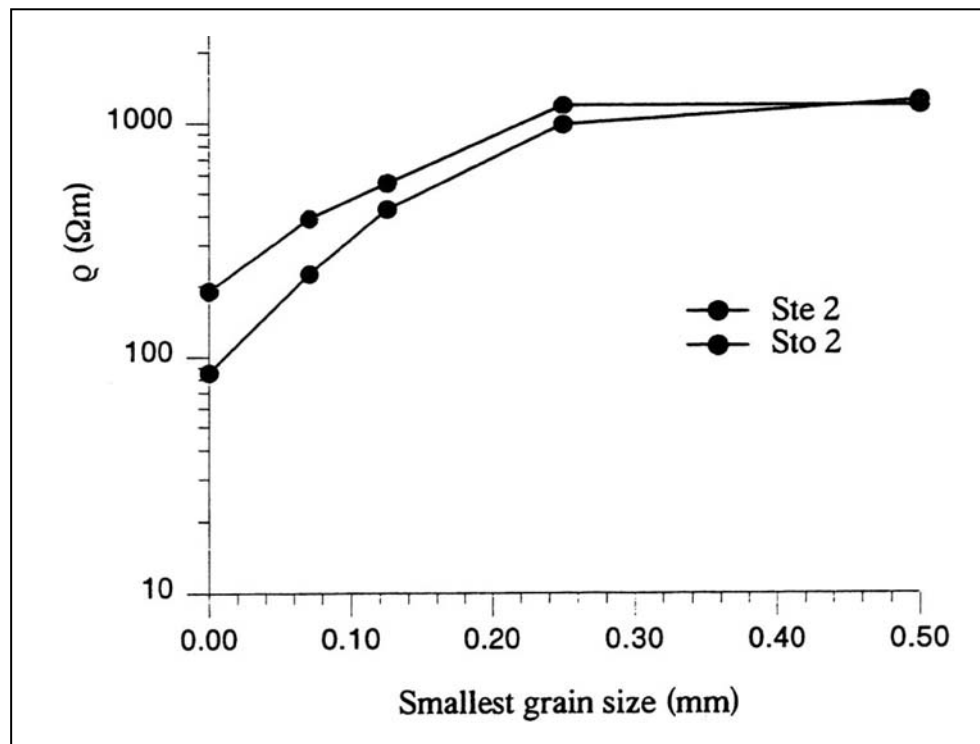


Figure 1: Importance of fines content on resistivity of soils. Results from an experiment simulating erosion in a glacial till used for sealing waste deposits, but similar to a dam core (Ste 2 and Sto 2 are named samples from two different sites) [1].

When internal erosion occurs, the fine particles of the soil are washed out from the core. This process affects the resistivity in two aspects, each working against the other. Firstly, the porosity of the core increases which leads to a decrease of the resistivity due to higher water content. Secondly the reduction of the fines content in itself increases the resistivity. In many fine-grained soils, the second aspect dominates. Laboratory test performed by Bergström [4] on some Swedish glacial tills used for sealing layers on waste deposits indicate a significant increase in resistivity when the fine content is removed (**Figure 1**). In the experiment conducted by Bergström, resistivity was measured on the same soil with different levels of fines removed, thereby simulating washout of fines as a result of internal erosion. The glacial till sample is similar to what is used in the cores of many Swedish dams. The resistivity rises approximately ten times after removal of fines smaller than 0.25 mm.

3 Materials and Methods

3.1 System Design

Installing electrodes along the crest has been the most practical design on existing dams. For zoned embankments with central cores it is most favourable to install the electrodes in the dam core. This secures good electrode contact and as the dam core is less resistive than the fill material, the current will have a channelling effect in the dam core, thereby focusing on the most interesting part of the dam [5]. Apart from these factors, dam geometry, material properties, water resistivity, error sources such as steel sheet piles or earthing cables, reservoir fluctuations, are examples of other factors influencing the choice of design.

3.2 Data Aquisition

There is a variety of resistivity measuring instruments or packages of instruments on the market for field use. Such equipment typically consists of a resistivity instrument, a relay switch (electrode selector), multi-electrode cables, stainless steel electrodes and various connectors. Most modern instruments have a built-in computer that can handle the entire data acquisition process and memory capacity to store days of measured data. Systems used for permanent installations for dam monitoring have some specific requirements. An important addition is lightning protection that should be designed with individual protection for each electrode input connected to the system, as well as for power supply and possibly a modem telephone connection. It is fundamental to provide sufficiently good and stable electrode contact, as too high contact resistance between electrode and ground is a common source of data quality problems. If Self Potential is to be measured special non-polarisable electrodes should be used.

3.3 Data Processing, Inverse Modelling and Interpretation

Processing of resistivity data includes data quality assessment, inverse numerical modelling and presentation and analysis of the results. Checking data quality is usually performed by plotting the pseudosection. Checking of data also includes removal of apparently erroneous data points, and in some cases weighting of data in relation to reliability can also be performed. Subsequently, inverse numerical modelling is carried out on the data set, and the final model or alternative models are presented and analysed. For standard resistivity investigations this is usually made by hand in steps. However, for long-term monitoring it easily becomes too time-consuming and instead automatic routines are necessary. Such automatic routines need to be robust and simple but still have the capacity to perform the individual steps of the data processing scheme.

4 Case Studies

4.1 Hällby

The embankment dams at Hällby have a total length of around 320 m. The maximum height is 30 m.

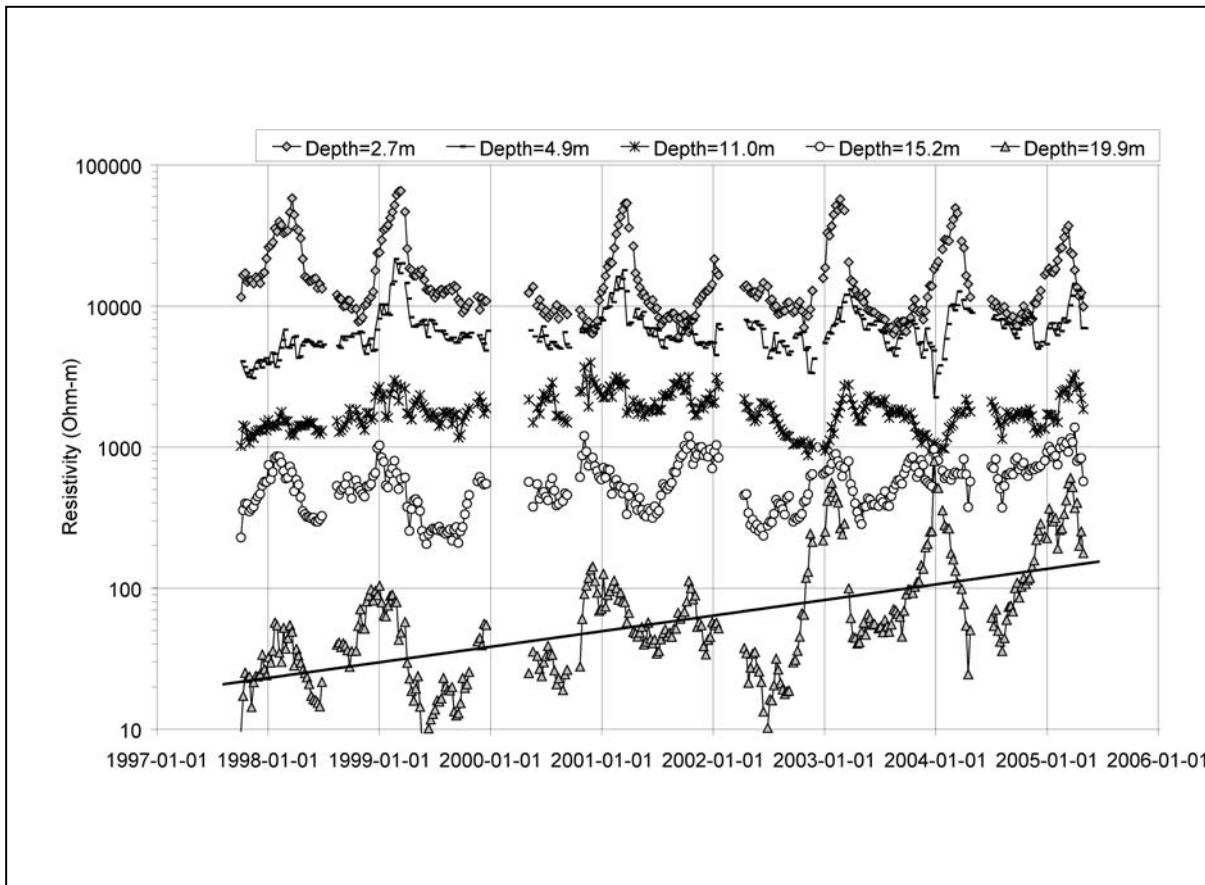


Figure 2: Resistivity at different depths in chainage -43 m on Hällby dam.

The dams are constructed as zoned rockfill embankment dams with vertical central glacial till cores. Hällby was the first Swedish embankment to get a permanently installed monitoring system intended for resistivity measurements. Daily measurements started to take place in 1996, which make these long-term monitoring data unique. In 2004-2005 the monitoring temporary halted as the dams were upgraded and the electrodes re-installed.

Resistivity in the dam varies seasonally (**Figure 2**). In general on the Hällby dam, the variation is high close to the crest, which is explained by extremely high winter resistivities due to ground freezing. The amplitude of the variation becomes lower at larger depths. This is consistent with theory as the impact from seasonal temperature variation in the reservoir or in the air decreases with distance from the reservoir. The data showed in Figure 2 is from an area adjacent to previously reported sinkholes. Here, contrary to the expectations, there are significant variations at large depths, which have not been seen elsewhere. Moreover, there are also signs of increasing variations and increasing absolute resistivities on large depth.

4.2 Sädva

The Sädva dam is located in the Skellefteälven River just south of the Arctic Circle.

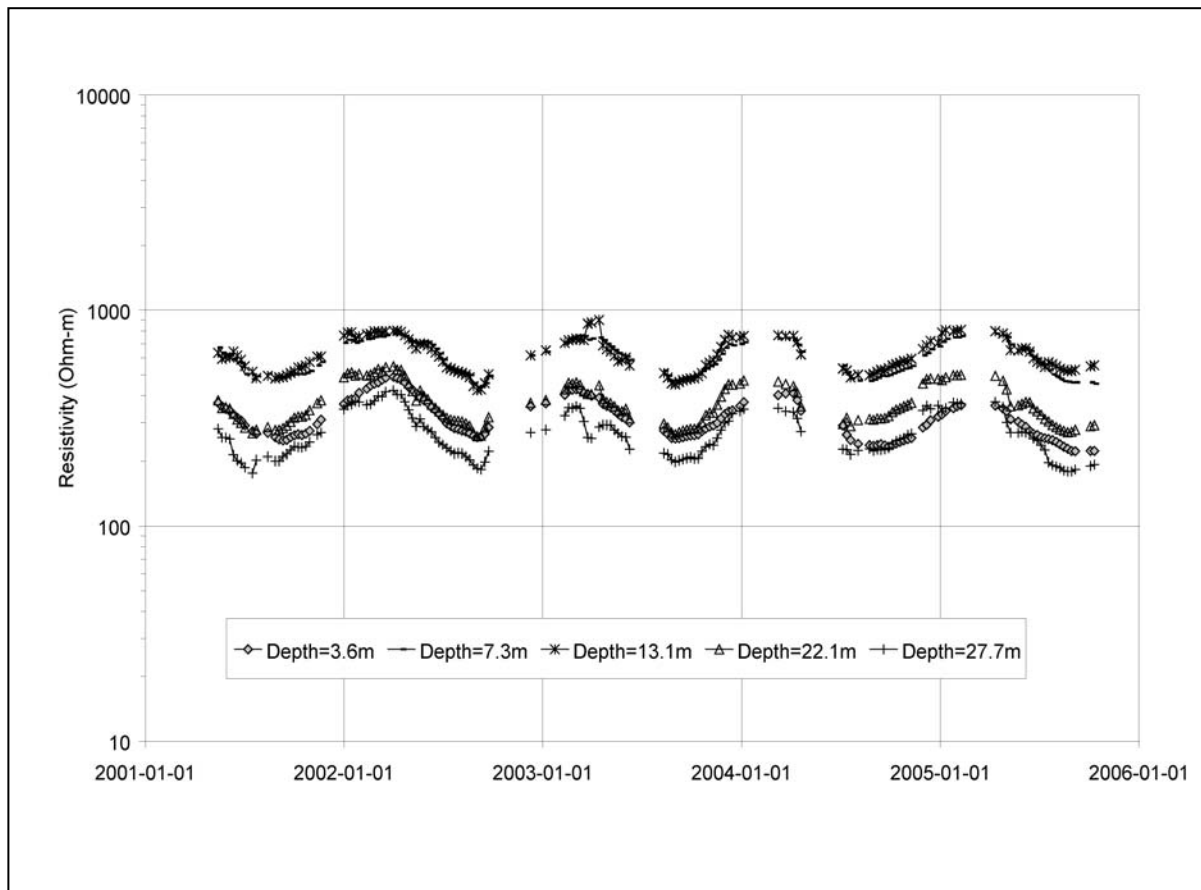


Figure 3: Resistivity at different depths in chainage 100 m on Sädva dam.

The total length of the dam is 620 m, and the maximum height is 32 m. The dam is a rock fill embankment dam with a slightly inclined central glacial till core. The monitoring installation comprises full instrumentation for resistivity measurements. Permanent electrodes are installed inside the top of the dam core along the full length of the dam and daily measurements have been carried out since 2001. The seasonal variation is obvious also in the Sädva dam (**Figure 3**). Comparing with Hällby, the variations are generally smaller and also consistent along the length of the dam, which may be a sign of a healthier dam with lower seepage flow rates. The homogeneous conditions in the dam are evident. Moreover, freezing effects and electrode contact problems were avoided by improved installations.

5 Conclusions

The resistivity method is a non-destructive method suitable for long-term monitoring. The rapid development in the areas of data acquisition and data processing has supported the possibilities of constructively using the method for dam applications. Long-term monitoring with spatially denser data points can now be achieved. This approach has been tried in two Swedish dams and similar installations are planned for another two dams.

Fundamental is the physical coupling between the resistivity parameter and seepage or seepage paths. The monitoring approach is based on two principal ideas, which both may be

identified by studying time-series. Firstly, washout of fines due to internal erosion will affect the resistivity in the dam. Secondly, seasonal resistivity variations in the reservoir, originating from variations in temperature and ion content, will affect the resistivity in the dam as the seepage water propagates through the dam.

Literature

- [1] Johansson, S.: Seepage monitoring in embankment dams, Doctoral Thesis, TRITA-AMI PHD 1014, ISBN 91-7170-792-1, Royal Institute of Technology, Stockholm, p 49, 1997
- [2] Johansson, S., Dahlin, T.: Seepage monitoring in an earth embankment dam by repeated resistivity measurements. European Journal of Engineering and Environmental Geophysics 1, Issue 3, p. 229-247, 1996
- [3] Ward, S.H.: Resistivity and induced polarization methods, In: Geotechnical and environmental geophysics, vol. 1, ed. Ward SH, Society of Exploration Geophysics, Tulsa, p. 147-189, 1990
- [4] Bergström, J.: Geophysical methods for investigating and monitoring the integrity of sealing layers on mining waste deposits, Licentiate Thesis, ISSN 1402-1757, ISRN LTU-LIC – 98/24 – SE, Luleå University of Technology, p 77, 1998
- [5] Sjödahl, P., Zhou, B., Dahlin, T.: 2.5D Resistivity Modeling of Embankment Dams to Assess Influence from Geometry and Material Properties, Geophysics 71, p. 107-114, 2006

Authors Name and Affiliation:

Pontus Sjödahl, Ph.D.
HydroResearch AB, Sweden
pontus.sjodahl@hydroresearch.se

Torleif Dahlin, Ph.D.
Engineering Geology, Sweden
torleif.dahlin@tg.lth.se

Sam Johansson, Ph.D.
HydroResearch AB, Sweden
sam.johansson@hydroresearch.se

Seepage Measurements and Internal Erosion Detection using the Passive Temperature Method

By Sam Johansson and Pontus Sjödahl

Abstract

Natural seasonal temperature variation in rivers and reservoirs provides a useful tool for seepage measurement in embankment dams. The method, sometimes called the “passive method”, has since long been used both for monitoring and investigations in Germany and Sweden. Fundamentals and evaluation methods are briefly described in this paper. Some result from manual temperature measurements, single temperature sensors, and distributed temperature sensing using optical fibres are also shown.

1 Introduction

Temperature is a seepage dependent parameter that may detect and quantify seepage anomalies in an embankment dam. The method, sometimes called the “passive method”, has since long been used both for monitoring and investigations in Germany and Sweden, Kappelmayer [1], Johansson [2]. In recent years the method has become more widely used. Research about thermal processes for temperature evaluation in dams were presented by Johansson [3] as a result of several research projects founded by the Swedish Power Association/ ELFORSK 1988-1996.

2 General Theory and Evaluation Methods

2.1 Fundamentals

The temperature in embankment dams depends mainly on the seasonal temperature variation in the air and the natural seasonal temperature variation that occurs in all surface water (such as lakes, reservoirs and rivers). These temperatures create a thermal response in the dam. Generally, a constant temperature will indicate a small seepage, while large seasonal variations may indicate significant seepage. At increasing seepage flows, the temperature in the dam will be changed, and the seasonal variation will increase. This variation is dependent on seepage flow, the seasonal variation at the inflow boundary, and the distance from the boundary to the measuring point. Temperature measurements can thus detect seepage flow changes, which may be associated with internal erosion.

The seasonal temperature variation in the upper part of the dam depends essentially on the air temperature at the surface. The influence from the air decreases with depth and can be ignored at depths exceeding 10 m. This process can be important in smaller dams.

2.2 Temperature in the Reservoir

Small reservoirs, or flowing water in a canal, have often a homogeneous temperature distribution. The seasonal temperature variation will be sinusoidal in moderate climate.

However, special consideration must be taken around at the equator and close to the artic where other temperature approximations are more appropriate. The impact of the stratification in large reservoirs is important to consider, as well as water level variations.

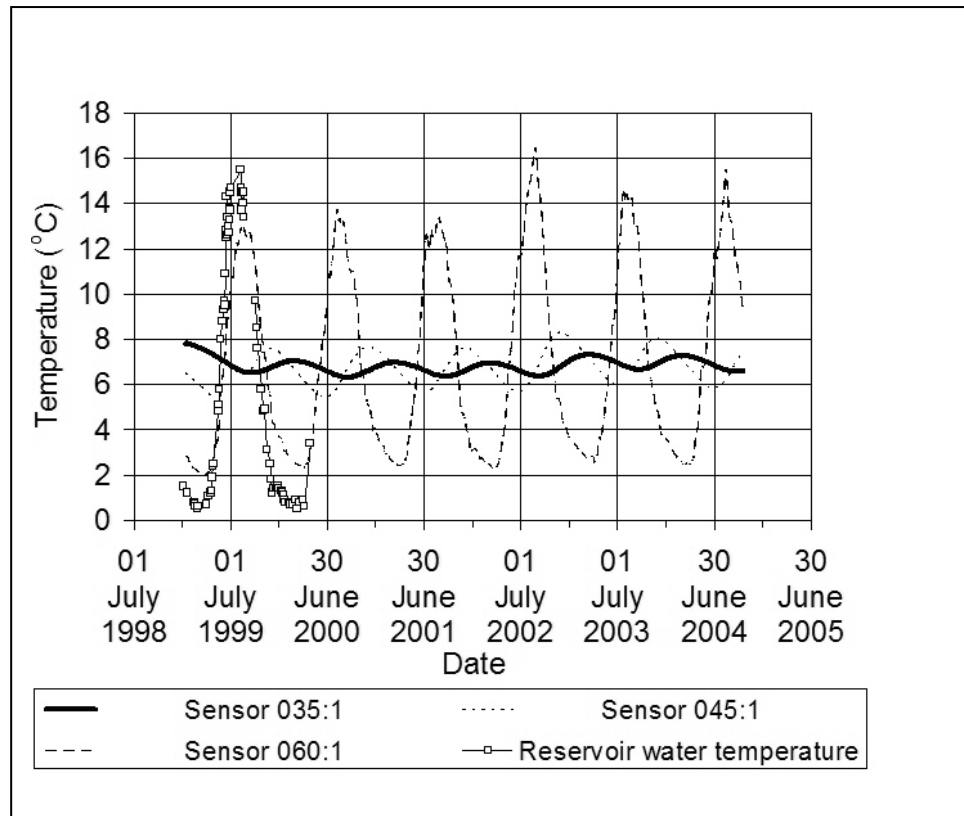


Figure 1: Temperature measurements at Lövön made in the piezometers 35:1, 45:1 and 60:1, located in the bedrock at chainage 35, 45 and 60.

2.3 Thermal Properties

Thermal properties of the dam material are well known. Typical values of specific heat capacity of rocks is between 700 and 850 (J/kg,K). The thermal conductivity of a water-saturated soil is determined by its mineral composition, especially the quartz content. The thermal conductivity of the water-saturated porous medium will decrease when the porosity increases. Typical values for normal soils used in embankment dams are around 2W/mK, ignoring the effect of thermal dispersion.

2.4 Qualitative Evaluation

A qualitative evaluation of the seepage can be performed by studying the seasonal variation in similarly located points. Figure 1 shows result from three sensors located similarly, but at different chainage (35 m, 45 m and 60 m). From the three examples it is easy to conclude that the highest seepage is found at sensor 60:1, and the lowest at sensor 35:1. Qualitative analysis can also be used to detect seepage changes just by comparing the temperature variations between different years.

2.5 Special Evaluation Tools

Experience from temperature monitoring in several dams has shown that concentrated seepage flow is common and can be 1000 times higher. The temperature field in the seepage zone and in the adjacent material is then mainly given by the flow in the higher permeable layer and the boundary condition. DamTemp is a software that calculates the thermal field is in two dimensions. The theory is described by Johansson [3] where a three layer is assumed with;

- an upper zone with heat conduction (in x- and y-direction) and no advection,
- a central seepage zone with advection (in x-direction) and heat conduction in y-direction; and
- a lower zone with heat conduction (in x- and y-direction) and no advection.

The temperature field is calculated for all three layers. One advantage with DamTemp is the limited amount of input data that have to be assumed.

2.6 Numerical Models

The thermo-hydraulic behaviour of an embankment dam is complex and includes heat conduction (from the dam crest and from the foundation due to geothermal flow), advection and radiation. The first two processes are partly coupled to each other because viscosity and density of water are temperature dependent. The problem is further complicated by the variation in material properties in the dam, and the different conditions in the saturated and unsaturated parts. The general problem has been studied using advanced coupled transport models, Johansson [2] or Aufleger [4].

3 Temperature Measurements in Embankment Dams

3.1 Single Point Sensors

Temperature is a basic parameter for many types of sensors, and is therefore measured in order to calibrate the readings from such sensors. If temperature data also is stored it will provide an excellent possibility for seepage evaluation from temperature measurements. One such example of this was shown above in Figure 1.

3.2 Vertical Profiles in Standpipes/Wells

Vertical temperature profiles in standpipes from different occasions give useful information. Manual measurements using a thermal probe are easy to carry out. Standpipes with a diameter up to 70 mm diameter can normally be used for temperature profiling without convection currents arising due to buoyancy effects within the standpipe. Another possible procedure is to measure and record temperature using thermistor strings, which eliminate any risk for mixing within the water column.

3.3 Distributed Temperature Sensors with Fibre Optics

The development of fibre optic systems improves the way of temperature measurements in dams, Dornstdälder [5], Johansson et al [6]. Such installations are now becoming more common. Sweden is one of the leading countries where about 30 dam sites are equipped with optical fibres in standpipes, along the downstream toe or in the drainage system. The accuracy may be down to 0.01 °C.

4 Measurements and Evaluations

4.1 Lövön

The embankment dam at Lövön was built between 1972 and 1973. Leakage water cannot be collected and measured by conventional leakage systems, due to a high downstream water level. When the dam was repaired in 1998, pressure and temperature sensors were installed (**Figure 1**). In addition, optical fibre were installed to measure the temperature upstream, above and downstream from the core. The first measurements were carried out in winter 1998/1999 using a DTS system with insufficient accuracy. In 2004 a second measurement was made using the Sentinel DTS, with an accuracy ten times better than the system used in 1998.

Evaluation using DamTemp, based on short-time DTS measurements 2004 and continuous temperature measurements in temperature sensors, indicated maximum seepage flow rates about $20\text{--}30 \cdot 10^{-3} \text{ m}^3/\text{s}/\text{m}$. A concentrated seepage flow about 0.05 l/s was detected at chainage 0/028. A wider seepage area was also detected between chainage 0/045 and 0/060 with total flow of about 0.5 l/s.

Näs

The longest temperature monitoring series in a Swedish embankment dam is at Näs power plant, where monthly measurements are performed since 1987. The embankment dam at Näs is

about 15 m high and located in the Dalälven River. No traditional leakage measurements are possible due to a high downstream water level.

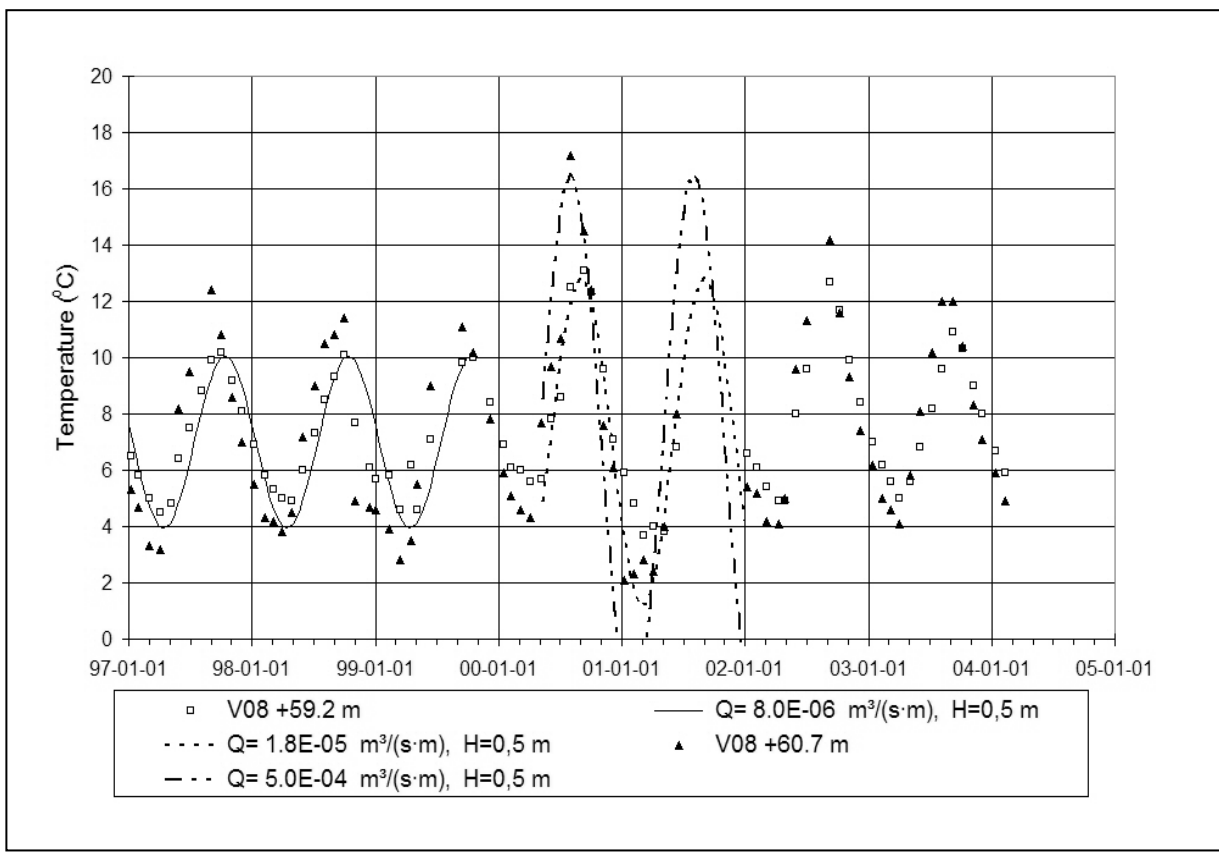


Figure 2: Measured and calculated temperature at observation well V08 at two levels.

An sudden temperature change was observed in standpipe V08 in year 2000 (**Figure 2**). After 13 years with a constant seasonal temperature variation between 4 and 11 °C, the maximum temperature increased to 17 °C, and the minimum temperature decreased to about 2 °C. Seepage calculations with DamTemp indicated a seepage increase from about $8 \cdot 10^{-6} \text{ m}^3/\text{s}\cdot\text{m}$ to about $1.8 \cdot 10^{-5} \text{ m}^3/\text{s}\cdot\text{m}$ at elevation +59.2 m and about $5 \cdot 10^{-4} \text{ m}^3/\text{s}\cdot\text{m}$ at elevation +60.7 m, i.e. a seepage increase of between 28 and 60 times. For the following three years a decreasing seasonal temperature variation was observed, indicating a decreasing seepage.

4.3 Suorva

The Suorva dams (Eastern, Western, and Sågvik dam) are positioned in the upper part of the Lule älv River. They were completed in 1972, creating the largest man made reservoir in Sweden. In order to further improve the monitoring system, fibre optical cables were installed in 2004-2005 in order to measure movements (strain) on the crest of the East and West dams, and the seepage flow of the West dam where a support toe berm was constructed.

Evaluation of a single measurement showed minor seepage flow between 10 and $60 \cdot 10^{-3} \text{ m}^3/\text{s}\cdot\text{m}$. A second measurement was made in May 2006 that confirmed those values as shown in the Figure 3. The interval for the estimated flow rates was also reduced to a value about $25 \cdot 10^{-3} \text{ m}^3/\text{s}\cdot\text{m}$.

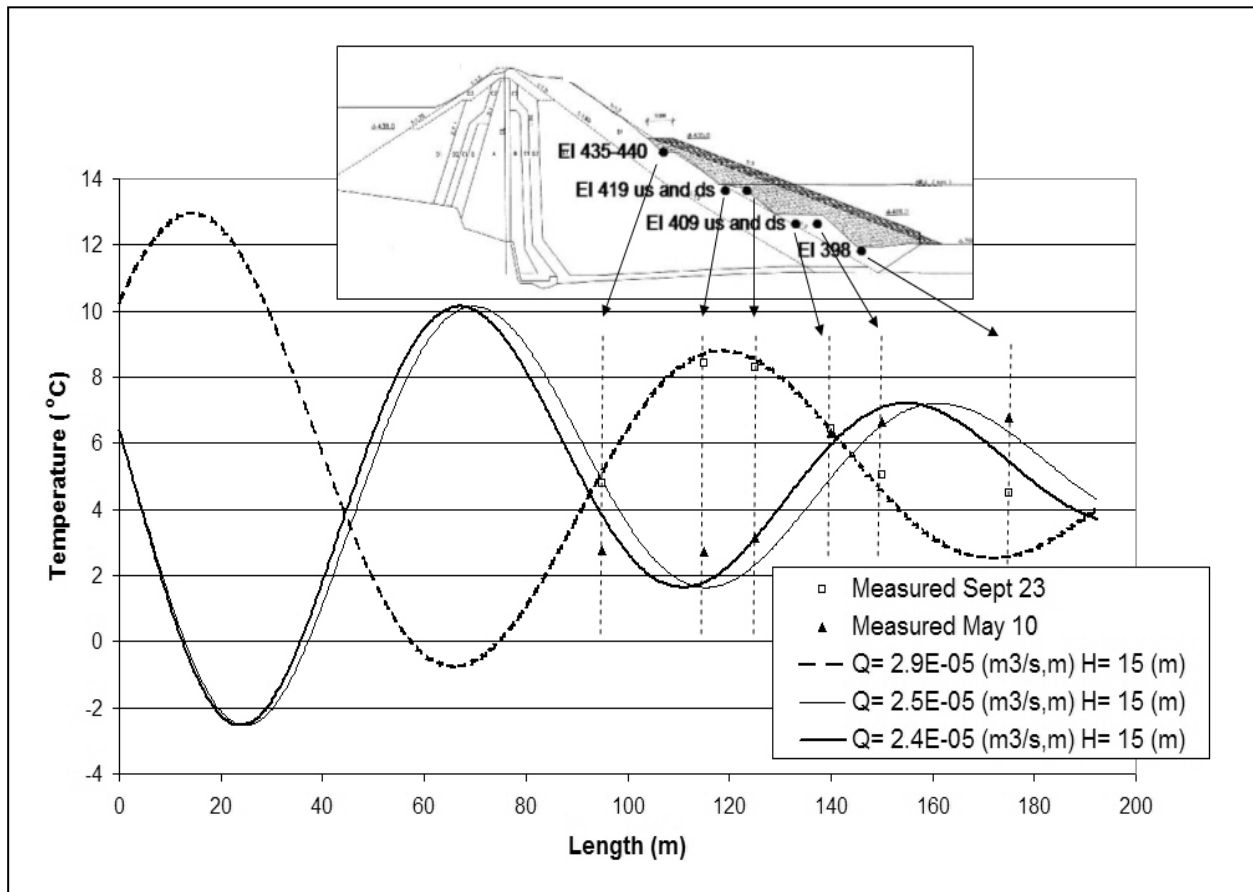


Figure 3: Measured and calculated temperature in the optical fibres at Suorva, West dam.

5 Conclusions

Temperature measurement is a sensitive method to detect seepage flow. The best application of the method is long term monitoring, where slow and small seepage flow changes can be detected. The sensibility is in the order of some $10^{-5} \text{ m}^3/\text{s/m}$ for normal dams. Measurements can be done using fibre-optic systems. Such installations are now common in Sweden, where new and old dams at about 30 dam sites are equipped with optical fibres.

Literature

- [1] Kappelmeyer, O.: The Use of Near Surface Temperature Measurements for Discovering Anomalies due to Causes at Depths. *Geophysical Prospecting*, Vol. 3, pp239-258, The Hague, 1957.
- [2] Johansson, S.: Localization and quantification of water leakage in ageing embankment dams by regular temperature measurements, Proc. ICOLD 17th Congress, Q65, R54, Vienna, Austria, 1991.
- [3] Johansson, S.: Seepage Monitoring in an Earth Embankment Dams, Doctoral Thesis, TRITA-AMI PHD 1014, ISBN 91-7170-792-1, Royal Institute of Technology, Stockholm, 1997.

- [4] AUFLEGER, M.: Presentation at Working Group on Internal Erosion in Embankment Dams, Symposium IREX/EWG, April 26-27, Paris 2004.
- [5] Dornstädter, J, "Detection of Internal Erosion in Embankment Dams", ICOLD 19th Congress, Q.73, R.7, Florence 1997.
- [6] Johansson, S and Farhadiroshan, M.: Fibre-optic System for Temperature measurements at the Lövön Dam. Elforsk Rapport 99:36, Stockholm, 25p, 1999.

Authors Name and Affiliation

Sam Johansson, Ph.D.
HydroResearch Sam Johansson AB, Sweden
sam.johansson@hydroresearch.se

Pontus Sjödahl, Ph.D.
HydroResearch Sam Johansson AB, Sweden
pontus.sjodahl@hydroresearch.se

Detection of Internal Erosion by Means of the Active Temperature Method

S. Perzlmaier, M. Aufleger, J. Dornstädter

Abstract

Detection plays an important role in handling the internal erosion risk. As internal erosion is on the one hand caused by seepage and on the other hand has an impact on the seepage pattern, the monitoring traditionally concentrates on leakage detection. However, conventional leakage detection strategies often lack of seamless and distributed information. Furthermore, the relevant parameters for internal erosion like degree of saturation and flow velocity can not directly be derived from the results. New monitoring tools have been developed to overcome this limitations. One of them is the active temperature method using distributed fiber optic temperature measurements. Beside some remarks about the principle and the performance of DTS (distributed temperature sensing) devices the thermodynamic fundamentals of the heat pulse concept are explained in this contribution. The calibration needed to translate the thermal response to flow velocity and degree of saturation is looked at theoretically and empirically. Finally, general recommendations for detection of internal erosion by means of the active temperature method are given.

1 Introduction

Internal erosion still is one of the major reasons for embankment dam failure. This leads to the assumption that an intractable risk seems to be inherent to the internal erosion phenomenon. Beside all design and construction efforts, monitoring can help to ease the evaluation of the internal erosion risk. Dams that do not satisfy modern design criteria concerning filter performance, may be operated with an acceptable risk utilizing powerful measures for early detection of internal erosion. The meaning of detection in the scope of risk assessment becomes evident, looking at the failure modes and the corresponding event trees for internal erosion. Efficient in time detection of initiation, continuation or progression may give time for intervention and help avoiding dam break incidents.

As internal erosion is caused by seepage and, furthermore, changes the seepage pattern (leakage), the monitoring generally focuses parameters related to seepage. Visual inspection as well as seepage water discharge and pore pressure measurement deliver either punctual or integral information that often lack of spatial resolution and do not directly address the relevant parameters which are degree of saturation concerning the slope stability relevant phreatic surface and flow velocity concerning the particle transport itself. Turbidity of seepage water does not refer to the driving forces of internal erosion but may doubtlessly indicate particle transport.

Most of the geophysical methods provide a high spatial resolution. An easy but powerful geophysical tracer for leakage is temperature (KBR 2004), measured either punctually by single temperature gauges or distributed by chains of several gauges. Today, temperature can be

displayed along fiber optic cables with a high spatial resolution using distributed temperature sensing (DTS), implemented for leakage detection in hydraulic engineering since the late nineties. The so called passive temperature method approach, using temperature as a simple tracer for seepage, is referred to in paper 14, 'Detection of internal erosion by means of the passive temperature method'. The following contribution describes a modified methodology, using an additional heat pulse, the so called active temperature method.

2 Active Temperature Method

2.1 Distributed Temperature Sensing (DTS)

The principle of distributed temperature sensing is based on the temperature-sensitive properties of the optical fiber. An optical impulse is sent into a fiber integrated in a cable by a powerful laser. The signal is backscattered with low intensity at every fiber position. A certain range of the backscattered light correlates with temperature and can be extracted by frequency analysis. The distance from the measured point to the laser can be determined by runtime (time domain OTDR) or by frequency (frequency domain OFDR). The cycle time for one measurement ranges from seconds to minutes. One measurement delivers temperature values distributed along the cable with a spacing of the data points minimum 0.25 to 1 m.

2.2 DTS Performance

Today DTS Instruments are available from several distributors, which differ quite a lot in price and performance. Concerning applications in hydraulic engineering, the following parameters are of interest:

- reliability,
- range (possible length of the fiber) and
- resolution (depending on fiber length, cycle time and spacing of data points).

Reliability is of particular interest if the device is used in a fixed installation (e.g. as alarming system). Standard measuring ranges go from 4 km to 10 km. The absolute temperature accuracy (constant offset on the whole fiber) is about ten times the relative accuracy. The latter is quantified by the standard deviation, either over a set of measurements (time step resolution) or over a number of data points along the fiber (spatial resolution). Figure 1 shows the principal dependency of the resolution on cycle time, fiber length and spacing of data points. The resolution can go down as far as 0,05 K with high end DTS devices (e.g. sensornet sentinel DTS-LR). Unfortunately, some DTS devices take several data points along the fiber to display steep temperature gradients or steps (see **Figure 2**).

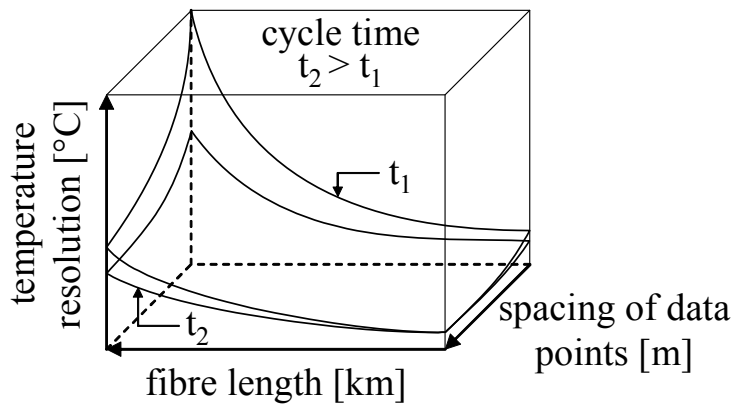


Figure 1: Impacts on the temperature resolution of DTS results

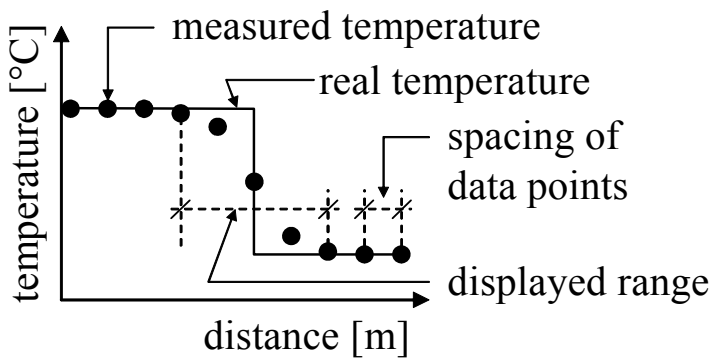


Figure 2: DTS result at a temperature step in comparison to the real temperature distribution

2.3 Applications for Leakage Detection

Due to its high information density, the DTS technology is ideally suited for monitoring temperature fields in dams, applied in the field of hydraulic engineering for leakage detection and concrete temperature observation. Meanwhile, DTS has become a standard tool for leakage detection in hydraulic engineering (Aufleger et al. 2005). The system is typically implemented by two major approaches: the passive method, which uses temperature as a tracer to detect anomalies in the flow pattern (see paper 14), and the active temperature method (formerly also called heat-up or heat pulse method) describing presence and movement of water in soil by evaluating the thermal response caused by a heat pulse. Recent development of these methods focuses on quantifying rather than only localizing leakage.

2.4 Heat Pulse Concept

Originally, the active method was developed for applications where the passive method was inapplicable, which is the case if there are neither sufficient temperature gradients between reservoir water and location of the temperature measurement (e.g. under facings, see Schäfer et al. 2003) nor adequate seasonal temperature variations of the reservoir water.

Recent development shows that the DTS active method can provide precise information on water content (degree of saturation) and movement in the direct surrounding of the cable. Accordingly, crucial needs of leakage detection in general and of detection of internal erosion in

embankment dams in particular are met, as information on the phreatic surface and the flow velocity is obtained distributed.

The method requires an adequate distributed heat input along the cable for about an hour. A.C. or D.C voltage produces such a linear heat input if put on the copper wires integrated in a heat-up cable (linear ohmic resistance). The wires and the optical fibers wind around the central strength member of the cable. Further structural components take stability and protection tasks. Cable diameters ranges from 3,5 to 15 mm. Where for exclusive leakage detection a heat input from 3 to 5 W/m is sufficient, the distributed flow velocity and degree of saturation measurement requires about 10 W/m. For cable sections of several kilometers either high voltage (transformer) or large copper cross section area (limited by cable diameter) are required, besides enough power.

The thermal response in the cable dT_i depends on the cable cross section (diameter, material) and the heat transport from the cable wall, either dominated by conduction in partly to fully saturated soils (**Figure 3, left**) or by convection in presence of flow velocities faster than 10^{-5} m/s (**Figure 3, right**). Accordingly, the temperature difference dT_i between the initial state T_∞ and the heated state T_i is composed of the difference between cable core and wall dT_c plus the difference between cable wall and infinity dT_s .

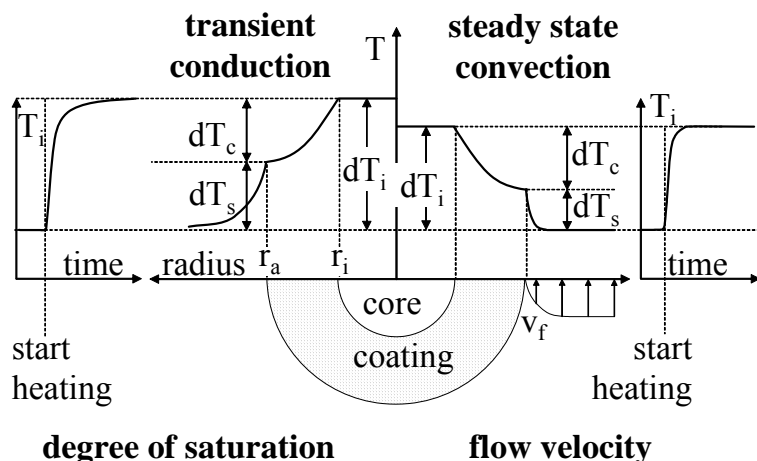


Figure 3: Temperature distribution over a schematic cable cross section with transient conduction and steady state convection

2.5 Conventional Temperature Measurement

In 1991 GTC Kappelmeyer GmbH developed a patented temperature based method - the heat pulse method (HPM) - for measuring the local pore velocity of seeping water in situ in existing embankment dams and their foundation. A line heat source with a well defined heat disturbance is generated by a heatable wire. Combined with a chain of conventional temperature sensors it is inserted in a hollow pipe of small diameter, rammed into the dam by a vibrating hammer before. Depending on grain size distribution, compaction and dam construction 40 to 45 meter have been reached by this so called temperature soundings in the past using special metal pipes.

After the heat source is switched on the temperature within the pipe rises quickly, allowing for a distinction between unsaturated condition and different seepage flow velocities, based on the heat pulse concept described in chapter 2.4. By switching off the heat source similar phenomena can be observed. With no fluid flow the cooling process is slow and the undisturbed temperature is only reached after a long time. High flow rates lead to a much faster adaptation to the undisturbed ground temperature.

Both temperature adaptation processes (heating and relaxation) can be modelled numerically for a variety of material parameters (heat conductivity, heat capacity), flow velocities and source strengths. By comparing the measured temperature-time curves to the modelled ones it is then possible to determine the actual pore velocity in the vicinity of the probe. The penetration depth of the HPM depends on heating time, source strength and pore velocity. With a heating power of several Watts to tens of Watts per m and a heating time interval of 6 to 12 hours a penetration depth of investigation of about 0.5 to 1 m can be reached with this method.

Combining this method with the distributed temperature sensing along fibre optic cables lead to the method described in the following chapters

If no power supply is available on site, the procedure is slightly modified and call Frost Pulse Method FPM. In that application liquid gas is injected into the hollow pipe. Due to the expansion of the gas and the change of the state of matter from liquid phase to the gas phase the pipe and the surrounding soil material is cooled. After the cooling procedure a chain of conventional temperature sensors is introduced into the pipe and the thermal relaxation is monitored. The analysis of the data is similar to the HPM procedure described above. For practical reasons it is easier to apply a heat pulse than a frost pulse.

3 Calibration of the Thermal Response

3.1 Distributed Flow Velocity Measurement

The relation between flow velocity and heat transfer coefficient at the wall valid for the heat transfer from a heated cylinder in presence of seepage in soil enables the DTS active temperature method to measure the Darcian flow velocity. The flow boundary layer and, accordingly, the thermal boundary layer on the wall decrease in thickness with increasing velocity. This forced convection effect makes the thermal response of the heated cable dependent on flow velocity. It is superposed by free convection only in very permeable soils ($k_D \geq 10^{-2} \text{ m/s}$) and else by conduction at slow flow velocities. While the cable influence dT_c can be quantified in tests, the heat transfer coefficient and, thus, dT_s can be calculated from empirical equations e. g. after Fand et al. (1993) using a dimensionless heat transfer coefficient called Nusselt number Nu

$$Nu = \frac{\alpha \cdot D}{\lambda_{eff}} = \frac{q_l}{\pi \cdot \lambda_{eff} \cdot dT_s} = f(Re_d, Re_D, Pr_{eff}) \quad (1)$$

where α is the heat transfer coefficient, D is the cable diameter, λ_{eff} is the effective thermal conductivity of the surrounding soil, q_l is the heat input in W/m, Pr_{eff} is the effective Prandtl number as a ratio of the cinematic viscosity of water and the effective thermal diffusivity of the porous medium soil, Re_D is the Reynolds number of the cable and Re_d is the Reynolds number

of the characteristic particle diameter. The flow velocity incorporated in the Reynolds numbers can be calculated from the measured temperature difference using such Nusselt equations.

The theoretical, thermodynamic fundamentals have been proven with a large number of tests at the laboratory of the Technische Universität München in the past three years. Figure 4 shows the good agreement of test data and theory for heat pulse tests carried out in sand with a heat input of 12 W/m and different cable diameters. It can be seen, that smaller cable diameters increase the span of temperature difference between small and fast flow velocities and thus make the evaluated signal larger compared to the accuracy of the measured temperature difference (see also **Figure 6**). The effect becomes even more obvious when wrapping the cable in an additional permeable low thermal conductivity geotextile fleece coating. Both of these measures combined with adequate heat input and accurate DTS devices provide the maximum measuring accuracy for distributed flow velocity.

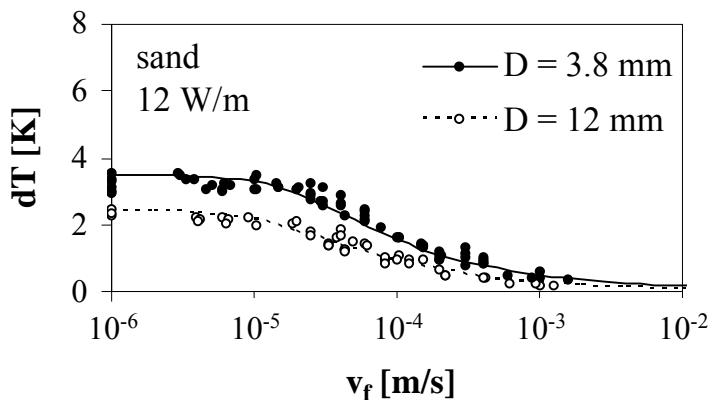


Figure 4: dT_s after 60 min versus Darcian flow velocity v_f at different cable diameter D in pure sand: test data (dots) and theory (lines)

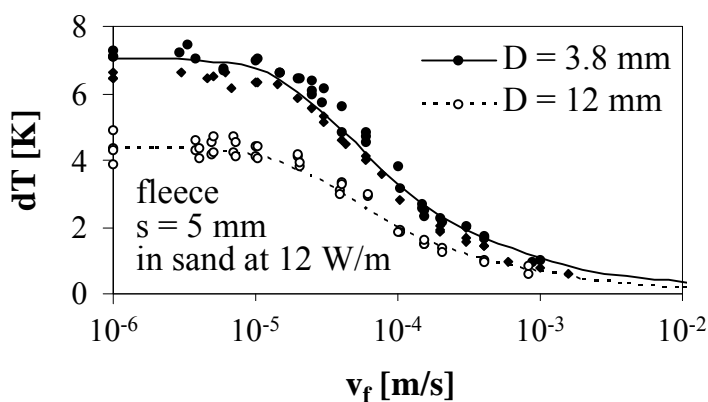


Figure 5: dT_s after 60 min versus Darcian flow velocity v_f at different cable diameter D with additional fleece coating: test data (dots) and theory (lines)

Detailed information on the thermo dynamical background and several hundred tests carried out for calibration with different cables, DTS devices and heat input in water and different soil (silt, sand, gravel), with and without additional geotextile fleece coating at different flow velocities and different flow directions against vertical and against the cable can be found in Perzlmaier et al.

(2004) and Perzlmaier (2007). This key work for the development of distributed flow velocity measurement gave the following general insights:

- Distributed in situ flow velocity measurements can be realized by the DTS active method for the first time.
- Different soil materials with Darcian permeability less than or equal to 10^{-2} m/s only show small variations concerning the dependence of the thermal response on the flow velocity (calibration).
- The measuring range typically ranges from 10^{-5} m/s to 10^{-3} m/s and is suited to detect velocities suspect to initiate internal erosion and suffusion.
- The angle of the flow against the cable has negligible effect on the dependence of the thermal response on the flow velocity as long as it does not differ from perpendicular more than $\pm 30^\circ$.
- The accuracy of the distributed flow velocity measurement increases if the span of temperature difference between small and fast flow velocities becomes large compared to the accuracy of the distributed temperature difference measurement (see **Figure 6**). The span of temperature measurement increases with decreasing cable diameter, increasing heat input, increasing accuracy of the DTS device and with additional several millimeter cable coating of a geotextile fleece (see **Figure 5**). By these measures extend the measuring range to 10^2 m/s.

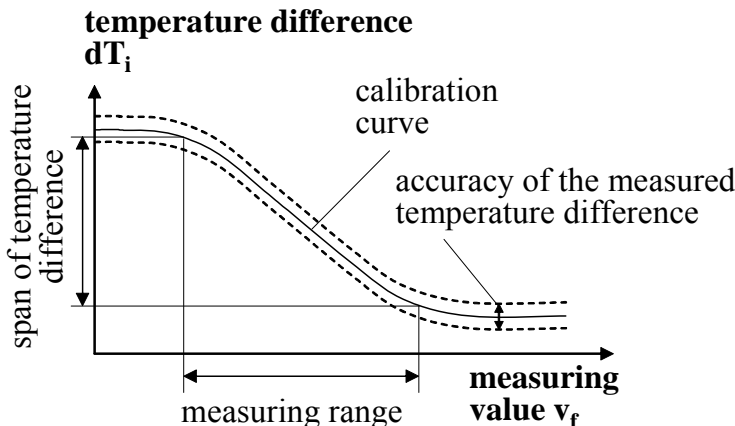


Figure 6: Calibration curve to calculate the measuring value v_f from the measured temperature difference

- The temperature accuracy of most of today's DTS devices (temperature resolution 0.1 to 0.2 K) requires a heat input not less than 10 W/m, limiting the range from 1 to 2 km using 400 V or to 3 to 4 km if the voltage is transformed to 1000 V. Any present or future device with better temperature accuracy will either allow for less heat input or higher accuracy of the distributed flow velocity measurement.

3.2 Distributed Determination of Degree of Saturation

The transient thermal response in the cable is dominated by conduction in partly to fully saturated soil and, thus, governed by the effective soil thermal conductivity λ_{eff} . Effective soil

thermal conductivity is dependent on the solid particle thermal conductivity λ_s , the porosity n and the degree of saturation S_r , which can either be shown by test results after Jessberger (1990) or by theoretical approaches. Johansen (1975) gives a formula (2) to derive the effective thermal conductivity of a partly saturated soil λ_{eff} from the thermal conductivities of the dry soil $\lambda_{\text{eff,d}}$ and the thermal conductivity of the fully saturated soil $\lambda_{\text{eff,sat}}$ as shown in Figure 7.

$$\lambda_{\text{eff}} = (\lambda_{\text{eff,sat}} - \lambda_{\text{eff,d}}) \cdot K_e + \lambda_{\text{eff,d}} \quad (2)$$

with $K_e = 0.68 \cdot \ln(S_r) + 1$ for coarse soil

and $K_e = 0.94 \cdot \ln(S_r) + 1$ for fine grained soil

(fine grained: $2\% < 0,002 \text{ mm}$)

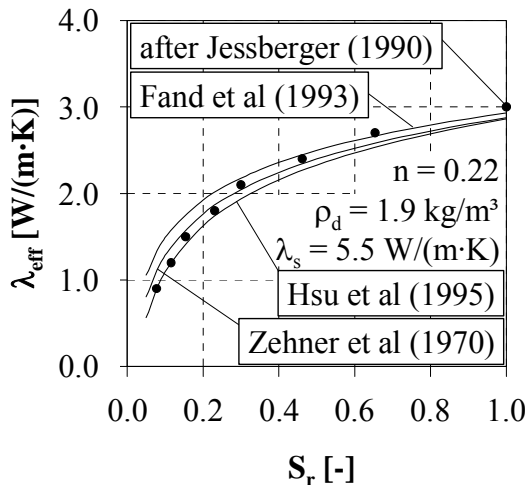


Figure 7: Effective thermal conductivity (λ_{eff}) of two phase mixes from literature modified after Johansen (1975) for partly-saturated soils and test results after Jessberger (1990) versus degree of saturation S_r

The transient conduction on a heated cable in soil can be described using a substitute system of a cylinder with infinite thermal conductivity coupled to the surrounding by a finite surface conductance H. The approximate solutions valid for long heating periods after Kristiansen (1982) allow for an easy description of the temperature difference between cable wall and surrounding dT_c

$$dT_c \approx \frac{q_1}{4 \cdot \pi \cdot \lambda_{\text{eff}}} \cdot \left(\ln(t) + \ln \left(\frac{4 \cdot \kappa_{\text{eff}}'}{r_a^2} \right) - 0.58.. \right), \quad (3)$$

where κ_{eff}' is the effective thermal diffusivity, r_a the cable radius and t the time. A detailed description of substitute systems and the analytical formulation of the transient conduction from a heated cable are given in Perzlmaier et al. (2004). The theoretical thermal response versus degree of saturation interrelationship described by (2) and (3) fits well to test data from DTS

heat pulse tests performed at the laboratory of the Institute of Hydraulic and Water Resources Engineering, TU München, as demonstrated in Figure 8.

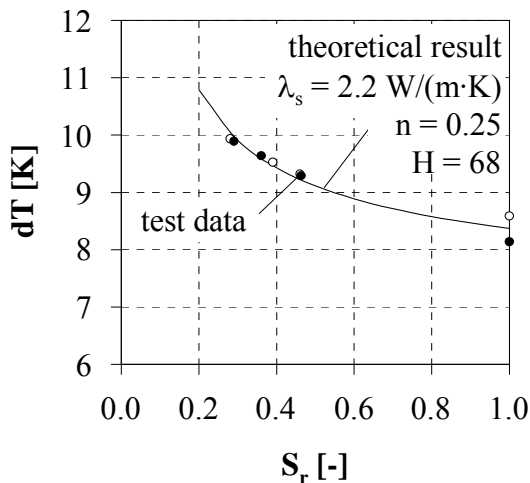


Figure 8: Thermal response dT after 110 minutes of a 12 W/m heat pulse versus degree of saturation S_r

For two reasons the degree of saturation S_r is displayed less accurate with the DTS active temperature method than with other methods available (e.g. TDR probe, dielectric aquameter). First, the span of the thermal response in moist to saturated soils is not large compared to the accuracy of the measured temperature difference and, second, the theoretical calculation of the degree of saturation from soil thermal conductivity additionally depends on porosity and particle thermal conductivity.

However, the method is adequate to distinguish dry, moist and saturated soil conditions at least in uncohesive soils and, furthermore, is outstanding in terms of information density. Hence, the method is relevant for dam engineering applications (e.g. location of line of seepage in coarse soils). An additional geotextile fleece cable coating (thickness s several mm) makes the differentiation of moist and saturated soils even more reliable.

Simplifying, it is assumed for coarse soils that at full saturation (matrix potential equal to zero) all pores are water filled and S_r is 1. In fact, a portion of the pores equal to about one half of the residual moisture remains air filled. For a porosity n of 0.25 and a residual moisture of 3 % (mass of water over the mass of the dried probe) S_r probably does not exceed 0.9.

3.3 Application Example MIK, Bavaria

E.ON Wasserkraft AG owns several hydro power channels mainly built at the beginning of last century. One of them is the Mittlere Isar Kanal (MIK), built from 1921 to 1929, which diverts water from the river Isar north of Munich for use in 5 hydro power plants situated along the channel. The channel was sealed with a 15 cm un-reinforced concrete lining placed on the slopes and the bottom of the trapezoid channel mainly for reduction of head losses and secondarily for sealing purposes.

A 10,8 km section of the channel was rehabilitated in 2005 with an additional concrete lining. In the early design phase of the rehabilitation works the owner identified the need for an efficient seepage control system for two major reasons:

- Since the channel embankment is fairly steep compared to state-of-the-art design standards, the load case "failure of the sealing element" and the inherent raising seepage line does not provide sufficient geotechnical stability to meet safety margins demanded in valid standards. Proving the functionality of the sealing system by monitoring the level of the seepage line seemed to be the only way to overcome this problem as there was no possibility for structural measures on the down stream sides.
- On the other hand, the chosen functional tendering lead to a EPC like contract in which the contractor commits to achieving a certain quality. As this quality had to be provable, the monitoring took an important part in the contract.

Excessive calibration and functionality testing of the DTS active temperature method monitoring concept designed for the job was carried out at the laboratory of the Institute of Hydraulic and Water Resources Engineering of the TU München (Perzlmaier et al 2006). 25 km of optical fibre were installed under the new sealing in the middle of the upstream slopes of left and right embankment (see **Figure 9**). The cable was bedded in an a geotextile fleece coating placed in a trench. The whole range was divided into 8 sections of max. 3,5 km length for measuring and heating with max. 10 W/m.

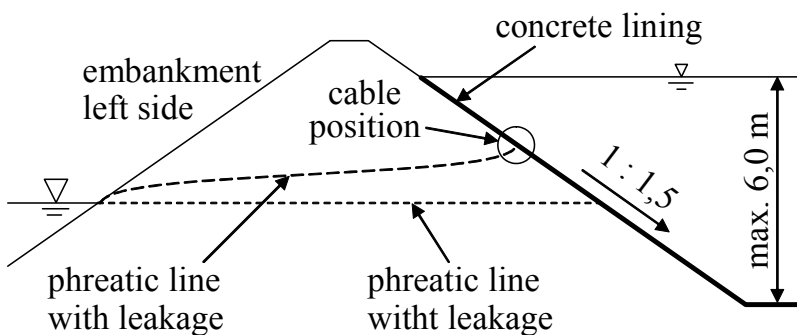


Figure 9: Cross section of the channel side embankment with cable position under the concrete lining

The system was demanded to distinguish precisely between a simple saturation of the cable surrounding, indicating a critical rise of the phreatic surface in the embankment, and a percolation across the cable, indicating small local leakage in the new concrete lining that do not affect stability.

Figure 10 shows the temperature difference measured in a 250 m section before (t_0), immediately after (t_1) and one month after the reimpoundment (t_2). The calibration curves defined analytically as well as empirically (similar to **Figure 4 and 8**) for the special configuration allowed to transfer the thermal response into information about the degree of saturation and, furthermore, to derive the leakage water discharge from the calculated flow velocities in places of local leakage through the new sealing. Before reimpoundment the cable surrounding was almost dry (t_0). As expected partial and full saturation referring to local leakage was monitored immediately after the channel was taken in operation (t_1), that decreased by time due to a natural sedimentation of the small joints and cracks (t_2). Generally, the new sealing passed the defined specification for water tightness and no critical increase of seepage was

monitored so far. No other system could have reliably monitored 25 km of embankment with a spatial resolution of 1 m at comparable effort. Meanwhile, the same concept was applied to a similar rehabilitation project near Munich successfully (E.ON-owned Mühltalkanal, 2006).

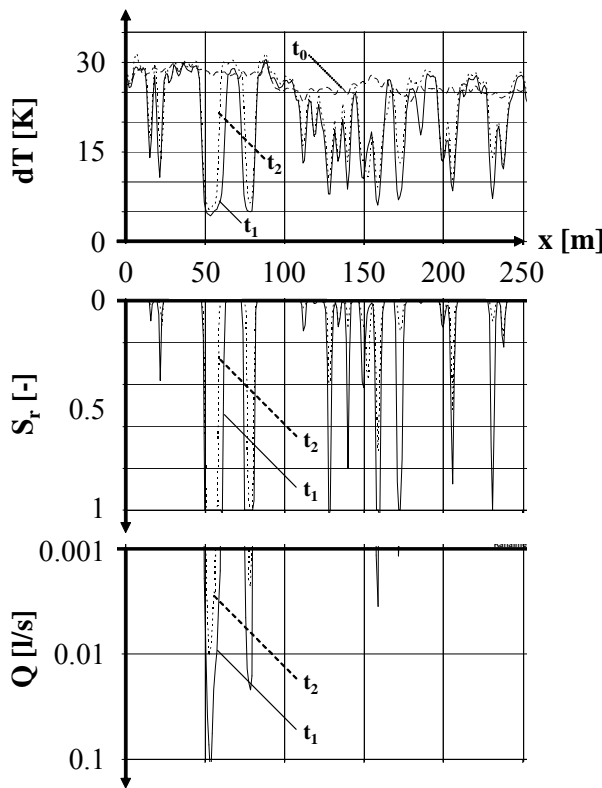


Figure 10: Distributed temperature measurements transferred to degree of saturation and discharge along the cable at the Mittlerer Isar Kanal, Bavaria

4 Detection of Internal Erosion

4.1 General

First of all, detection of internal erosion shall answer the question ‘where and to which extent does internal erosion take place and influence the dam stability?’. Therefore, the impact of internal erosion on the seepage pattern is focused. As continuation and progression of internal erosion often go hand in hand with increased leakage, detection of internal erosion is frequently considered equivalent to leakage detection. Excessive internal erosion may be ruled out by reliable leakage detection proving the absence of any leakage anomalies.

However, the risk level related to internal erosion is hard to quantify by exclusive leakage detection. Even without any apparent seepage anomalies, the erosion process might already have started. Estimating the margin left between an actual no leakage stage and the different phases of internal erosion, needs a more detailed consideration of the parameters dominating potential particle transport. Comparing the hydraulic load on the particles derived from detection with their theoretical drag force (see paper on ‘Hydraulic criteria for internal erosion in cohesionless soil’) may help estimating the likelihood of the different erosion phases to take

place and continue. Similar concepts are required, if leakage has already been detected in times and places.

Finally, the parameters dominating internal erosion like particle size, cohesion, filter performance, hydraulic gradient, permeability, flow velocity and others are known to vary a lot even within one dam. Failure occurs at random spots, where this set of parameters exceeds critical limits. Even though, certain areas in an embankment dam are known to bear a disproportional high risk of initiation (see typical locations for concentrated leaks in paper 3 'Locations') the detection needs adequate spatial resolution over the whole structure to be successful and reliable.

4.2 Leakage Detection

The active temperature method has become a standard tool for leakage detection in the last decade. As described above the detection of internal erosion is first of all leakage detection. Therefore, the renown advantages of the method for leakage detection applications are as well valid for the detection of internal erosion. Leakage detection by means of the active temperature method has to bee taken into consideration if:

- the length of the observed structure makes standard detection methods like seepage water discharge measurement unfeasible or inefficient,
- any required re-instrumentation of an existing dam does not allow for conventional detection strategies,
- the site conditions (e.g. dam structure, damage potential) require special measures like automated alarming systems,
- the high spatial resolution, inherent to the active temperature method, helps making the evaluation more precise and reliable,
- the passive temperature method is inapplicable because neither sufficient temperature gradients between reservoir water and location of the temperature measurement (under surface sealing or at the downstream toe) nor adequate seasonal temperature variations of the reservoir water are given,
- and if the local information on degree of saturation and flow velocity are rather required than integral information on leakage anomalies provided by the passive method.

4.3 Direct Interpretation

Regarding leakage detection in small but long dams a fratic surface critical for slope stability can be defined by geotechnical calculations (see example in chapter 3.3). Any leakage, no matter from which source, can be evaluated as noncritical, as long as this critical line of seepage is not reached. Placing a fiber optic cable somewhere underneath this critical phreatic surface and applying the concept of distributed estimation of the degree of saturation (see chapter 3.2) allows for a direct interpretation of the actual state of stability. This concept is only applicable if slope failure due to increasing phreatic surface is found to be the critical failure mode.

Combining monitoring results (e.g. pore water pressure) and hydraulic criteria to evaluate the risk of internal erosion is traditionally done looking at hydraulic gradients. More precisely, critical

flow velocities can be evaluated (see paper on 'Hydraulic criteria for internal erosion in cohesionless soil'). The distributed flow velocity measurement by means of the active temperature method described above, provides a measuring range of the Darcian flow velocity between 10^{-5} m/s and maximum 10^{-2} m/s, corresponding to critical pore velocities 4 to 8 times higher. Compared to the critical velocities for particle transport presented in the paper 'Hydraulic criteria for internal erosion in cohesionless soil', the risk of particle transport to initiate in uncohesive soil can be derived from the monitoring results for particle sizes up to several millimeters using the distributed flow velocity measurement. Thus, the particle size most relevant for internal erosion, to big to have noteworthy cohesion and to small to resist the hydraulic load, can be targeted by this detection method.

Combining monitoring results (e.g. pore water pressure) and hydraulic criteria to evaluate the risk of internal erosion is traditionally done looking at hydraulic gradients. More precisely, critical flow velocities can be evaluated (see paper 5 'Hydraulic criteria for internal erosion in cohesionless soil'). The distributed flow velocity measurement by means of the active temperature method described above, provides a measuring range of the Darcian flow velocity between 10^{-5} m/s and maximum 10^{-2} m/s, corresponding to critical pore velocities 4 to 8 times higher. Compared to the critical velocities presented in paper 5, Figure 4 'critical velocity over particle diameter', the risk of particle transport to initiate in uncohesive soil can be derived from the monitoring results for particle sizes up to several millimeters using the distributed flow velocity measurement. Thus, the particle size most relevant for internal erosion, to big to have noteworthy cohesion and to small to resist the hydraulic load, can be targeted by this detection method.

4.4 Cable Layout

Typical applications using the active temperature method either for a high spatial resolution leakage detection or for a more sophisticated evaluation of degree of saturation and flow velocity generally require fiber optic heat-up cables installed behind the sealing element. If the cable is placed in a surrounding more permeable than the sealing element (e.g. in a filter or drainage layer) leakage flow is forced to pass the cable increasing reliability and decreasing the installation effort. Figure 9 gives some examples for the cable layout.

Cables installation inside a dam (**Figure 11, example A**) is more practical for implementation in newly constructed embankment dams, where the passive method is feasible as well. Which of the two methods or a combination of both to chose, depends on the information looked for as described in chapter 4.2 and 4.3. Installations under surface sealing elements (**Figure 11, example C**) or in a new toe berm (**Figure 11, example B**) often afford the use of the active method due to the lack of sufficient natural temperature gradients.

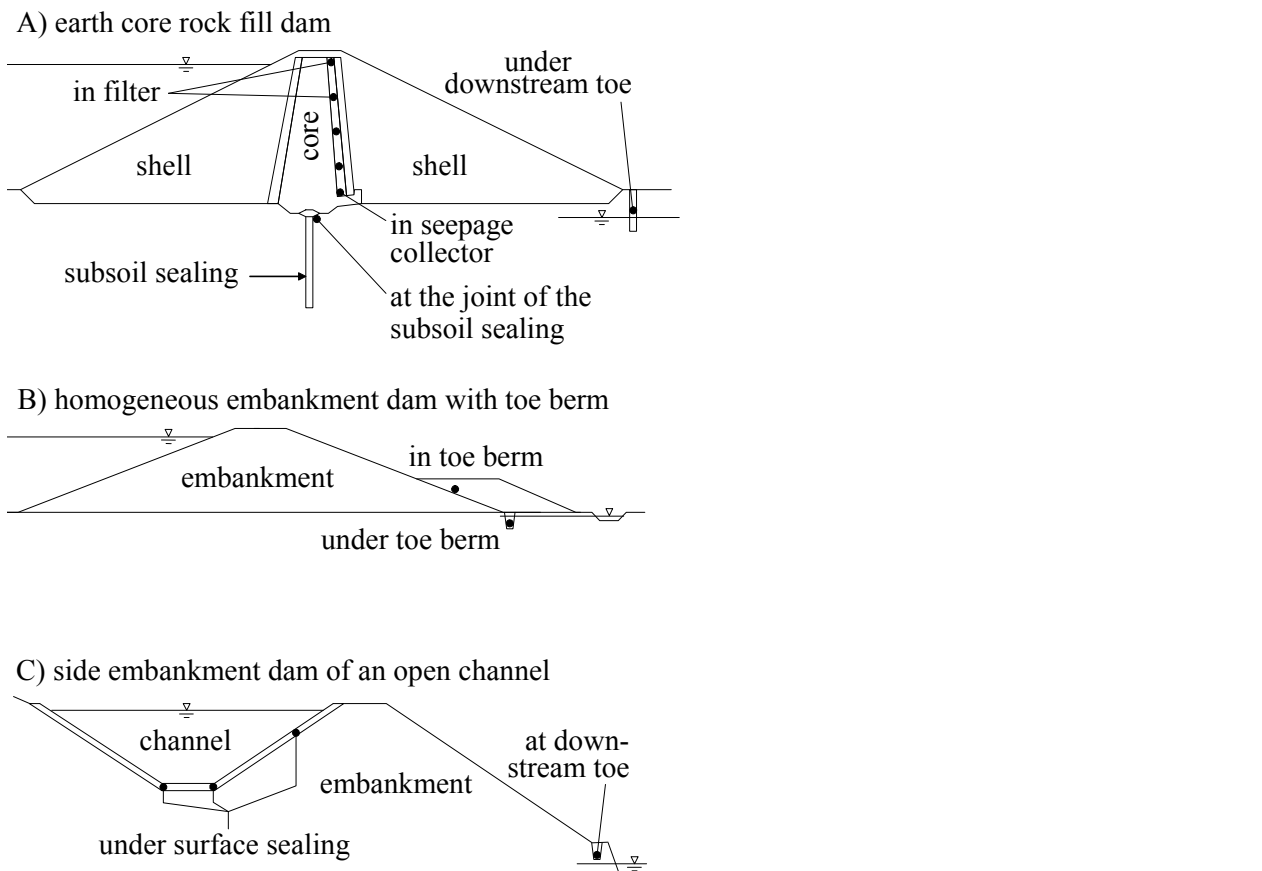


Figure 11: Different embankment dam cross sections with cable positions (black dots) relevant for applying the active temperature method

Conclusion

To be finished for the Frising paper (deadline 5th of Mai 2007) after the Aix le Bains meeting and further contribution of J. Dornstädter

Literature

- [1] Aufleger, M.; Conrad, M.; Perzlmaier, S.; Porras, P. 2005: Improving a Fiber Optics Tool for Monitoring Leakage. *HRW*, Volume 13, Number 4, Sept. 05.
- [2] Fand, R. M.; Varahasamy, M.; Greer, L. S. 1993: Empirical correlation equation for heat transfer by forced convection from cylinders embedded in porous media that accounts for wall effects and dispersion. *Int. J. Heat and Mass Transfer* Vol. 36, No. 18, p. 4407 – 4418.
- [3] Hsu, C. T.; Cheng, P.; Wong, K. W. 1995: A lumped parameter model for stagnant thermal conductivity of spatially periodic porous media. *ASME J. Heat Transfer*, Vol. 117, S. 264 – 269.
- [4] Jessberger, H. L. 1990: Bodenfrost und Eisdruck. In: *Grundbautaschenbuch / Teil 1*. edt.: Smoltczyk, U. Verlag Wilhelm Ernst & Sohn. Berlin, München, Düsseldorf.
- [5] Johansen, O. 1975: *Varmeledningserne AV Jardarter - Thermal conductivity of soils*. NTH Trondheim, Dissertation. (CRREL Draft Translation 637, 1977).

- [6] KBR 2003: *Early detection of internal erosion, feasibility report, Vol. 1 of 2: main report.* Defra, Research Contract Reservoir Safety Advice, England.
- [7] Kristiansen, J. I. 1982: *The transient cylindrical probe method for determination of thermal parameters of earth materials.* Laboratory of Geophysics, Aarhus, Denmark. GeoSkrifter No. 18, ISSN 0105-824X.
- [8] Perzlmaier, S.; Aufleger, M.; Conrad, M. 2004: Distributed Fiber Optic Temperature Measurements in Hydraulic Engineering – Prospects of the Heat-up Method. *Proceedings of the 72nd Annual ICOLD Meeting.* Seoul, Korea.
- [9] Perzlmaier, S. 2006: Der Wärmeübergang vom Heizzylinder an gesättigte und durchströmte Schüttungen. *Tagungsband Workshop: Anwendung und Grenzen physikalischer und numerischer Modelle im Wasserbau.* Wallgau, Sept. 05. Berichte des Lehrstuhls und der Versuchsanstalt für Wasserbau und Wasserwirtschaft der TU München, Heft 104.
- [10] Perzlmaier, S.; Straßer K.-H.; Strobl, Th.; Aufleger, M. 2006: Integral Seepage Monitoring on Open Channel Embankment Dams by the DFOT Heat Pulse Method. *Proceedings of the 22nd Congress of the International Commission on Large Dams (ICOLD),* June 06, Barcelona, Spain, Q. 86 – R12, S. 145 – 164.
- [11] Perzlmaier, S. 2007: Verteilte Filtergeschwindigkeitsmessung in Staudämmen. Berichte des Lehrstuhls und der Versuchsanstalt für Wasserbau und Wasserwirtschaft der TU München, Heft 109.
- [12] Schäfer, P.; Perzlmaier, S.; Conrad, M.; Strobl, Th.; Aufleger, M. 2003: Rehabilitation of dam facings monitored by an advanced technology for leakage detection. *Proceedings of the 21st ICOLD congress,* Montréal, Canada.
- [13] Zehner, P.; Schlünder, E. U. 1970: Wärmeleitfähigkeiten von Schüttungen bei mäßigen Temperaturen. *Chemie - Ing. Technik,* 42, S. 933 – 941.

Authors Name and Affiliation

S. Perzlmaier
 TIWAG – Tiroler Wasserkraft AG
 sebastian.perzlmaier@tiwag.at

M. Aufleger
 University of Innsbruck, Austria
 Unit of Hydraulic Engineering / Institute of Infrastructure
 markus.aufleger@uibk.ac.at

J. Dornstädter
 GTC Kappelmeyer GmbH, Germany
 dornstaedter@gtc-info.de

Dam Strengthening by Diaphragm Walls

By Jean-Jacques Fry and Michel Chopin

Abstract

Existing water retaining structures lacking filter or with deficiencies in their filtering system need an assessment of the risk of internal erosion in order to determine the type of maintenance. Considering the remedial maintenance, two main rehabilitations improve the resistance for internal erosion. The first one is to lay an intercepting filter on the downstream side and construct on it a toe-berm. The second one is to repair the sealing element damaged by internal erosion. This paper deals with the second kind of rehabilitation and focuses on diaphragm walls. After a short introduction on the philosophy of dam strengthening, the main methods of cut-off and sealing repair by diaphragm wall, that are currently being used in France, are presented in this paper.

1 Introduction

1.1 Two Kinds of Internal Erosion Repair

Internal erosion damages the watertightness function. Repair does not necessarily hinge on upgrading that watertightness function. Theoretically, assuming that the filtration is not fully provided, repair consists in strengthening a barrier against one of the successive phases of the failure mode :

- Initiation is stopped by upgrading the sealing element. Both, flow rate and erosion are stopped by a new impervious and resistant material.
- Continuation is stopped by installing a downstream filter under weighting. Erosion is stopped but not flow rate.

1.2 Criteria for Selecting the Kind of Repair

1.2.1 First Criteria: Excessive Loss of Water

The choice of the method of rehabilitation depends on the consequences of the hazard:

- if water is being lost and the economic viability is being jeopardized, the sealing system must be upgraded,
- if stability may be lost with no excessive loss of water, a downstream filter blanket and a downstream stabilising bank may be provided,

1.2.2 Order of Magnitude of the First Criteria Threshold

The thumb rule for repair design, compiled from case studies of large dams and hydropower canals, is based on the average permeability K of the deteriorated sealing element or on the global discharge flow Q .

Table 1: First criteria for repair compiled from case studies

Intervention	downstream filter, drainage system and weighing are enough	Special survey is needed to select repair according to the mode of failure	upgrading of watertightness is relevant : repair of the sealing element
Average permeability of the sealing element	$K < 10^{-6}$ m/s	10^{-6} m/s $< K < 10^{-5}$ m/s	$K > 10^{-5}$ m/s
Global discharge flow Q (m^3/s) in dam	$Q < 10^{-3}$ to 10^{-2} m^3/s	10^{-3} $\text{m}^3/\text{s} < Q < 10^{-1}$ m^3/s	$Q > 10^{-2}$ to 10^{-1} m^3/s
linear discharge flow Q ($\text{m}^3/\text{s}/\text{m}$) in dyke	$Q < 10^{-5}$ – 10^{-4} $\text{m}^3/\text{s}/\text{m}$	$10^{-5} < Q < 10^{-3}$ $\text{m}^3/\text{s}/\text{m}$	$Q > 10^{-4}$ to 10^{-3} $\text{m}^3/\text{s}/\text{m}$

Practically, the previous criteria, compiled from experience in table 1, is a first attempt for decision making. Before using them, some remarks must be kept in mind :

Remark 1: the criteria thresholds in table 1 are for situations where internal erosion is under development. For instance, too much money may be expended in a view to reducing larger seepage flow in karstic foundations to the critical value of table 1.

Remark 2: the criteria thresholds in table 1 are not triggering the erosion initiation. For instance, let assume in a stratified alluvial foundation that contact erosion is going on at the interface of a very fine layer of silt ($d=0,003$ mm) through the adjacent coarse gravelly sand layer whose the thickness is 0,1m. In such condition the critical flow velocity is 10^{-5} m/s, the discharge for initiation is 10^{-6} $\text{m}^3/\text{s}/\text{m}$, lower than the critical threshold in table 1.

Remark 3: the thresholds in table 1 are not the absolute or mandatory condition of repair. Let assume that in a thick gravel foundation, with 1 mm particle diameter and 10 m thickness, the critical flow velocity is 10^{-1} m/s, the safety discharge should be 10^{-1} $\text{m}^3/\text{s}/\text{m}$, well larger than the values in table 1.

1.2.3 Second Criteria: Assessment of the Progression Phase after Repair

It is clear that the internal erosion assessment is the only way to propose a safety criteria for repair decision. For instance the permeability criteria lower than 10^{-6} m/s is not a guarantee of good behaviour: an homogeneous dam in clay without filter and with $K= 10^{-10}$ m/s may suddenly fail. Why? A crack or an animal hole may initiate a sudden piping. To select the best investment for strengthening the dam, the engineer has to answer the following question: " what kind of continuation phase may going on after repairing the dam? ". To answer that question, it is noteworthy to separate cohesive constitutive soils and soils with no cohesion.

Embankment made with clay and without filter or founded on clayey material may suffer erosion along a crack as the most frequent initiation mode. In such situation, the development of progression leads to piping. A filter downstream any potential crack should be required. In consequence, an intercepting filter on the downstream face, let in a compression state by a weighting, dimensioned for all the possible future situations, should be recommended and

controlled by preventive maintenance. Repair design has to control stability with high pressure caused by filter plugging.

Embankment made with non cohesive material cannot hold the roof for a long time and suffer probably not piping but mainly suffusion, contact and backward erosions. Repairs go and change the flow velocities: most of the flow velocities decrease after strengthening, however the areas where flow velocities are unchanged or increased are of the utmost importance. The new flow velocities in the repaired dam and its foundation, calculated by flow analysis, have to be compared with the critical flow velocity criteria, proposed by S. Perzlmaier and P. Muckenthaler. Progression can be predicted and consequences taken into account. For instance, the flow velocities at the borders of the diaphragm wall are the basic parameters to dimension the depth and the length of the effective and long term strengthening. At Cusset dyke, erosion was triggered at the lateral edges of the thin wall. In a similar way, the future trend of progression in the core is a key parameter to justify downstream filter and weighting on the downstream toe as the long term solution.

In any case, criteria is checked according to past behaviour, soil type in the dyke and type of mode of failure.

1.2.4 The Third Criteria is the Level of Consequences of the Failure

The hazard created by reservoir size is partly quantified by the peak flood failure flow. As a first estimate, that flow would be proportional to $H^2\sqrt{V}$ where H is dam height (m) and V reservoir volume (millions m³). In France, $H^2\sqrt{V} > 200$ is considered as a high consequence dam and $H^2\sqrt{V} < 20$ as a low consequence dam (however other items are considered in the risk assessment). Of the structures that have undergone rehabilitation, the dykes are generally less than 10 m high, the small dams are 10 m high on average, and the large dams vary in height, always over 15 m. For dykes, considered as low consequence structures, the works have involved cheap improvement in the drainage canal by means of drainage shafts, repairing the downstream filter and weighting the downstream side and cheap sealing system (dumping clay or silt on the upstream side, thin central wall). For large dams, the most common rehabilitation technique has been the diaphragm wall. Repair of the sealing system is more necessary when the dam is high, since watertightness is the dam's main function.

1.2.5 The Repair of the Watertightness

The field of application of sealing repair methods depends on four main parameters:

- Location, dimensions and particularly depth,
- ground permeability,
- ground strength,
- cost.

Upstream sealing systems have been increasingly used, and their rehabilitation are now considered. Methods of detection are quite efficient to find localised defects or incidents. Method of rehabilitation of upstream systems are too numerous to give an overview of their various applications: they are not presented in that paper.

Referring to the repair of a central sealing system, the use of grouting techniques is flexible, it does not require major mechanical means, and adapts to a wide variety of grounds. However, the main purpose of grouting is to fill in voids, cavities or open cracks, as its field of application is limited by permeability. It cannot penetrate ground with permeability equal to or less than 10^{-5} m/s without hydraulic fracturing, which should be avoided when the dam is low. Grouting is also costly and tricky in ground with high permeability. They are used in critical and local situations where, for instance, seepage flow in foundation can lead to piping. Grouting shall not be detailed in that paper.

From another standpoint, most of engineers want to achieve watertightness in a more tangible and easy to control fashion than is possible with grouting; in this case they speak of a "positive cut off", a term borrowed from the Americans that corresponds quite simply to a diaphragm wall. The different kinds of diaphragm walls are introduced in that paper.

Finally, in some cases there are advantages to combining the two last methods of repair, i.e. grouting and diaphragm wall. For instance, in front of major problems, consolidation must be restored before the sealing system is upgraded. This can be done by compaction grouting, to permit construction of a diaphragm wall under acceptable safety conditions and with satisfactory results.

2 The Diaphragm Walls

2.1 Economical Ranking

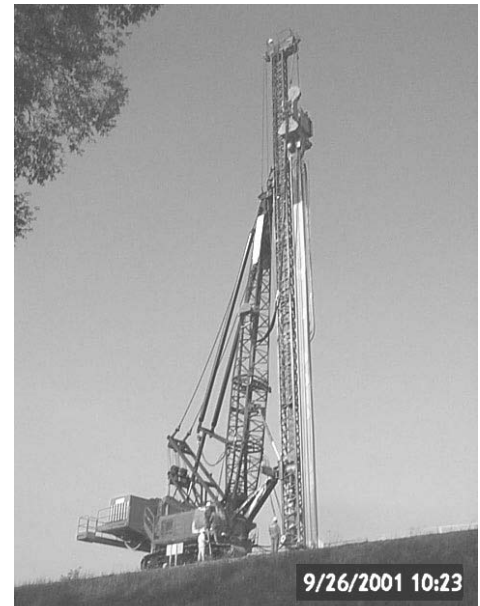
It is useful to rank the most commonly used techniques according to their cost and to discuss their field of application. The following list is an attempt for ranking the methods of construction used in France, from an economical point of view:

- 1 Thin wall or vib wall,
- 2 Trench mix
- 3 Slurry wall with back hoe
- 4 Cement Soil Mixing
- 5 Plastic wall with clam shell
- 6 Steel pile wall
- 7 Concrete wall with Cutter excavation
- 8 Pile wall
- 9 Jet grouting

2.2 Thin or Vib Wall

Principle

This type of diaphragm wall is built by driving a steel profile (i.e. a kind of sheet pile) into the ground to the required depth, then a cement grout mix is injected through injection pipes fixed in the steel profile, which is lifted up to the surface. The wall is created by filling the empty space remaining, when the profile is removed and by permeation of the ground porosity. The grout mix



9/26/2001 10:23

Figure1: vib wall under construction

used is a self-setting cement slurry that fills up the empty space left by the steel profile. The average permeability of a thin wall (0.10m thickness) is in a range of 10^{-7} to 10^{-8} m/s.

Construction procedure

The construction sequence includes the following steps:

- Step 1: excavation of a trench in the centreline of the wall to store slurry ready for use.
- Step 2: the profile is driven in by hammering or by vibration, an additional high-pressure jetting can be used to ease the penetration and increase thickness.
- Step 3: when the designed depth has been reached, as the pile rises, a jet of high-pressure (a few dozen MPa) slurry is injected towards the panel being built, causing mixing and blending of the earth with the slurry, to prevent that panel from closing as the current panel is driven in, thus eliminating any risk of "holes" in the thin diaphragm wall and increasing the thickness.
- Step 4: when a stroke is completed, the machine moves a step forward to repeat the same process, overlapping the previous trench by a dozen centimetres.

Control

Monitoring the verticality is the major issue. Grout mix characteristics are also sensitive therefore frequent controls of grout mix are required (viscosity and specific gravity). Temperature measurements are carried out after completion to check efficiency.

Field of application

Thin wall is the cheapest technology which is commonly used for dykes built of alluvial fill. It can be used in any type of soil (natural ground or fill) into which a cone penetrometer test can be driven. But the process is not operative in heterogeneous ground with boulders or hard layers due to lack of penetration or deviation. The thickness of the diaphragm wall, relies mainly on the ground porosity. It may vary from a few centimetres in fine sand, to several decimetres in gravel; when there are alternating layers of cohesive soil and soils with coarse grading, discontinuities may crop up in the wall near transition zones. The maximum depth is 25 m with the most powerful equipment available today.

Case studies

ST-EGREVE dam (1990) 3 000 m² of drilling, no problem after 17 year.

CUSSET dyke (10 repaired areas since 1995-1999) total 4km and 40,000 m² of drilling, 8 to 12 m deep. In 4 areas, leakages appear 10 years after ; in most of the cases, lateral extension of the wall was not enough.

STRASBOURG polder dyke (2001) 58 000 m² 19 to 24 m max deep production 26 m²/h average take 225l/ m² (**Figure 1**). Not enough time for feedback.

2.3 The Trench Mixing

Principles

The trench mixing consists of continuous mixing with cement by a rotating tool.

Construction procedures

The equipment is a trenching machine built for pipe or drainage installation

(Figure 2). The trench width is 0,40m. The construction process is carried out whether in using:

- Dry Method: which consist of introducing and mixing a dry cement powder to create soil-cement mixture by adding water, or using:
- Wet Method: which consist of introducing and mixing a cement - bentonite slurry to create soil-cement mixture as well (Figure 2)

Control

Control is based on the consistency of the mixing, take (200-250 l/m), tomography panel, CPT.

Field of application:

Dry Method is suited for shallow depth construction down to 6 m, while wet Method can be performed down to 10 m depth. The dry method has less environmental concerns.

Case studies

The HAUCONCOURT dyke, improved by the dry method in 2006, successfully withstood a major flood.

2.4 Slurry Wall

Principle

Slurry wall is excavated with bentonite-cement slurry, which stabilises the trench along drilling, after setting, its forming a sand mix material so called the cut-off. The slurry is having the function to support the trench walls and create a watertight medium (permeability 10^{-8} m/s when fully set).

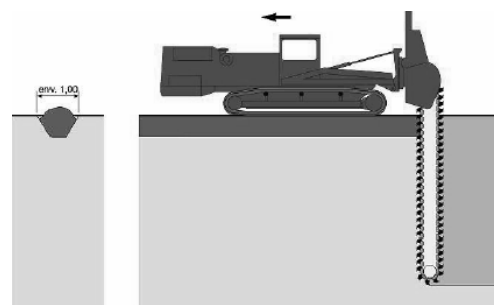


Figure 2: trench mixing



Figure 3: The wet method



Figure 4: trench excavated by backhoe

Procedure

The trench is excavated by backhoe or a clam shell. The cement bentonite slurry is prepared in storage tanks or ponds and pumped into the trench as excavation take place. The slurry filled the trench and set in place. To reach the full depth of the trench may take some hours, and the sand mix with the slurry increases the shear strength, the grout mix composition is usually C/W ratio < 0.3, with a fluidifier. Therefore the period of setting is increased to several weeks. The construction of a diaphragm wall is completed in only step. Usually continuous drilling is employed, with each primary panel being as long as the clamshell works; overlap is considered equal to the thickness of the wall plus the maximum expected deviation at the base of the wall. Alternating panels can be achieved as well, as the clamshell can bite into the freshly set slurry, when the secondary panels are drilled.

Control

Cement bentonite slurry characteristics: viscosity Specific gravity unconfined strength (>100 KPa) Grout consumption is to be continuously controlled as well

Field of application

This is the most commonly used method when the only purpose of the diaphragm wall is watertightness. The use of slurry walls is often restricted to low dams, as at first consideration it would seem to be the most economical and adaptable solution. The process requires as well some significant space available for the slurry pools. The continuity of the wall should be checked to some extent of the cutoff. Some core boreholes drilled through the slurry give relevant detail on the grout performances. Some Slurry wall deterioration may be caused by lack of setting inhibitor in ground foundation (La Prade dam) or by aggressive water (acid Ph<4, water with sulphate or chlorides).

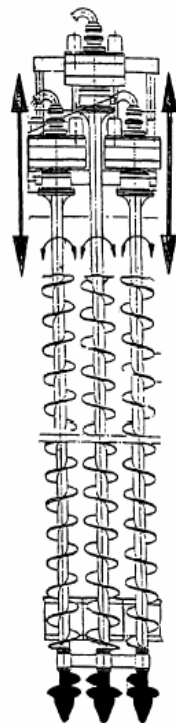
Case studies

The embankments of the ST-EGRÈVE dam were repaired in 1991 with that method: no problem has been reported since that repair.

2.5 The Mixed in Place

Principle

Existing soil is mixed continuously with cement by a rotating tool. Drilling is done in alternating panels: first the primary panels are drilled, secondary panels are drilled after the adjacent primary ones with half a diameter connection, finally primary panels are mixed one more time.



Construction procedures

The tool is a machine with one row of three augers with 35 cm diameter. The soil is mixed up with around 300l/m³ of bentonite-cement slurry (15% in volume). There are two drill machines: one with depth less than 14m, the other for depth higher. The diameter is 55 cm.

Control

Control is based on DIN 18136 checking in laboratory permeability < 10 – 8 m/s and unconfined strength $q_{u28d,i} \geq 0,5$ MPa, bulk density may be checked > 2.1, the control on site is based on drilling, temperature probe tests.

Field of application

Well suited for alluvium with gravel. The depth is currently limited to 24 m.

Case studies

A 520 m leaking section of the Gerstheim dyke was successfully repaired by this method.

2.6 Deep Mixing

Principle

Deep soil mixing is a process involving a continuous mixing with cement by a rotating tool.

Construction procedures

The tool is the metal frame with two horizontal-axis parallel cutting drums with cutters driven by two slowly rotating motors at the bottom. The width is 0.5m.

Figure 5: the working tool with three augers



Figure 6: Soil Cutter

Control

Grout mix consistency is to be monitored, absorption recording, tomography panel, CPT

Field of application

That new technology should be suited for large range of depth and soils conditions.

Cases studies

The 20m wall of Le Havre Harbour (**Figure 5**) made in dual step with 210 l/m of bentonite and 300 l/m of grout C/E=2 gets $R_c > 2 \text{ MPa}$ and Permeability $< 2 \cdot 10^{-10} \text{ m/s}$.

2.7 Plastic Concrete Wall – Clam Shell Excavation

Principle

Diaphragm wall consists in soil excavation and concrete casting according to primary and secondary sequence. The excavation unit is a clam shell, consisting of a heavy body with two half-shells at the bottom, the clamshell is linked to a crane with heavy duty wires, allowing displacements opening & closing. Different clamshell may be selected according to soil characteristics (5 to 12tons).

The conventional diaphragm wall is constructed in two steps:

- Excavation phase using bentonite slurry, to stabilise the trench and protect from loss of water.
- Concrete casting with plastic concrete or plastic mortar. Generally this type of diaphragm wall is 0.50 to 1.50 m thick.

Construction procedures

"Guide walls" are first constructed (trench 1 to 1.5 m deep and 30 to 50 cm) to guide the clamshell and set the panels before drilling.

During drilling a bentonite slurry used to stabilise the trench thanks to its thixotropic properties. Drilling is done in alternating panels: primary panels are first drilled, to the designed depth.

A primary panel is usually drilled 5 to 8 m wide. Secondary panels are drilled after the adjacent primary ones have been concreted, and are generally shorter.

Control

Deviation, Slurry properties and concrete progress are the main issues for control. Plastic concrete UCS should be in a range of 700 kPa to 1200 KPa after 28 days.

Field of application

The clamshell technique can be used in any type of soil except hard ground. This means that the technique is routinely used to build diaphragm walls up to 40 m deep.

The process is losing efficiency with depth and round hardness.

Case studies

The cut-off of La Ganguise dam was constructed with that method.

2.8 Concrete Wall with Cutter Excavation

Principle

In rock or deep foundation the clamshell is of low effectiveness. Then a powerful cutting tool was issued, some 20 years ago, to do very deep wall or large range of foundations.

The double cutting tool mounted at the bottom of a metal frame consists of two horizontal-axis parallel cutting drums with cutters and driven by two slowly rotating motors.

A third motor drives a mud pump to carry the cuttings up to the surface. The mud is then sent back to a filtration unit from which it emerges screened and without sand.

Construction procedure

Construction mode is quite simple: the equipment is installed and an elementary panel element is drilled to the required depth. An elementary vertical panel often measures 2.40 m wide (in the plane of the wall) and is between 0.65 and 1.5 m thick. A primary panel is composed of several elementary panels and can be up to 10 m wide.

Once drilling is finished, concreting can start and the slurry pumped back to the storage plant. Primary panels are isolated by un drilled sections (2.2 m wide).

Those columns are the basis of the secondary panels that the cutter drills, with a 0.10 m overbite into the concrete of the adjacent primary panels. A good quality joint is produced with no special arrangements. Maximum drilling speed can reach 30 to 40 m²/h.



Figure 7: Cut-off of La Ganguise dam

Control

A great deal of effort has been made to give this equipment a great accuracy. It is now fitted with a number of sensors to constantly monitor verticality, by means of built-in inclinometers and to correct any deviation enabling high accuracy drilling (deviations $\leq 1/1000$).

Field of application

When the dam is high and there are no boulders in it, the most commonly used cutter today is from SBY (so called Hydrofraise). It can be used to build diaphragm walls in loose ground or rock foundations having a compressive strength of more than 120 MPa.

Cases studies

Several dams are excellent evidence of the technique's efficiency: FONTENELLE, NAVAJO and MUD MOUNTAIN dams were repaired with 45, 140 and 120 m deep diaphragm walls in the core



Figure 8: 120m diaphragm wall of Mud mountain dam

2.9 Sheet Pile Wall

Principle

Sheet pile wall is built by driving a sheet piles into the ground to the required depth, the wall is created by a continuous driving of typical sheet profiles (flat, Z or similar modulus).

Construction procedure

The construction sequence is including the following steps:

- Step 1: the profile is driven in by hammering or by vibration,
- Step 2: When the maximum friction has been reached, the sheet pile advance decrease to refusal criteria. The process of driving is completed.
- Step 3: When a stroke is completed, the machine moves a step forward to repeat the same process, with another sheet pile connected in the previous one.

Control

Monitoring the verticality and refusal is the major issue.

Field of application

Sheet pile wall was one of the cheapest technology which is commonly used for dykes built of alluvial fill. The steel market makes it more expensive now. It can be used in any type of soil (natural ground or fill) into which a penetrometer can be driven. The process is not operative in heterogeneous ground with boulders or hard layers due to lack of penetration or deviation. The maximum depth is 25 m with the most powerful equipment available today.

Case studies

This method was used for strengthening the eroded core of La Saulce embankment (2005). The main reasons were quick repair and no environmental concern.

2.10 Jet Grouting Wall

Principles

Jet grouting wall consists in drilling and jetting up to 40 to 50 MPa to remove most of loose sand or weathered soil layers to set out a resistant soil mixed structure. Such a wall is somewhat irregular due to soil or rock hardness. Primary-secondary" principles can be respected as well as fresh in fresh method which consist in drilling and jetting in continuity along the diaphragm walls section.

Construction procedure

The main techniques commonly used for building the columns are:

- The monojet technique, which is using Cement jetting only (Basic parameter is Cement pressure 40 to 50 MPa)
- The Bi-jet technique, which is using Cement & air jetting (Basic parameters Cement pressure 40 to 50 MPa - Air pressure 1.2 to 2.0 MPa)
- The triple jet technique, which uses Water, Cement & air pressure (Basic parameters Water pressure 25 to 35 MPa - Cement pressure 40 to 50 MPa - Air pressure 1.2 to 2.0 MPa)

Each borehole is drilled down to the required depth, then the jet starts and the soil mix appears at low pressure at the borehole. This material composed of soil and grout mixed (spoil) is collected and stored until it is set. The jet grouting process is driven according to theoretical energy based calculations. Column diameter may vary from (0.5m to 1.80m) according to soil characteristics and jetting energy (usual data are varying in a range of 15 to 80 MJ/m). The grout mix commonly used is W/C =1 (with or without admixture upon cement quality).

Control

Verticality measurements, jet parameters and grout mix characteristics are the main items to check continuously to guarantee that columns overlap is sufficient to do a watertight cutoff.

Field of application

Jet grouting is to be considered when conventional method is not applicable (heterogeneity, soft rock and loose soil and boulders).

Cases studies

That technique was used in the Petit Saut Dam (1999) to improve the watertightness of the foundation from the top (residual soil) to the bottom (slightly weathered rock). Discharge flow was divided by two and downstream pore pressure were significantly reduced.

2.11 Pile Wall

Principle

Pile Wall consists in casting piles one next to the other in order to form a watertight wall. Such a wall is usually made of plastic concrete. The piles are built according to the same "primary-secondary" principles used for diaphragm walls.

Construction procedure

The both main techniques for building the piles in a secant pile cut-off are recall hereafter:

- Conventional technique based on slurry drilling, sometimes using a temporary tube. The piles are then concreted using a tremie pipe,
- Alternative pile construction using a large-diameter excavator (bucket up to 1.50 m or more) hydraulic or pneumatic hammer at the bottom of the drillhole, attached to a series of rods running along a powerful rail installed at the surface.

Control

The main requirement is to guarantee that two adjacent piles overlap to ensure that the wall is continuous and watertight.

Field of application

The second technique can be used to build diaphragm walls with secant piles in especially hard or abrasive ground, where the excavation methods involved in grab or hydrofraise techniques are not applicable. In this kind of exceptional case, it is wise to check that grouting would not be the most efficient and economical solution.

Cases studies

That technique was used in MONTEZIC dam (1985) to improve the watertightness of the fissured and weathered granite. No problem after repair.

Literature

- [1] Internal erosion: typology, detection and repair French Committee on Large Dam 1997
- [2] Ecran étanche de Strasbourg rétention des crues P. Bonnet Colloque Technique sur les digues du 26 novembre 2004 Comité français des Grands Barrages

Acknowledgement

The authors Thank Bachy-Soletanche for providing pictures in that paper.

Authors Name and Affiliation

Jean-Jacques Fry
EDF CIH, France
jean-jacques.fry@edf.fr

Michel Chopin
MC Consulting, France
m.chopin@mcconsulting.fr

Function Analysis and Strengthening by Adding a d/s Berm

By Maria Bartsch and Åke Nilsson

Abstract

The new Swedish dam safety guidelines require high consequence dams to safely withstand the “maximum possible leakage” that can be expected during their lifetime. Methods to assess this maximum possible leakage, as well as measures to increase the resistance for leakage are considered to be of utmost importance.

Since leakage and internal erosion is a frequent cause of failures, defensive design measures such as intercepting filters, zoning of the dam to minimise arching and good compaction have been developed during the years to protect new dams against piping. However, for existing dams lacking or with deficiencies in such features, there is commonly a need to improve the resistance for seepage in order to have capability to meet the maximum possible leakage.

Experience of leakage incidents in dams with moraine cores, as in most Swedish embankment dams, indicate that a sudden leakage usually seals itself after a short period of time. One possibility for improvement of existing dams is to construct a toe-berm of coarse material along the d/s toe of the dam. The philosophy of strengthening a dam by adding a coarse reverse filter at the toe and along the d/s slope is to provide the time necessary for self-healing. It also provides time to perform measures such as strengthening works, lowering of the reservoir or emergency actions.

In Sweden such toe-berms are designed, as a preventive measure, to improve both the erosion resistance and the stability of the embankment in the event of large leakage. By extending the toe-berm all the way up to the dam crest also local overtopping of the dam crest, due to sinkholes caused by internal erosion, can be eliminated. The principles that are currently being used for determination of the design leakage for existing dams and design of toe-berms are presented in this paper.

1 Introduction

Close after overtopping by floods, the second most frequent cause of failure of embankment dams has been internal erosion and/or leakage. Embankment dams always have some seepage due to the permeability of the core of moraine (glacial till) and the foundation. Experiences from existing dams show that sudden leaks may occur a long time after completion of a dam. The causes of the leaks have been hard to determine. However, they are commonly judged to be the result of relatively small details in the design or construction. Examples of such factors are a combination of:

too coarse segregated d/s filters due to the maximum grain size being too large in the broadly graded sandy gravel material

a moraine core compacted at a water content on the dry side of Proctor optimum and low compaction rate adjacent to concrete structures and sheet pile walls, with resulting loose horizontal layers, arching and hydraulic fracturing of the core.

In order to compensate for deficiencies in existing dams with moraine core and broadly graded d/s filters the Swedish dam safety guidelines require that high consequence dams should withstand the “maximum possible leakage” that can be expected during their lifetime.

The maximum possible leakage is considered to be unique for each dam, and methods to assess this maximum leakage, as well as measures to increase the resistance for leakage, are considered to be of utmost importance. This paper describes the procedure in the Swedish guidelines for determining the design leakage for existing embankment dams with moraine cores, and outlines the considerations for design of stabilising toe berms. During the last couple of years a large number of dams in Sweden have been upgraded with a stabilising berm, zoned as a reverse filter, along the d/s slope. The berms are considered as preventive measures improving the ability of the dam to safely pass large leakage.

For dams, which have experienced deficiencies in the core, it also has to be considered to improve the sealing element of the dam, and thus reduces the potential for occurrence of large leakage (**Figure 1**). There are several potential means to improve the water tightness, for example remediation by adding a slurry trench, sheet pile walls, jet grouting etc. In some cases retrofitting of filters and drains have been used. Further discussion on such measures directed towards improvement of the sealing element and filters have been outside the scope of this paper.

2 Experiences of Leakage and Internal Erosion in Swedish Dams

Swedish experiences of leakage, internal erosion and sinkholes based on a survey which has been conducted on large embankment dams, shows that most of the observed sinkholes and leakage cases reported in the survey are assumed to have been caused by internal erosion within the impervious core [1] and [2]. The survey comprised 35 incidents related to leakage, but there were no failure cases. In general the incidents occurred many years after the first filling of the reservoir. Still, in many cases an evaluation has been made that the causes of this type of deterioration can be related to inadequate design or construction procedures of the filter d/s of the impervious core. E.g. experience shows that settlements, sinkholes and leakage have often occurred at the junction between an embankment dam and concrete structures. Contributing factors are:

- Difficulties to use heavy compaction equipment close to the concrete structure
- The core material has often been compacted at a lower water content, drier than Proctor optimum, to facilitate compaction with hand held compaction equipment
- The low water content results in larger saturation settlement upon the first filling, and may lead to arching and low stress zones at the contact to concrete structures and sheet pile walls, which increases the potential for hydraulic fracturing.

An inventory of the gradation of d/s filters of earth or rock-fill dams with an impervious central core of moraine shows that most of the filters do not fulfil the current filter criteria. Important factors are:

- The grain size D15 in several dams does not meet modern criteria for fine filters down stream of moraine cores, where $D15 \leq 0.7$ mm is one of the present criteria.
- The maximum grain size has not been limited to the preferable 20-25 mm, but is often in the order of 60 mm or larger, which means that the broadly graded filter material has been sensitive for stone segregation during handling and construction.

It is assumed that the deterioration in most cases could have been avoided if all the filters in the drainage arrangements d/s from the core (d/s filters, filter blankets, toe drains, etc.) had been properly graded in accordance with the current filter criteria. The susceptibility for internal erosion caused by the filter gradation in Swedish dams has been evaluated and a clear correlation exists [3]. However, there is with the present knowledge not possible to rule out the possibility of internal erosion in any of the dams. Therefore, in the present guidelines all high consequence dams are in principle considered to be susceptible to internal erosion.

For most existing dams it is neither practically nor economically achievable to replace these coarse filters with new filters meeting the modern requirements. After reported incidents surveillance has been increased in most cases, by more frequent inspections and/or additional monitoring. Grouting of core and foundation has been used at several dams after incidents with sinkholes and muddy leakages. The primary intent of the grouting has been to stop the leakage. An additional potential benefit is increased compaction and increased stresses within the core material, which results from the grouting process itself. In one case a diaphragm wall of plastic concrete was constructed in the centre of the impervious core. Construction of a berm along the d/s damtoe has also been used after incidents in order to increase the stability and the erosion resistance.

Initiating root causes of leakage and resulting failure mechanisms caused by through flow are illustrated in Figure 1, together with possibilities to intervene in the different phases of a leakage scenario. Governing factors for initiation, continuation and progression of a leakage scenario, and methods for estimating the potential for failure of embankment dams by internal erosion and piping are described by Fell et al (2004) [4].

International experiences of historical dam failures due to leakage and internal erosion indicate that the failure cases have been embankments dams with the d/s shoulder founded on natural soil. Rock-fill dams founded on rock have knowingly not been among the reported failure cases. However, the shoulder material used in Swedish rock-fill dams commonly originate from blasting of underground caverns and tunnels. The resulting rock-fill can have a relatively fine grading curve with resemblance to earth-fill.

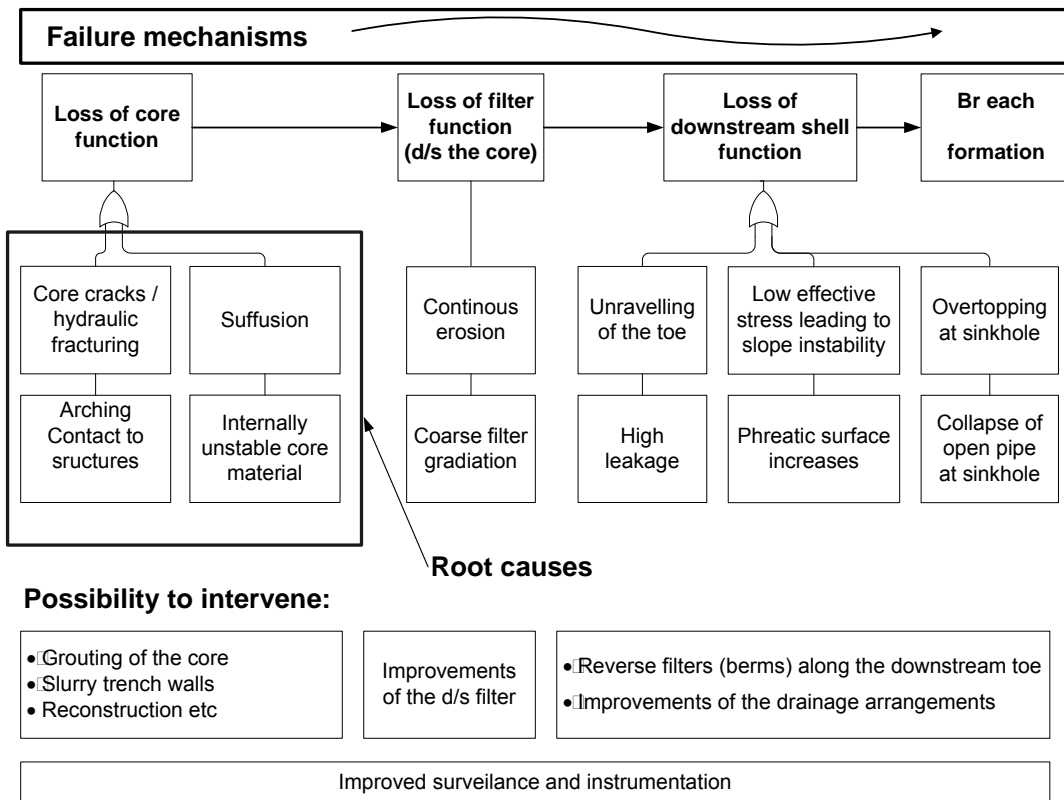


Figure 1: Failure mechanisms caused by through-flow and possibilities to intervene in different phases. Modified from [5].

In the Swedish guidelines (RIDAS 2002), it is required that the maximum possible leakage that may occur during its life time should be determined for high consequence dams, and it should be safeguarded that they can meet this design leakage. This refers to both existing and new high hazard dams. Corresponding measures including increased surveillance and stabilising measures should also be considered for existing dams with smaller failure consequences, where the described deficiencies in the filter and core have showed up e.g. by sinkholes or leakage incidents.

The purpose of increased surveillance and stabilising berms are to provide an early warning and make sure the dam can safely withstand a potential leakage scenario sufficiently long to provide time for self healing and/or emergency measures. In this way, the increased probability for initiation of a concentrated leakage and internal erosion is compensated for, by minimising the effect of a potential leakage incident. This philosophy has lead to that several major embankment dams are currently being upgraded by adding coarse toe berms along the downstream shoulder.

The application guide regarding determination of the design leakage and design of toe berms were updated in 2004, and is summarised below. Also, recent findings from large scale through flow tests in the field and in laboratory in Norway [6] are described and are proposed in principle to be used for revision of the Swedish guidelines.

3 Failure Modes Initiated by Leakage

The Swedish guidelines prescribe that high consequence dams should be designed to have sufficient drainage capacity and erosion resistance to withstand potential failure modes related to leakage, and possible associated internal erosion, as illustrated in Figure 2. The main failure mode is leakage followed by slope unravelling or scouring at the d/s toe (pathway no. 1). The risk for failure induced by leakage has usually been assessed assuming that the discharge flow, toe-stone size and slope angles are the governing factors [6].

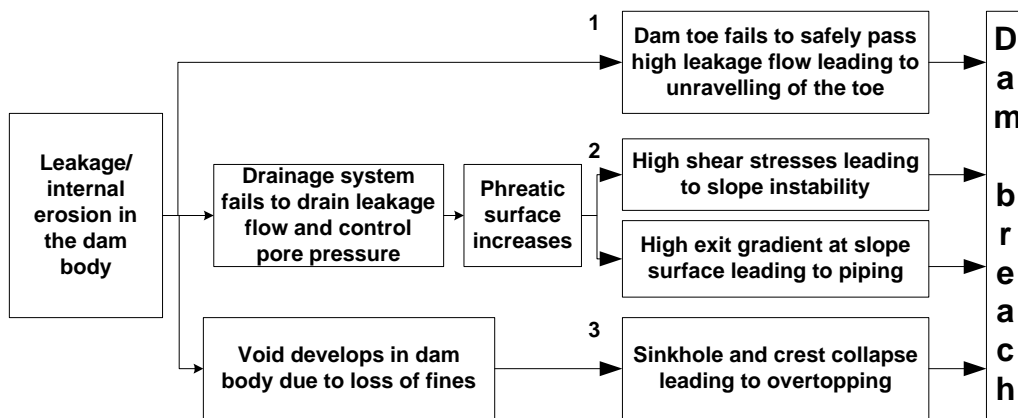


Figure 2: Failure scenarios initiated by leakage/internal erosion in the dam body

Mass sliding is another potential failure mode, where the friction angle, the slope angle and the pore pressure distribution are the governing factors. If the drainage system fails to drain the leakage and control the pore pressure, the phreatic surface will increase in the d/s shell (pathway no. 2). Leakage may spring from the d/s slope causing local stability problems (or piping) close to the point of leakage. With time further slides may progress backwards and cause overall instability and overtopping following settlement of the crest. One possible means to prevent such stability problems in existing dams is to construct a stabilising toe-berm of coarse material along the d/s toe of the dam. The gradation of the fill material of the toe-berm should be coarse enough to permit safe passage of maximum possible leakage and prevent scouring at the down stream toe.

A third possibility is that of wash-out of fines resulting in cavities in the dam body. The collapse of such a cavity may lead to sinkholes causing the crest to collapse and overtopping (pathway no. 3). This failure mode should be considered particularly for dams with a small free board and/or a narrow crest. A possible measure to decrease the vulnerability to this failure scenario is to extent a stabilising toe-berm to cover the d/s slope of the dam all the way up to the crest of the dam. Thereby the crest will be wider and overtopping of the crest is prevented in the event of a major sinkhole in the area of the core.

4 Design Considerations for Existing Dams

4.1 Design Leakage

There is always seepage through a dam and its foundation. Experiences show that sudden leakage incidents can occur also long time after the first filling of the reservoir. The Swedish guidelines have introduced the concept of "design leakage". The design leakage refers to the largest possible through flow, related to internal erosion, that may occur through the foundation, core or filter zone above the core, under the lifetime of a dam. Guidance on how the design leakage can be assessed for dams with a moraine core is given below.

For earth-fill dams the design leakage can be assessed in a very conservative manner by the assumption that the shoulder material determines the leakage rate. Thus the fines in the core material are assumed to have been lost by internal erosion and transported through possible filters and through the materials in the shoulders. The calculation is done without regard of the permeability of the core material. The permeability of the filter zone may also be disregarded, if the filter is narrow or if it may be eroded into the shoulder material in the event of severe leakage. In the most conservative case both the core and the filters are assumed to be damaged by internal erosion to such a degree that the dam is assumed to be homogeneous and with the same permeability as the material in the shoulders (**Figure 3**).

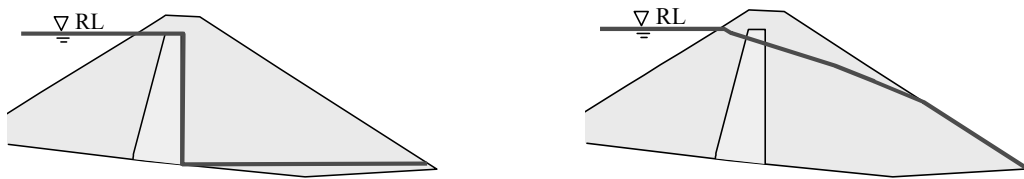


Figure 3: Normal ground water pressure (left) and assumed water pressure at design leakage (right)

This assumption on homogeneous permeability may also be applicable for rock fill dams with shoulder material with a large content of fines. For example if d_{10} , that to a large degree determines the permeability of the material, is of similar grain size as for an earth fill dam with gravel shoulders. The flow may be either laminar or turbulent, or a combination of the two. The through flow is estimated by a flow net or finite element analysis (e.g. using SEEP/w or similar) and determination of the hydraulic conductivity of the shoulder material from its grain size distribution. A 2-dimensional calculation may be sufficient, but the possibility for 3-dimensional effects, such as concentrated outflow due to the shape of the valley and the layout of the dam structure, has to be addressed.

For rock fill dams the flow can be turbulent, and the design leakage must also be assessed from case to case. For high dams a total design leakage of $5 \text{ m}^3/\text{s}$, or a flow per meter of $0.5 \text{ m}^3/\text{s}$, is expected to give a considerable increase of the time available for self-healing if a large quantity of leakage would occur due to internal erosion. However, for many Swedish rock fill dams a smaller design leakage can be justified since the shoulders usually consist of fairly fine-grained

rock-fill originating from required excavations of tunnels and underground power stations. In such cases, the above indicated very conservative assumption that the shoulder material governs the flow could still be used. In many cases this results in practical sizes for the material in a berm along the toe.

The Swedish guidelines have adopted Eq. (1) for the permeability for turbulent flow [7].

$$k_t = \frac{1.7 \cdot d_{10} \cdot g \cdot n^3}{\beta_\circ \cdot (1-n)} \quad (1)$$

where:

k_t = turbulent permeability, cm^2/s^2

β_\circ = grain form coefficient, (3,6 for crushed rock)

d_{10} = grain size for the 10 % passing material, ($1.7 \cdot d_{10}$ = dominant grain size)

n = porosity (assessed to 0.3)

g = gravity acceleration (assumed to 9.81 m/s^2)

The turbulent permeability is used to calculate the velocity (v) by Eq. (2). The velocity, and thus the design leakage (q), through the assumed homogeneous dam is assessed from the gradient (i) from a flow net, which is assumed to be similar to that for laminar flow conditions. A_{mean} is the mean through flow area for the leakage, where the mean height can commonly be assumed to be $2/3 H$, where H is the height of the dam.

$$v^2 = k_t \cdot i \quad q = v \cdot A_{mean} \quad (2)$$

When the flow velocity has been calculated Reynolds number should be determined in order to verify the flow conditions. When Reynolds number is greater than 600 the flow condition can be assumed to be fully turbulent. When Reynolds number is smaller than 1 or 2 the flow is assumed to be fully laminar. It is always conservative to assume turbulent flow. For values of Reynolds number that is in the lower range say below 100 an interpolation can be justified, where a corrected permeability coefficient is used [7].

4.2 Discussion on the Order of Magnitude of the Design Leakage

Some guidance on the order of magnitude of the potential leakage flow in a rock fill dam is given from historical incidents. At the Suorva dam in the Lule River it is known that leakage in the order of 200 l/s has occurred. Experiences from a few leakage incidents in Norway reports leakage rates of the same magnitude. At the Bullileo Dam in Chile there are reports of leakage that under longer periods of time were in the order of $1 \text{ m}^3/\text{s}$ and experienced short term peaks of up to $8 \text{ m}^3/\text{s}$. At this dam there were no filter between the sealing layer and the rock fill shoulder.

Rock-fill dams has a capacity to withstand large leakages, at least of the down stream shoulder in founded on rock. However, in many cases it has to be noted that rock fill from tunnelling work etc is used as he shoulder material, which means that the rock fill contains a lot of fines and may have a similar permeability as an earth fill. This is the case for several Swedish rock fill

dams. In order to determine the gradation curve of the shoulder material it is often practical to dig test pits at the down stream toe (**Figure 4**).



Figure 4: Test pit at the down stream toe at a typical rock fill dam. Determination of content of material 0-60, 60-120, 120-200 and > 200 mm in the field.

The height and layout of a dam will have great influence on the rate of the design leakage. The design leakage for a typical earth-fill dam, 30 m high or lower, on a horizontal foundation may normally be in the order of one or a few hundred l/s. Higher rock-fill dams may be designed for a total leakage flow of a few m³/s, with the above mentioned experience of historical incidents as a basis. Rock-fill dams that are designed for a design leakage of 0.5 m³/s/m or a total leakage of 5 m³/s can be assumed to remain stable under a long time from the initiation of the leakage. If the geometry of the site may result in concentration of the outflow of the dam toe, then this higher leakage per meter along the dam axis should be used in the design.

5 Vulnerability to Leakage Failure Modes and Design of Toe Berms

Guidance on estimation of the ability to resist design leakage is given below, together with possible measures for upgrading.

5.1 Stability

Determination of the safety factor for stability of existing dams may require field investigations as uncertainty in the input parameters (primarily the internal friction angle and pore water pressures) can have great influence on the results. An increase in the pore water pressures will reduce the factor of safety, and the safety factor during design leakage should be at least 1.1. Another possibility where material parameters are uncertain is to calculate the relative change in the safety factor that additional loads, such as an increase in pore water pressure, would result in. Stabilising measures should then be designed to compensate for the additional loads with a margin. Experiences from operation and measurements of displacements over the years should also be taken into consideration.

5.2 Drainage Capacity

The down stream shoulder should have sufficient erosion resistance to withstand through flow of the design leakage. This is to a large extent dependent on the design and material (stone

size) at the downstream toe. Also, the geometry of the valley will influence the rate of the outflow at different points of the dam toe, as well as the rate of flow along the dam toe. Where the leakage may be concentrated to certain exit points, or flow along the toe at steep abutments, the situation has to be investigated and the stone size and the design has to be adjusted to the existing foundation.

5.3 Sinkholes in the Dam Crest

For breach to occur by sinkhole development (due to collapse of an open erosion pipe through the core), the sinkhole would need to be sufficiently large to settle the crest to close to or below reservoir level. The enlargement of the sinkhole is normally a slow process, whereas the breach formation after initiation of overtopping can be expected to be rapid. Some factors influencing the likelihood of overtopping at a large sinkhole is given in Table 1 [4]. Further factors influencing the risk of breaching due to the overtopping if the overtopping height will be small are the type of material in the down stream zone (loose fine material – coarse free draining rock fill), down stream slope inclination (steeper than 1V:1.4 H – flatter than 1V: 1.75 H).

Table 1: Factors influencing risk of overtopping at sinkhole (adopted from [4])

Factor	More likely	Neutral	Less likely
Freeboard at the time of the incident	< 2 m	~ 3 m	> 4 m
Width of crest	< 4 m	~ 6 m	> 9 m

5.4 Design of the Downstream Stabilising Berm

Toe berms will improve the drainage capacity and stability of an existing dam, and thus to some extent compensate for potential deficiencies in existing dams in the core and filter that may result from older design standards. However, it is important to stress that the potential for initiation of a leakage scenario is not reduced (**Figure 1**). The berm along the dam toe is designed according to the following principles:

- Stones with sufficient size to withstand design outflow are placed along the toe of the d/s slope at the contact to the foundation
- The d/s slope should have a sufficiently gentle slope, or be stabilised with coarse berm material, so that sliding will not occur if design leakage results in high pore pressures in the shoulder material.

The material gradation of the material in the berm is selected to have the required erosion resistance. The relationship between a stable stone size D in a granular fill material, flow per meter q , and slope inclination γ , has been described by [7] and that relationship Eq. (3) is at present adopted in the present Swedish Dam Safety Guidelines.

$$D = 1,5 \cdot q^{2/3} \cdot (\sin \gamma)^{7/9} \quad (3)$$

where:

D = Stone size D_{50} , m

q = Flow m^3/s , m

γ = Slope inclination, deg.

According to recent comprehensive laboratory and field tests in Norway [8] the above relationship by Solvik, based on small scale laboratory tests, is found to be very conservative. From recent field tests the relationship according to Eq. (4) is recommended to be applied to determine the D_{50} size in the lower part of the d/s berm. The relationship includes a load factor of minimum 1.5. This gives a margin to failure or collapse in the rock-fill (damages are accepted but no failures) and a margin to the uncertainty in the estimation of the unit flow.

$$D_{50\ dim} = 0.60 \cdot S_0^{0.43} \cdot q^{0.78} \quad (4)$$

where

$D_{50\ dim}$ = rock size in metres (load factor 1.5)

S_0 = down stream slope of rock fill (1V: S_0 H)

q = unit discharge in m^3/s , m

The size according to Eq. (4) is conservative when used also for higher elevations of the berm. The required D_{50} for material at the toe according to Eq. (3) and (4) are compared in Figure 5. The diagram is for a d/s slope inclination 1V:1.5H and horizontal foundation.

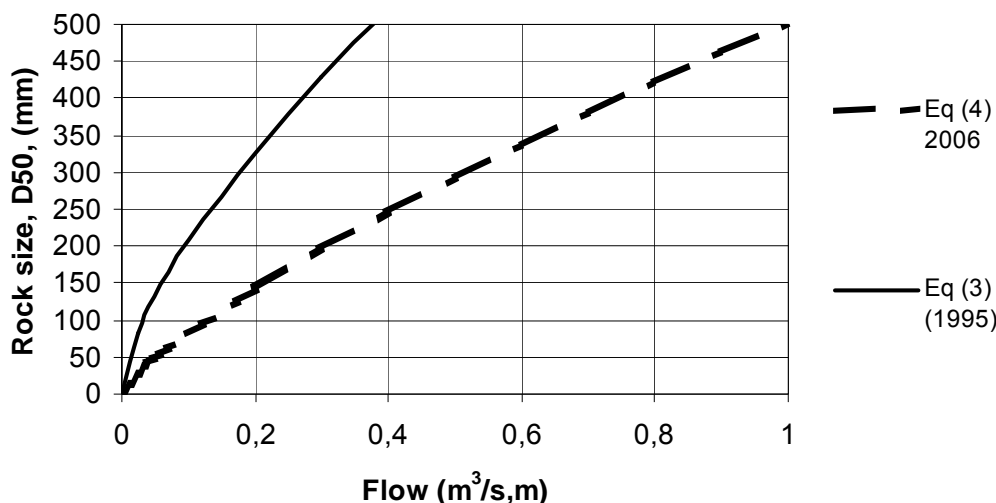


Figure 5: Rock size in relations to through flow for a d/s slope 1V:1.5H. Recommended size according to Eq (4) compared to earlier applied size according to Eq (3).

The height of the berm is designed with marginal to protect a possible exit point of the phreatic surface (**Figure 6**). The potential for having a larger hydraulic conductivity in the horizontal direction than in the vertical direction should be taken into consideration in order not to underestimate the level for the phreatic surface and the exit point.

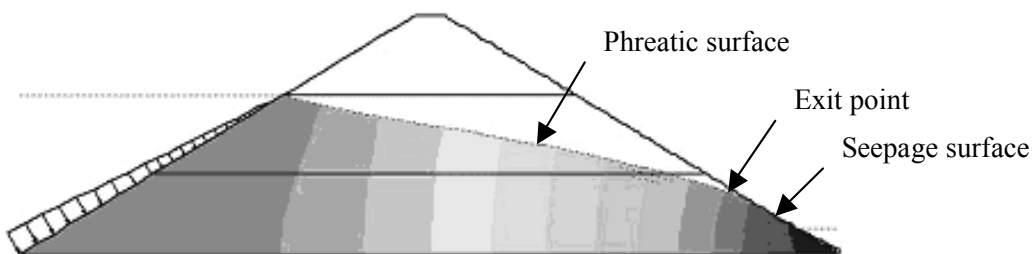


Figure 6: Determination of exit point and required height of the berm

The thicknesses of the rock-fill and possible transition layer in the berm are designed using ordinary geotechnical stability analyses with slip surfaces governed by assumed friction angles together with the phreatic line shown above. However, in many cases the analysis methods show that a fairly thin berm is required to achieve stability; in these cases the actual thicknesses are determined based on practical requirements involved in placement of these materials. If it is considered necessary to protect against overtopping at potential sinkhole in the crest the berm could be extended along the whole d/s slope all the way up to the crest.

A recent example of the design and construction of a toe berm is given in Figure 7-10.

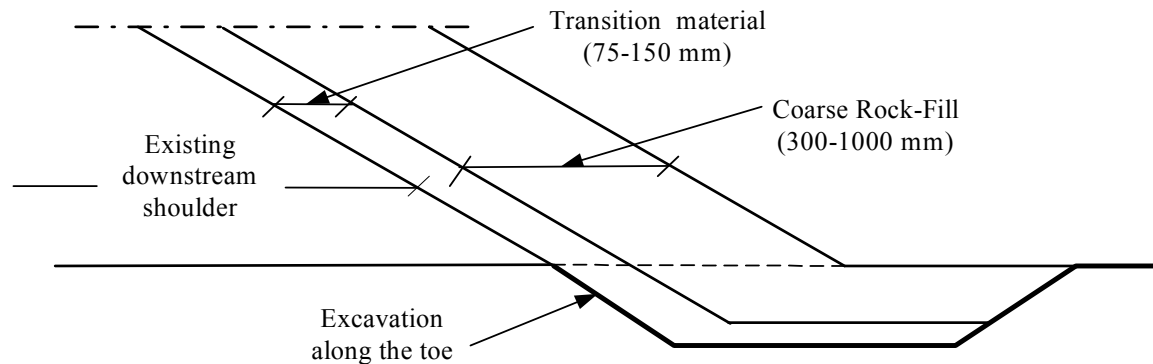


Figure 7: Foundation of toe berm at existing fine-grained rock fill shoulder founded on soil.

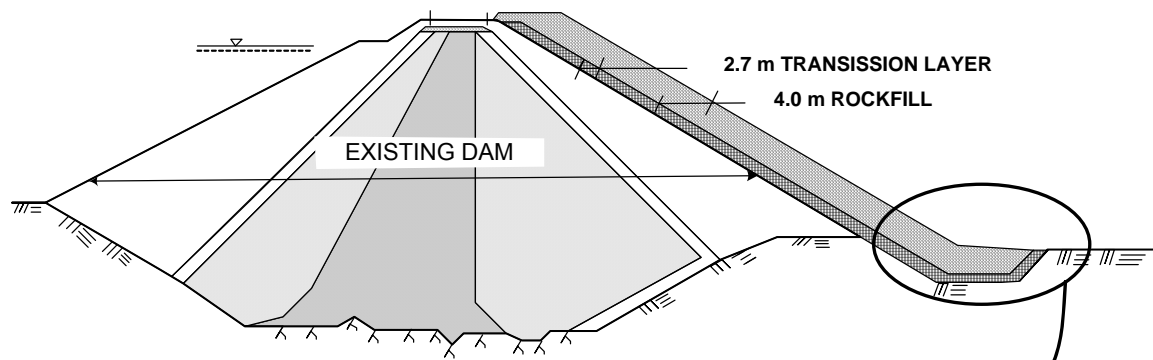


Figure 8: Example where the toe-berm has been extended up to the crest



Figure 9: Foundation of the toe-berm



Figure 10: Construction of the berm half way up to the crest of the dam

Literature

- [1] Bartsch, M. (1995): Safety Analysis of Swedish Dams – Dam Performance and incident Data Analysis, Licentiate Thesis, Division of Hydraulic Engineering, Royal Institute of Technology.
- [2] Norstedt, U.; Nilsson, Å. (1997): "Internal erosion and ageing in some of the Swedish earth and rock fill dams". ICOLD, Q73, R20, Florence 1997.
- [3] Nilsson, Å.; Norstedt, U. (2004b): Reverse filters on the d/s slope to compensate for coarse graded filters in Swedish dams. Canadian Dam Association 2004 Conference. The Canadian Dam Association, Ottawa, 2004.
- [4] Fell, R. et al. (2004): Methods for estimating the probability of failure of embankment dams by internal erosion and piping – piping through the embankment. UNICIV report No. R-428.
- [5] Nilsson, Å.; Rönnqvist, H. (2004a): Measures to strengthening embankment dams in order to stop or control a possible through-flow process. International Seminar, Stability and Breaching of Embankment Dams, Oslo, Norway.

- [6] Bartsch, M.; Nilsson, Å. (2004): Leakage Through Embankment Dams. Failure Modes and Design of Toe-Berms, ICOLD Seoul, Korea
- [7] Solvik, Ø. (1995): Stenfyllningsdammars stabilitet vid genomströmning, VASO Dam Committee, Report No.17.
- [8] EBL (2006): Stability and breaching of embankment dams. Report on Sub-project 2. Stability of downstream shell and dam toe during large through-flow. Publication nr: 186-2005 EBL Kompetense AS. Revised January 2006.

Authors Name and Affiliation

Maria Bartsch
Principal Engineer, Dr. Eng. (CE)
Vattenfall Power Consultant AB, Sweden
maria.bartsch@vattenfall.com

Åke Nilsson
Manager Dam Safety Department, M. Sc. (CE)
Vattenfall Power Consultant AB, Sweden
ake.nilsson@vattenfall.com

Active and Passive Defences against Internal Erosion

By Olivier Artières, Stéphane Bonelli, Jean-Paul Fabre, Cyril Guidoux, Krzysztof Radzicki, Paul Royet, Christophe Vedrenne

Abstract

A reliable early localization and warning system for both gradual and catastrophic dam and dike failure is being developed. This monitoring system is based on the combination of geosynthetic functions, integrated fibre optic sensors and a related instrumentation to detect the first steps of internal erosion processes and hydraulic works instability. The detection of the leaks, early stage of the internal erosion process, is assessed through temperature changes measurement using the passive method without heating. The HydroDetect system has been tested on several 1:1 scale experimental works and real dikes in-use. The results from 2 of them are very promising.

1 Improved Hydraulic Structure Safety

Owners of dams and dikes are managing a wide number of works with a large variety of ages and stages. The problem facing the dike owner today is to limit the impact of this aging phenomenon and the most serious task is to eliminate the risk of failure and repair costs. In the last decade a large number of dam and dike failures occurred, causing several hundreds of billions of Euros in damages.

For this purpose, a technical solution that detects and localizes malfunctions (erosion, blocking, breaches, sliding, settlements), which are the precursors of failure was developed.

2 Seepage Detection by Thermometry in Unsaturated Dikes

Fibre optic distributed measurements now make it possible to measure temperatures and deformations over lengths of up to 30 km (Selker, 2006). The two following methods are based on temperature measurements and are used for seepage detection (see chapter 6 of this document).

The active method (or heat-pulse method) is used for determining the saturation level and the rate of flow of the fluids in the structure with high accuracy (Perzlmaier, 2006). However, the use of this method implies the consumption of between 3 and 10 W/m power for seepage detection and the estimated seepage flow rate, respectively.

The passive method (or gradient method) also allows a seepage location to be detected and the flow to be measured, and without heating the fibre. But this method is based on the hypothesis that the fibre has to be in the groundwater and that the effect of the air temperature on it is negligible (Johansson, 1997).

There is a shortcoming in the case of the gradient method (because they are more economical or able to supply the necessary heating power) performed on dry dikes and also to take

advantage of the reinforcement (refilling) works to instrument a structure. In this case, the fibre can be outside the groundwater and near the surface, with an influence of air temperature on that of the fibre, meaning a need for suitable analyses. For the instrumentation of a structure during reinforcement, the advantage of coupling a distributed measurement system with the geotextile used, as already done for deformation measurement in civil engineering structures, becomes obvious

3 The HydroDetect system.

The purpose of the Eureka E!3361 SafeDike project is to develop a technical solution which is a practical answer to the problems of dike owners, who have to manage the risk of failure of their work, either due to internal erosion or due to overall instability.

Concerning internal erosion, the first defence level for a hydraulic work is the use of a filtration system which stabilizes the soil particles of the dike body. The purpose of the HydroDetect system is to combine this first classical level made of a geotextile filter with a second monitoring level with optical fiber sensors increasing the global level of safety by early detection of leaks for instance.

HydroDetect is a full system which includes both the hardware (product, sensors, instrumentation) and the related software based on the data analysis methodology described hereafter.

The partners of this project are: Cemagref, Cetmef, EDF, FOS&S, Grenoble University and TenCate Geosynthetics.

4 Associated Analysis Methods (of Outside Groundwater)

The principles

In theory, there are many environmental variables: Outside temperatures (air, water), radiative effects, wind, precipitation. When the fibre is placed in a saturated zone, the Johannson approach can be generalized by integrating these variables to detect and quantify a rate of seepage. Conversely, when the fibre is based in an unsaturated zone (outside the groundwater during normal operation), because of the influence of the hydric condition of the ground, evaluating a seepage rate is now an open question. However, we are going to demonstrate that detection is possible.

We have used two methods of analysis. The first (STa) is derived from the HST Thermic method (PENOT, 2003), developed to explain that the movement of arch dams under the effect of phenomena like hydrostatic effects, time and effects related to temperature. The STa model informs us that some physical parameters, especially the delay times of OF measurements compared to those made in the air, may be linked with the presence of seepage. When flow variations appear, statistical parameters like the residuals (differences between measurements and model) or the sum square errors (SSE) can also be seepage detection and quantification parameters.

The second method is the Impulse Response Function Analysis (IRFA). This model has been designed to simulate the pore pressures measured in and around dams, which are influenced

by the reservoir and rainfall levels (Bonelli and Radzicki, 2007), or to simulate temperature measured in dams as a function of air and water temperature (Bonelli and Felix, 2001). This is a two-parameters analysis. The first parameter, α (dimensionless), characterizes the damping. The second parameter, η , is a characteristic diffusion time: the system has some memory of the previous values of the loading time series. The role of this parameter is given by harmonic analysis: if the input is $\sin(\omega t)$, the output will be $\alpha \sin(\omega(t-\eta))$, under slowly varying loading conditions ($(\omega\eta)^2 \ll 1$). The characteristic time η quantifies the time elapsing between the onset of the loading and the response.

5 Experimental Sites

5.1 Oraison

The Oraison canal was built between 1959 and 1962; its main characteristics are as follows:

- Maximum height on natural ground: 27 m – Length: 21,430 m
- Coating: Sealed of un-reinforced concrete (redone in asphalt concrete in some areas).
- Volume of materials: 5,400,000 m³ excavation, 6,300,000 m³ backfill
- Foundation land: Valensole pudding on the left bank and forming an embankment, Durance alluvial matter containing pudding lenses and marl passages with a high void index on the right bank



Figure 1: Aerial view of Oraison canal

- In 2002, the optical fibre was buried at the toe of the dike over a length of 2300 m upstream of the plant, and to a depth of 0.80 m.
- Over the first 1000 m, the optical fibre is in a low location at the foot of the dike near the counter canal. After 1000 m, the optical fibre is in a high location on the shoulder of the dike (**Figure 2**).

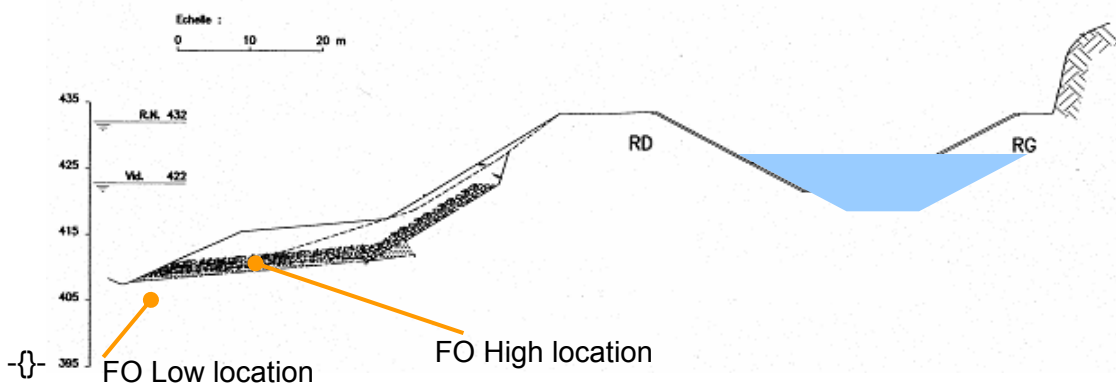


Figure 2: Sectional view of dike

5.2 Aix-en-Provence Experimental Basin

To test and validate the Hydrodetect system, as well as other equipment and methods dedicated to detecting and quantifying leaks from a real structure, an experimental basin was built during the second quarter of 2006 on the Cemagref site in Aix-en-Provence, France (Guidoux, 2007).

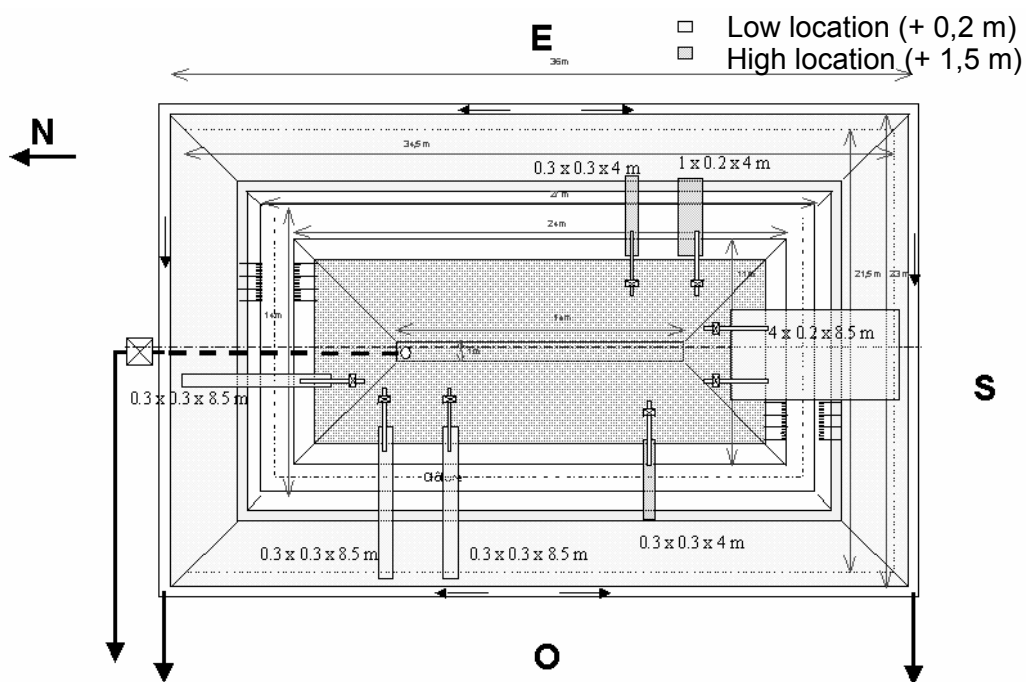


Figure 3: View of experimental basin

The main characteristics of the experimental basin (**Figure 3**) are as follows:

- Volume of materials: Approximately 1200 m^3 of clayey materials (permeability at saturation of 10^{-11} m/s) for the dikes, approximately 225 m^3 for refilling.
- Perimeter: 118 m at the foot, 78 m at the head.
- Coating: None (for the data investigated here; a geo-membrane was installed subsequently in December 2006)
- Approximate water volume: 200 m^3

Among the various materials, a device (associated with a geotextile) for measurements of temperature distributed along an optical fibre (OF) was tested. This device consists of an OF arranged on a geotextile having three levels (referred to as T2, M2 and B2, respectively for top, middle and bottom) along the downstream embankment. The geotextile and the OF retained by a refill (**Figure 4**).

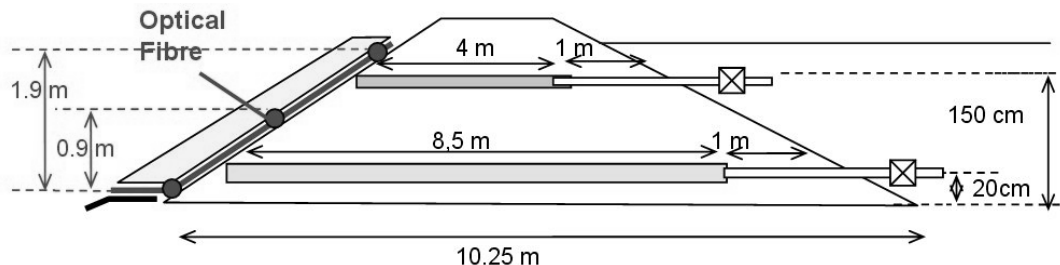


Figure 4: Sectional view of one face of basin

There are several devices situated at two different heights: Between OFs T2 and M2 and between OFs M2 and B2, fitted to the structure. These comprise geotextile envelopes filled with sand and connected on the upstream side by a PVC tube terminating in a valve designed for qualitative and quantitative control of seepage (**Figure 4**). This provides a maximum flow rate of approximately 10 l/min.

6 Results Obtained

6.1 Oraison: Case of Abrupt Leakage

From of the canal air and water temperature data, FE modeling was carried out to represent the temperature measured at the OF. This modeling reveals good correlation between the results of the model and the measured values (using the hypothesis of zero flow through the model). These simulations were reproduced for various flow rates (1, 10 and 100 l/min/m). The data analysis model was tested on these modeling results.

The first graph (**Figure 5**) illustrates a case without leakage and we see that the level of the residuals values is low (< 0.3 °C) and stable in the course of time.

The second graph (**Figure 6**) illustrates this case with the appearance of leakage of 1 l/min/m during the second year of measurement. We also see a definite increase in the residuals values (> 1.5°C).

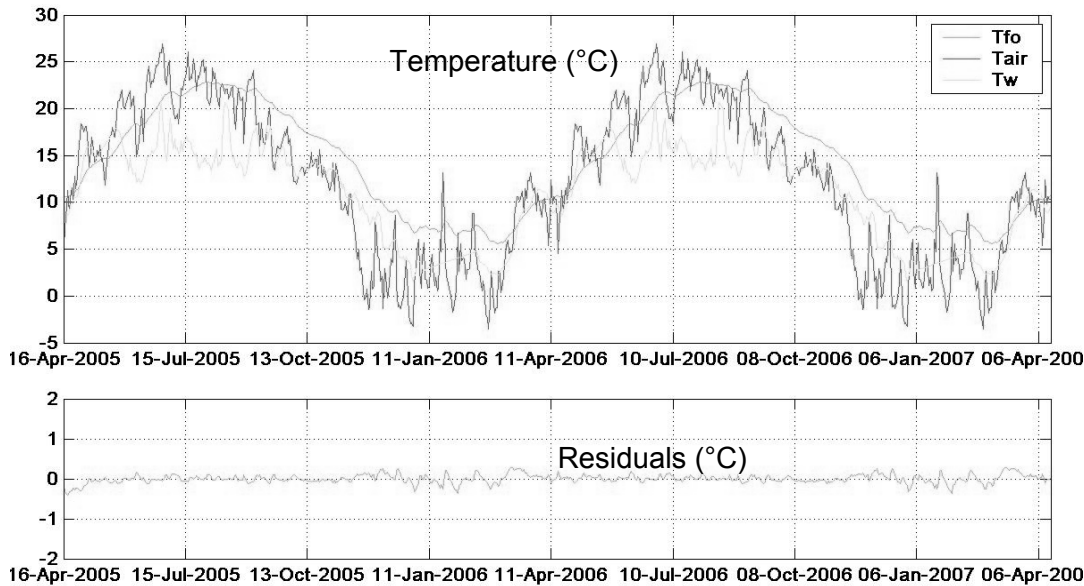


Figure 5: Results of modeling and analysis – Case without leakage

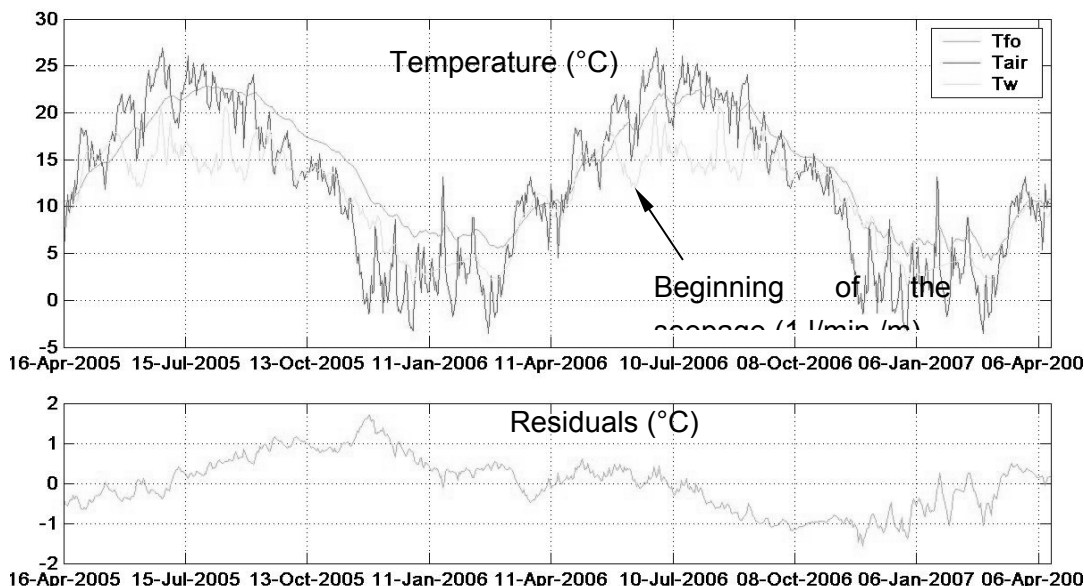


Figure 6: Results of modeling and analysis – Case with leakage

Similar tests were performed for flow rates of 10 l/min/m and 100 l/min/m. For each result, the sum square error (SSE) was calculated and we see that there is apparently a relationship between the SSE and the leakage flow rates (when a leak appears) (**Figure 7**).

$$SSE = \sum_{i=1}^n \varepsilon_i^2 \quad (1)$$

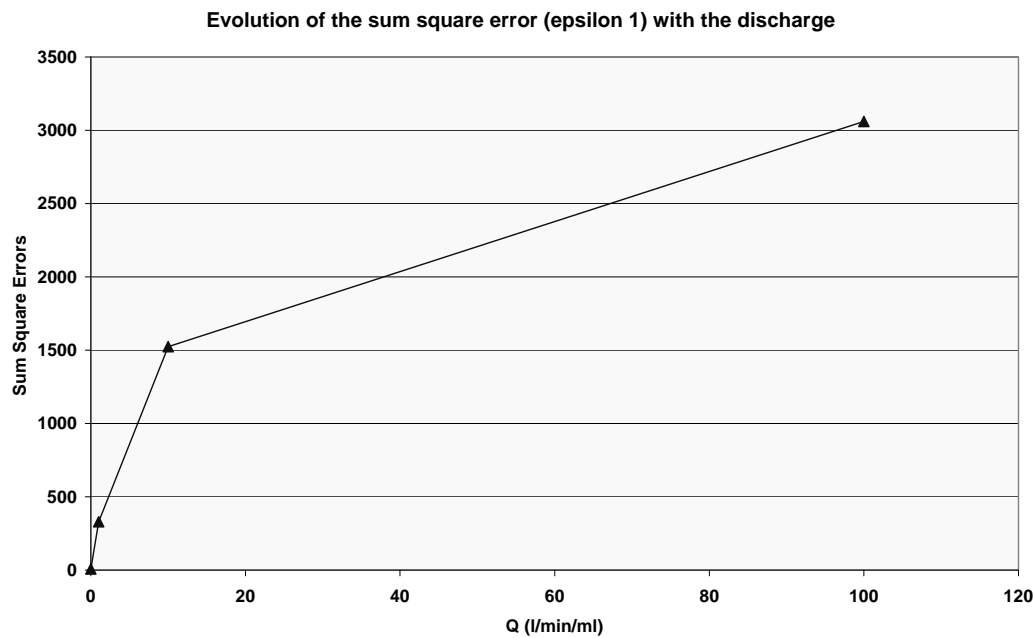


Figure 7: evolution of SSE according to leak flow rate

6.2 Aix-en-Provence Experimental Basin Diffuse Leaks

Experiments in the Aix-en-Provence basin, situated on the CEMAGREF site, made it possible to test the detection method on a real site.

We applied the method to the data measured on the West face between September and November of 2006 (**Figure 8**). There are three leakage devices on this face. The first is above OF M2 (leaks visible on OF M2 and B2 of figure 9) and the other two between the OFs M2 and B2.

Leak detection is possible from analysis of the residuals and the sum square error (SSE) (cf. **figure 9**).

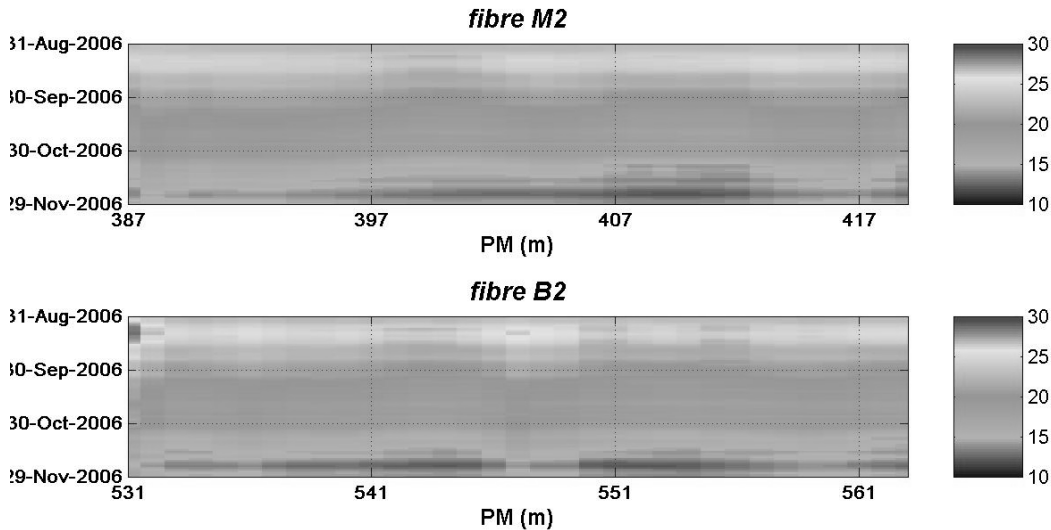


Figure 8: Evolution of temperatures measured along the OF – West Face

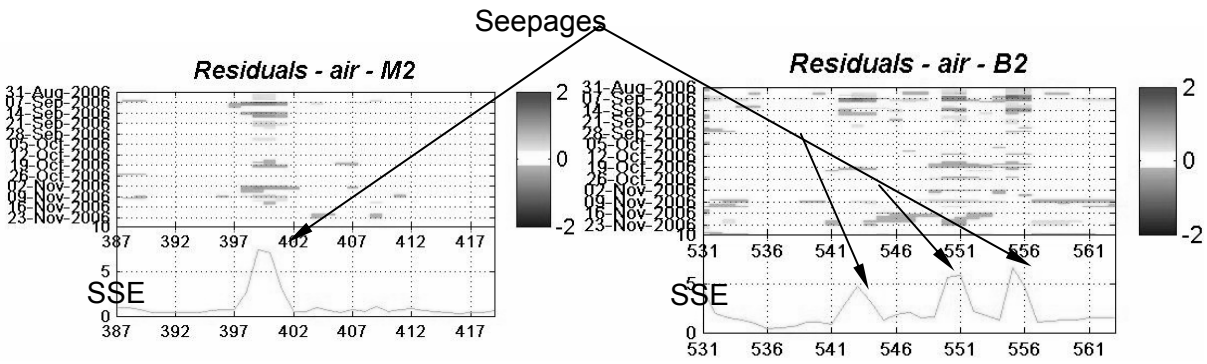


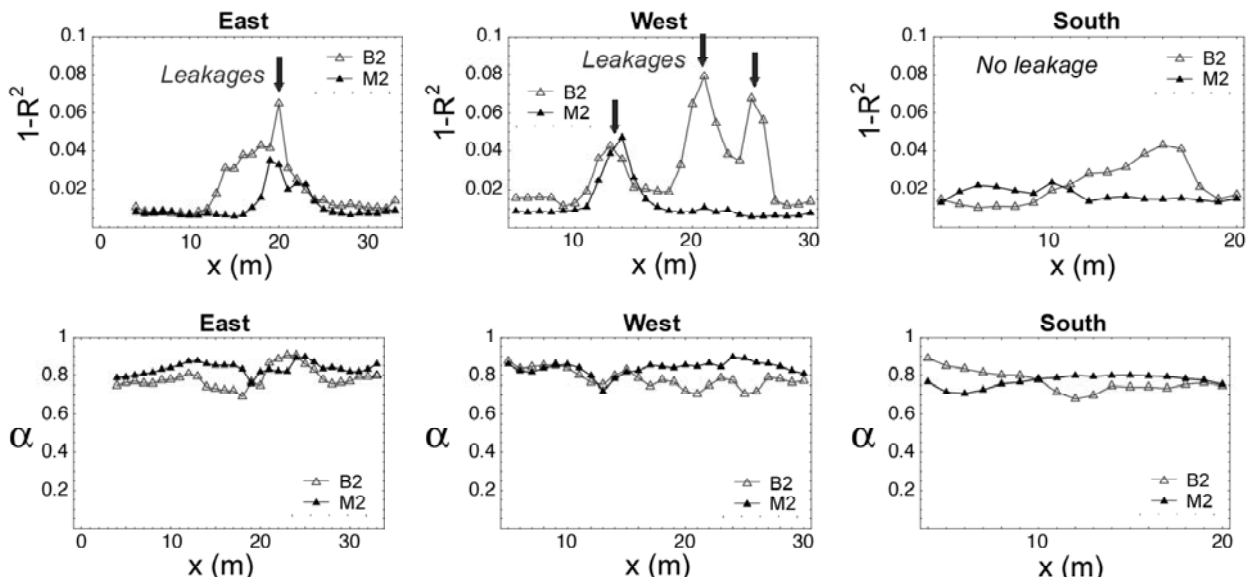
Figure 9: Residue after analysis and SSE – West Face

The Impulse Response Function Analysis (IRFA) has been applied in two steps. Firstly, the three OF temperature measurement has been expressed a delayed response of the air temperature. For conciseness, results are not detailed. The delay η is about 15 days for B2 and M2, and 5 days for T2.

Secondly, B2 and M2 has been expressed a delayed response of T2. This technique has several advantages: 1) the air temperature is not necessary, 2) the top temperature is here considered as an explanatory variable, accounting for all the complexity of the system (air convection, radiation, inhomogeneity of the soil, pluviometry, ...). As a consequence, the parameters (α, η) should be x -independent. In other words, a local variation may be interpreted as the influence of a local leakage.

Obtained results confirm the validity of this approach. All the (artificial) leaks have been clearly identified on the east and west sides, while no leakage has been detected on the south side (**Figure 10**).

Deep analysis of the mechanical equations shows that η is as a function of (S, Pe) , while α is a function of Pe only, S being the saturation degree and Pe being the Peclet number (leakage velocity/thermal velocity). In the present situation, values of Pe around the OF (near the ground surface) are almost zero. We conclude that local variation of η may be interpreted as the consequence of S (actually on the local thermal diffusivity).



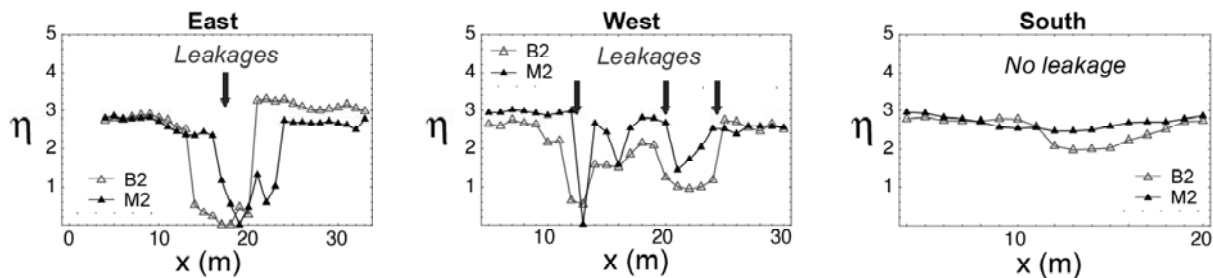


Figure 10: results of IRF analysis of bottom temperature (B2) and middle temperature (M2) as a function of top temperature (T2) (η in days)

7 Conclusions - Perspectives

The passive method used here is associated with a geotextile designed to detect leaks in the case of an OF placed outside the groundwater. There are a few remaining validation steps to render the overall system operational.

Literature

- [1] BONELLI S., RADZICKI K.: Impulse response function analysis of pore pressures in earthdams, *European Journal of Civil Engineering*, accepted for publication.
- [2] BONELLI S., RADZICKI K. (2007): The Impulse Response Function Analysis of Pore Pressures Monitoring Data, *5th International Conference on Dam Engineering*, 14-16 February, Lisbon, Portugal.
- [3] BONELLI S., FÉLIX H. (2001): Interpretation of measurement results, delayed response analysis of temperature effect, *6th ICOLD Benchmark Workshop on Numerical Analysis of Dams*, Oct 17-19, Salzburg.
- [4] GUIDOUX C. et al (2007): Measurement Results on Full Scale Field Experiment using Optical Fibre Detection Methods. 14th German Symposium of the international commission on large dams (ICOLD), Freising, Germany, September 17-19, 2007.
- [5] PENOT I., DAUMAS B. and FABRE J.P. (2003) : Behaviour on civil engineering structures, taking into account air temperature “Thermal H.S.T.” method, WaterPower, dec. 2005
- [6] JOHANSSON S. (1997): Seepage Monitoring in Embankment Dams. Doctoral Thesis, Royal institute of Technology, Stockholm, Sweden, 1997.
- [7] PERZLMAIER S. et al (2006): Integral seepage monitoring on open channel embankment dams by the DFOT heat pulse method, 22nd major dams congress, Barcelona, June 2006.
- [8] SELKER J.S. et al (2006), Distributed fibre-optic temperature sensing for hydrologic systems, *Water Resour. Res.* 42, W12202, doi:10.1029/2006WR005326.

Authors Name and Affiliation:

Olivier Artières
TenCate Geosynthetics Europe, France
o.artieres@tencate.com

Stéphane Bonelli, Krzysztof Radzicki, Paul Royet
Cemagref, France
stephane.bonelli@cemagref.fr
krzysztof.radzicki@cemagref.fr
paul.royet@cemagref.fr

Jean-Paul Fabre, Christophe Vedrenne
EDF, France
jean-paul.fabre@edf.fr
christophe.vedrenne@edf.fr

Cyril Guidoux
Laboratoire des Transferts en Hydrologie et Environnement (LTHE), France
cyril.guidoux@ujf-grenoble.fr

Dam Breaching – Case Studies

Jean-Robert Courivaud and Jean-Jacques Fry

Abstract

Engineers need validated software for modelling dam breaching by internal erosion, for managing emergency plan surveys. Although an extensive research effort was devoted to that extreme phenomena, a lot of hypothesis are not well founded. In consequence, evaluation of observed large scale field tests and of real cases of dam failure is a crucial step of the task. The last step is the validation of the theoretical framework for erosion law at large velocities.

1 Introduction

During the last decade, an extensive research effort has been performed both in Europe and USA to improve comprehension and modelling capabilities of breach processes: EU CADAM and IMPACT projects, Norwegian project “Stability and Breaching of Embankment Dams”, USDA-ARS-HERU research, DSIG project “Erosion of Embankment Dams” and French project “ERINOH”. These projects have provided an improvement in the understanding of physics and have also pointed out the necessity to improve the evaluation and validation of breach numerical models. One of the key components to reach this objective is to acquire reliable and well documented data from case studies.

Some results from the evaluation of large scale field test of piping, laboratory tests of breach widening and real-world case studies of embankment dam breaching are discussed.

2 Large Scale Field Test of Piping

In the frame of the Norwegian project “Stability and Breaching of Embankment Dams” and the EU project IMPACT, a large scale field test of piping has been conducted in 2003. A documentation of this test is provided in [1] and [2]. The main characteristics of this test are:

- test dam height: 4.3 m
- test dam length: approximately 40 m
- test dam crest width: 2.8 m
- test dam upstream slope: 1:1.4
- test dam downstream slope: 1:1.4
- test dam material: homogeneous moraine
- Moraine characteristics:
 - i. $D_{10} = 0.06 \text{ mm}$
 - ii. $D_{50} = 5.5 \text{ mm}$
 - iii. $D_{\text{Max}} = 200 \text{ mm}$

- iv. Cohesion = 0
- v. Porosity = 0.24
- vi. Moisture content = 0.06

- piping initiation mechanism: trigger pipe surrounded by sand. No filter between the sand envelope and the moraine material.

The homogenous moraine dam as constructed before the test is shown in the figure 1a. The downstream outlet of the trigger pipe is shown in the figure 1b. The piping process is shown in the figure 1c, before the roof collapse. The breach widening phase is shown in the figure 1d.

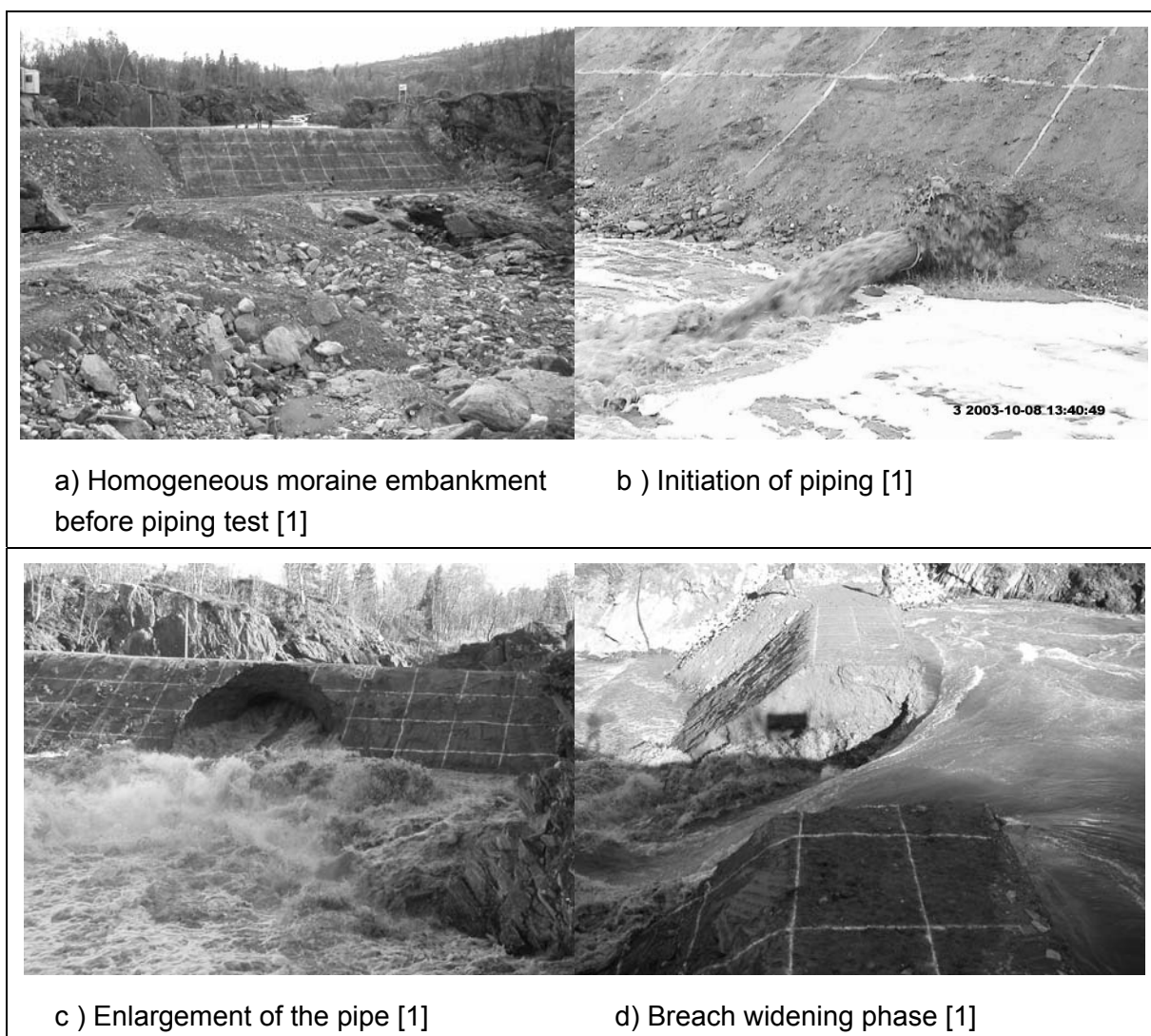


Figure 1: Piping test of the Norwegian project “Stability and Breaching of embankment dams

A video analysis of the enlargement of the pipe enabled to determine the evolution in time of the pipe radius (**Figure 2**)

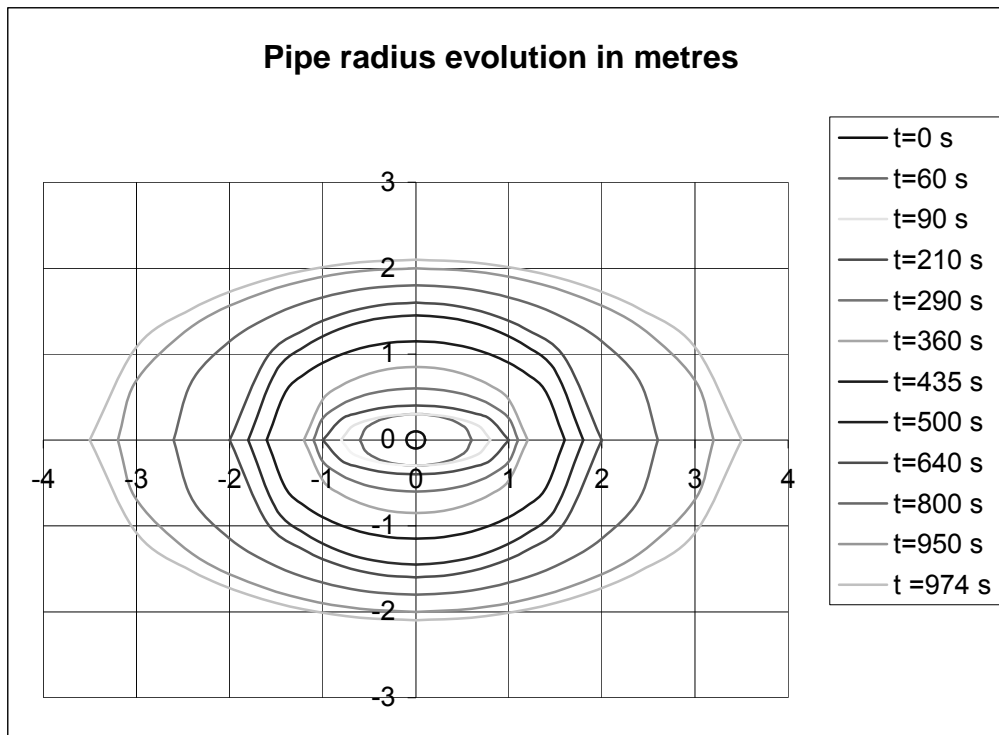


Figure 2: Downstream pipe section evolution in time (Norwegian large scale piping test)

This analysis shows that the pipe section is elliptic rather than circular (**Figure 2**). Upcoming experimental research efforts in piping should confirm if in one hand anisotropy in resistance to erosion is the cause of elliptic shape of the pipe section and if on another hand the elliptic shape has to be considered rather than a circular one.

The horizontal and vertical radius evolution of the pipe (downstream outlet of the pipe) in time is shown in the figure 3.

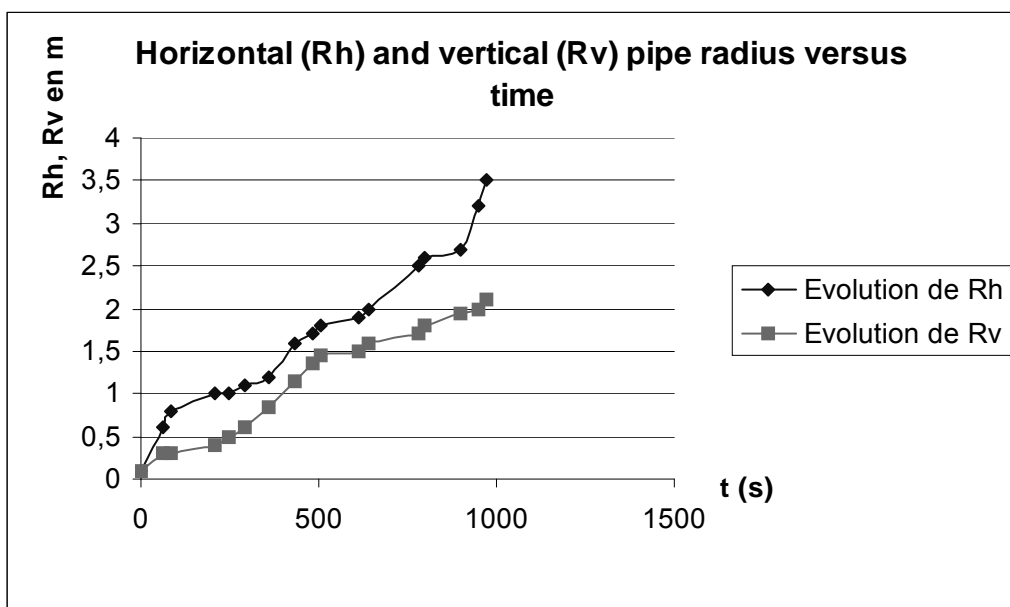


Figure 3: Enlargement of pipe radius (horizontal and vertical) during the Norwegian piping test

It is remarkable to notice that the evolution in time of the pipe radius has been roughly linear with an average rate of enlargement of 0.13 m/minute for the vertical radius. The ongoing research efforts should permit to identify the influence of the driven parameters of this rate of pipe radius enlargement: soil erodibility and hydraulic conditions (upstream and through the pipe). According to this test, the ratio horizontal radius over vertical radius does not seem constant, as shown in the figure 4.

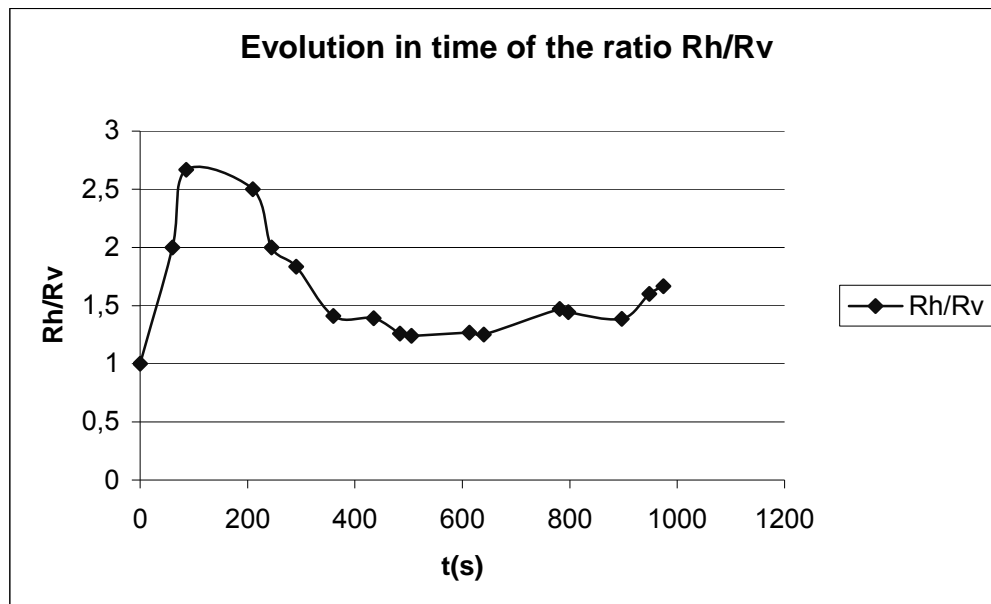


Figure 4: Ratio horizontal radius over vertical radius during the Norwegian piping test

3 Breach Widening Process

3.1 Results from Laboratory and Field Tests

The breach widening processes have been studied in laboratory experiments for both non cohesive and cohesive embankments [7]. Norwegian large scale field tests provided also unique data related to that physics [1].

According to Hunt, Hanson, Cook and Kadavy [7], laboratory researches that investigated widening processes provided significantly different results depending on the cohesive or non cohesive nature of the embankment material [7]. Researches that focused on widening processes in non cohesive materials concluded that widening rate was not a function of the embankment material. On the contrary, researches that investigated widening process in cohesive embankment found that widening rates is strongly influenced by soil properties, including water content, density, erodibility, strength and compaction [7].

Norwegian large scale field tests provide unique information on widening process for different types of embankment materials: homogeneous clay, homogeneous sandy-gravel,

homogeneous moraine and a zoned embankment with a moraine core and rock fill shoulders. Investigated initiation processes of failure were overtopping and piping.

The same general process of erosion was observed in all tests, but it occurred with different celerity and continuity depending on the type of material. This process presented the following characteristics [1]:

- lateral erosion of the embankment material due to the flow occurred mainly at the base of the breach sides, leading to an undermining on each side of the breach.
- In parallel to this undermining process, crack lines occurred in the embankment, mostly parallel to the flow and relatively close to the breach sides.
- The main material detachment process was slumps of the undercut parts of the embankment.
- Once the slumps have fallen in the flow, they are carried out downstream.

This general process occurred in steps and was discontinuous for the homogeneous clay embankment, as for the homogeneous moraine and the zoned embankment, but it was much more continuous for the homogeneous sandy-gravel embankment (slumping of material more frequent and of small volume) [1].

This process of erosion during breach widening observed during Norwegian large scale field tests was similarly observed by ARS-HERU researchers during breach widening lab experiments on cohesive embankments (see **Figure 5** hereafter).

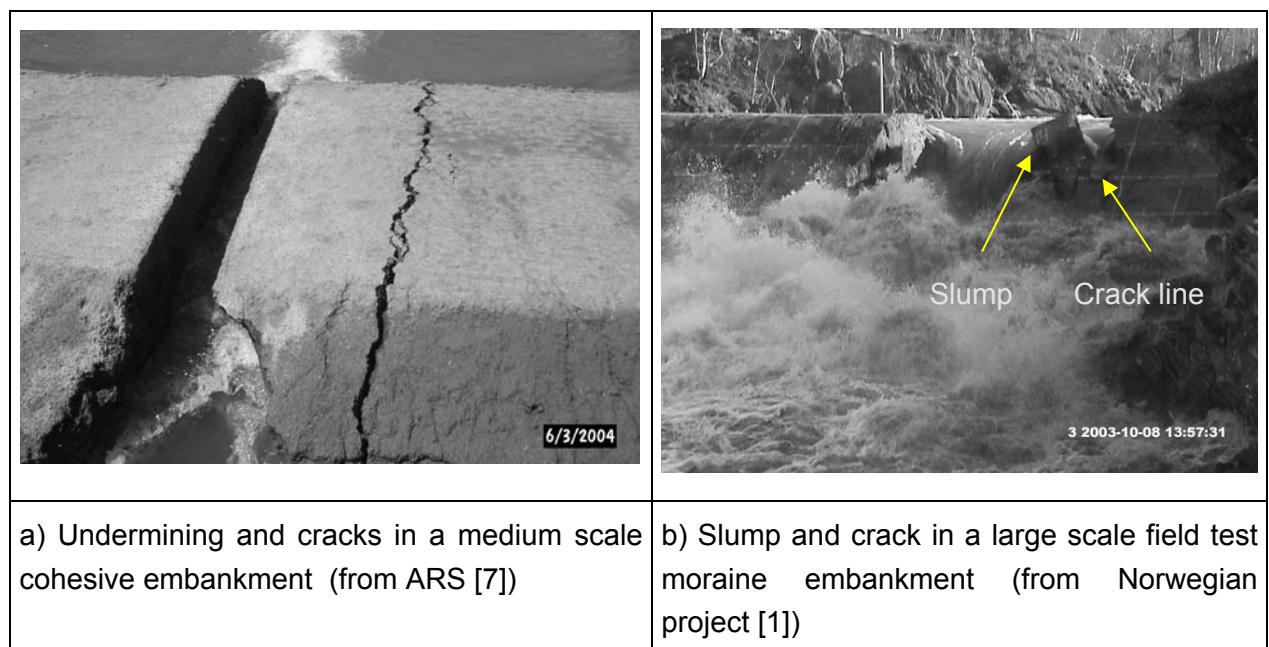


Figure 5: observed process of breach widening

In addition to these qualitative descriptions of physical processes, both ARS medium scale tests and Norwegian large scale tests provided average breach widening rates for the different tested embankment materials. Although the widening process is discontinuous and therefore non linear, a linear trend of the enlargement can be considered during the breach widening phase, at rather constant reservoir elevation. This trend is illustrated by the analysis of the breach widening phase of the Norwegian piping large scale field test (**Figure 6**).

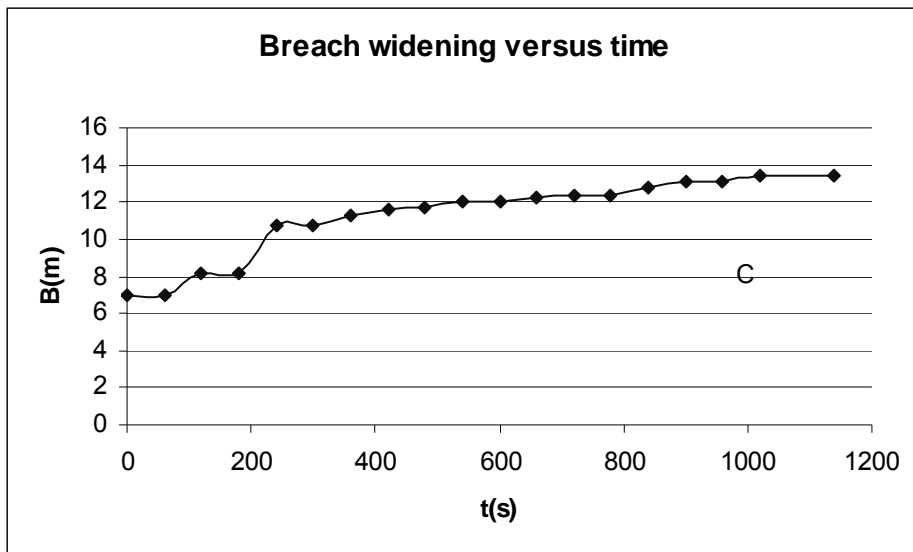


Figure 6: Evolution in time of the breach widening in the Norwegian large scale piping test

The graph of the figure 6 plots the half of the breach length versus time (considered as breach widening rate). The average rate of breach widening is between 0.25 m/minute and 0.34 m/minute depending on the analysis method. These estimates of breach widening rates are presented in Table 1 hereafter.

Table 1: Breach widening rates measured for medium and large scale embankments

Test identification	Embankment height (m)	Type of embankment material	Breach widening rate (m/min)
ARS-HERU W1 [7]	1.3	Silty sand 6% < 2 μ m NP w = 12.2%	0.00225
ARS-HERU W2 [7]	1.3	Silty sand 6% < 2 μ m NP w = 10.7%	0.0073
ARS-HERU W3 [7]	1.3	Lean clay 26% < 2 μ m PI = 17 w = 16.2%	0.00018
Norwegian test 1-02 [1] Homogeneous clay	5.9	Homogeneous clay. D ₅₀ = 0.007 mm. D _{max} = 1 mm w = 30%	0.15
Norwegian test 2-02 [1] Homogeneous gravel	5	Gravel. D ₅₀ = 4.75 mm. D _{max} = 76 mm w = 7%	0.7
Norwegian test 1-03 [1] Zoned (moraine core and rock fill shoulders)	5.9	Core material = moraine D ₅₀ = 5.5 mm. D _{max} = 200 mm w = 6%	0.8
Norwegian test 3-03 [1] Homogeneous moraine	4.3	Homogeneous moraine D ₅₀ = 5.5 mm. D _{max} = 200 mm w = 6%	0.25 to 0.34

3.2 Evaluation of Real-World Case-Studies Data

An evaluation of the database of real-world case studies of embankment dam failures developed for the DSIG project “Erosion of Embankment Dams” [8] provided widening rate estimates for ten case studies of failures (cf. Table 2 hereafter).

Table 2: Breach widening rate estimates of real-world case studies of embankment dam failures

Dam Name	Dam Material	Dam Height	Reservoir capacity right before failure	Mean breach widening rate estimate
Machhu 2	Hand made earth dam, very weak compaction	20.4 m	219.4 Mm ³	6 to 7 m/min
Oros	Zoned embankment, with thick clay core	35.5 m	730 Mm ³	0.14 to 0.26 m/min
Salles de Oliveira	Homogeneous earth, probably weak compaction	32 m	71.5 Mm ³	1.9 to 2.8 m/min
Euclides da Cunha	Homogeneous earth, probably weak compaction	40 m	23.03 Mm ³	1.7 m/min
El Guapo	Zoned embankment with core	60 m	180.8 Mm ³	1.1 m/min
Castlewood	Gravel and rock fill, masonry face	21.3 m	5.54 Mm ³	1.4 m/min
South Fork	Rock and earth fill, weak compaction	21.1 m	18.8 Mm ³	1.6 m/min
Noppikoski	Zoned embankment with moraine core and rock fill shoulders	18 m	1.1 Mm ³	0.56 m/min
Belci	Central clay core with sand gravel filter. Concrete slab upstream face.	14 m	12.89 Mm ³	0.6 m/min
Glashütte	Silt loam and clay with gravel and sand	8 m	0.07 Mm ³	0.26 m/min

These ten case studies cover a range of dam heights from 8 m to 60 m. Reservoir volumes are ranging from 0.07 Mm³ to 730 Mm³. Material embankment vary from hand-made earth embankment with a very weak compaction to zoned embankment made of a thick and well compacted clay core. Therefore this sample of case studies is significantly representative of dam heights, reservoir volumes and embankment material erodibilities that can be encountered in real-world dams.

Breach widening rate estimates presented in Table 2 are ranging from 0.14 m/min to 13 m/min. The value of 13 m/min obtained for Machhu 2 dam failure corresponds to the simultaneous

development of two breaches (one breach in each of the two embankments of the dam) which had approximately the same length each. Therefore, it would be more realistic to consider the half of this value for the breach widening rate of Machhu 2 dam failure, that is 6 to 7 m/min.

These estimate of the breach widening rate are consistent with the observed widening rates from the Norwegian large field scale test s: Glashütte Dam and the homogeneous moraine Norwegian embankment are similar in their heights and materials. Their breach widening rate estimates are similar (0.26 m/minute for Glashütte Dam and 0.25 to 0.34 m/min for the Norwegian test). Oros Dam was constituted from a thick clay core with material characteristics rather similar to the homogeneous clay Norwegian embankment. Their breach widening rates are also similar (0.14 to 0.26 m/min for Oros Dam and 0.15 m/min for the Norwegian test).

3.3 First Tentative Interpretation and Perspectives

It is noteworthy to notice that breach widening rates controls the maximum discharge of the failure hydrogramme. The maximum discharges released by failure in the large scale filed test in Rossvatn (Norway) show clearly that influence (**Figure 7**).

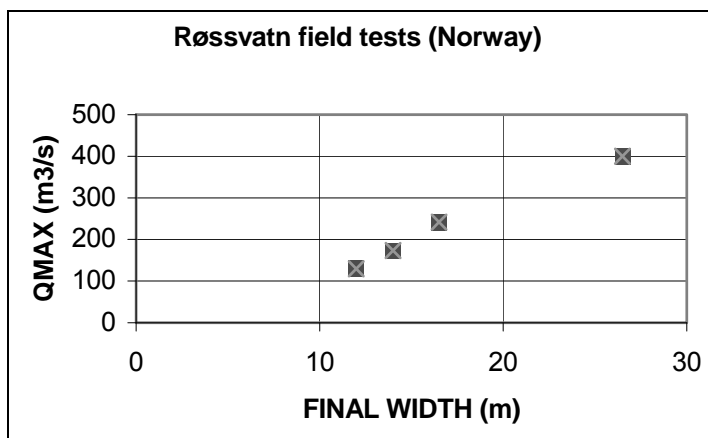


Figure 7: Influence of the breach widening rate on the peak discharge flow

Assuming that the breach widening rate is constant and equals to the value, c , from the beginning to the end of the breach formation phase, it can be demonstrated that Q_{MAX} the peak of released discharge by the failure of a H_o high dam retaining a V_o water capacity is:

$$Q_{MAX} = c^{1/2} H_o^{3/4} V_o^{1/2} \quad (1)$$

Taking into account the results of Greg Hanson that the breach widening rate is proportional to erosion coefficient k_d , and that the range of field k_d vary in a range from 1 to 10^4 , the peak of discharge may vary theoretically from 1 to 100, depending on material properties.

However, the breach widening rates from ARS tests are two up to three orders of magnitude lower than widening rates from Norwegian tests. This difference could not be explained by differences in embankment material properties only. A probable explanation is the influence of hydraulic head. Taking into account the results of Greg Hanson [7] that the breach widening rate is proportional to the product of erosion coefficient k_d and the shear stress, it appears that the breach widening rate should be proportional to the hydraulic head H at power 1,5. That

relationship could explain that the breach widening rate from ARS test is one order of magnitude lower than the ones measured at Rossvatn, according to the ratio of hydraulic head used in both field tests.

Lempérière, Courivaud and Fry [8] have proposed a relationship based on statistics, from dam failure data base, linking the peak discharge to the square root of the reservoir capacity and to the square of the hydraulic head. More theoretical research is needed to confirm such a relationship.

The first comparisons carried out at USBR between the hole erosion test and jet erosion test leads to the result that the erosion coefficient with the Jet test is around one order higher than the erosion coefficient measured in the Hole Erosion Test. Higher water velocity could lead to higher erosion coefficient. A deeper assessment of the test conditions (both hydraulic and soil properties) and a better interpretation need to be done to quantify the shear stress at very high velocity and qualify the erosion law. The application of the erosion law proposed by Bonelli [9] could be helpful for the interpretation of that tests.

Regional and local dispersion of erosion resistance, like in rock mechanics, may cause scale effects. An important issue of this evaluation will be to determine the influence of that scale effects on breach widening rates and on erosion law in general.

4 Conclusions

Some evidences and order of magnitudes on breach phenomena have been demonstrated from large scale field tests of dam failure. Breach widening rate can be known from real-world case studies of embankment dam failure. Nevertheless, a theoretical framework is missing to describe and integrate the erosion law at large water flow velocity. Emphasis has to be put on the scale effects in the future research, in order to developing software for engineers modelling dam breaching.

Literature

- [1] EBL Kompetanse, "Stability and Breaching of Embankment Dams – Report on Sub-project 3 (SP3): Breaching of Embankment Dams".
- [2] EU Impact project, "Impact_DetailedTechnicalReport_v2_2.pdf", www.impact-project.net
- [3] T. L. Wahl, "Prediction of Embankment Dam Breach Parameters. A Literature Review and Needs Assessment". DSO-98-004. USBR, July 1984.
- [4] "Lessons from Dams Incidents", ICOLD 1974, computerized version 1999.
- [5] "Dams less than thirty metres high", ICOLD 1997, bulletin n°109.
- [6] A. Vogel, "Bibliography of the History of Dam Failures" (database on CD-ROM).
- [7] S. L. Hunt, G. J. Hanson, K. R. Cook, K. C. Kadavy, "Breach Widening Observations from Earthen Embankment Tests", Transactions of the ASCE, Vol. 48(3): 1115-1120, 2005.
- [8] F. Lempérière, J.-R. Courivaud, J.-J. Fry, "A new analysis of embankment dam failures by overtopping", 22nd ICOLD Congress, Barcelona, June 2006.

- [9] Bonelli, S.; Brivois, O.; Borghi, R.; Benahmed, N. 2006. On modelling of piping erosion. Comptes Rendus de Mécanique, 8-9(334), 555-559.

Authors Name and Affiliation

Jean-Robert Courivaud
EDF CIH
jean-robert.courivaud@edf.fr

Jean-Jacques Fry
EDF CIH
jean-jacques.fry@edf.fr

A framework for the Management of Risk from Internal Erosion

A.J Brown

Abstract

This paper describes the use of Risk Management techniques as a framework for both assessing the risk from internal erosion to the safety of the dam, and a tool for deciding when additional risk reduction measures would be warranted.

1 Introduction

The European Working Group on Internal Erosion (EWG) has been active since 1993, with Progress Reports by Charles in 2001 and 2002. The current report represents meetings and dialogue since 2003. This includes meetings at Aussois in 2005 (Fell,2007) and Stockholm (www.swedcold.org/SwedCOLD/index.html) in 2006 as well as various ongoing research projects in Europe, reported as appropriate in the various chapters of the report.

As well as advancing technical knowledge and understanding of internal erosion, the key outputs from EWG should include tools for practical risk management. This is the process whereby decisions are made as to whether the level of existing risk is tolerable, or whether the risk needs to be reduced by some form of intervention. It aims to address the “So what” questions about internal erosion with the conclusions in a form that is understandable by dam owners, regulatory authorities, politicians, the media and public.

There is a significant existing literature on risk assessment, both qualitative and quantitative. This paper is therefore limited to presenting the principles of risk management relevant to internal erosion and providing key references. It refers to other chapters of the report by the European Working group on Internal Erosion. The limitations of current knowledge in internal erosion should be appreciated, and should form part of the risk assessment.

It is preferable that the risk analysis uses quantitative risk assessment (QRA) as this can provide significant insights into relative importance of different factors, as well as providing a robust audit trail for dam safety decisions. Nevertheless it is noted that QRA is still developing as a science, and qualitative assessments can still be of significant value in understanding risks from internal erosion. Key references to QRA are the Interim Guide to Quantitative risk assessment of UK Reservoirs (UK Guide) (Brown and Gosden, 2004) which provides a screening level quantitative assessment, and “Risk and Uncertainty in dam safety” (Hartford et al, 2004) which provides a detailed description of the theoretical principals. The process of risk management is summarized in Figure 1, as two concentric circles.

2 Risk Analysis

Risk analysis can be broken down into several elements

- What are the mechanisms by which internal erosion occurs (modes of failure)?
- What are the consequences of ongoing internal erosion?
- What is the annual probability of occurrence of each mode of failure?
- What are the consequences of failure of the reservoir?

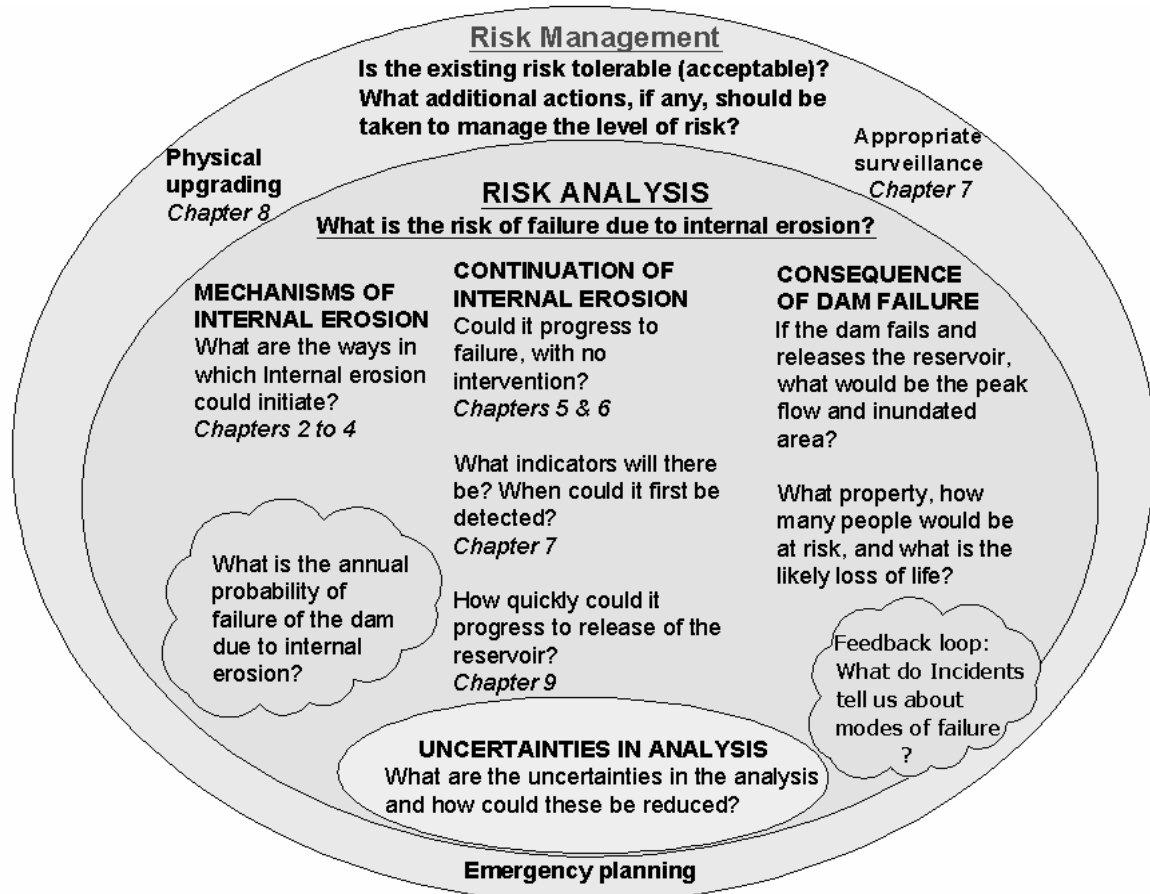


Figure 1: Relationship of risk analysis to risk management.

2.1 Mechanisms of Internal Erosion

This is covered in Chapters 2 to 4. It is important that assessment of mechanisms of internal erosion considers all possible mechanisms in a systematic way, and does not make presumptions about what will be the most critical mechanisms. The limitations of current understanding of behavior should also be noted, such that assessment should include consideration of all of the following

- Precedent – what do case histories of poor behavior of similar types of dam tell us?
- Analysis – what does theoretical analysis tell us?
- Investigations – what do field investigations and laboratory testing tell us?

Particular issues that need careful consideration are

- Structures through the watertight element of an embankment, as these often provide preferential leakage paths, along which internal erosion can develop rapidly
- the local groundwater regime, both in terms of levels and geochemistry
- the viscosity of water changes significantly with temperature, and can lead to seasonal changes in seepages

Consideration should also be given as to what is unknown, and uncertainties in what is known, as these may have significant effect on the risk of internal erosion. These includes consideration of the potential presence and type of singularities. These are features which are often not shown on "as-built" construction drawings and which may have a significant effect on the mode of, and rate of deterioration due to, internal erosion. These include irregularities in the foundation, construction stage features such as access routes, local drainage and variations in materials; and trial pits/ or other localized excavation and backfilling within the dam. In addition consideration should be given as how site and regional conditions may change in future, and how these may influence the risk of failure (e.g. increased risk of desiccation from climate change)

A risk assessment should include an assessment of the quality of the data on which it is based, the unknowns for which assumptions have had to be made and how the uncertainties could be reduced.

2.2 Ongoing Internal Erosion

The issue of whether internal erosion will continue, and if so the means by which it may be detected and how likely this is to lead to catastrophic failure of the dam is covered in Chapters 5 to 6 and 8. The issues relating to assessment of mechanisms of internal erosion also apply to the issue of continuation. A key issue is the rate at which mechanism of internal erosion could progress to failure, as this is key to determining the practicality of surveillance and emergency planning as practicable risk management tools.

2.3 Annual Probability of Failure due to Internal Erosion

There is no analytical method for estimating the annual probability of failure due to internal erosion (as there is for floods), such that recourse has to be made to historic probability and judgment, some of which are summarized in Table 1. Further detail on alternative methods is given in Hartford and Baecher (2004). Ideally such estimates would also provide how the probability varies with time to failure.

Table 1: Alternative methods to assess the annual probability of failure due to internal erosion

	Method	Advantages	Disadvantages
A Historic probability			
A1	McCann, Stanford University, USA, 1985	Rapid method	Scope for variable interpretation of condition score Base data now quite old
A2	Foster & Fell, University of New South Wales, Australia, 1998	Based on historic data	Data is mainly from the US and Australia and may not apply elsewhere. System based on extrapolation from median point for median dam Relatively little importance given to current condition, such that major leak would not necessarily lead to low probability of failure
A3	Interim (Defra) Guide, 2004	Based on UK data. Interpolation between end points Structural works give benefits only where used to treat and remove indicators of poor performance	Scope for variable interpretation of Current Condition score Little weight given to Intrinsic Condition, such that major structural works would give little apparent benefit in reducing the AP of failure where there had been no indicators of poor performance
B Judgment			
B1	Predefined Event Trees used by US BOR (Cyganiwicz, JM 2005)	Structured system based on US experience Alternative to systems based on historic data	May not be fully applicable to dams outside US
B2	Event or fault tree defined by User e.g. B5760:1991	Flexibility in adapting to subject dam	Need to calibrate users if meaningful results are to be obtained
B3	Expert Elicitation (Brown & Aspinall, 2004)	Viable alternative to those based on historic data, and event trains	Expensive, as to be meaningful a minimum of five, and preferably more, "experts" are required, together with the facilitator Output dependent on the reliability of the "experts"

2.4 Consequences of Dam Failure

This aspect of risk assessment is outside the scope of this report on Internal Erosion, and is covered in other texts, such as the UK Guide and Hartford et al (2004). It comprises assessing the hydrograph for the dam failure flood wave, routing this downstream from the dam, and assessing the consequences in terms of property damage and likely loss of life.

2.5 Annual Risk of Failure due to Internal Erosion

In principle the output from a QRA would provide estimates of both likely loss of life and property damage per annum. This is of value in comparing the risks between different dams and with other high hazard installations, and to provide a means to evaluate what cost would be proportionate in terms of reducing risk.

3 Risk Management - General

Risk assessment is the process of deciding whether a risk is sufficiently significant to require additional control measures. There are a variety of tools to decide when no further control measures are warranted, for example as described in Section 3.3 of Hartford et al.

The Health and Safety Executive in UK note that the cost of risk reduction works should be “reasonably practicable”, stating in para 4 of Appendix 3 of HSE (2001):

“Of particular importance ... is Edwards v. The National Coal Board (1949). This case established that a computation must be made in which the quantum of risk is placed on one scale and the sacrifice, whether in money, time or trouble, involved in the measures necessary to avert the risk is placed in the other; and that, if it be shown that there is a gross disproportion between them, the risk being insignificant in relation to the sacrifice, the person upon whom the duty is laid discharges the burden of proving that compliance was not reasonably practicable.”

In terms of application of this principle Item 9 of the HSE statement (2001) “Principles and guidelines to assist HSE in its judgments that duty-holders have reduced risk as low as reasonably practicable” (ALARP) states

“This process can involve varying degrees of rigour which will depend on the nature of the hazard, the extent of the risk and the control measures to be adopted. The more systematic the approach, the more rigorous and more transparent it is to the regulator and other interested parties. However, duty-holders (and the regulator) should not be overburdened if such rigour is not warranted. The greater the initial level of risk under consideration, the greater the degree of rigour HSE requires of the arguments purporting to show that those risks have been reduced ALARP”

It is thus implicit that all risk management action should be subject to an ALARP assessment, both in terms of adequacy of existing arrangements and case for enhanced measures. This test can either be entirely judgment based, or can use a quantitative analysis.

The primary control measures to reduce risk from internal erosion are

- Surveillance and monitoring (detection leading to intervention);
- Emergency planning (planning of measures to be taken in the event that internal erosion is detected, which could lead to failure to the dam)
- Physical works to reduce vulnerability to internal erosion

The following sections describe the process for deciding when costs are disproportionate, and then describes the alternative means to reduce risk.

4 Proportionate Costs

The favored tool for assessing whether risk is tolerable, or whether risk reduction measures should be implemented to reduce risk, is the ALARP (As Low As Reasonably Practicable) approach. With this approach the reduction in risk that would be achieved from possible works is measured against the cost of the works, to assess whether the cost of the works is proportionate to the reduction in risk achieved.

The approach calculates the cost to prevent a fatality (CPF) as follows

$$\text{CPF} = \frac{\text{Cost of risk reduction measures} - \text{Present Value } (\Delta \text{ Pf} \times \text{Damage})}{\text{Present value } (\Delta \text{ Pf} \times \text{Likely Loss of Life (LLOL)})}$$

where $\Delta \text{ Pf}$ is the change in annual probability of failure due to the proposed risk reduction works. At its simplest where the CPF is less than the “value of preventing a fatality” (VPF) then the candidate works would be proportionate risk reduction measures; whilst where CPF exceeds VPF then the cost is disproportionate.

The value that should be assigned to VPF is a difficult decision and includes consideration of

- Direct costs (measurable) such as earning potential of the victims, injury and long term health impairment of other victims not included in the LLOL value, and emergency services costs
- Indirect (business losses)
- Intangibles (Psychological impact on people, Environmental damage) – it could be argued that a value should be assigned to the Intrinsic Value of a Human Life (irrespective of age, health, education etc)

However, HSE (2002, para 25) notes that gross” disproportion is required before ALARP is satisfied and defines a Proportion Factor (PF):

$$\text{PF} = \frac{\text{Cost to Prevent a Fatality (CPF)}}{\text{Value to Prevent a Fatality (VPF)}}$$

The purpose of a PF “grossly” greater than unity is to allow for the imprecision of estimates of costs and benefits and also to ensure that the duty holder robustly satisfies the ALARP principle. HSE guidance (HSE, 2002, para 26 onwards) notes the proportion factor should always be gross, that the value is likely to vary with level of risk and should be argued in the light of particular circumstances. Guidance issued by individual directorates in UK quote Proportion factors of 1 to in excess of 10, using VPF of £1M.

Application of the ALARP approach is illustrated in Figure 2, where the proportionate cost of risk reduction works is plotted against the existing annual probability of failure, for a variety of consequences of failure in terms of likely loss of life (LLOL), a VPF of £1M/life, a proportion factor of 5 and property damage of £1M/life.

For example for an initial probability of failure of 2×10^{-5} where works which would reduce the annual probability of failure by 5 are identified, it would be proportionate if these cost £10,000/year for a dam where the likely loss of life in event of failure is 100, but the proportionate cost would only be £100/year for a dam where the likely loss of life in event of failure is 1. It can be seen that proportionate cost varies significantly depending on the level of risk i.e. annual probability of failure and consequences in terms of likely loss of life.

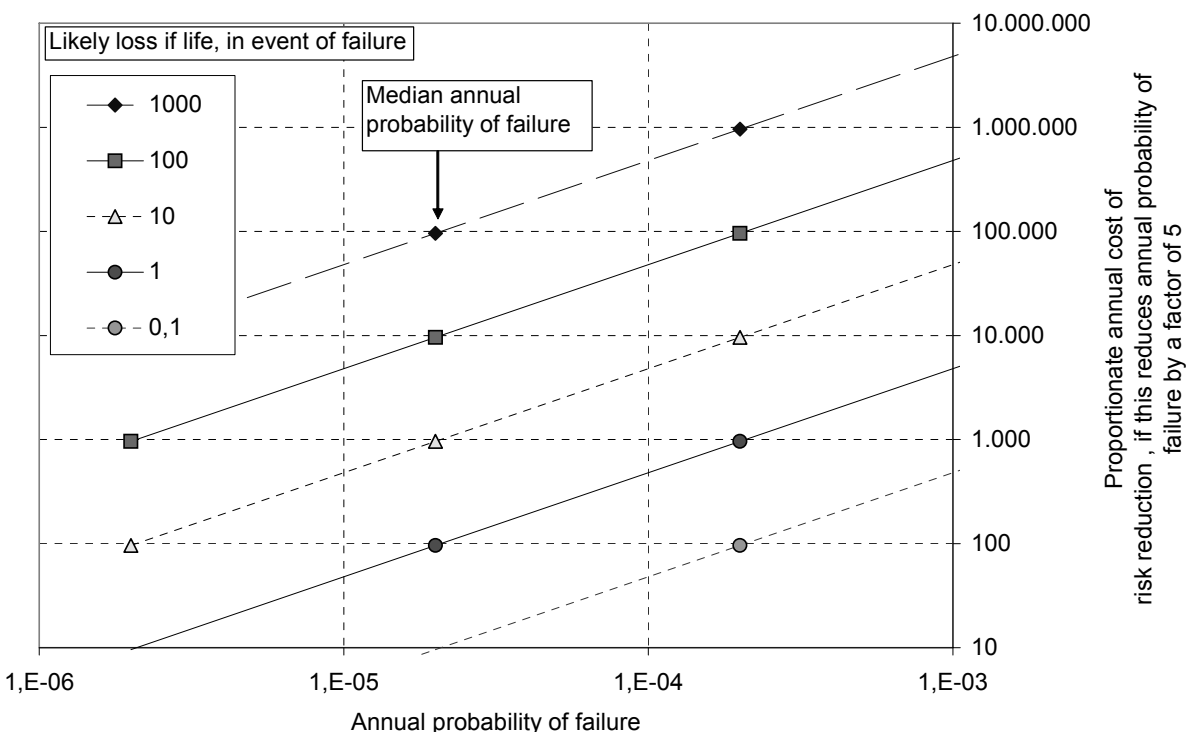


Figure 2: Illustration of how proportionate cost of risk reduction works varies with annual probability of failure and consequences

5 Appropriate Surveillance

An important issue in defining the strategy for surveillance is the balance between the options of surveillance (visual observation) and instrumentation; and whether the latter should include real time monitoring.

Surveillance has the major advantage that the whole of the visible dam surface can be inspected, such that it should provide early detection when internal erosion is occurring at an unexpected location. Instrumentation has the advantage that the precision of monitoring instrument is likely to be much higher than the human eye, and is not prone to human error/fallibility. Real time monitoring has the advantage that changes in readings can automatically trigger alarms in a control room (although it would be necessary to check that this is not a false alarm). However, the advantages of the latter are unlikely to be realized unless the dam owner has a control room which is manned 24 hours a day. Although in principle dam owners without this facility could obtain the service through some form of service provider, this is likely to be disproportionately costly for owners without existing 24-hour control rooms.

It is suggested that surveillance should remain the primary means for the detection of internal erosion. However, for high consequence dams and those vulnerable to rapid deterioration it is likely to be appropriate to install real time monitoring systems, with these identified on the basis of the most likely failure modes. Further information on automated monitoring is given in ICOLD Bulletin No 118 (2000).

It is important that the adoption of any real time monitoring must not result in any reduction in the frequency of surveillance visits. In terms of monitoring the choice of which indicators best provide for the early detection of internal erosion should be based on their value to the "early detection of progressive internal erosion", and the risk of failure of the dam

An assessment for UK dams is given in the research report carried out for Defra (KBR, 2003) and available on the Defra website. This concluded that the order of preference for UK embankment dams was turbidity meter, then seepage flow rate, followed by crest settlement. It is noted that where temperature sensors are installed within the dam temperature monitoring should be a high priority. It was suggested that the need for, and level of, monitoring would depend on the consequence class of the dam.

ANCOLD have produced "Guidelines on Dam safety management" (2003) which includes tables with indicative frequency of inspections and dam monitoring. The latter depends on hazard category, with five levels of hazard, each with an indicative frequency of monitoring of rainfall, reservoir level, seepage, pore pressures and movements. The frequency of routine visual inspection varies from daily for extreme hazard dams to monthly for low hazard.

In the United Kingdom this concept has been extended to provide a risk matrix, with consequences of failure along the horizontal axis, and vulnerability of the dam to failure on the vertical. This is shown in Table 2. The frequency of surveillance visits, both by operating staff and the overseeing dam engineer is defined for each of the five surveillance regimes, varying from daily for Regime α to monthly for Regime δ .

A key part of the surveillance system is setting "trigger levels" which define thresholds of normal behavior. These trigger values are typically categorized as: green, yellow and orange/red. These should be linked to actions by dam supervisory staff, and by senior management. An example of possible escalation of levels of concern and associated actions, both in terms of surveillance and emergency planning, is given in Table 3.

Table 2: Suggested risk matrix to select the surveillance and monitoring regime at a dam

Vulnerability to internal erosion, based on risk analysis ²	Consequence Class of dam ³				
	A1	A2	B	C	D
High	α	β	β	γ	δ
Medium	β	β	γ	δ	ε
Low	γ	γ	δ	ε	ε

Notes

- This is the suggested starting point, for application and adjustment on a dam specific basis, following the principle that the cost should be proportionate to the benefits obtained.
- Where this is annual probability of failure, then the suggested boundaries between the three categories of risk to the public are overall risk from dam failure of loss of life of 1 in 100 (10^{-2}) per year and 1 in 10,000 (10^{-4}) per year (i.e. the sloping lines on the FN chart on Sheet 11.3 of the Interim Guide to QRA (2004))
- The dam owner may select a higher consequence class if failure of the dam would include significant business or other losses, for example it was the only source of water to a major town
- Although this matrix applies to “early detection of internal erosion”, the same principles can be applied in relation to other failure modes, for example failure of pipework.

Table 3: Suggested range of Dam owner’s response matrix (as given in 2006 draft Guide to Emergency planning for UK reservoirs)

Alarm level	Trigger	Possible actions by		Local Resilience Forum
		Undertaker		
Watch	An earthquake has occurred, or major flood is predicted/ has occurred. <u>Instrumentation exceeds “orange” trigger level</u>	Instrumentation checked to see if instrument error.. Immediate surveillance visit to the dam by the Supervising Engineer		None (not notified, with actions internally within the Undertaker’s organization only)
Alert	<u>Instrumentation reading exceeds predefined “red” trigger level</u> some other aspect of behavior is outside the normal range of behavior	Increasing escalation of actions Repeat readings to confirm correct Inform Reservoir Safety Manager and the Supervising Engineer immediately		

		Increase the frequency of readings Panel Engineer to visit site and determine what further action is required	
Advisory	A serious structural problem has been detected. Precautionary drawdown is being carried out to reduce the likelihood of failure to an acceptable level	External notification to the Local Resilience Forum of the alarm level. Regular contact and updates should then continue until such time as the incident is deemed to be routine maintenance	Nominated members of the Local Resilience Forum should be given early notification (put on standby)
Alarm	Emergency drawdown is required to avert failure		Category 1 responders to take
Imminent failure	Control of the reservoir has been lost and failure (release of the reservoir) is inevitable	Internal actions include appointing a expert Dam Engineer to provide advice	phased escalation of actions including warning/ evacuation of the public, closure of major transport and service infrastructures.
Failed	The dam has failed (a large uncontrolled release of water has occurred)		
Recovery	Flooding due to dam break has dissipated; police have removed their cordons and handed control back to the local authority	Steps to minimize the consequential environmental impacts in and adjacent to the reservoir	Actions to reinstate infrastructure and rebuild the community

6 Emergency Planning

There are generally three sections in an emergency plan as shown in Table 4. Elements 2 and 3 are separated partly because the lead is generally taken by the dam owner and emergency services respectively, and also because legal powers to take actions vary depending on the owner of the land where the actions are being taken.

Table 4: Elements comprising an emergency plan

	Element	Objectives
1	Impact assessment	An assessment of the consequences if the hazard escaped from the owner's land
2	On-site	Actions which would be taken to prevent a failure of the dam
3	Off-site	Actions which would be taken to reduce loss of life in the event of a failure

Careful consideration should be given as to when it is proportionate to produce any element, and the level of detail of each element. The ongoing costs of maintaining each element,

including training for those who would be involved in an emergency and periodic exercising to ensure the plans would be effective can be significant and should not be underestimated.

7 Physical Upgrades

One of the available risk control measures is to carry out physical upgrades. Chapter 7 describes the strengthening of dams in Sweden, based on numerous incidents of internal erosion. Addition of toe berms was adopted in Northern Ireland in the late 1970's, when the principles of the UK Reservoirs Act 1975 were applied (Cooper, 1987).

In choosing between structural works and enhanced surveillance and monitoring consideration should include:

- currently it is not often possible to reliably predict those dams where internal erosion would progress rapidly, rather than at a slow rate
- pipes and culverts appear to be the largest risk; effective upgrade measures need to be developed for these
- if the mechanisms and singularities present at a dam cannot be fully quantified, then upgrades could lead to a false sense of security if they were incomplete in not addressing all potential failure modes. (e.g. if carrying out an upgrade led to a reduction in surveillance, this could increase the probability of failure due to progressive internal erosion)

8 Summary and Conclusion

Risk management may be used as a tool to link the understanding of internal erosion processes at a dam to the practical measures that can be taken to reduce the risk of failure. A key part of the processes is the speed at which internal erosion could progress, in the limit to failure of the dam. An important part of the risk assessment is identifying the uncertainties in the assessment, including limits of current knowledge on internal erosion.

The appropriate suite of risk management measures will vary between dams, depending on the vulnerability of the dam to internal erosion, the uncertainties of the assessment and the consequences if the dam did fail

Where quantitative risk assessment can be carried out, this provides a means to quantify the risk, and thus carry out an "As low as reasonably practicable" (ALARP) analysis, namely an assessment of when the cost of risk reduction measures would be proportionate to the reduction in risk achieved.

Literature

ANCOLD (2003) Guidelines on dam safety management. August. 52pp excl appendices

BROWN A J and GOSDEN J D (2004) Interim Guide to Quantitative Risk assessment for UK Reservoirs. Thomas Telford. 161pp. Supplement No 1 produced in June 2006, and available on Defra website.

BROWN and ASPINALL W, 2004, Use of expert opinion elicitation to quantify the internal erosion process in dams . Proc European Conference Canterbury Publ Thomas Telford

BSI (1991) Reliability of systems, equipment and components. BS 5760 Part 5. Guide to failure modes, effects and criticality analysis (FMEA and FMECA). 38pp British Standards Institution.

CHARLES J A (2001) Internal erosion in European embankment dams. ICOLD European Symposium, Geiranger, Norway, supplementary volume pp19-27

CHARLES J A (2002) Internal erosion in European embankment dams. British Dam Society Conference. 378-393

COOPER G A (1987) IWES Summer Conference, Torquay 1987 – The Reservoir Safety Programme in Northern Ireland.

CYGANANIEWICZ, John M (2005) Bureau of Reclamation Experience with Evaluating Internal Erosion of Embankment Dams" In Fell(2007)

FELL (2007) "Internal Erosion of Dams and Their Foundations: Selected Papers from the Workshop on Internal Erosion and Piping of Dams and Their Foundations, Aussois, France, 25-27 April 2005" To be published by Taylor & Francis May 2007

FOSTER , FELL and SPANNAGLE, 1998. Risk assessment – estimating the probability of failure of embankment dams by piping. ANCOLD 1998. Reproduced in A method for assess the relative likelihood of failure of embankment dams by piping. Canadian Geotechnical Journal. Vol. 37 No 5. PP1025-1061

HARTFORD DND and BAECHER GB (2004) Risk and uncertainty in dam safety. Thomas Telford. 391pp

HSE (2001) Reducing risks, protecting people (R2P2). Dec 2001 74pp. Available at www.hse.gov.uk

Health and Safety Executive (2002) Principles and Guidelines to assist HSE in its Judgments that Duty-Holders Have Risk as Low as Reasonable Practicable. www.hse.gov.uk/dst/alarp1.htm.

ICOLD (2000) Automated dam monitoring systems – Guidelines and case histories Bulletin 118.

JACOBS (2006) Draft Guide to Emergency Planning. Defra website

JACOBS (2007) Guide to early detection of internal erosion. Defra website

KBR (2003) Task B: Early Detection of Internal Erosion, Feasibility Report, Volume 1 of 2, Main Report, Defra website

McCANN et al, 1985, Preliminary safety evaluation of existing dams. Dept of Civil Eng. Stanford University.

Authors Name and Affiliation:

A.J Brown
Jacobs, Thorncroft Manor
Alan.J.Brown@Jacobs.com

Bisher erschienene Berichte des Lehrstuhls und der Versuchsanstalt für Wasserbau und Wasserwirtschaft, Technische Universität München

- Nr. 1 **Häusler Erich:** Energieumwandlung bei einem frei fallenden, kreisrunden Strahl in einem Wasserpolster, 1962, *vergriffen*
- Nr. 2 **Spiekermann, Günter:** Instabile Formen des Schußstrahles beim Abfluß unter Schützen und seine Kraftwirkungen auf die Schützenkonstruktion, 1962, *vergriffen*
- Nr. 3 **Linder Gaspar:** Über die Gestaltung von Durchlaßausläufen, 1963, *vergriffen*
- Nr. 4 **Knauss Jost:** Modellversuche über die Hochwasserentlastungsanlagen an kleinen Rückhaltespeichern in Südbayern, 1963, *vergriffen*
- Nr. 5 **Mahida Vijaysinh:** Mechanismus der Schnellsandfiltration, 1964, *vergriffen*
- Nr. 6 **Rothmund, Hermann:** Energieumwandlung durch Strahlumlenkung in einer Toskammer, 1966, *vergriffen*
- Nr. 7 **Häusler Erich:** Luftsiphons für den pneumatischen Verschluß von Wassereinlauföffnungen, 1966, *vergriffen*
- Nr. 8 **Seus Günther J.:** Die Anfangskavitation, 1966, *vergriffen*
- Nr. 9 **Knauss Jost:** Schießender Abfluß in offenen Gerinnen mit fächerförmiger Verengung, 1967, *vergriffen*
- Nr. 10 **Häusler Erich; Bormann Klaus:** Schießender bzw. strömender Abfluß in Bächen
Schultz Gert A.: Die Anwendung von Computer-Programmen für das Unit-Hydrograph-Verfahren am Beispiel der Iller
Bauch Wolfram: Untersuchungen über Wasserstandsvorhersagen an einem 600 m langen Modell der Donaustrecke Regensburg-Straubing, 1967, *vergriffen*
- Nr. 11 **Schultz Gert A.:** Bestimmung theoretischer Abflußganglinien durch elektronische Berechnung von Niederschlagskonzentration und Retention (Hyreun-Verfahren), 1968, *vergriffen*
- Nr. 12 **Raumer Friedrich von:** Verteilung von Bewässerungswasser in Kanälen - Eine Systematik großer Kanalsysteme zur Verteilung von Bewässerungswasser unter besonderer Berücksichtigung von Regulier- und Meßvorgängen, 1968, *vergriffen*
- Nr. 13 **Bormann Klaus:** Der Abfluß in Schußrinnen unter Berücksichtigung der Luftaufnahme, 1968
- Nr. 14 **Scheuerlein Helmut:** Der Rauhgerinneabfluß, 1968, *vergriffen*
- Nr. 15 **Koch Kurt:** Die gegenseitige Strahlablenkung auf horizontaler Sohle, 1968
- Nr. 16 **Bauch Wolfram:** Die Hochwasserwelle im ungestauten und gestauten Fluß, 1968
- Nr. 17 **Marr Gerhard:** Vergleich zweier Differenzenverfahren in einem mathematischen Modell zur Berechnung von instationären Abflußvorgängen in Flüssen, 1970, *vergriffen*
- Nr. 18 **Herbrand Karl:** Der räumliche Wechselsprung, 1970, *vergriffen*
- Nr. 19 **Seus Günther J.:** Betrachtungen zur Kontinuitätsbedingung der Hydromechanik;
Zielke Werner: Zur linearen Theorie langer Wellen in Freispiegelgerinnen, 1971
- Nr. 20 **Häusler Erich:** Entnahmetürme mit Luftsiphons, 1971, *vergriffen*
- Nr. 21 **Herbrand Karl:** Das Tosbecken mit seitlicher Aufweitung, 1971
- Nr. 22 **Knauss Jost:** Hydraulische Probleme beim Entwurf von Hochwasserentlastungsanlagen an großen und kleinen Staudämmen, 1971, *vergriffen*
- Nr. 23 **Zielke Werner:** Brechnung der Frequenzganglinien und Eigenschwingungen von Rohrleitungssystemen
Zielke Werner; Wylie E. Benjamin: Zwei Verfahren zur Berechnung instationärer Strömungen in Gasfernleitungen und Gasrohrnetzen, 1971
- Nr. 24 **Knauss Jost:** Wirbel an Einläufen zu Wasserkraftanlagen, 1972, *vergriffen*
- Nr. 25 **Kotoulas Dimitrios:** Die Wildbäche Süddeutschlands und Griechenlands, Teil 1, 1972, *vergriffen*
- Nr. 26 **Keller Andreas:** Experimentelle und theoretische Untersuchungen zum Problem der modellmäßigen Behandlung von Strömungskavitation, 1973, *vergriffen*
- Nr. 27 **Horn Heinrich:** Hochwasserabfluß in automatisch geregelten Staustufen, 1973
- Nr. 28 **Bonasoundas Markos:** Strömungsvorgang und Kolkproblem am runden Brückenpfeiler, 1973
- Nr. 29 **Horn Heinrich; Zielke Werner:** Das dynamische Verhalten von Flußstauhaltungen, 1973

- Nr. 30 **Uslu Orhan:** Dynamische Optimierung der Fließbeiwerte in mathematischen Flußmodellen und Berücksichtigung der Vorlandüberströmung - Eine Anwendung des Operations Research im theoretischen Flußbau, 1974
- Nr. 31 **Kotoulas Dimitrios:** Die Wildbäche Süddeutschlands und Griechenlands, Teil 2, 1975, *vergriffen*
- Nr. 32 **50 Jahre Versuchsanstalt Obernach**
Hartung Fritz: Einführung: Was treiben eigentlich die Obernacher?
Knauss Jost: Strategien und Entscheidungshilfen beim Hochwasserschutz in Städten, dargestellt am Beispiel der Hochwasserfreilegung der Stadt Harburg an der Wörnitz
Häusler Erich: Abstürze und Stützschwellen in hydraulischer und konstruktiver Betrachtung (Mindestfallhöhen zur Erzielung einer genügenden hydraulischen Wirksamkeit)
Seus Günther J.; Hack Hans-Peter: Erster Vergleich der Ergebnisse des physikalischen Modells in Obernach mit denen des neuen mathematischen Modells
Uslu Orhan; Schmitz Gerd: Parameteridentifikation und Sensitivitätsanalyse bei mathematischen Modellen in der Hydrologie
Keller Andreas; Zielke Werner: Veränderung des freien Gasgehaltes in turbulenten Rohrströmungen bei plötzlichen Druckabsenkungen
Herbrand Karl: Zusammenführung von Schußstrahlen. Zwei praktische Beispiele konstruktiver Lösungen aus Modellversuchen
Zielke Werner: Grenzen der deterministischen Betrachtungsweise in der Strömungsmechanik, 1976
- Nr. 33 **Probleme der Arbeit des beratenden Ingenieurs in der Wasserwirtschaft der Entwicklungsländer.** Symposium am 13.10.1976 in Wallgau
Bauch Wolfram: Besondere Probleme bei der Planung und Ausführung der Gesamtentwässerung Busan/Korea
Bormann Klaus: Wasserkraftstudie West Kamerun und Bau der Wasserkraftanlage Batang Agam, Indonesien, zwei Entwicklungshilfe-Projekte unter extremen Bedingungen
Raumer Friedrich von: Zielvorstellungen und Verwirklichung eines wasserwirtschaftlichen Mehrzweckprojektes in Ecuador
Krombach Jürgen: Der beratende Ingenieur in Entwicklungsländern gestern und heute: Berater, Kontrolleur, Entwicklungshelfer oder Geschäftsmann? (am Beispiel wasserwirtschaftlicher Projekte), 1977
- Nr. 34 **50 Jahre Versuchsanstalt Obernach,** Feierstunde am 14.10.1976 in Wallgau
Hartung Fritz: Die Wasserbauversuchsanstalt Obernach im Strom der Zeit
Bischofsberger Wolfgang: Laudatio für Professor Dr.-Ing. E. Mosonyi
Mosonyi Emil: Wasserbau, Technik oder Kunst? 1977
- Nr. 35 **50 Jahre Versuchsanstalt Obernach,** Ausleitungen aus geschiebeführenden Flüssen, Seminar am 15.10.1976 in Obernach
Cecen Kazim: Die Verhinderung des Geschiebeeinlaufes zu Wasserfassungsanlagen
Midgley D.C.: Abstraction of water from sediment-laden rivers in Southern Africa
Jacobsen J.C.: Geschiebefreie Triebwasserfassungen - Modellversuche am Beispiel des sogenannten Geschiebeabzuges
Scheuerlein Helmut: Die Bedeutung des wasserbaulichen Modellversuchs für die Gestaltung von Ausleitungen aus geschiebeführenden Flüssen, 1977
- Nr. 36 **Hack Hans-Peter:** Lufteinzug in Fallschächten mit ringförmiger Strömung durch turbulente Diffusion, 1977
- Nr. 37 **Csallner Klausotto:** Strömungstechnische und konstruktive Kriterien für die Wahl zwischen Druck- und Zugsegment als Wehrverschluß, 1978
- Nr. 38 **Kanzow Dietz:** Ein Finites Element Modell zur Berechnung instationärer Abflüsse in Gerinnen und seine numerischen Eigenschaften, 1978
- Nr. 39 **Keller Andreas; Prasad Rama:** Der Einfluß der Vorgeschichte des Testwassers auf den Kavitationsbeginn an umströmten Körpern - Ein Beitrag zur Frage der Rolle der Kavitationskeime bei Strömungskavitation, 1978
- Nr. 40 **Hartung Fritz:** 75 Jahre Nilstau bei Assuan - Entwicklung und Fehlentwicklung, 1979, *vergriffen*
- Nr. 41 **Knauss Jost:** Flachgeneigte Abstürze, glatte und rauhe Sohlrampen
Scheuerlein Helmut: Wasserentnahme aus geschiebeführenden Flüssen
Häusler Erich: Unkonventionelle neuere Stauhaltungswehre an bayerischen Flüssen als gleichzeitige Sohsicherungsbauwerke, 1979, *vergriffen*

- Nr. 42 **Seus Günther J.; Joeres Erhard P.; Engelmann Herbert M.:** Lineare Entscheidungsregeln und stochastische Restriktionen bei Bemessung und Betrieb von Speichern, 1979, *vergriffen*
- Nr. 43 **Meier Rupert C.:** Analyse und Vorhersage von Trockenwetterabflüssen - Eine Anwendung der Systemhydrologie, 1980, *vergriffen*
- Nr. 44 **Treske Arnold:** Experimentelle Überprüfung numerischer Berechnungsverfahren von Hochwasserwellen, 1980, *vergriffen*
- Nr. 45 **Csallner Klausotto; Häusler Erich:** Abflußinduzierte Schwingungen an Zugsegmenten - Ursachen, Sanierung und allgemeine Folgerungen
Herbrand Karl; Renner Dietrich: Aufnahme und Wiedergabe der Bewegung von Schwimmkörpern mit einem Video-Meßsystem
Keller Andreas: Messungen des Kavitationskeimspektrums im Nachstrom eines Schiffes - die ersten Großausführungsmessungen mit der Laser-Streulichtmethode
Knauss Jost: Neuere Beispiele für Blocksteinrampen an Flachlandflüssen
Scheuerlein Helmut: Der gelbe Fluß - nach wie vor Chinas Sorge oder die Unerbittlichkeit der Natur gegenüber 4000 Jahren menschlicher Bemühungen
Seus Günther J.: Nochmals: Das Muskingum-Verfahren. Fingerübungen zu einem bekannten Thema als "gradus ad parnassum" sowie neue Gedanken zur Interpretation des Anwendungsbereiches und eine Lösung des Problems der Nebenflüsse
Treske Arnold: Hochwasserentlastung an Dämmen. Zwei konstruktiv ähnliche Lösungen im Modellversuch, 1981, *vergriffen*
- Nr. 46 **Schmitz Gerd:** Instationäre Eichung mathematischer Hochwasserablauf-Modelle auf der Grundlage eines neuen Lösungsprinzips für hyperbolische Differentialgleichungs-Systeme, 1981, *vergriffen*
- Nr. 47 **Scheuerlein Helmut:** Der wasserbauliche Modellversuch als Hilfsmittel bei der Bewältigung von Verlandungsproblemen in Flüssen
Knauss Jost: Rundkronige und breitkronige Wehre, hydraulischer Entwurf und bauliche Gestaltung
Keller Andreas: Maßstabseffekte bei der Anfangskavitation, 1983, *vergriffen*
- Nr. 48 **Renner Dietrich:** Schiffahrtstechnische Modellversuche für Binnenwasserstraßen - Ein neues System und neue Auswertungsmöglichkeiten, 1984, *vergriffen*
- Nr. 49 **Sonderheft: Erhaltung und Umbau alter Wehre** (Wasserbau im historischen Ensemble, drei Beispiele aus dem Hochwasserschutz bayerischer Städte), 1984, *vergriffen*
- Nr. 50 **Knauss Jost; Heinrich B.; Kalcyk H.:** Die Wasserbauten der Minyer in der Kopais - die älteste Flußregulierung Europas, 1984, *vergriffen*
- Nr. 51 **Hartung Fritz; Ertl Walter; Herbrand Karl:** Das Donaumodell Straubing als Hilfe für die Planung und Bauausführung der Staustufe Straubing, 1984
- Nr. 52 **Hahn Ulrich:** Lufteintrag, Lufttransport und Entmischungsvorgang nach einem Wechselsprung in flachgeneigten, geschlossenen Rechteckgerinnen, 1985
- Nr. 53 **Bergmann Norbert:** Entwicklung eines Verfahrens zur Messung und Auswertung von Strömungsfeldern am wasserbaulichen Modell, 1985
- Nr. 54 **Schwarz Jürgen:** Druckstollen und Druckschächte - Bemessung und Konstruktion, 1985, *vergriffen*
- Nr. 55 **Schwarz Jürgen:** Berechnung von Druckstollen - Entwicklung und Anwendung eines mathematischen Modells und Ermittlung der felsmechanischen Parameter, 1987
- Nr. 56 **Seus Günther J.; Edenhofer Johann; Czirwitzky Hans-Joachim; Kiefer Ernst-Martin; Schmitz Gerd; Zunic Franz:** Ein HN-Modellsystem für zweidimensionale, stationäre und instationäre Strömungen beim Hochwasserschutz von Städten und Siedlungen, 1987
- Nr. 57 **Knauss Jost:** Die Melioration des Kopaisbeckens durch die Minyer im 2. Jt.v.Chr. – Kopais 2 - Wasserbau und Siedlungsbedingungen im Altertum, 1987
- Nr. 58 **Mtalo Felix:** Geschiebeabzug aus Kanälen mit Hilfe von Wirbelröhren, 1988
- Nr. 59 **Yalin M. Selim; Scheuerlein Helmut:** Friction factors in alluvial rivers
Yalin M. Selim: On the formation mechanism of dunes and ripples
Keller Andreas: Cavitation investigations at one family of NACA-hydrofoils at different angles of attack, as a contribution to the clarification of scale effects at cavitation inception, 1988

- Nr. 60 **Schmitz Gerd H.:** Strömungsvorgänge auf der Oberfläche und im Bodeninneren beim Bewässerungslandbau. Grundlagen, Kritik der herkömmlichen Praxis und neue hydrodynamisch-analytische Modelle zur Oberflächenbewässerung, 1989
- Nr. 61 **Muckenthaler Peter:** Hydraulische Sicherheit von Staudämmen, 1989, *vergriffen*
- Nr. 62 **Kalenda Reinhard:** Zur Quantifizierung der hydraulischen Versagenswahrscheinlichkeit beweglicher Wehre, 1990
- Nr. 63 **Knauss Jost:** Kopais 3, Wasserbau und Geschichte, Minysche Epoche - Bayerische Zeit (vier Jahrhunderte - ein Jahrzehnt), 1990
- Nr. 64 **Kiefer Ernst-Martin, Liedl Rudolf, Schmitz Gerd H. und Seus Günther J.:** Konservative Strömungsmodelle auf der Basis krummliniger Koordinaten unter besonderer Berücksichtigung von Wasserbewegungen im ungesättigt-gesättigten Boden, 1990
- Nr. 65 **Hartung Fritz:** Der ägyptische Nil 190 Jahre im Spiel der Politik (1798-1988)
Hartung Fritz: Gedanken zur Problematik der Nilwehre
Döscher Hans-Dieter und Hartung Fritz: Kritische Betrachtungen zum Stützwehr im Toschka-Entlastungsgerinne des Assuan-Hochdammes, 1991
- Nr. 66 **Schmitz Gerd H., Seus Günther J. und Liedl Rudolf:** Ein semi-analytisches Infiltrations-modell für Füllung und Entleerung von Erdkanälen
Keller Andreas P.: Chinese-German comparative cavitation tests in different test facilities on models of interest for hydraulic civil engineering, 1991
- Nr. 67 **Liedl Rudolf:** Funktionaldifferentialgleichungen zur Beschreibung von Wasserbewegungen in Böden natürlicher Variabilität - Beiträge zur Theorie und Entwicklung eines numerischen Lösungsverfahrens, 1991
- Nr. 68 **Zunic Franz:** Gezielte Vermischung bestehender Kanalisationssysteme - Methodische Studien zur Aktivierung freier Rückhalteräume unter besonderer Berücksichtigung der Abflusssteuerung, 1991
- Nr. 69 **Eickmann Gerhard:** Maßstabseffekte bei der beginnenden Kavitation - Ihre gesetzmäßige Erfassung unter Berücksichtigung der wesentlichen Einflußgrößen, 1991
- Nr. 70 **Schmid Reinhard:** Das Tragverhalten von Erd- und Steinschüttböden mit Asphaltbeton-Kerndichtungen, 1991
- Nr. 71 **Kiefer Ernst-Martin:** Hydrodynamisch-numerische Simulation der Wasserbewegung im ungesättigten und gesättigten Boden unter besonderer Berücksichtigung seiner natürlichen Variabilität, 1991
- Nr. 72 **Strobl Th., Steffen H., Haug W. und Geiseler W.-D.:** Kerndichtungen aus Asphaltbeton für Erd- und Steinschüttböden, 1992
- Nr. 73 **Symposium: Betrieb, Unterhalt und Modernisierung von Wasserbauten.**
Garmisch-Partenkirchen, 29. - 31. Oktober 1992
- Nr. 74 **Heilmair Thomas; Strobl Theodor:** Erfassung der sohnahen Strömungen in Ausleitungsstrecken mit FST-Halbkugeln und Mikro-Flowmeter - ein Vergleich der Methoden, 1994
- Nr. 75 **Godde Dominik:** Experimentelle Untersuchungen zur Anströmung von Rohrturbinen - Ein Beitrag zur Optimierung des Turbineneinlaufs, 1994
- Nr. 76 **Knauss Jost:** Von der Oberen zur Unteren Isar
Alte und neue Wasserbauten rund um die Benediktenwand. Bachumleitungen - Treibholzfänge - durchschwälzte Rohre - eine besondere Entlastungsanlage
Sohlensicherung an der Unteren Isar. Sohlstufenkonzept - Belegung der Sohle mit größeren Steinen in offener Anordnung, 1995
- Nr. 77 **Knauss Jost:** Argolische Studien: Alte Straßen - alte Wasserbauten. Talsperre von Mykene; Flußumleitung von Tiryns; Hydra von Lerna; Küstenpass Anigraia, 1996
- Nr. 78 **Aufleger Markus:** Ein Beitrag zur Auswertung von Erddruckmessungen in Staudämmen, 1996
- Nr. 79 **Heilmair Thomas:** Hydraulische und morphologische Kriterien bei der Beurteilung von Mindestabflüssen unter besonderer Berücksichtigung der sohnahen Strömungsverhältnisse, 1997
- Nr. 80 **Maile Willibald:** Bewertung von Fließgewässer-Biozönosen im Bereich von Ausleitungskraftwerken (Schwerpunkt Makrozoobenthos), 1997
- Nr. 81 **Knauss Jost:** Olympische Studien: Herakles und der Stall des Augias. Kladeosmauer und Alpheiosdamm, die Hochwasserfreilegung von Alt-Olympia, 1998

- Nr. 82 **Symposium: Planung und Realisierung im Wasserbau - Vergleich von Zielvorstellungen mit den Ergebnissen**, Garmisch-Partenkirchen 15. – 17. Oktober 1998
- Nr. 83 **Hauger Stefan:** Verkehrssteuerung auf Binnenwasserstraßen – Ein Beitrag zur Optimierung der Schleusungsreihenfolge in Stillwasserkanälen und staugeregelten Flüssen, 1998
- Nr. 84 **Herbrand Karl:** Schiffahrtstechnische Untersuchungen der Versuchsanstalt Obernach; Ein Rückblick auf ein traditionelles Untersuchungsgebiet der VAO, 1998
- Nr. 85 **Hartlieb Arnd:** Offene Deckwerke – Eine naturnahe Methode zur Sohlstabilisierung eintiefungsgefährdeter Flußabschnitte, 1999
- Nr. 86 **Spannring Michael:** Die Wirkung von Buhnen auf Strömung und Sohle eines Fließgewässers – Parameterstudie an einem numerischen Modell, 1999
- Nr. 87 **Kleist Frank:** Die Systemdurchlässigkeit von Schmalwänden. Ein Beitrag zur Herstellung von Schmalwänden und zur Prognose der Systemdurchlässigkeit, 1999
- Nr. 88 **Lang Tobias:** Geometrische Kriterien zur Gestaltung von Kraftwerkseinläufen. Experimentelle Untersuchungen an Rohr-S-Turbine und Durchströmturbine, 1999
- Nr. 89 **Aufleger Markus:** Verteilte faseroptische Temperaturmessungen im Wasserbau, 2000
- Nr. 90 **Knauss Jost:** Späthelladische Wasserbauten. Erkundungen zu wasserwirtschaftlichen Infrastrukturen der mykenischen Welt, 2001
- Nr. 91 **Festschrift** aus Anlass des 75-jährigen Bestehens der Versuchsanstalt für Wasserbau und Wasserwirtschaft der Technischen Universität München in Obernach – Oskar v. Miller-Institut, 2001
- Nr. 92 **Wildner Harald:** Injektion von porösem Massenbeton mit hydraulischen Bindemitteln, 2002
- Nr. 93 **Wildbach Naturversuche**
Loipersberger Anton; Sadgorski Constantin: Schwemmholt in Wildbächen: Problematik und Abhilfemaßnahmen; Geschiebeuntersuchungen; 1D und 2D Abflussmodelle in einem Wildbach
Rimböck Andreas: Naturversuch Seilnetzsperren zum Schwemmholtzrückhalt in Wildbächen: Planung, Aufbau, Versuchsdurchführung und Ergebnisse
Hübl Johannes; Pichler Andreas: Zur berührungslosen Erfassung der Fließtiefe und Fließgeschwindigkeit in einem Wildbachgerinne zum Zeitpunkt des Durchganges der Hochwasserwelle, 2002
- Nr. 94 **Rimböck Andreas:** Schwemmholtzrückhalt in Wildbächen – Grundlagen zu Planung und Berechnung von Seilnetzsperren, 2003
- Nr. 95 **Nothhaft Sabine:** Die hydrodynamische Belastung von Störkörpern, 2003
- Nr. 96 **Schmautz Markus:** Eigendynamische Aufweitung in einer geraden Gewässerstrecke – Entwicklung und Untersuchungen an einem numerischen Modell, 2003
- Nr. 97 **Neuner Johann:** Ein Beitrag zur Bestimmung der horizontalen Sicherheitsabstände und Fahrrinnenbreiten für Wasserstraßen, 2004
- Nr. 98 **Göhl Christian:** Bypasseinrichtungen zum Abstieg von Aalen an Wasserkraftanlagen, 2004
- Nr. 99 **Haimerl Gerhard:** Groundwater Recharge in Wadi Channels Downstream of Dams - Efficiency and Management Strategies, 2004
- Nr. 100 **Symposium: Lebensraum Fluss – Hochwasserschutz, Wasserkraft, Ökologie.**
Band 1; Wallgau, Oberbayern, 16. bis 19. Juni 2004
- Nr. 101 **Symposium: Lebensraum Fluss – Hochwasserschutz, Wasserkraft, Ökologie.**
Band 2; Wallgau, Oberbayern, 16. bis 19. Juni 2004
- Nr. 102 **Huber Richard:** Geschwindigkeitsmaßstabseffekte bei der Kavitationserosion in der Scherschicht nach prismatischen Kavitatoren, 2004
- Nr. 103 **Exposed Thermoplastic Geomembranes for Sealing of Water Conveyance Canals,** Guidelines for Design, Supply, Installation, 2005
- Nr. 104 **Workshop „Anwendung und Grenzen physikalischer und numerischer Modelle im Wasserbau“.** Wallgau, Oberbayern, 29. und 30. September 2005
- Nr. 105 **Conrad Marco:** A contribution to the thermal stress behaviour of Roller-Compacted-Concrete (RCC) gravity dams – Field and numerical investigations, 2006
- Nr. 106 **Schäfer Patrick:** Basic Research on Rehabilitation of Aged Free Flow Canals with Geomembranes, 2006

- Nr. 107 **Deichertüchtigung und Deichverteidigung in Bayern.** Beiträge zur Fachtagung am 13. und 14. Juli 2006 in Wallgau, Oberbayern, 2006
- Nr. 108 **Porras Pablo:** Fiber optic temperature measurements – Further Development of the Gradient Method for Leakage Detection and Localization in Earthen Structures, 2007
- Nr. 109 **PerzImaier Sebastian:** Verteilte Filtergeschwindigkeitsmessung in Staudämmen, 2007
- Nr. 110 **Wasserbau an der TU München** – Symposium zu Ehren von Prof. Theodor Strobl am 16. März 2007 in Wallgau, Oberbayern, 2007
- Nr. 111 **Haselsteiner Ronald:** Hochwasserschutzdeiche an Fließgewässern und ihre Durchsickerung, 2007
- Nr. 112 **Schwarz Peter; Strobl Theodor:** Wasserbaukunst - Oskar von Miller und die bewegte Geschichte des Forschungsinstituts für Wasserbau und Wasserwirtschaft in Obernach am Walchensee (1926-1951), 2007

Ab Band 113 ist Prof. Peter Rutschmann der Herausgeber der Berichte.

Die Berichtsbände können über den Lehrstuhl und die Versuchsanstalt für Wasserbau und Wasserwirtschaft der Technischen Universität München und über den Buchhandel bezogen werden.

- Nr. 113 **Flutpolder: Hochwasserrückhaltebecken im Nebenschluss.** Beiträge zur Fachtagung am 19. und 20. Juli 2007 in Wallgau, Oberbayern, ISBN 978-3-940476-03-6, 240 Seiten, Preis: 34,80 €, 2007
- Nr. 114 **Assessment of the Risk of Internal Erosion of Water Retaining Structures: Dams, Dykes and Levees.** Intermediate Report of the European Working Group of ICOLD, ISBN 978-3-940476-04-3, 284 Seiten, Preis: 29,80 €, 2007
- Nr. 115 **14. Deutsches Talsperrensymposium** (14th German Dam Symposium) and **7th ICOLD European Club Dam Symposium.** Beiträge zur Tagung am 17. bis 19. September 2007 in Freising (Contributions to the Symposium on 17 - 19 September 2007 in Freising, Germany, ISBN 978-3-940476-05-0, 560 Seiten, Preis: 49,80 €, 2007

